1995

Higher order spectra and their use in digital communication signal estimation

Yayci, Cihat

Monterey, California. Naval Postgraduate School

NAVAL POSTGRADUATE SCHOOL
Monterey, California

THESIS

HIGHER ORDER SPECTRA AND THEIR USE IN DIGITAL COMMUNICATION SIGNAL ESTIMATION

by

Cihat Yayci

March 1995

Thesis Advisor: Ralph Hippenstiel
Thesis Co-Advisor: Donald L. Walters

Approved for public release, distribution is unlimited.

REPORT DOCUMENTATION PAGE

Form Approved
OMB No. 0704-0188

1. AGENCY USE ONLY (Leave blank)	2. REPORT DATE	3. REPORT TYPE AND DATES COVERED
	March 1995	Master's Thesis

4. TITLE AND SUBTITLE
HIGHER ORDER SPECTRA AND THEIR USE IN DIGITAL COMMUNICATION SIGNAL ESTIMATION

5. FUNDING NUMBERS

6. AUTHOR(S)
Cihat Yayci

7. PERFORMING ORGANIZATION NAME(S) AND ADDRESS(ES)
Naval Postgraduate School
Monterey, CA 93943-5000

8. PERFORMING ORGANIZATION REPORT NUMBER

9. SPONSORING/MONITORING AGENCY NAME(S) AND ADDRESS(ES)

10. SPONSORING/MONITORING AGENCY REPORT NUMBER

11. SUPPLEMENTARY NOTES
The views expressed in this thesis are those of the author and do not reflect the official policy or position of the Department of Defense or the United States Government.

12a. DISTRIBUTION/AVAILABILITY STATEMENT
Approved for public release; distribution unlimited.

12b. DISTRIBUTION CODE

13. ABSTRACT *(Maximum 200 words)*

This thesis compared the detection ability of the spectrogram, the 1-1/2D instantaneous power spectrum (1-1/2D$_{IPS}$), the bispectrum, and outer product (dyadic) representation for digitally modulated signals corrupted by additive white Gaussian noise.

Four detection schemes were tried on noise free BPSK, QPSK, FSK, and OOK signals using different transform lengths. After determining the optimum transform length, each test signal is corrupted by additive white Gaussian noise. Different SNR levels were used to determine the lowest SNR level at which the message or the modulation type could be extracted.

The optimal transform length was found to be the symbol duration when processing BPSK, OOK, and FSK via the spectrogram, the 1-1/2D$_{IPS}$, or the bispectrum method. The best transform size for QPSK was half of the symbol length. For the outer product (dyadic) spectral representation, the best transform size was four times larger than the symbol length. For all processing techniques, with the exception of the outer product representation, the minimum detectable SNR is about 15 dB for BPSK, FSK, and OOK signals and about 20 dB for QPSK signals. For the outer product spectral method, these values tend to be about 10 dB lower.

14. SUBJECT TERMS	15. NUMBER OF PAGES
spectrogram, bispectrum, 1-1/2D$_{IPS}$, outer product representation simulation methods	213
	16. PRICE CODE

17. SECURITY CLASSIFICATION OF REPORT	18. SECURITY CLASSIFICATION OF THIS PAGE	19. SECURITY CLASSIFICATION OF ABSTRACT	20. LIMITATION OF ABSTRACT
Unclassified	Unclassified	Unclassified	UL

Approved for public release; distribution is unlimited

HIGHER ORDER SPECTRA AND THEIR USE IN DIGITAL COMMUNICATION SIGNAL ESTIMATION

by

Cihat Yayci
Lieutenant J. G., Turkish Navy
B.A., Turkish Naval Academy, 1988

Submitted in partial fulfillment of the
requirements for the degree of

MASTER OF SCIENCE IN ELECTRICAL ENGINEERING
MASTER OF SCIENCE IN APPLIED PHYSICS

from the

NAVAL POSTGRADUATE SCHOOL

March 1995

Author: [redacted]
Cihat Yaycı

Approved by: [redacted]
Ralph Hippenstiel, Thesis Advisor

[redacted]
Donald L. Walters, Co-Advisor

[redacted]
Michael A. Morgan, Chairman
Department of Electrical and Computer Engineering

[redacted]
William Colson, Chairman
Department of Physics

ABSTRACT

This thesis compared the detection ability of the spectrogram, the 1-1/2D instantaneous power spectrum (1-1/2D_{IPS}), the bispectrum, and outer product (dyadic) representation for digitally modulated signals corrupted by additive white Gaussian noise.

Four detection schemes were tried on noise free BPSK, QPSK, FSK, and OOK signals using different transform lengths. After determining the optimum transform length, each test signal is corrupted by additive white Gaussian noise. Different SNR levels were used to determine the lowest SNR level at which the message or the modulation type could be extracted.

The optimal transform length was found to be the symbol duration when processing BPSK, OOK, and FSK via the spectrogram, the 1-1/2D_{IPS}, or the bispectrum method. The best transform size for QPSK was half of the symbol length. For the outer product (dyadic) spectral representation, the best transform size was four times larger than the symbol length. For all processing techniques, with the exception of the outer product representation, the minimum detectable SNR is about 15 dB for BPSK, FSK, and OOK signals and about 20 dB for QPSK signals. For the outer product spectral method, these values tend to be about 10 dB lower.

TABLE OF CONTENTS

LIST OF FIGURES

LIST OF TABLES

ACKNOWLEDGMENT

I wish to thank my thesis advisor Professor Ralph Hippenstiel for his guidance and encouragement in this research. Also, I thank my wife, Muserref, my parents, Habibe and Yaşar, my son, Baybars Omer, and my sister, Ayşegül for their support.

I. INTRODUCTION

A. OVERVIEW

The estimate of the power spectral density of discrete-time deterministic or stochastic signals is a useful tool in digital signal processing. In spectral estimation, the distribution of power as a function of frequency is obtained. The information contained in the power spectrum is related by the Wiener-Khintchine theorem to the autocorrelation sequence. This is sufficient for the complete statistical description of a Gaussian signal. However, one has to look beyond the power spectrum (autocorrelation) of a signal to extract information about deviations from Gaussianity or phase relationships.

Higher order spectra (polyspectra) defined in terms of higher order statistics ("cumulants") of a signal, contain such information. Particular cases of higher order spectra are the third and fourth-order spectra called the bispectrum and trispectrum, respectively. These are Fourier transforms of their respective third and fourth-order moments. Higher-order statistics and their spectra can be defined in terms of moments and cumulants. Moments and moment spectra can be useful in the analysis of deterministic (transient and periodic) signals whereas cumulants and cumulant spectra are of great importance in the analysis of stochastic signals [Ref. 1, 2, 9, 17].

There are several reasons for using higher-order spectra. The first one is based on the property that for Gaussian signals, all cumulant spectra of order greater than two are identically zero. If a non-Gaussian signal is received along with additive Gaussian noise, the use of the higher-order cumulant will suppress the Gaussian noise component.

The second reason is that polyspectra (cumulant and moment) preserve the true phase character of signals. This provides a technique to identify non-minimum phase systems or to reconstruct non-minimum phase signals. For

example, the Knox-Thompson and triple correlation techniques use the bispectrum to remove random phase distortions in images degraded by the propagation medium [Refs. 27, 28].

The third reason is based on the fact that most "real world" signals are non-Gaussian and thus have non-zero higher-order spectra. Hence, a signal can be decomposed into its higher-order spectral functions where each one of them contains information about the signal. This allows determination of the degree of deviation from Gaussianity.

Finally, higher-order spectra are useful in analyzing the nonlinearity of a system operating with a random input. Polyspectra can play a key role in detecting and characterizing the type of nonlinearity in a system from its output. This allows detection and characterization of nonlinear properties in signals or systems.

In this work, the spectrogram, the bispectrum, the 1-1/2D instantaneous power spectrum, and outer product (dyadic form) spectrum were studied with respect to detection and classification performance. Four detection scheme were tried on noise free binary phase shift keyed (BPSK), quadrature phase shift keyed (QPSK), frequency shift keyed (FSK), and on-off keyed (OOK) signals using different transform lengths. After determining the optimum transform length, each test signal was corrupted by additive white Gaussian noise. Different SNR levels were used to determine the lowest SNR level at which the message or the modulation type can be extracted.

B. THESIS OUTLINE

The thesis is presented as follows; Chapter II defines cumulants and their relationship to moments. Each spectral method is presented. Chapter III defines the generation of the test signals. Chapter IV shows how the spectrogram, the 1-1/2D_{IPS}, bispectrum, and the outer product representation perform on noise

free signals. The best transform length for each method is then determined. Chapter V establishes the lowest SNR level for extracting the message or the modulation parameters. Chapter VI presents conclusions and suggestions for future work. The appendices contain the Matlab programs.

II. PROCESSING TECHNIQUES

This chapter describes the processing techniques used in this thesis. Detailed information is presented to develop an understanding of each method. We first define cumulants and show how they are used to form polyspectra. This is followed by the spectrogram, bispectrum, 1-1/2D_{IPS} spectrum, and the outer product (dyadic) form.

A. CUMULANTS AND MOMENTS

Given a set of n real valued random variables $\{x_1, x_2, ..., x_n\}$, their joint moments of order $r = k_1 + k_2 + ... + k_n$ are given by

$$Mom[x_1^{k_1}, x_2^{k_2}, ..., x_n^{k_n}] = E\{x_1^{k_1}, x_2^{k_2}, ..., x_n^{k_n}\}$$

$$= (-j)^r \frac{\partial^r \Phi(w_1, w_2, ..., w_n)}{\partial w_1^{k_1} \partial w_2^{k_2} \partial w_3^{k_3} .... \partial w_n^{k_n}} \Big|_{w_1=w_2=...=w_n=0} . \quad (2.1)$$

where $\Phi(w_1, w_2, ..., w_n) = E\{\exp(j(w_1 x_1 + w_2 x_2 + ... + w_n x_n))\}$ is their joint characteristic function and E{ } denotes the expectation operation. For example, for two random variables {x_1, x_2}, we have the second-order moments Mom[x_1, x_2] = E{x_1, x_2}, Mom[x_1^2] = E{x_1^2}, and Mom[x_2^2] = E{x_2^2}.

The joint second characteristic function is defined as the natural logarithm of $\Phi(w_1, w_2, ..., w_n)$; [Ref. 1, 14] i.e.,

$$\Psi(w_1, w_2, ..., w_n) = \ln[\Phi(w_1, w_2, ..., w_n)]. \quad (2.2)$$

The joint cumulants (also called semi-invariants, [Ref.1]) of order r, of a set of random variables, are defined as the coefficients of the Taylor expansion of the second characteristic function about zero. Thus, the joint cumulants can be expressed in terms of the joint moments of a set of random variables. The cumulants are given by

$$Cum[x_1^{k_1}, x_2^{k_2}, ..., x_n^{k_n}] = (-j)^r \frac{\partial^r \Psi(w_1, w_2, ..., w_n)}{\partial w_1^{k_1} \partial w_2^{k_2} \partial w_3^{k_3} .... \partial w_n^{k_n}} \Big|_{w_1=w_2=....=w_n=0}. \quad (2.3)$$

1. Moments and Cumulants of Stationary Processes

If { X(k) }, k = $0, \pm1, \pm2, \pm3, ...$ is a real stationary random process and its moments up to order n exist, then

$$Mom[X(k), X(k+\tau_1), ..., X(k+\tau_{n-1})] = E\{X(k)X(k+\tau_1).....X(k+\tau_{n-1})\}. \qquad (2.4)$$

will depend only on the time differences $\tau_1, \tau_2, ..., \tau_{n-1}$. [Ref. 1] We define the moments of a stationary random process as:

$$m_n^x(\tau_1, \tau_2, ..., \tau_{n-1}) = E\{X(k)X(k+\tau_1).....X(k+\tau_{n-1})\} \quad . \qquad (2.5)$$

Similarly , the nth-order cumulants of {X(k)} are (n-1)-dimensional functions defined as

$$c_n^x(\tau_1, \tau_2, ..., \tau_{n-1}) = Cum\{X(k)X(k+\tau_1).....X(k+\tau_{n-1})\}. \qquad (2.6)$$

Thus, the joint cumulants can be expressed in terms of the joint moments of a set of random variables. Since we only deal with a given random process, we simplify the notation as shown,

$m_1 = Mom\ [x_1] = E\{x_1\}$ $\qquad$ $m_2 = Mom\ [x_1, x_1] = E\{x^2_1\}$

$m_3 = Mom\ [x_1, x_1, x_1] = E\{x^3_1\}$ $\qquad$ $m_4 = Mom\ [x_1, x_1, x_1, x_1] = E\{x^4_1\}$.

The moments are related to the cumulants as given by

$c_1 = Cum\ [x_1] = m_1$

$c_2 = Cum\ [x_1, x_1] = m_2 - m^2_1$

$c_3 = Cum\ [x_1, x_1, x_1] = m_3 - 3m_2 m_1 + 2m^3_1$

$c_4 = Cum\ [x_1, x_1, x_1, x_1] = m_4 - 4m_3 m_1 - 3m^2_2 + 12m_2 m^2_1 - 6m^4_1$.

The general relationship between moments of $\{x_1, x_2, ..., x_n\}$ and joint cumulants $Cum\ [x_1, x_2, ..., x_n]$ of order r = n is given by [Ref. 1, 17]

$$Cum[x_1, x_2, ..., x_n] = \Sigma(-1)^{p-1}(p-1)!E\{\prod_{i\in s_1} x_i\}E\{\prod_{i\in s_2} x_i\}....E\{\prod_{i\in s_p} x_i\} \quad , \tag{2.7}$$

where the summation extends over all partitions $(s_1, s_2, ..., s_p)$, p = 1,2 ,.....,n, of the set of integers (1,2,...,n). The first order cumulant is equal to the first order moment since only one unique partition exists for one random variable. The first three orders of cumulants, expressed in terms of the component indices of a set of random variables, are

$c_1 = Cum\ [x_1] = E\{x_1\} = m_1$,

$c_2 = Cum\ [x_1, x_2] = E\{x_1, x_2\}\ E\{x_1\}\ E\{x_2\} = m_{1,2} - m_1\, m_2$,

$c_3 = Cum\ [x_1, x_2, x_3] = E\{x_1, x_2, x_3\} + 2E\{x_1\}\ E\{x_2\}E\{x_3\} - E\{x_1, x_2\}E\{x_3\} - E\{x_1, x_3\}E\{x_2\} - E\{x_2, x_3\}E\{x_1\}$

$= m_{1,2,3} + 2m_1m_2\, m_3 - m_{1,2}\, m_3 - m_{1,3}\, m_2 - m_{2,3}\, m_1$.

2. Properties of Moments and Cumulants

Inspection of the moment-cumulant expressions show that dependencies among random variables are removed when cumulants are calculated. In fact, both the second and third order cumulants are zero if all the random variables are independent of each other.

Another observation regarding the above moment-cumulant expressions applies in the commonly encountered situation where the means of the random variables are equal to zero. When this is true, the first order cumulant is zero since it equals the mean, the second order cumulant simply equals the variance, and the third order cumulant equals the third order moment.

The relationship (2.7) implies that the computation of joint order r requires knowledge of all moments up to order r.

Cumulants have three properties that make them more desirable than moments when it comes to higher order statistics:

Cumulants have three properties that make them more desirable than moments when it comes to higher order statistics:

1. Each cumulant is independent of all lower order cumulants. Consequently, all cumulants of order greater than two are equal to zero for a Gaussian processs, as a Gaussian process is completely characterized by its first and second order moments. Higher order moments, on the other hand, can contain information about lower order moments. Hence, the cumulants of order greater than two, measure the non-Gaussian nature of a time series. [Ref. 2, 25]

2. If a set of n random variables can be divided into more than one statistically independent subset, then the n^{th} order cumulant, unlike the n^{th} order moment, is equal to zero. [Ref. 2, 18 (p. 330)]

3. Unlike moments, the cumulants of the sum of two independent stationary random processes is equal to the sum of the corresponding cumulants of each process. [Ref. 2]

B. CUMULANT SPECTRUM

Suppose that the process {X(k)}, k = ...,-2,-1,0,1,2,.... is a real, stationary process with n^{th} order cumulant sequence $c_n^x(\tau_1, ..., \tau_{n-1})$ defined by (2.6).

Assuming that the cumulant sequence satisfies the conditions

$$\sum_{\tau_1=-\infty}^{+\infty} .... \sum_{\tau_{n-1}=-\infty}^{+\infty} |c_n^x(\tau_1, ..., \tau_{n-1})| < \infty,$$

$$\sum_{\tau_1=-\infty}^{+\infty} .... \sum_{\tau_{n-1}=-\infty}^{+\infty} (1 + |\tau_j|)|c_n^x(\tau_1, ..., \tau_{n-1})| < \infty. \qquad (2.8)$$

for j = 1,2,....,n-1, the n^{th} order cumulant spectrum $C_n^x(\ w_1,....,w_{n-1}\ )$ of {X(k)} exists, is continuous, and is defined as the (n-1) - dimensional Fourier transform of the n^{th} order cumulant sequence; [Ref.1, 22]. The conditions in (2.8) describe the usual conditions for a Fourier Transform to be well defined. The n^{th} order cumulant is thus defined:

$$C_n^x(w_1, ..., w_{n-1}) = \sum_{\tau_1=-\infty}^{+\infty} ..... \sum_{\tau_{n-1}=-\infty}^{+\infty} c_n^x(\tau_1, ..., \tau_{n-1}) \exp\{-j(w_1\tau_1 + w_1\tau_1 + ... + w_{n-1}\tau_{n-1})\} \tag{2.9}$$

where $|w_i| \leq \pi$, for i=1,2,....,n-1 and $|w_1 + w_2 + ... + w_{n-1}| \leq \pi$.

In general, $C_n^x(w_1,....,w_{n-1})$ is complex, i.e., has magnitude and phase. It can be written as

$$C_n^x(w_1, ..., w_{n-1}) = |C_n^x(w_1, ..., w_{n-1})| \exp\{j\Psi_n^x(w_1, ..., w_{n-1})\}. \tag{2.10}$$

The cumulant spectrum is also periodic with period 2π , i.e.,

$$C_n^x(w_1, ..., w_{n-1}) = C_n^x(w_1 + 2\pi, ..., w_{n-1} + 2\pi).$$

C. POWER SPECTRUM

The cumulant spectrum of order 2 is the power spectrum. It is given in (2.11) below.

$$C_2^x(w) = \sum_{\tau=-\infty}^{+\infty} c_2^x(\tau) \exp\{-j(w\tau)\}, \tag{2.11}$$

for $|w| \leq \pi$, where $c_2^x(\tau)$ is the covariance sequence of {X(k)}. Equation (2.11) is also known as the Wiener-Khintchine theorem.

As we stated earlier, the 2nd order cumulant is given by

$$c_2^x(\tau_1) = m_2^x(\tau_1) - (m_1^x)^2 \qquad \text{(covariance sequence)}$$

$$= m_2^x(-\tau_1) - (m_1^x)^2 = c_2^x(-\tau_1) \ , \tag{2.12}$$

where $m_2^x(-\tau_1)$ is the autocorrelation sequence. Thus, we see that the 2nd order cumulant sequence is the covariance function while the 2nd order moment sequence is the autocorrelation function. From equations (2.11) and (2.12), we have

$$c_2^x(\tau) = c_2^x(-\tau)$$

$$C_2^x(w) = C_2^x(-w) \qquad (2.13)$$

$C_2^X(w) \geq 0$ (real, nonnegative function) [Ref. 1, 9].

D. THE BISPECTRUM

The bispectrum is defined as the two dimensional Fourier transform of the third order cumulant:

$$C_3^X(w_1, w_2) = \frac{1}{(2\pi)^2} \sum_{\tau_1=-\infty}^{+\infty} \sum_{\tau_1=-\infty}^{+\infty} c_3^x(\tau_1, \tau_2) \exp\{-j(w_1\tau_1 + w_2\tau_2)\} \qquad (2.14)$$

where $|w_1| \leq \pi, \quad |w_2| \leq \pi, \quad |w_1 + w_2| \leq \pi$.

Here $c_3^x(\tau_1,\tau_2)$ is the third - order cumulant sequence of {X(k)} described by:

$$c_3^x(\tau_1, \tau_2) = m_3^x(\tau_1, \tau_2) - m_1^x[m_2^x(\tau_1) + m_2^x(\tau_2) + m_2^x(\tau_1 - \tau_2)] + 2(m_1^x)^3 \qquad (2.15)$$

and $m_3^x(\tau_1, \tau_2)$ is the third - order moment sequence.

Analogous to the power spectrum, the bispectrum can also be defined with frequency domain quantities. Given N samples of stationary signal *x(n)*, its Fourier transform is

$$X(w) = \sum_{n=0}^{N-1} x(n) \exp(-jwn) \qquad (2.16)$$

Assuming that the third - order cumulant in (2.14) is computed with the conjugation scheme (zero mean case), i.e.;

$$c_3^x(\tau_1,\tau_2) = E\{x^*(n)x(n+\tau_1)x(n+\tau_2)\}, \qquad (2.17)$$

then the equivalent frequency domain expression for the bispectrum is obtained through an extension of the periodogram of the form:

$$C_3^x(w_1,w_2) = \tfrac{1}{N}X(w_1)X(w_2)X^*(w_1+w_2) \quad . \qquad (2.18)$$

Equations (2.14) and (2.18) represent two different non - parametric methods that can be used to calculate the bispectrum. The approach in (2.14) is called the indirect method, while the approach in (2.18) is known as the direct method.

In general, the bispectrum's region of support is a hexagon centered at the origin of the (w_1, w_2) bispectral plane. Evaluation of the mean product of three Fourier amplitude terms shows that the bispectral plane exhibits certain symmetries. For a stationary, real, continuous time signal the expected value of the product of three Fourier components is:

$$E\{X_c(w_1)X_c(w_2)X_c(w_3)\} = C_c(w_1,w_2)\delta(w_1+w_2+w_3); \qquad (2.19)$$

where the subscript *c* denotes continuous time quantities.

Three properties of (2.19) determine the bispectral symmetry. First, since the frequency indexes must sum to zero, $w_3 = - w_1 - w_2$. Second, the frequency indexes in the expectation operation can be interchanged. Third, for the bispectrum of a real signal, conjugate symmetry results since $C(-w_1, -w_2) = C(w_1, w_2)$. Using the first property to express w_3 in terms of w_1 and w_2, the symmetry lines for a continuous time signal are [Ref. 9 & 20]

$$w_1 = w_2,$$

$2w_1 = -w_2$ (from $w_1 = w_3$),

$2w_2 = -w_1$ (from $w_1 = w_3$),

$w_1 = -w_2$,

$w_2 = 0$ (from $w_1 = -w_3$)

$w_1 = 0$ (from $w_2 = -w_3$).

Important symmetry conditions follow from the properties of moments:

$$c_3^x(\tau_1, \tau_2) = c_3^x(\tau_2, \tau_1) = c_3^x(-\tau_2, \tau_1 - \tau_2) = c_3^x(\tau_2 - \tau_1, -\tau_1)$$

$$= c_3^x(\tau_1 - \tau_2, -\tau_2) = c_3^x(\tau_1, \tau_2 - \tau_1).$$

As a consequence, knowing the third-order cumulants in any of the six sectors of Figure 2.1 enable us to find the entire third - order cumulant sequence. These sectors include their boundaries so that, for example sector I is an infinite wedge bounded by the lines $\tau_2 = 0$ and $\tau_1 = \tau_2, \tau_1 \geq 0$.

The definition of the bispectrum and the properties of the third - order cumulants give

$$C_3^x(w_1, w_2) = C_3^x(w_2, w_1) \tag{2.20}$$

$$= C_3^{x*}(-w_2, -w_1) = C_3^x(-w_1 - w_2, w_2)$$

$$= C_3^x(w_1, -w_1 - w_2) = C_3^x(-w_1 - w_2, w_1)$$

$$= C_3^x(w_2, -w_1 - w_2).$$

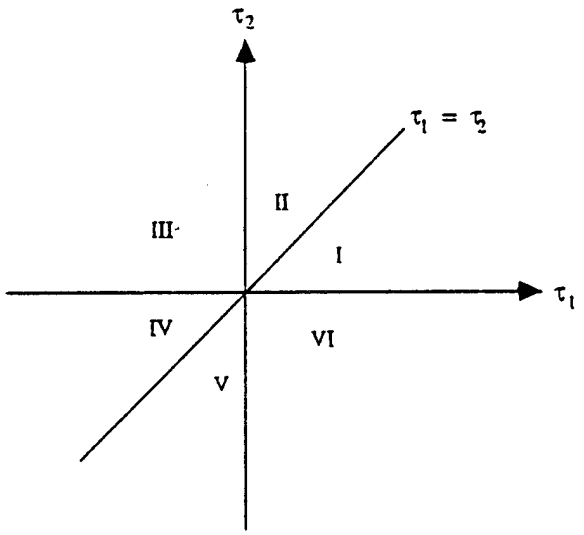

Figure 2.1: The Time Domain Plane

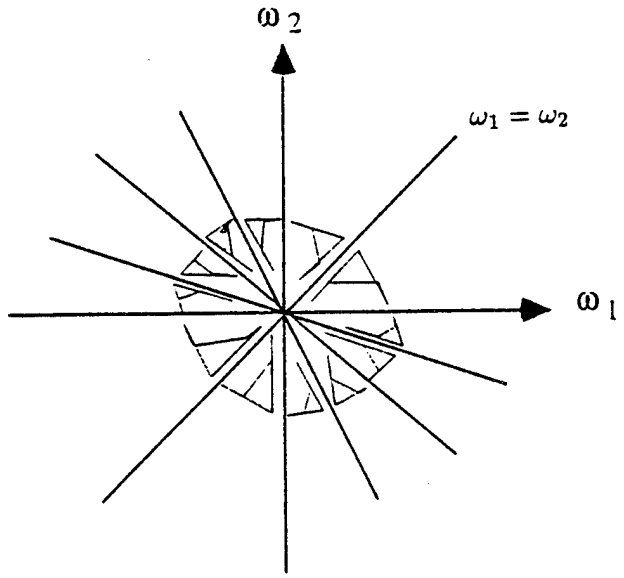

Figure 2.2: The Bispectral Plane

Thus knowledge of the bispectrum in the triangular region $w_2 \geq 0,\ w_1 \geq w_2,\ w_1 + w_2 \leq$ as shown in Figure 2.2 is sufficient for a complete description of the bispectrum. For real valued processes, the bispectrum has 12 symmetry regions.

Bispectral techniques have other applications, particularly in image restoration. For example, when an electromagnetic wave or sound wave propagates through a turbulent medium such as the ocean or the atmosphere, random phase perturbations scramble the phase front and induce intensity fluctuations from multipath interference. Images formed from these distorted waves lose their high spatial frequencies and become blurred. One technique, the Knox-Thompson and the related tripple correlation technique, utilize bispectral methods to combine a sequence of degraded images, while preserving the correlations between small frequency differences. Consequently, an ensemble average of the bispectra of several hundred degraded images allows the reconstruction of the original image, by computing the phase of the image from the statistical average of the phase differences. [Refs. 27, 28]

E. THE 1-1/2 D INSTANTANEOUS POWER SPECTRUM

The 1-1/2 D instantaneous power spectrum (1-1/2 D_{IPS}) is a combination of the standard 1-1/2 D spectrum (1-1/2 D_{STD}) and the Instantaneous Power Spectrum (IPS). It is shown that in some respects the1-1/2 D_{IPS} performs better than the conventional spectrogram. [Ref. 9, 16, 21] When used to process dynamic signals, 1-1/2 D_{IPS} is observed to have a quicker rise and fall time than the spectrogram. In addition, the 1-1/2 D_{IPS} method also appears to be a good at detecting low SNR stationary signals. [Ref. 16]

The standard 1-1/2 D spectrum is a degenerate form of the bispectrum. When the first lag of the third order cumulant expression is set to zero, the third order cumulant expression becomes

$$c_3^x(0,\tau_2) = E\{x^*(n)x(n)x(n+\tau_2)\} \tag{2.21}$$

$$= E\{|x(n)|^2 x(n+\tau_2)\}. \tag{2. 22}$$

A one-dimensional Fourier transform of (2.21) produces the 1-1/2 D_{STD} spectrum. [Ref. 2]

The instantaneous Power Spectrum is defined as the average of the derivatives of Page's running spectrum, [Ref. 9, 21]

$$\rho(t,f) = \frac{\partial}{\partial t} \int_{-\infty}^{t} |s(\tau)\exp(-j2\pi f\tau)d\tau|^2 \quad ; \tag{2.23}$$

and Levin's backward running spectrum, [Ref. 9, 21]

$$\rho^b(t,f) = \frac{\partial}{\partial t} \int_{t}^{\infty} |s(\tau)\exp(-j2\pi f\tau)d\tau|^2 \ . \tag{2.24}$$

A discrete version of IPS is obtained by taking the Fourier transform of windowed correlation estimates formed using simple lag products:

$$IPS(n,w) = \frac{1}{2}\sum_{k=0}^{N-1}\{x(n)x^*(n-k) + x^*(n)x(n+k)\}w(k)\exp(-jwk) \tag{2.25}$$

where w(k) is a window function, and N is the length of the sampled data sequence [Ref. 9, 16, 21]. The 1-1/2D_{IPS} is defined as

$$1 - 1/2D_{IPS}(n,w) = \frac{1}{2}\sum_{k=0}^{N-1}\{|x(n)|^2 x^*(n-k) + |x(n)|^2\}x(n+k)\}w(k)\exp(-jwk) \qquad (2.26)$$

as given in [Ref. 16].

F. OUTER PRODUCT (DYADIC) FORM

The outer product is the two dimensional periodogram of the sample at frequencies f_1 and f_2 [Ref. 23]. In particular,

$$P_o(f_1,f_2,m) = X(f_1,m)X^*(f_2,m) \quad , \qquad (2.27)$$

where

$$X(f_i,m) = \sum_{n=(m-1)k}^{(km-1)} x(n)e^{-j2\pi f_i n} \qquad m = 1,....,M, \qquad (2.28)$$

and M is the total number of segments, k is the transform length, and m is the segment number.

Note that the entries of the two dimensional spectrogram have complex symmetry and that they are the complex conjugates of the each other.

The outer product is averaged in a coherent and incoherent fashion. For the coherent averaging; all complex valued matrices are added and the absolute value of the resultant matrix is taken.

$$P(f_1,f_2,m)_{COH} = \left|\sum_{m=1}^{M} P_o(f_1,f_2,m)\right| \quad . \qquad (2.29)$$

For incoherent averaging; the absolute value of the matrices are added.

$$P(f_1,f_2,m)_{INCOH} = \sum_{m=1}^{M} |P_o(f_1,f_2,m)| \qquad (2.30)$$

Note, the entries along coordinate (f_i, f_j) correspond to a conventional averaged (coherent or incoherent) periodogram.

III. SIGNAL GENERATION

In this chapter, we introduce the signals, BPSK, QPSK, OOK, and FSK that are generated to serve as test data. The computer plots of these signals are shown in this chapter. This chapter also covers the algorithms that are used in the generation of these signals. Matlab code is used for the generation of signals and the noise.

A. BINARY - PHASE SHIFT KEYING (BPSK)

Suppose the information is to be transmitted one bit at a time at some uniform rate R bits/s. The modulator maps the binary digit 0 into a waveform $s_1(t)$ and binary digit 1 into a waveform $s_2(t)$. In this manner, each bit from the channel encoder is distinctly encoded. We call this process a binary modulation.

In binary data transmission, only one of two possible signals are sent during each bit interval T_b. On the other hand, in an M-ary data transmission system, any one of M possible signals can be sent during each signaling interval T [Ref. 10, 11, 12]. The binary data transmission system is a special case of an M-ary data transmission system.

Binary phase shift keying (BPSK) is one of the most common binary bandpass signaling techniques. The phase of a sinusoidal carrier is shifted by 0° or 180° relative to the reference sinusoid with a unipolar binary signal. It is equivalent to PM signaling with a digital waveform and is also equivalent to modulating a DSB-SC signal with a polar digital waveform. [Ref. 10, 12]

A sinusoidal carrier wave of fixed amplitude A_c and fixed frequency f_c is used to represent both symbols 1 and 0 . A typical BPSK is shown in Figure 3.1 and given by

$$s(t) = A_c \cos(2\pi f_c t), \qquad \text{for symbol 1}$$
$$s(t) = A_c \cos(2\pi f_c t + \pi) \qquad \text{for symbol 0.}$$

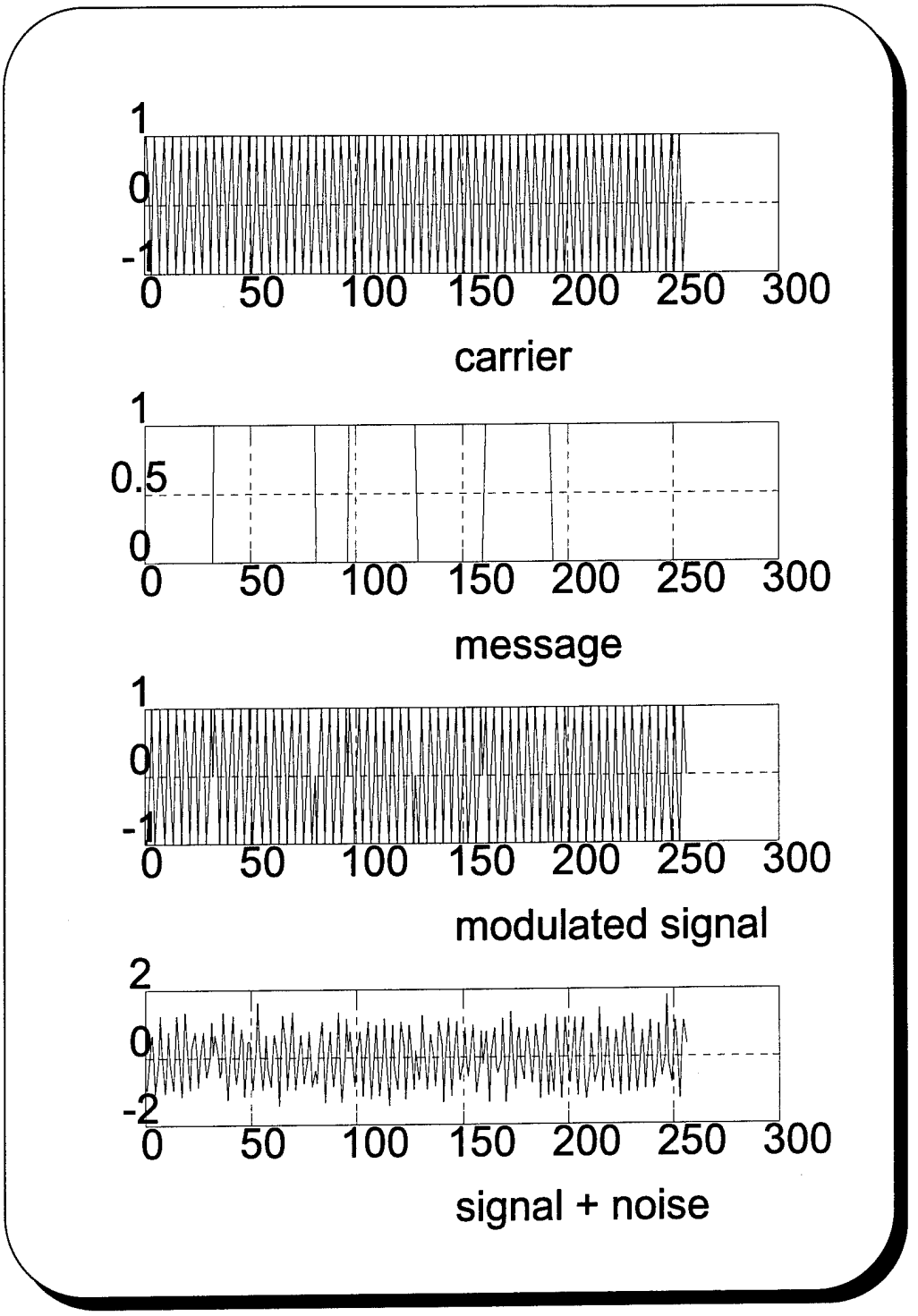

Figure 3.1: Binary Phase Shift Keying Generation

The algorithm that is used for the generation of BPSK signal consists of the following steps:

1. Creation of the message, (i.e., 1010)

2. Creation of the sinusoidal carrier wave.

3. Adding an appropriate phase shift (180° or 0°) to modulate the carrier. The transmitted signal is either in phase or out of phase with the carrier when signalling a binary 1 or 0, respectively.

4. Expressing every symbol in a message as a group of bits, so that a group of bits represent a unit of information. For example, four bits represents a symbol of message. In this case, the message of step 1 will become 1111000011110000.

5. Adding noise (for analyzing noisy signals).

B. FREQUENCY - SHIFT KEYING (FSK)

Frequency-shift keying (FSK), consists of shifting the frequency of a sinusoidal carrier from a mark frequency (corresponding to a binary 1) to a space frequency (corresponding to a binary 0) according to the baseband digital signal.

In an FSK system, two sinusoidal waves of the same amplitude A_c but different frequencies f_1 and f_c are used to represent binary symbols 1 and 0, respectively. That is, we may express the binary FSK wave s(t) as

$$s(t) = A_c \cos(2\pi f_1 t), \quad \text{for symbol 1}$$
$$s(t) = A_c \cos(2\pi f_c t), \quad \text{for symbol 0.}$$

The algorithm that is used for the generation of FSK signal consists of the following steps:

1. Creation of the message, (i.e., 1010).

2. Creation of the sinusoidal carrier wave at frequency f_c.

3. Changing the frequency to f_1 for representing symbol 1, otherwise using f_c as the carrier frequency.

4. Expressing every symbol in the message as a group of bits. So that a group of bits represents a unit of information. For example, four bits represent one symbol of the message.

5. Adding noise (for analyzing noisy signals).

A typical FSK signal is shown in Figure 3.2.

C. ON - OFF KEYING (OOK , ASK)

On-off keying (OOK), also called amplitude shift keying (ASK), consists of keying (switching) a carrier sinusoid on or off with a unipolar binary signal. It is identical to unipolar binary modulation on a DSB-SC signal [Ref.10, 11, 12].

In an ASK system, the binary symbol 1 is represented by transmitting a sinusoidal carrier wave of fixed amplitude A_c, and fixed frequency f_c for the bit duration T_b seconds, whereas the binary symbol 0 is represented by switching off the carrier for T_b seconds. In mathematical terms, we may express the binary ASK wave s(t) as:

$$s(t) = A_c \cos(2\pi f_c t), \quad \text{for} \quad \text{symbol 1}$$
$$= 0 \ , \quad \text{for} \quad \text{symbol 0.}$$

The algorithm that is used for the generation of OOK signal consists the following steps:

1. Creation of the message (i.e., 1010)

2. Creation of the sinusoidal carrier wave.

3. Multiplying the carrier by 1 or 0 for representing the symbol 1 or 0, respectively.

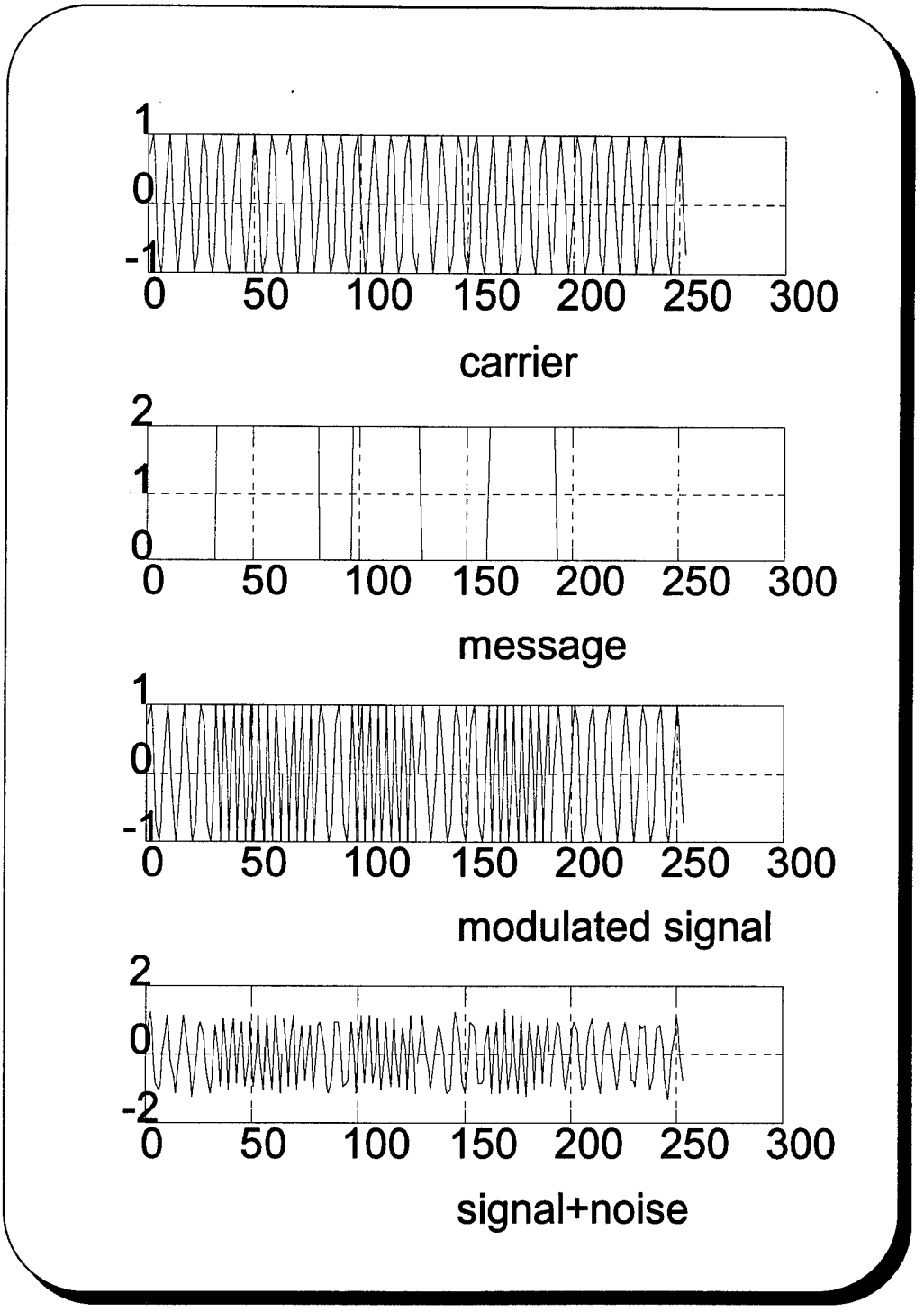

Figure 3.2: Frequency Shift Keying Generation

4. Expressing every symbol in the message as a group of bits, so that a group of bits represent a unit of information. For example, four bits represent a symbol of the message. In this case, the message will be 1111000011110000.

5. Adding noise (for analyzing noisy signals).

A typical OOK signal is shown in Figure 3.3.

D. QUADRATURE PHASE (QUADRIPHASE) - SHIFT KEYING (QPSK)

The quadriphase-shift keying (QPSK) is an example of M-ary data transmission with M = 4. In quadriphase-shift keying, one of four possible signals is transmitted during each signaling interval, with each signal uniquely related to a dibit (pairs of bits are termed dibits) [Ref. 10, 12, 20]. For example, we may represent the four possible dibits 00, 10, 11, and 01 (in Gray-encoded form) by transmitting a sinusoidal carrier with one of four possible phase values, as follows;

$s(t) = A_c \sin(2\pi f_c t + 2\pi)$, for dibit 00

$s(t) = A_c \sin(2\pi f_c t + \pi/2)$, for dibit 10

$s(t) = A_c \sin(2\pi f_c t + \pi)$, for dibit 11

$s(t) = A_c \sin(2\pi f_c t + 3\pi/2)$, for dibit 01

where $0 \le t \le T_s$ and T_s as symbol duration.

Clearly, QPSK represents a special form of phase modulation. This is done by expressing s(t) as

$s(t) = A_c \sin(2\pi f_c t + \phi(t))$,

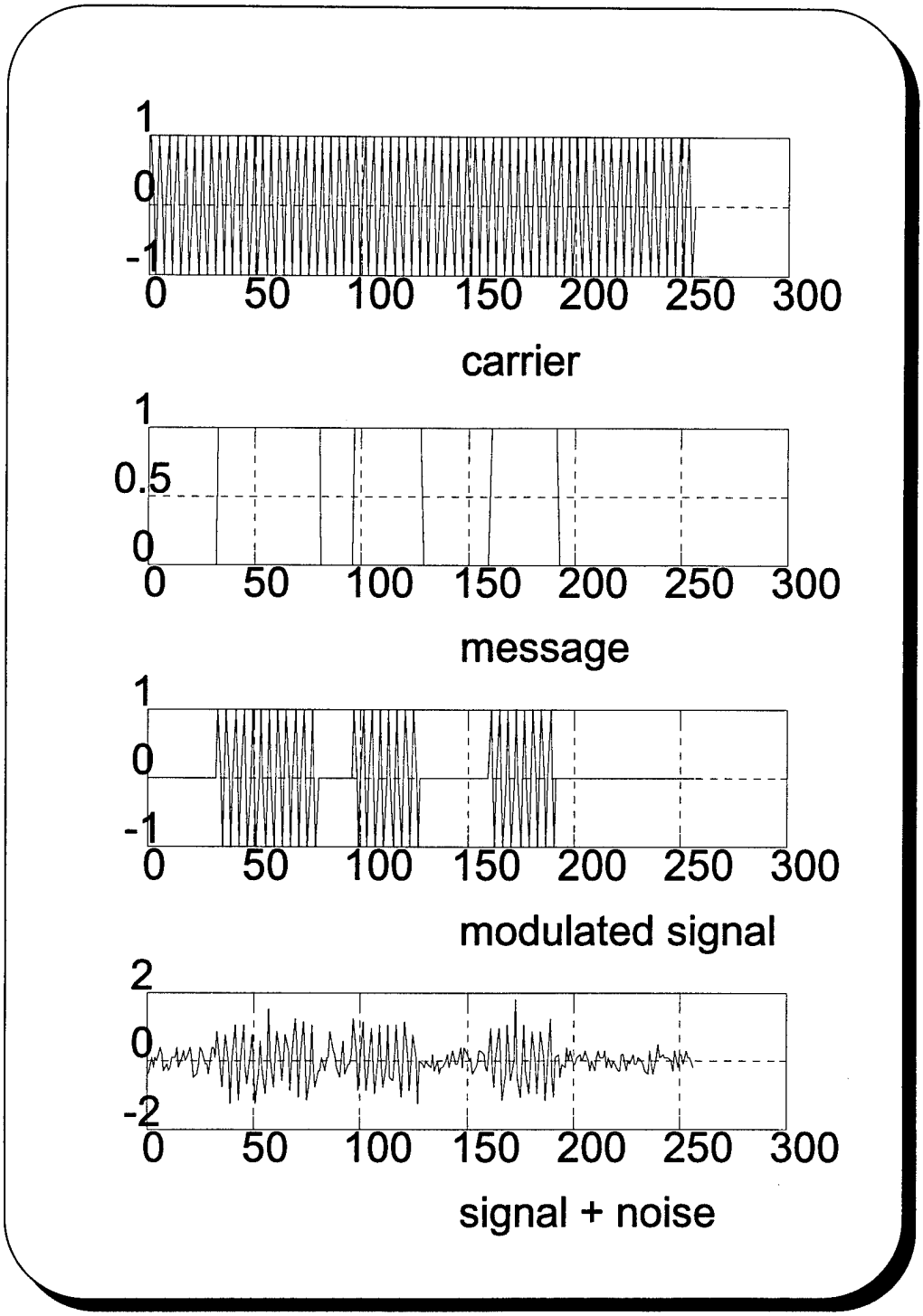

Figure 3.3: On - Off Keying Generation

where the phase $\phi(t)$ assumes a constant value for each dibit of the incoming data stream. Specifically, we have

$\phi(t) = 2\pi$ for dibit 00,
$\phi(t) = \pi/2$ for dibit 10,
$\phi(t) = \pi$ for dibit 11,
$\phi(t) = 3\pi/2$ for dibit 01.

The symbols can be expressed as dibits or 0, 1, 2, and 3 (or any other four message units). A typical QPSK signal is shown in figure 3.4.

The algorithm that is used for the generation of an QPSK signal consists of the following steps:

1. Creation of the message that consists of four possible signals.

2. Creation of the sinusoidal carrier wave.

3. Adding 0° phase shift for the symbol 0, (00) (i.e., leaving it as it is), adding 90° phase shift for the symbol 1, (10), adding 180° phase shift for the symbol 2, (11), adding 270° phase shift for the symbol 3, (01).

4. Expressing every symbol in the message as a group of bits, so that a group of bits represent a unit of information.

5. Adding noise (for analyzing noisy signals).

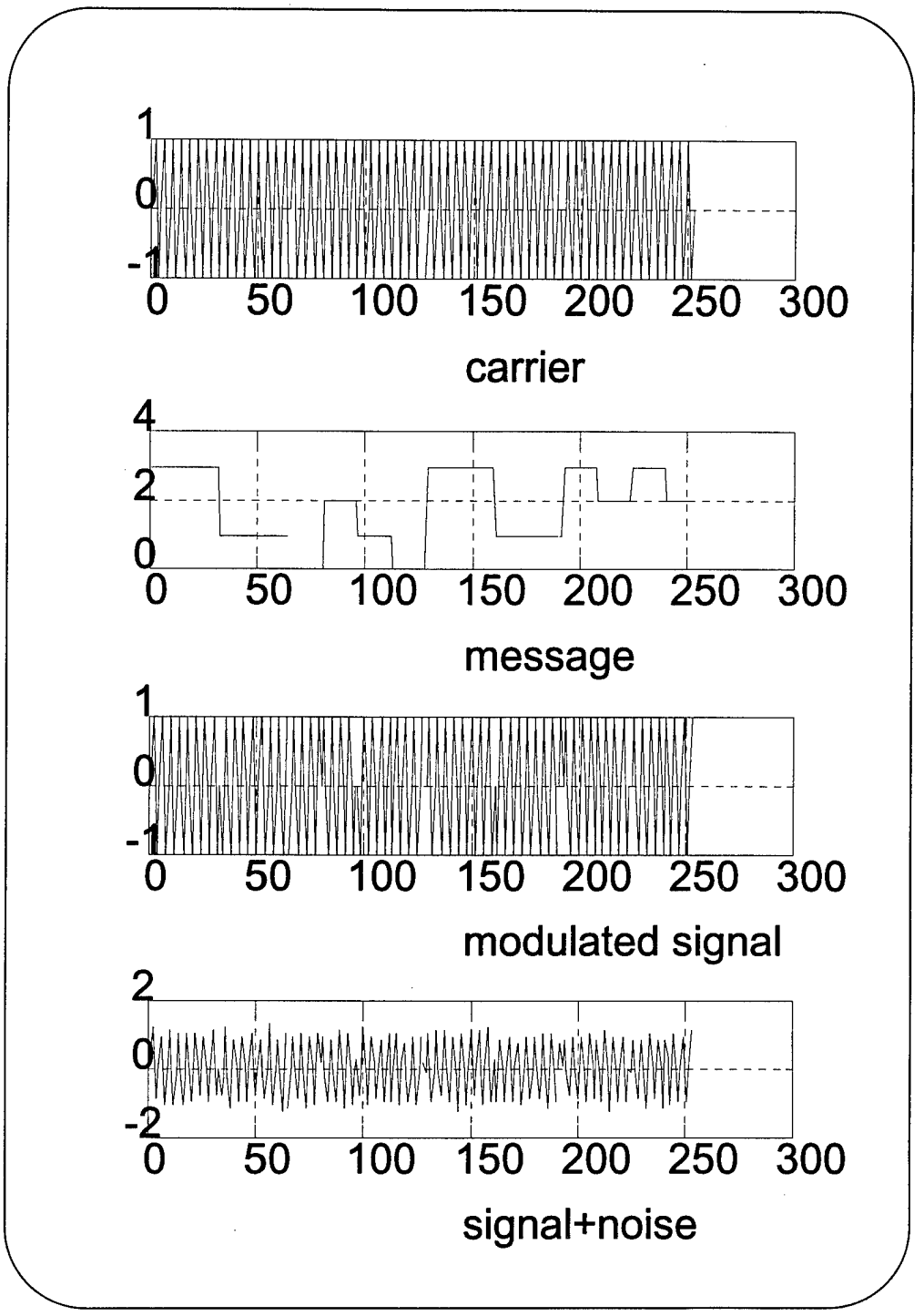

Figure 3.4: Quadrature Phase Shift Keying Generation

IV. SIMULATION

In this chapter we compare the performance of the spectrogram, the 1-1/2 D_{IPS}, the bispectrum, and the outer product representation. Matlab programs were used to conduct the computer simulations contained in this chapter. Simulation results are interpreted to see how each method treats the signal and noise components.

For comparison BPSK, FSK, OOK, and QPSK signals were used as input data. Initially, simulation programs were run with signals using differently sized Fourier transforms. This allowed the determination of the optimum transform length for comparing the different methods.

A. SIMULATION PROGRAMS

1. SPECTRO

The SPECTRO algorithm is given in Appendix E. It computes the spectrogram. The periodogram is computed as:

$$P_{per}(w,m) = \left| \sum_{n=m}^{(winlen-1)+m} x(n)w(n)\exp(-jwn) \right|^2; \qquad m = 0, 1, \ldots \qquad (4.1)$$

where m = time index, and winlen = data length. The data segment was padded with zeros to the desired transform length, and *w(n)* was a window function.

The user must specify the window function:

wintype : '0' for a rectangular window

'1' for a Hamming window.

winlen : The desired length of data window.

The time step was fixed at one and the spectrogram surface was calculated with non-normalized periodograms.

The time-frequency (spectrogram) surface was calculated and stored in a location denoted by the 'P' matrix. The columns of 'P' matrix were the frequency bins while the rows are the time steps.

The spectrogram program created a series of five plots. In the upper row of the spectrogram figures such as Figure 4.2 the first picture was a mesh plot , the second one is the corresponding contour plot. The third figure is obtained by averaging the "P" matrix over frequency. The first picture in the lower row was obtained by averaging the "P" matrix over time and the second figure was the power spectrum of the signal using all available data.

2. ONE_HALF D_{IPS}

The 1-1/2 D_{IPS} algorithm was implemented in [Ref. 16] with the extrinsic Matlab function ONE_HALF. Modifications were made to the original program to remove some undesirable smoothing steps. The revised ONE_HALF algorithm is contained in Appendix F. It has the same input and output format as the SPECTRO code.

The user specifies an input data sequence, the size of the data window, a step increment, and a window function. ONE_HALF returns the time-frequency representation of the input sequence. The ONE_HALF algorithm was based upon (2.26) but was windowed to avoid undesirable product term interference that may form spurious peaks in the time-frequency representation. First the following sequence was generated:

$$prod1 = \left| element(0)element(1)....element(\tfrac{winlen}{2} - 1) \right|; \qquad (4.2)$$

where

$$element(k) = |x(n)|^2 \{x^*(n-k) + x(n+k)\}, \quad (4.3)$$

winlen was the specified data window length, and *x(n)* was the input data segment. A second sequence, designated as *prod2*, was formed by deleting the first element in *prod1,* adding one more element to it (i.e., $element(\frac{winlen}{2})$) and then reversing the order of the conjugated remaining elements [Ref. 9]:

$$prod2 = [element^*(\frac{winlen}{2}), element^*(\frac{winlen}{2} - 1), ..., element^*(1) \quad (4.4)$$

The two sequences were then concatenated with a zero inserted between them to form a proper correlation function having a real valued Fourier transform. The 1-1/2 D_{IPS} estimate was obtained by multiplying the real part of the transformed sequence by one-half. The program computed the magnitude via the real part of the transform:

$$1\text{-}1/2\ D_{ips} = |\ \tfrac{1}{2}\ \ F\{[prod1\ 0\ prod2]\}| \quad (4.5)$$

where F denotes the Fourier transform.

The 1-1/2 D surface characteristics were determined by the selection of window type (wintype), window length (winlen) and the distance that the window was moved through the data sequence (step).

The inputs are:

data : The input observations vector. The length should be a power of 2, e.g., 64, 128 , 512.

wintype : '0' for Rectangular window
'1' for Hamming window

winlen : The desired width of the window, normally half of the input length.

step : The desired time step, can be '1' or any integer (typically a power of 2 is used).

The time-frequency surface was calculated and stored in a location denoted by the 'P' matrix. The columns of 'P' matrix were the frequency bins while the rows are the time steps. Time-frequency axis labeling vectors, 'freqindex' and 'timeindex' were returned to aid in the plotting of the results.

In the upper row of the 1-1/2D spectra figures (such as Figure 4.7) also, the first picture was a mesh plot, while the second one was the corresponding contour plot. The third figure was obtained by averaging the "P" matrix over frequency. The first picture in the lower row was obtained by averaging the "P" matrix over time and the second figure is the power spectrum of the signal using all available data.

3. BISPECTRUM

Bispectrum methods produce a frequency versus frequency representation instead of a time-frequency representation. The direct method for computing the bispectrum was realized through the Hi-Spec Matlab function BISPEC_D of [Ref. 13]. This function returned the complex bispectrum matrix and a frequency axis labeling vector. The user specifies an input data sequence, the desired Fast Fourier Transform (FFT) size, the number of samples per segment, the amount of overlap between data segments, and the desired form of the smoothing window. The three window options available were the unit hexagonal window, the Parzen window, and the optimum window (also known as the minimum bias supremum window).

The user must specify:

y : data vector or time series

nfft : FFT length

wind : window specification for frequency-domain smoothing

nsamp : samples per segment

overlap : percentage overlap

The output of BISPEC_D.M was denoted by *Bspec.* The output plots of Bspec were an nfft x nfft array with the origin at the center, with axes pointing up and to the right. The another output was *waxis* which is a vector of frequencies associated with the row and column indices of Bspec. The sampling frequency was assumed to be 1.

In the upper row of the bispectrum figures such as Figure 4.12, the first picture is the mesh plot, and the second one is the contour plot. In the lower row, the first picture is the frequency average plot of the ' Bspec ' matrix , and the second one is the power spectrum of the signal.

4. OUTER PRODUCT (DYADIC) FORM

The outer product is the two dimensional periodogram of the sample at frequencies f_1 and f_2 [Ref. 23]. In particular,

$$P_o(f_1,f_2,m) = X(f_1,m)X^*(f_2,m) \quad , \tag{4.6}$$

where

$$X(f_i,m) = \sum_{n=(m-1)k}^{(km-1)} x(n)e^{-j2\pi f_i n} \qquad m = 1,2,...,M \quad , \tag{4.7}$$

where M is the total number of segments, k is the transform length, and m is the segment number.

Note that the entries of the two dimensional spectrogram have complex symmetry and that they are the complex conjugates of each other.

We averaged the outer product in both coherent and incoherent fashions. For the coherent averaging; all complex valued matrices were added and the absolute value of the resultant matrix was taken.

$$P(f_1,f_2,m)_{COH} = \left| \sum_{m=1}^{M} P_o(f_1,f_2,m) \right| \tag{4.8}$$

For incoherent averaging; the absolute value of the matrices were added.

$$P(f_1,f_2,m)_{INCOH} = \sum_{m=1}^{M} |P_o(f_1,f_2,m)| \tag{4.9}$$

The general procedure for averaging the outer product coherently and incoherently was as follows;

1. The data, which has a length of N, was divided into segments with respect to the chosen transform length, so that we will have N/k segments of data. For example, for 256 data points and a 64 point transform length then we will have 4 segments of data which consist of data points 1 through 64, 65 through 128, 129 through 192, and 193 through 256.

2. The Fourier transform of each segment was taken.

3. Each Fourier transform was multiplied in an outer product form by its complex conjugate to produce k x k matrices, we have N/k matrices and each matrix was of size k x k.

4. For coherent averaging; all complex valued matrices are added and the absolute value of the final matrix was taken (4.8) . For incoherent averaging; the absolute value of each matrix was taken and then added (4.9).

In the upper row of the outer product representation figures such as Figure 4.17, the first picture is the mesh plot of the final matrix, and second one is the corresponding contour plot. In the lower row, the first one is a scatter plot, and the second one is the sum plot of the final matrix. The scatter plot is the plot of

all the rows (or the columns) of the final matrix. Note that the entries along coordinate (f_i, f_j) are equivalent to an averaged periodogram. In this study, the first quadrant of the contour plots was chosen for the analysis of contour plots since the contour plots had four symmetric quadrants. The outer product algorithm is given in Appendix G.

B. FFT LENGTH SELECTION

Different Fourier Transform (FFT) lengths were tried to find an optimal length for each of the test signal. The test message was 16 symbols long with each symbol of length 16, resulting in a data length of 256. In all simulations, Figure 4.1 through Figure 4.104 only noise free signals were used.

1. BPSK

The message consisted of ones and zeros. In the BPSK scheme, the transmitted signal was either in phase or out of phase with the carrier when signaling a binary 1 or 0, respectively. Generally, the sinusoidal carrier can be represented as follows:

carrier s(n) = $\cos(2\pi\frac{k}{N_1}n)$

where n = 0,1,.....,255.

In this formulation, N_1 was the number of samples per symbol, and k was the number of cycles per symbol. Over N_1 samples exactly k cycles (periods) were produced. In this work, k was 4 and N_1 was 16. Hence we know the carrier frequency, f_c , was $(k / N_1)f_s = (4 / 16)f_s = 0.25\ f_s$.

This means that 16 samples represent 4 cycles. The data set was 256 samples long, having 64 carrier cycles and representing 16 symbols. The

transform lengths which were used in this study are N_1 /4, N_1 /2, N_1, $2N_1$, and $4N_1$ where N_1 was the symbol length (i.e., N_1 = 16).

The 16 symbol message { 0 0 1 1 1 0 1 1 0 0 1 1 0 0 0 0} used for BPSK was also used for FSK, and OOK. Since every symbol was 16 data points, we expect a 180° phase shift at locations 33, 81, 97, 129, 161, 193.

Figure 4.1 shows the plot of the sinusoidal carrier, the message, and the BPSK modulated signal. Figure 4.2 through Figure 4.6 shows spectrograms for the noise free case for FFT sizes 4, 8, 16, 32, and 64. A Hamming window was used.

It can be seen that the message or the phase shifts at the relevant locations can be determined with window lengths of N_1 /2 (which is 8), N_1 (which is 16) and 2 x N_1 (which is 32). For the other window lengths, it was difficult to determine the message. For a length of 32 (in Figure 4.5), the contour plot was not showing, accurately, the phase shifts at their relevant locations and for a length of 8 (in Figure 4.3), the time averaged plot was not centered. Therefore, the Figure (4.4) for size 16 was the best in localizing the transition points.

Figure 4.7 through Figure 4.11 show the 1-1/2 D spectrum for FFT sizes of 4, 8, 16, 32, and 64. A Hamming window with a step size of 2 were used. The phase transition points can be seen on the mesh, contour and frequency averaged plots when using an FFT size of 8,16 and 32 (in Figures 4.8, 4.9, and 4.10). For a length of 32 (in Figure 4.10), the frequency averaged plot was hard to interpret and for a length of 8 (in Figure 4.8), the time averaged plot was not centered. A size of 16 (i.e., matched signal bit length) was chosen as the optimum transform length for the 1-1/2 D spectral analysis since the time averaged plot showed the total spectral range (in Figure 4.9).

Figure 4.12 through Figure 4.16 show the bispectrum for FFT sizes 4, 8, 16, 32, and 64. The window type was '1' , the overlap was 50 percent, and the number of samples per segment (nsamp) was 4. For bispectral analysis on

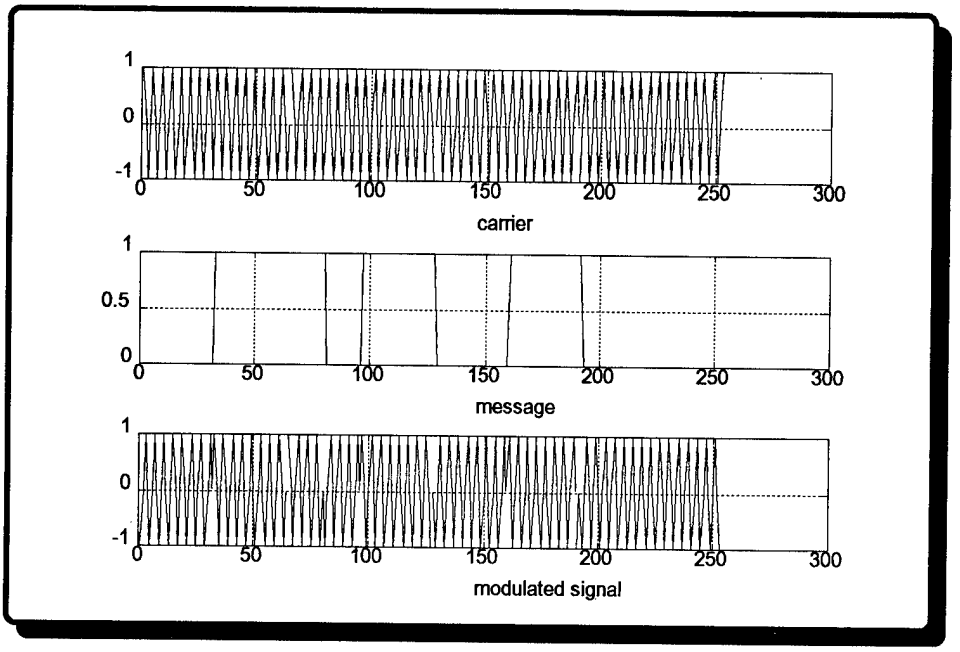

Figure 4.1: BPSK Generation

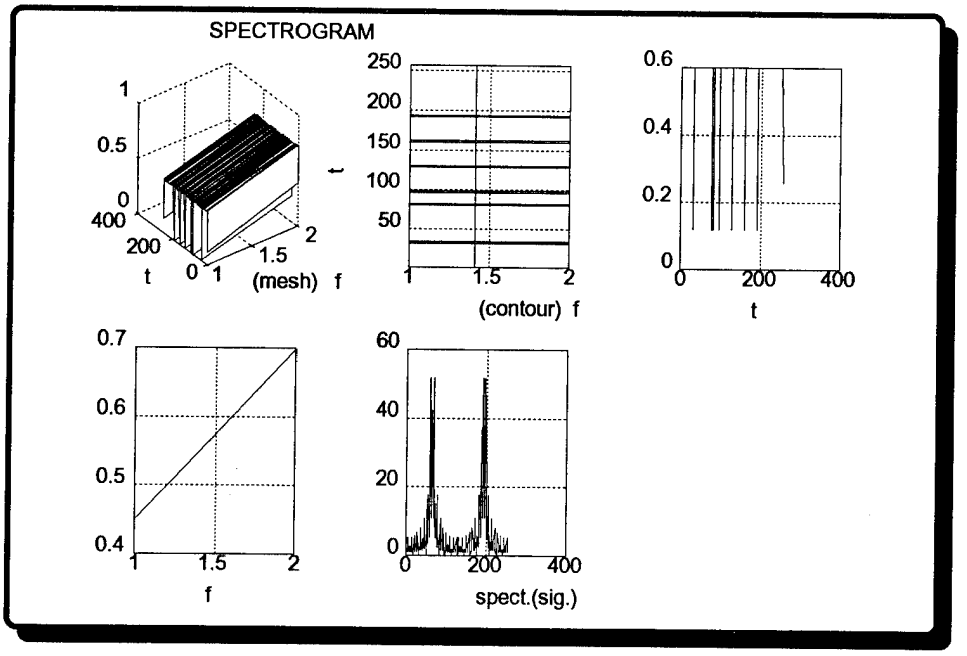

Figure 4.2 : BPSK Spectrogram (Window Length is 4)

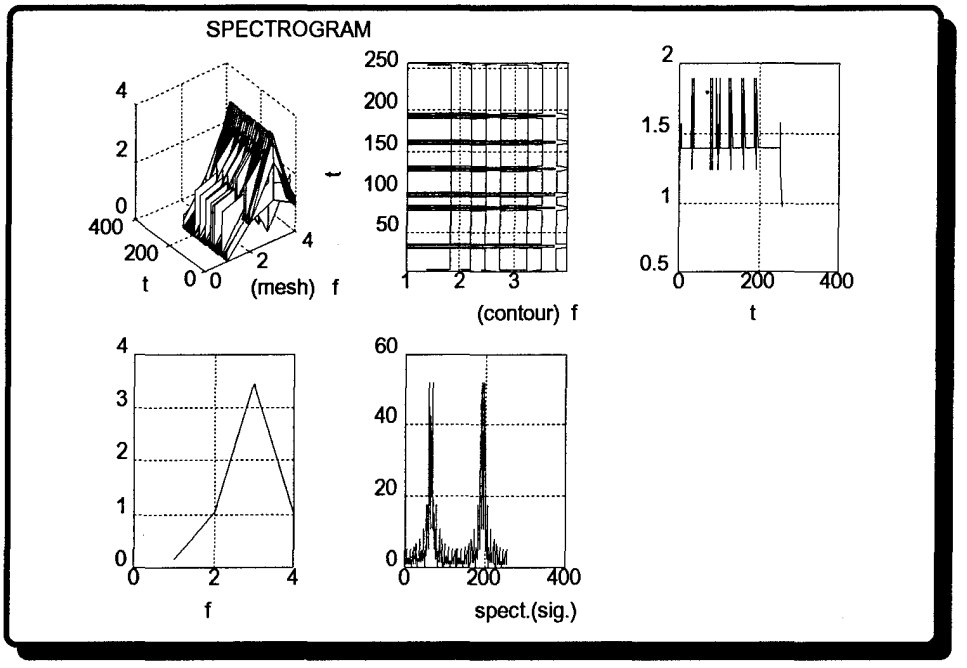

Figure 4.3: BPSK Spectrogram (Window Length is 8)

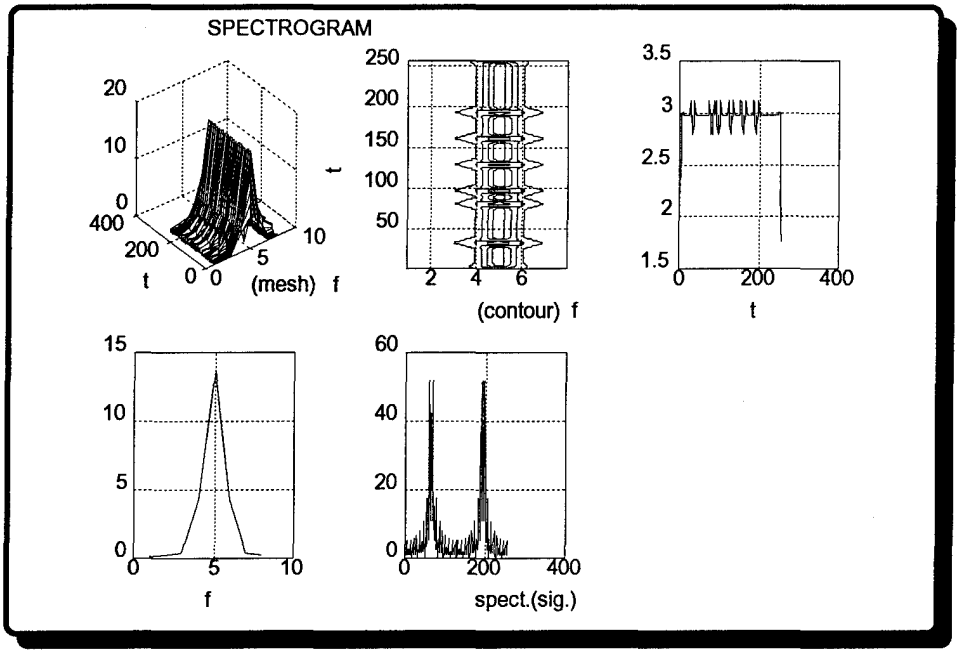

Figure 4.4: BPSK Spectrogram (Window Length is 16)

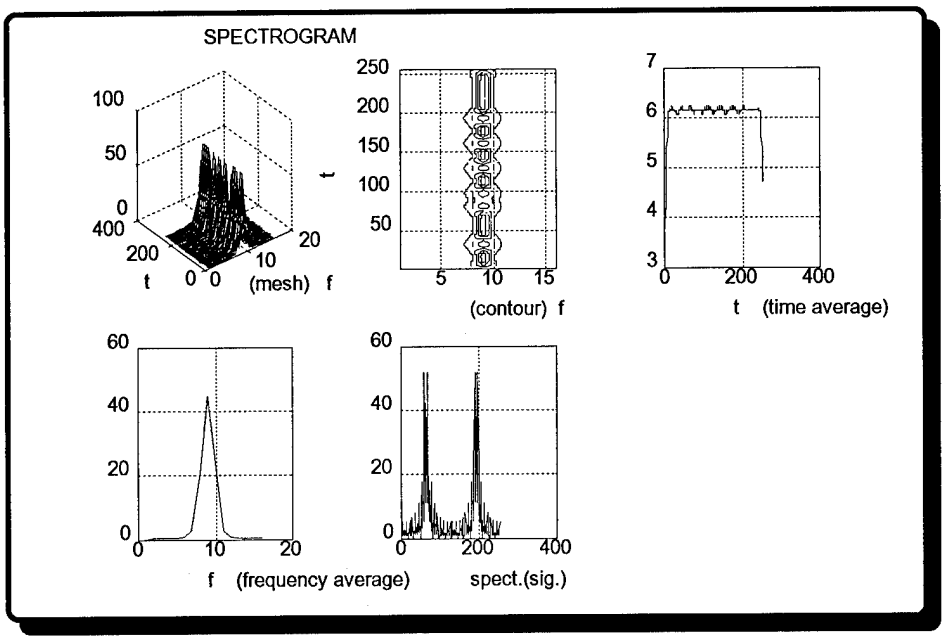

Figure 4.5: BPSK Spectrogram (Window Length is 32)

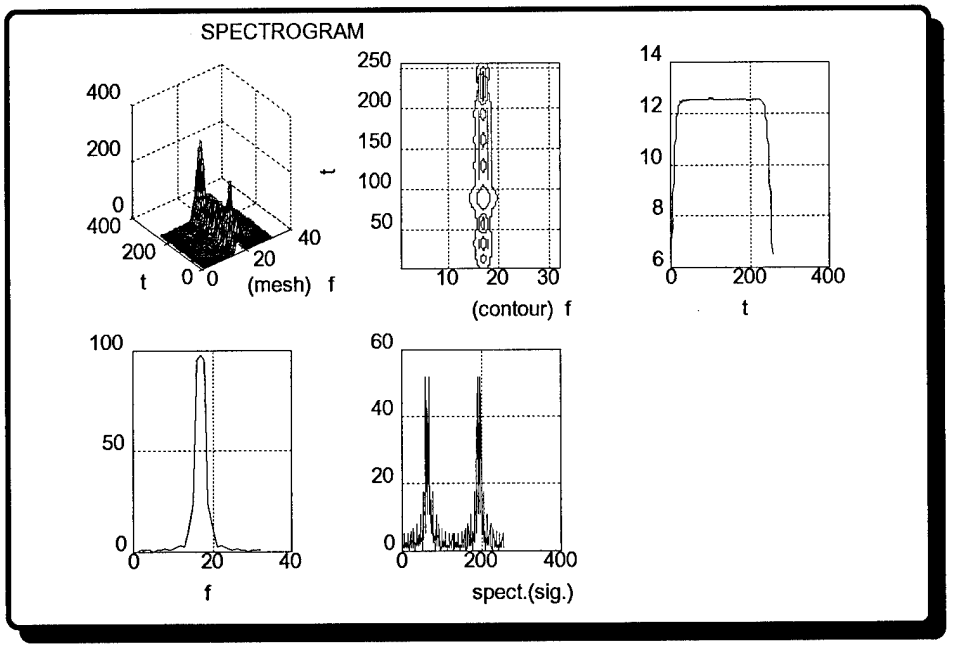

Figure 4.6: BPSK Spectrogram (Window Length is 64)

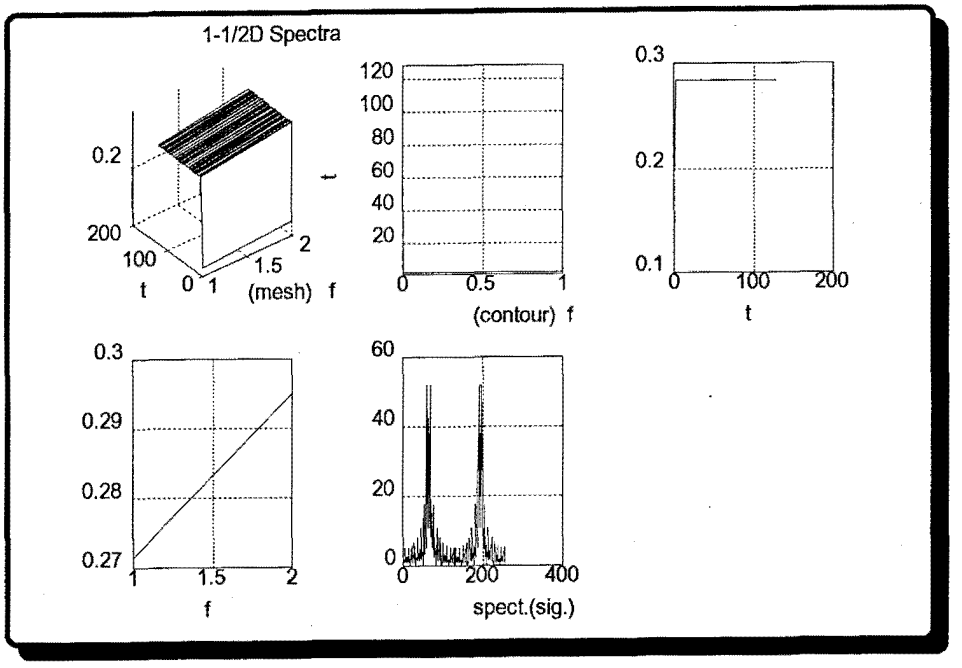

Figure 4.7: BPSK 1-1/2D Spectra (Window Length is 4)

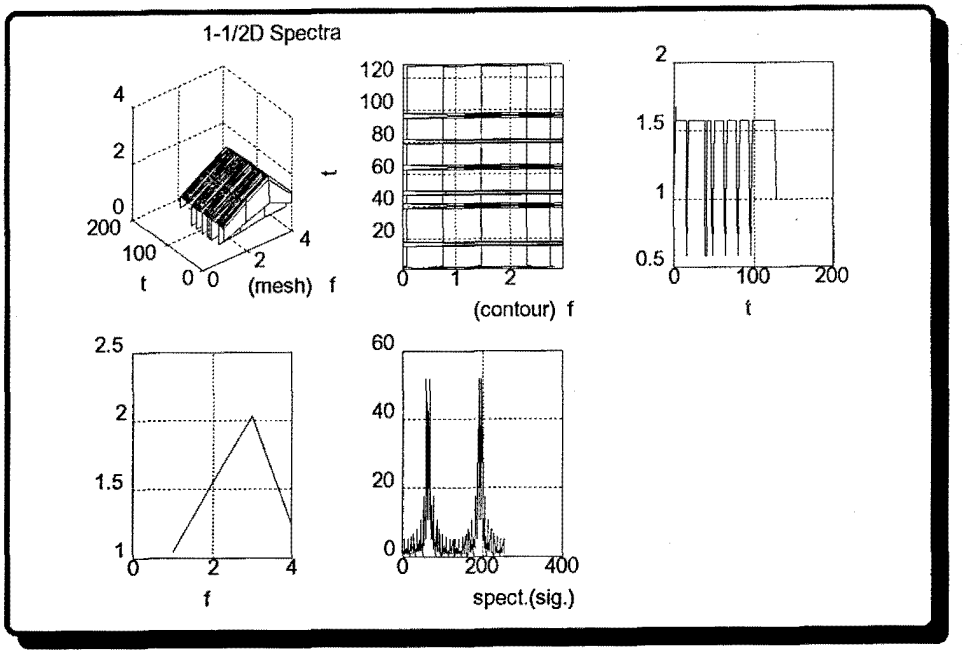

Figure 4.8: BPSK 1-1/2D Spectra (Window Length is 8)

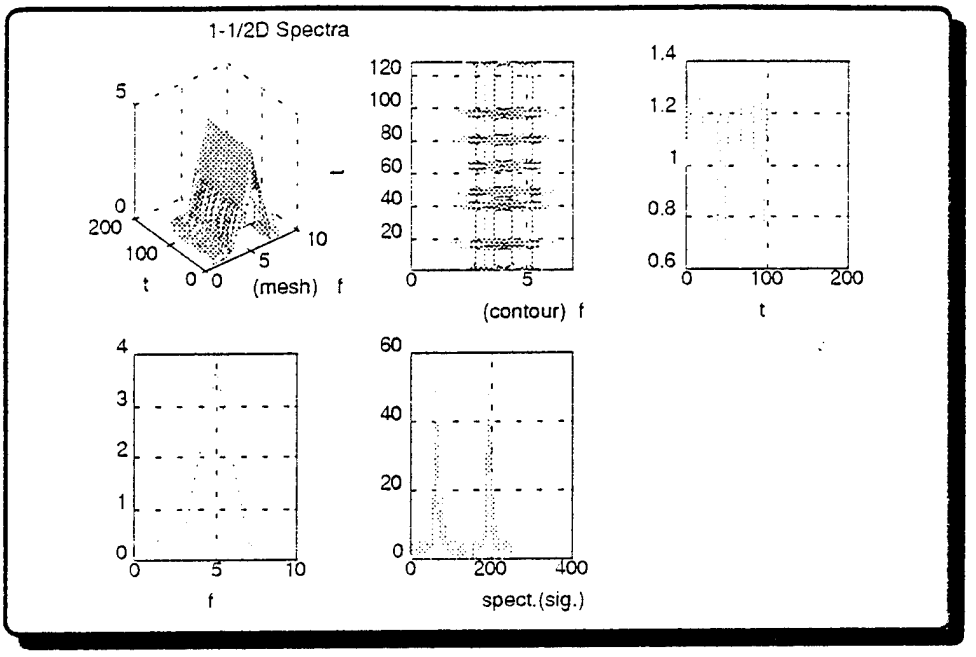

Figure 4.9: BPSK 1-1/2D Spectra (Window Length is 16)

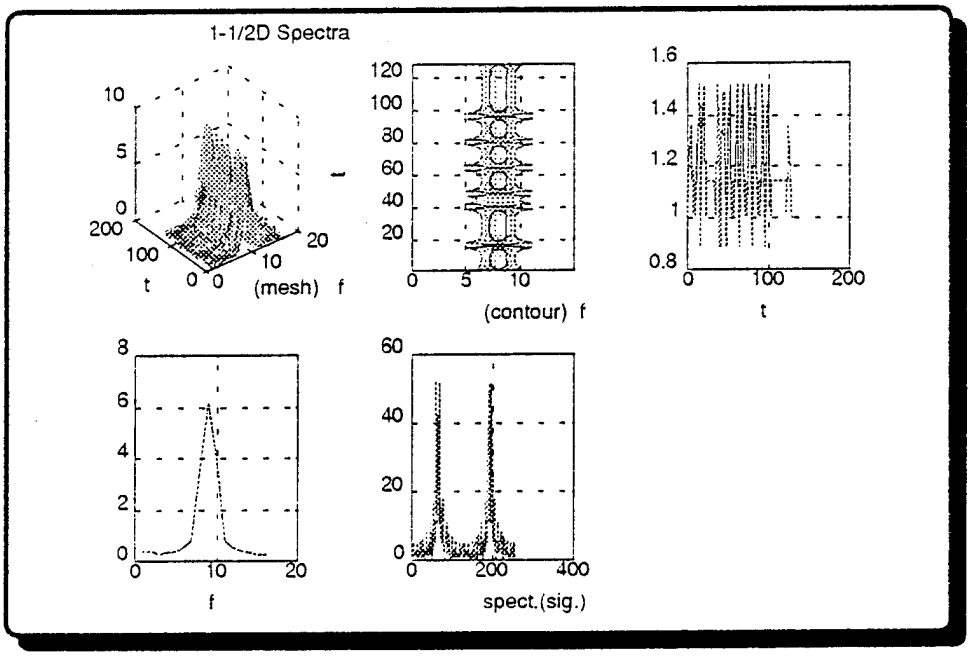

Figure 4.10: BPSK 1-1/2D Spectra (Window Length is 32)

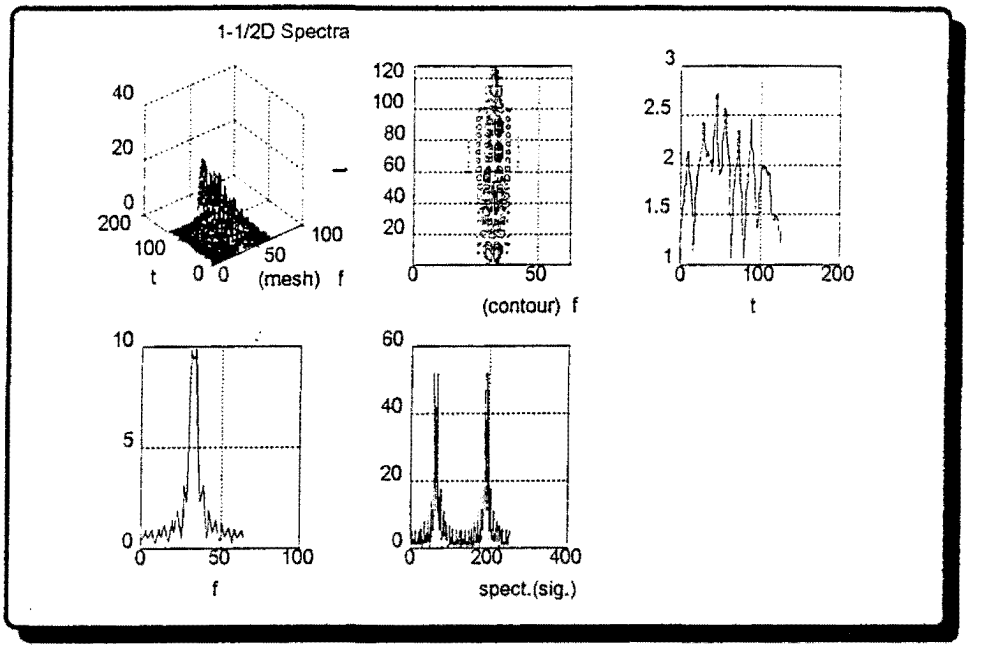

Figure 4.11: BPSK 1-1/2D Spectra (Window Length is 64)

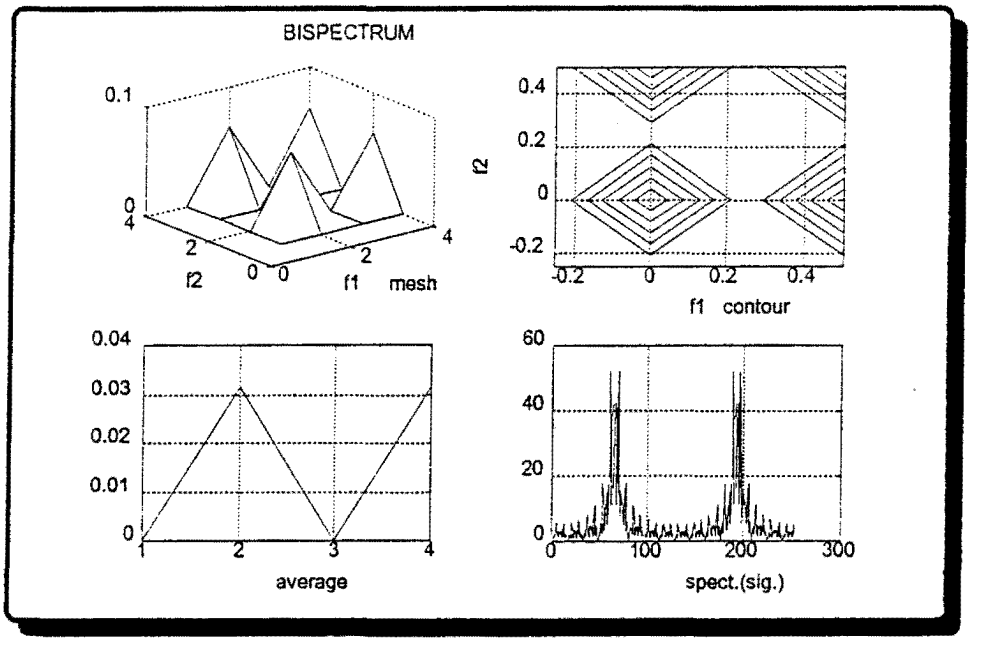

Figure 4.12: BPSK Bispectrum (Fast Fourier Transform Length is 4)

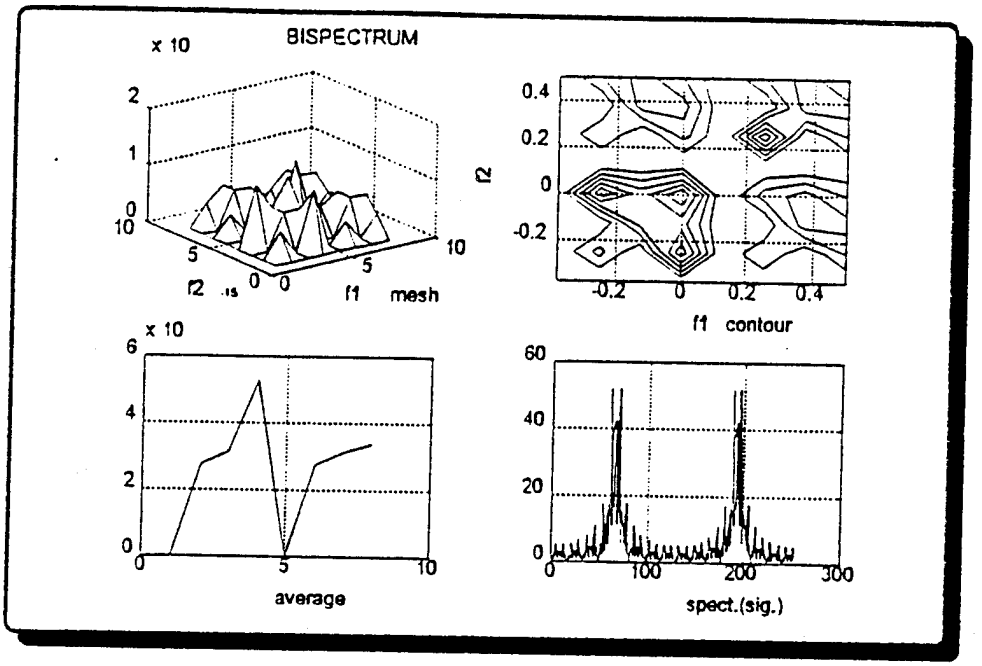

Figure 4.13: BPSK Bispectrum (Fast Fourier Transform Length is 8)

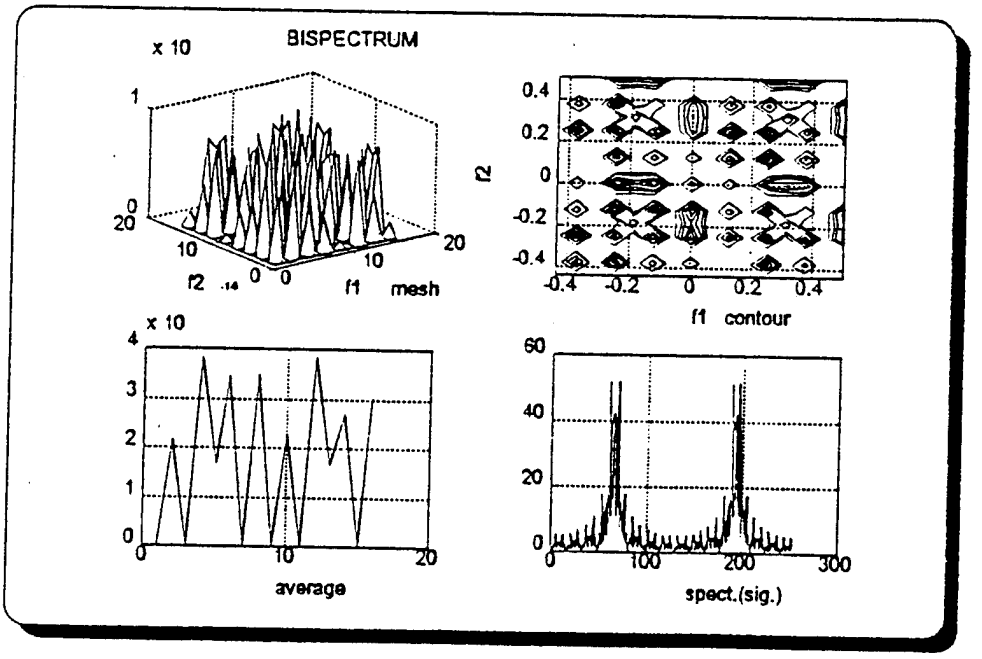

Figure 4.14: BPSK Bispectrum (Fast Fourier Transform Length is 16)

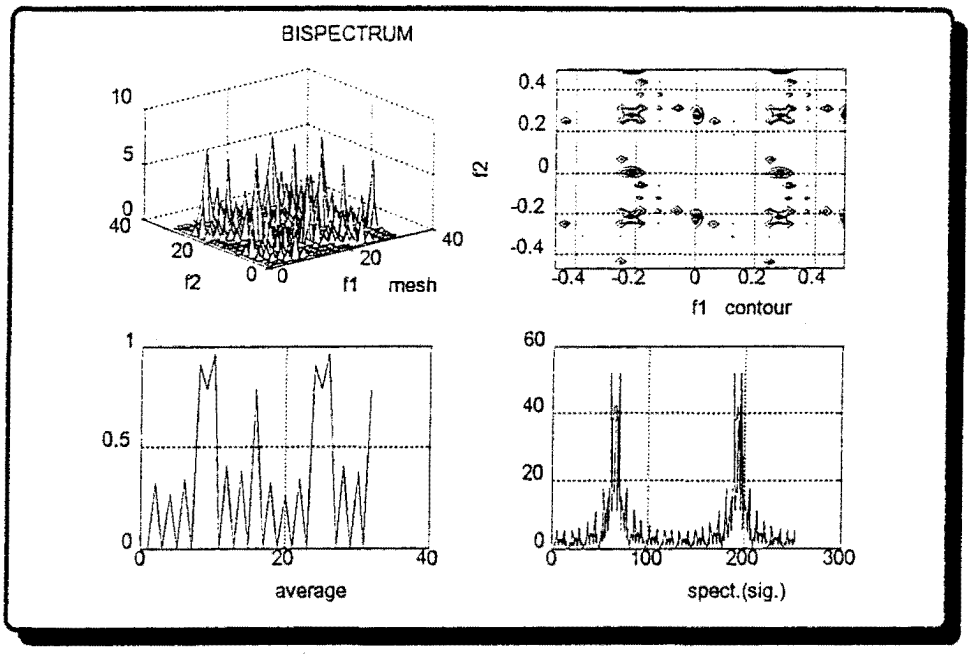

Figure 4.15: BPSK Bispectrum (Fast Fourier Transform Length is 32)

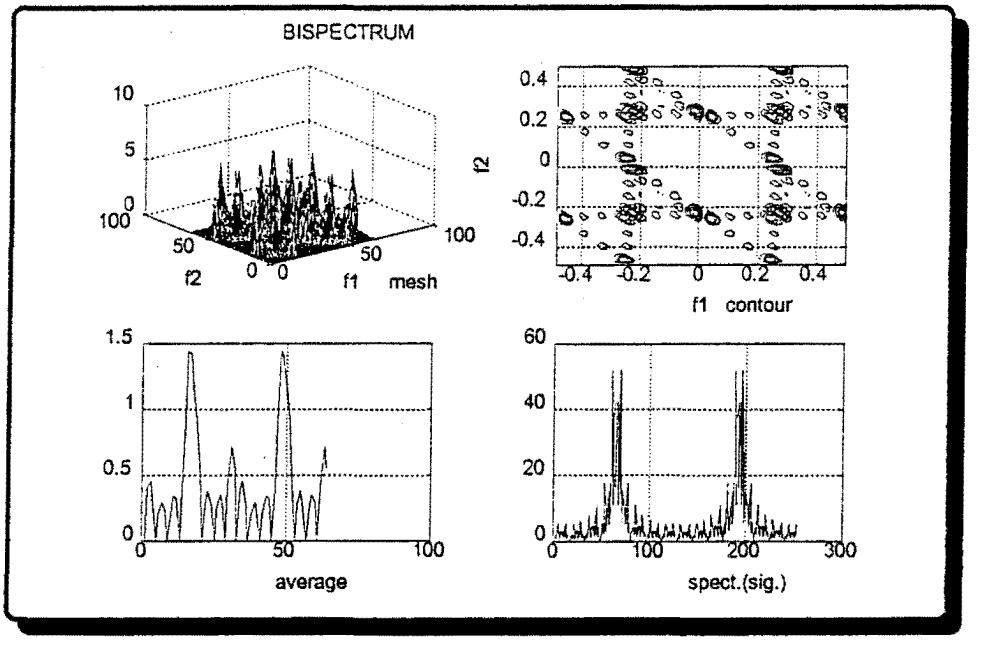

Figure 4.16: BPSK Bispectrum (Fast Fourier Transform Length is 64)

BPSK signals, we chose an FFT length of 16 (i.e., matched signal bit length) for the remainder of this study. The transform length of 16 provided good frequency information extraction from the frequency averaged plots while adhering to the symbol length (see Figure 4.14).

Figure 4.17 through Figure 4.26 are the outer product representation of BPSK for FFT sizes of 4, 8, 16, 32, and 64. The 4, 8, and 16 point spectra do not give clues nor present unique spectra about the modulation. Figures 4.23 through 4.26 for sizes 32, and especially 64 do give clues about the modulation scheme. The contour plots in Figures 4.25, and 4.26 for the BPSK signal for a FFT size of 64 presents a picture that looks similar to the pound (#) sign which was very useful for differentiating BPSK from other modulation types and the frequency sum plots for this size presents the identical spectra for BPSK signal. Therefore, we choose 64 point sample for the outer product representation of the BPSK signal.

2. FSK

The simulation message consisted of ones and zeros. In the FSK scheme, there was no frequency change for the symbol 0, while there was a frequency change (or increase) for the symbol 1.

For the FSK scheme, the modulated signal can be expressed as;

$$X(n) = \sin(2\pi(\frac{k+a}{N_1})n) \quad ,$$

where a = 0 for symbol 0

a = 1 for symbol 1

k = 4

$N_1 = 16$

n = 0,1,.....,255.

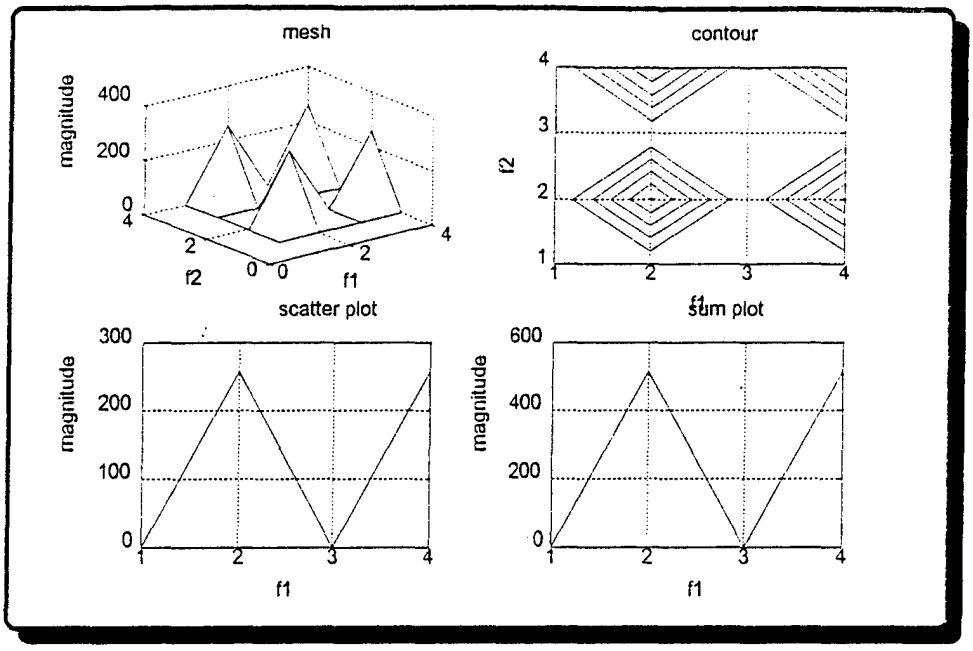

Figure 4.17: BPSK Outer Product Representation (Transform Length is 4, Coherent)

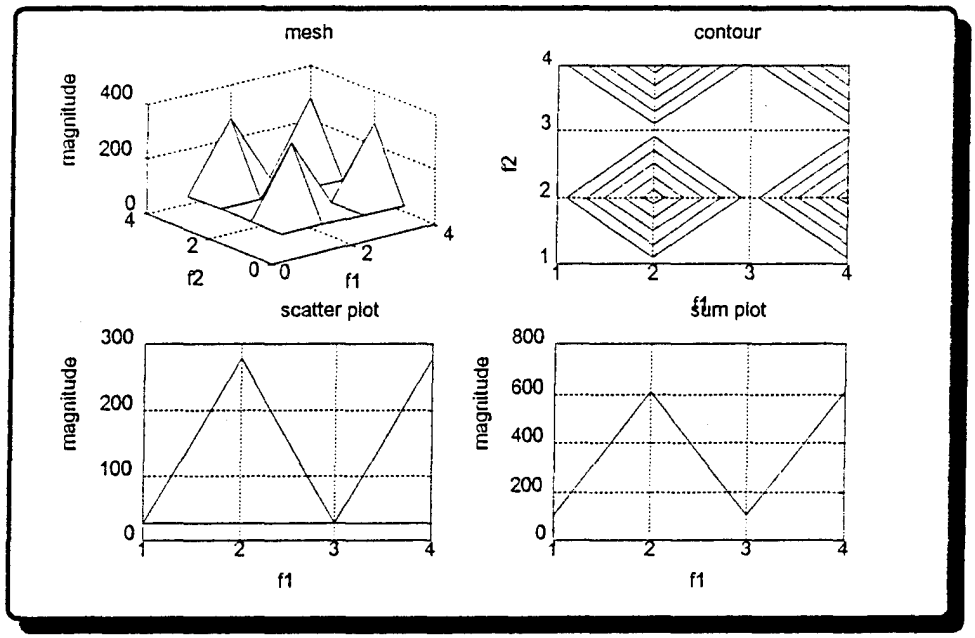

Figure 4.18: BPSK Outer Product Representation (Transform Length is 4, Incoherent)

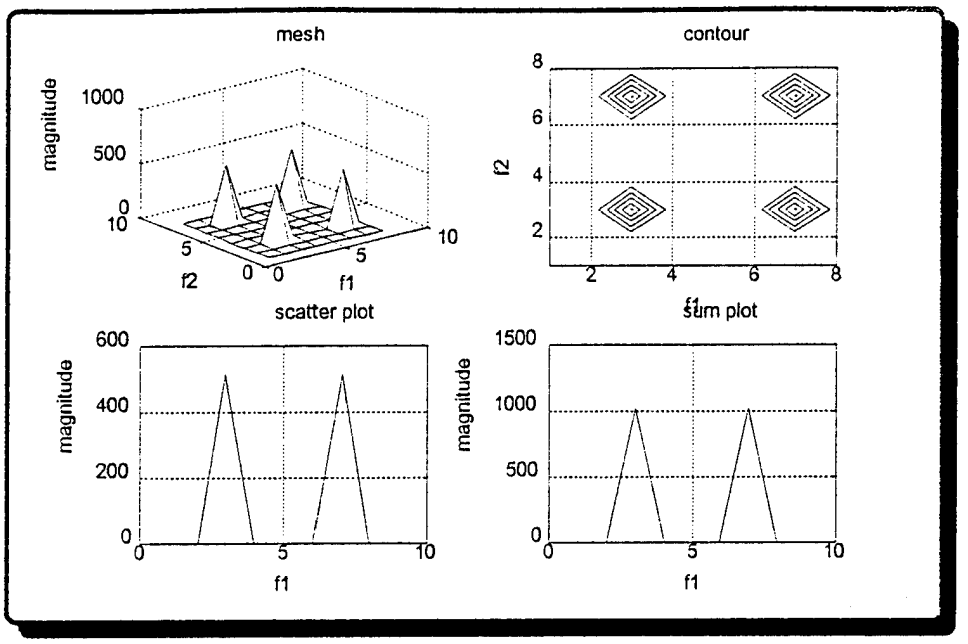

Figure 4.19: BPSK Outer Product Representation (Transform Length is 8, Coherent)

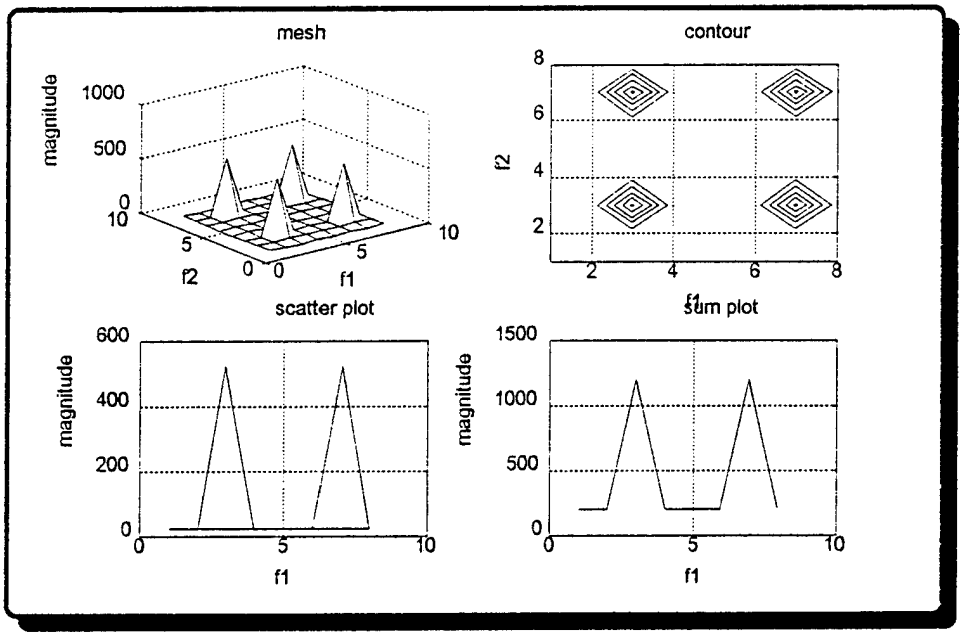

Figure 4.20: BPSK Outer Product Representation (Transform Length is 8, Incoherent)

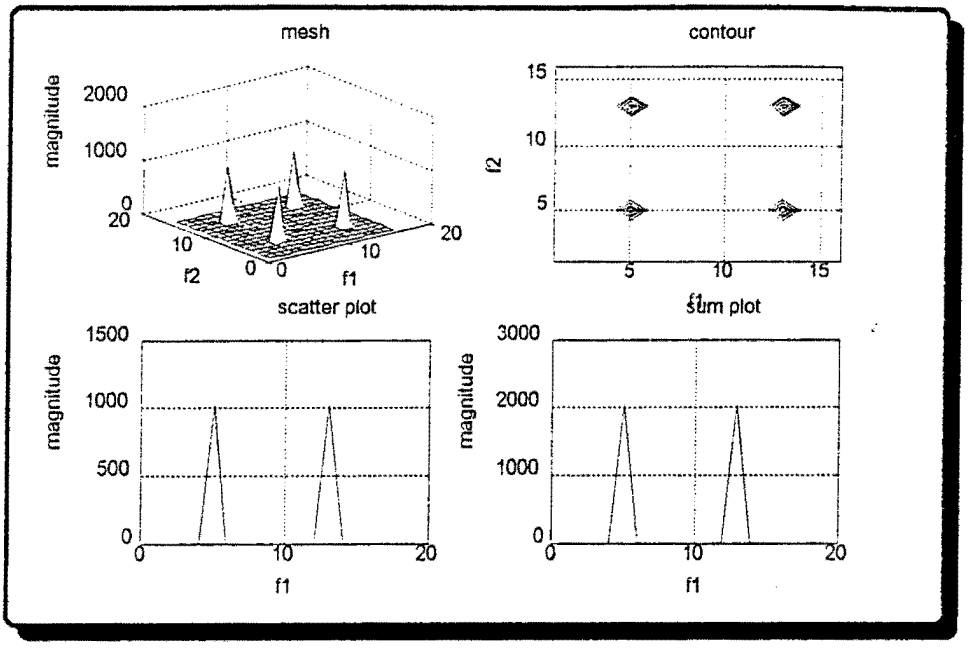

Figure 4.21: BPSK Outer Product Representation (Transform Length is 16, Coherent)

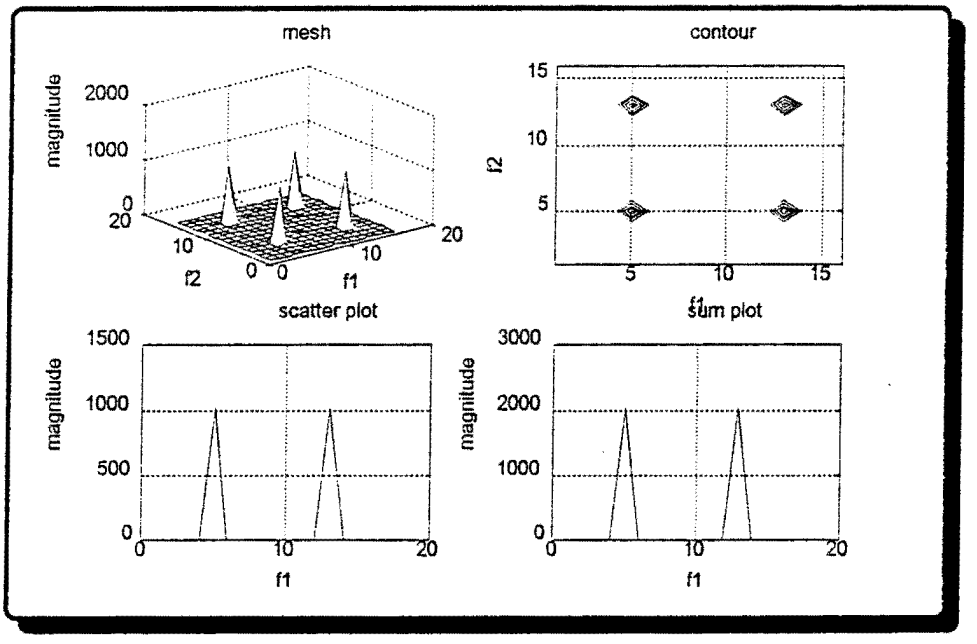

Figure 4.22: BPSK Outer Product Representation (Transform Length is 16, Incoherent)

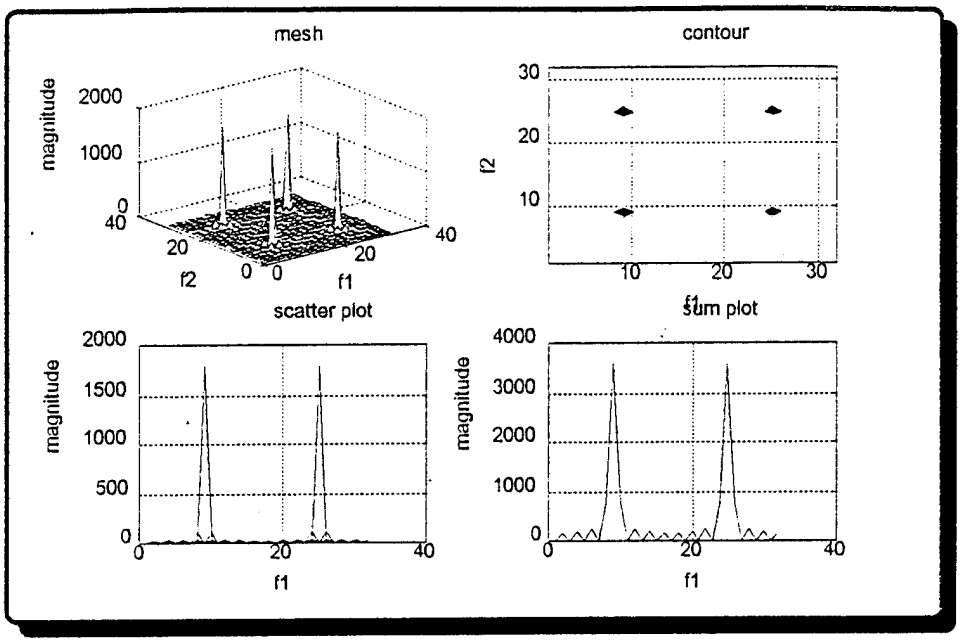

Figure 4.23: BPSK Outer Product Representation (Transform Length is 32, Coherent)

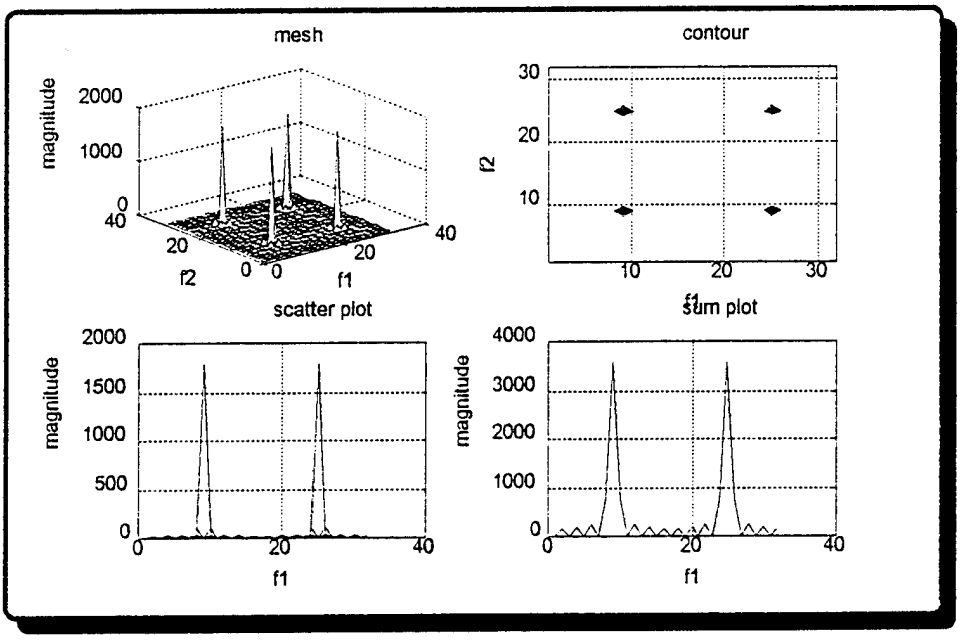

Figure 4.24: BPSK Outer Product Representation (Transform Length is 32, Incoherent)

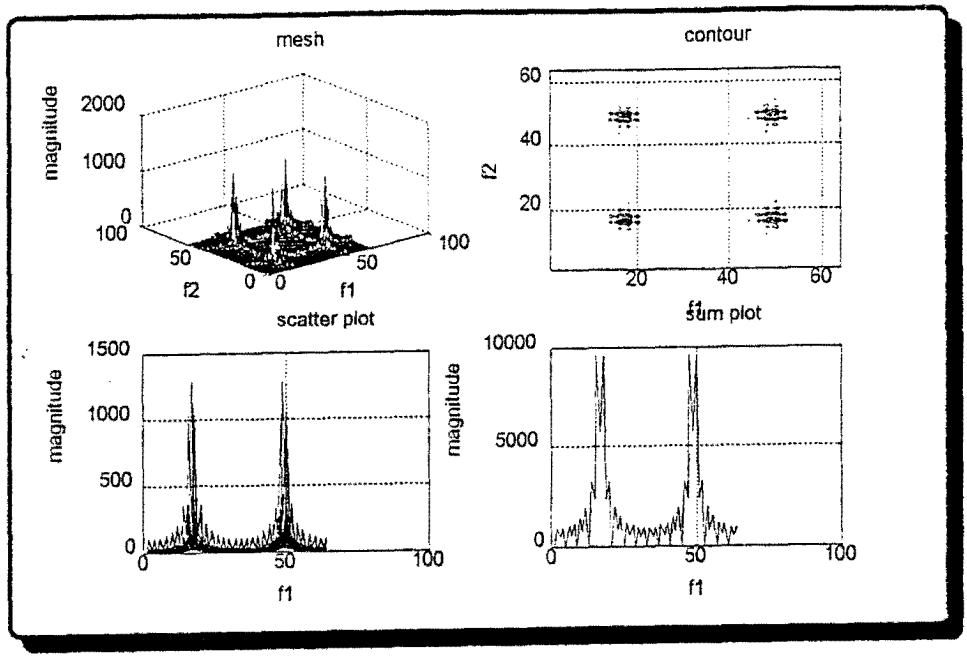

Figure 4.25: BPSK Outer Product Representation (Transform Length is 64, Coherent)

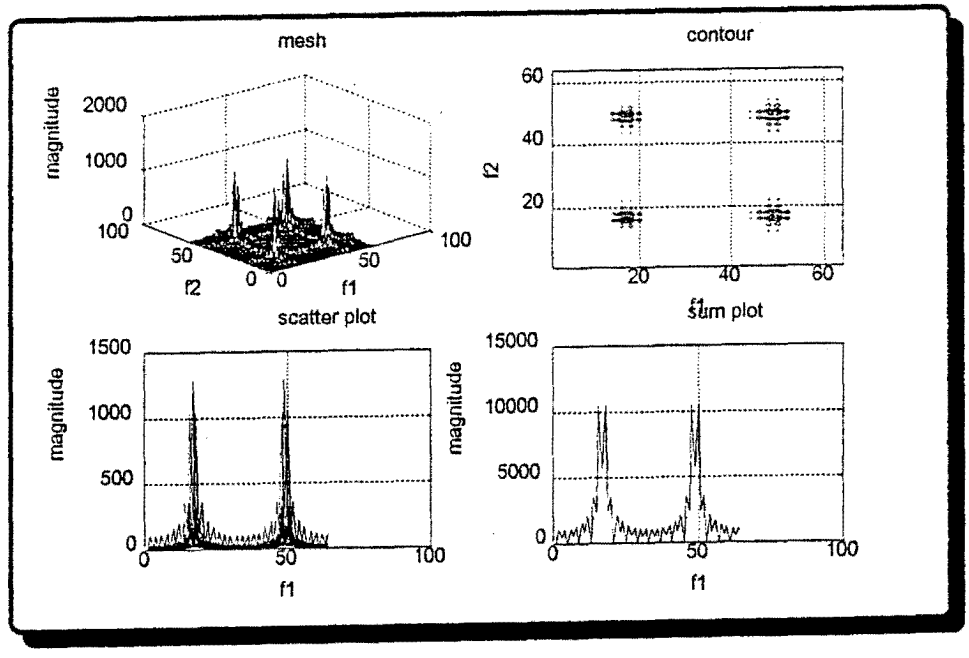

Figure 4.26: BPSK Outer Product Representation (Transform Length is 64, Incoherent)

This means that there was an increase of 1 cycle per message bit (i.e., 5 cycles per symbol) for symbol 1 and no frequency change (i.e., 4 cycles per symbol) for symbol 0. Since every symbol had 16 data points, we expect frequency shifts of plus 1 cycle at the segments of the modulated signal between 33 and 81, 97 and 129, and 161 and 193.

Figure 4.27 shows the plot of the sinusoidal carrier, the message, and the FSK modulated signal. Figure 4.28 through Figure 4.32 show spectrograms for FFT sizes 4, 8, 16, 32, and 64. A Hamming window was used. Frequency shifts at the proper locations were determined for FFT sizes N_1 /2 (which is 8), N_1 (which is 16) and 2 x N_1 (which is 32). For the other window lengths, it was difficult to determine message signals. From Figure 4.30 the contour plot for a FFT size 16 shows well separated frequencies and the time averaged plot provided centered spectra. Therefore we choose 16 as the optimum transform length for FSK signal spectrogram analysis.

Figure 4.33 through Figure 4.37 show the 1-1/2 D spectrum for FFT sizes 4, 8, 16, 32, and 64. The window was a Hamming window and the step size was 2. On the figures, transition points (at the right times) can be seen on the mesh, contour and frequency averaged plots, for lengths of 8,16 and 32. But in Figure 4.36 (for length of 32), the frequency averaged plot of 1-1/2 D spectra had more spikes than Figure 4.34 (for length of 8), the contour plot was not as clear as for the length 16. We choose 16 as the optimum transform length for 1-1/2 D spectral analysis of the FSK signal (see Figure 4.32).

Figure 4.38 through Figure 4.42 show the bispectrum for FFT sizes 4, 8, 16, 32, and 64. The window type was '1', the overlap was 50 percent, and the number of samples per segment (nsamp) was 16. For the bispectral analysis on FSK signals, an FFT length of 16 (in Figure 4.40) was chosen for the remainder of this study to adhere to the symbol length and to conform with the choice of the other spectral methods.

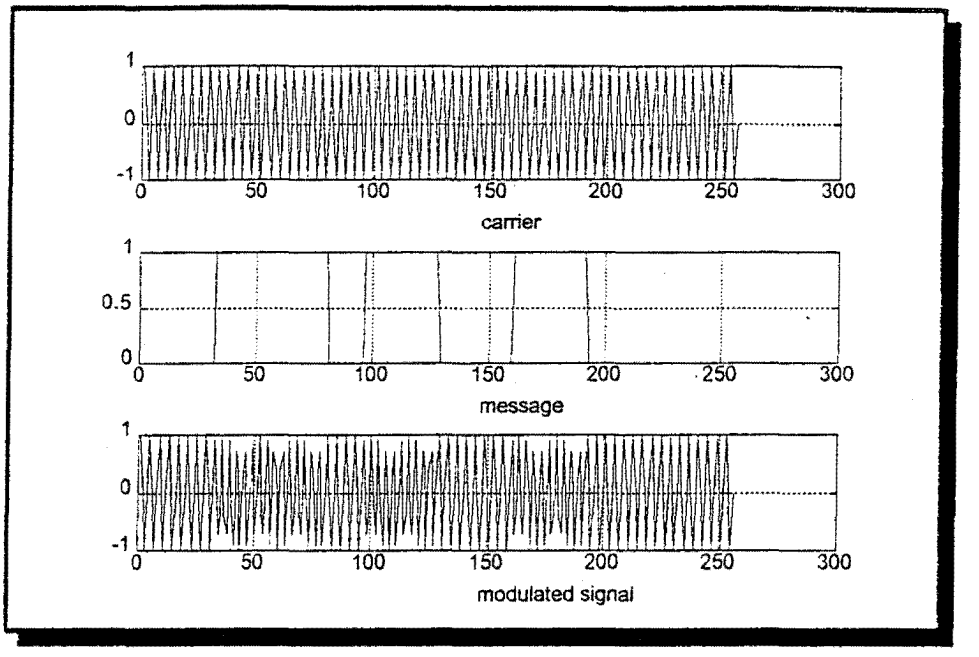

Figure 4.27: FSK Generation

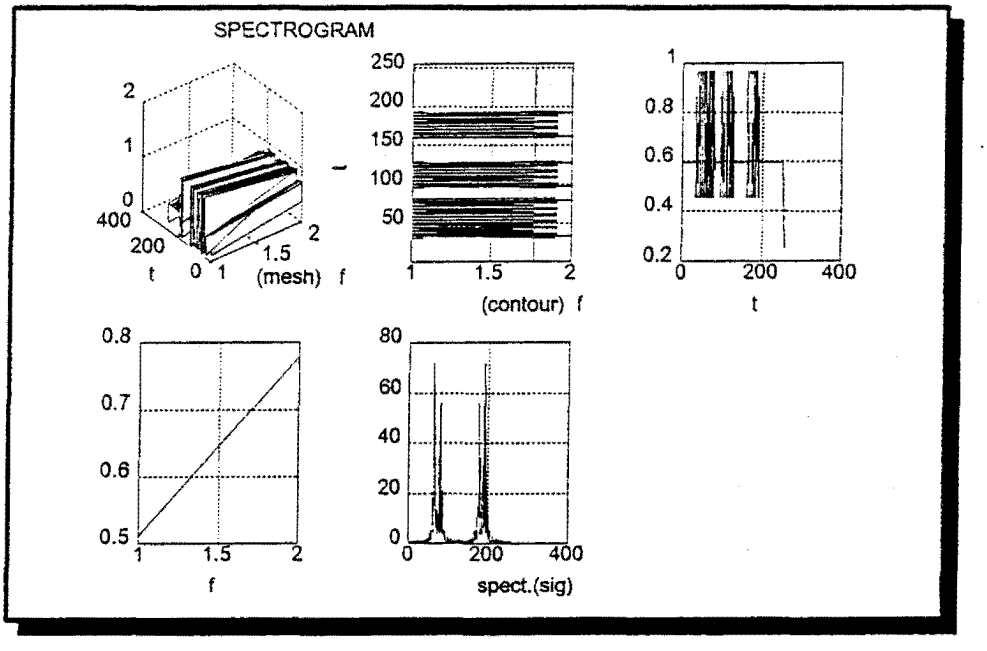

Figure 4.28: FSK Spectrogram (Window Length is 4)

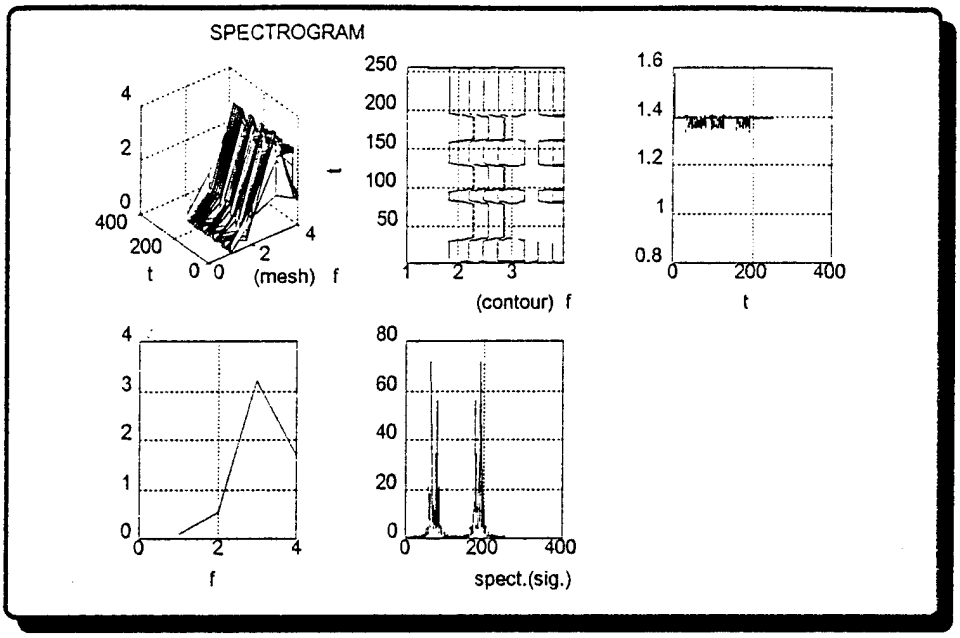

Figure 4.29: FSK Spectrogram (Window Length is 8)

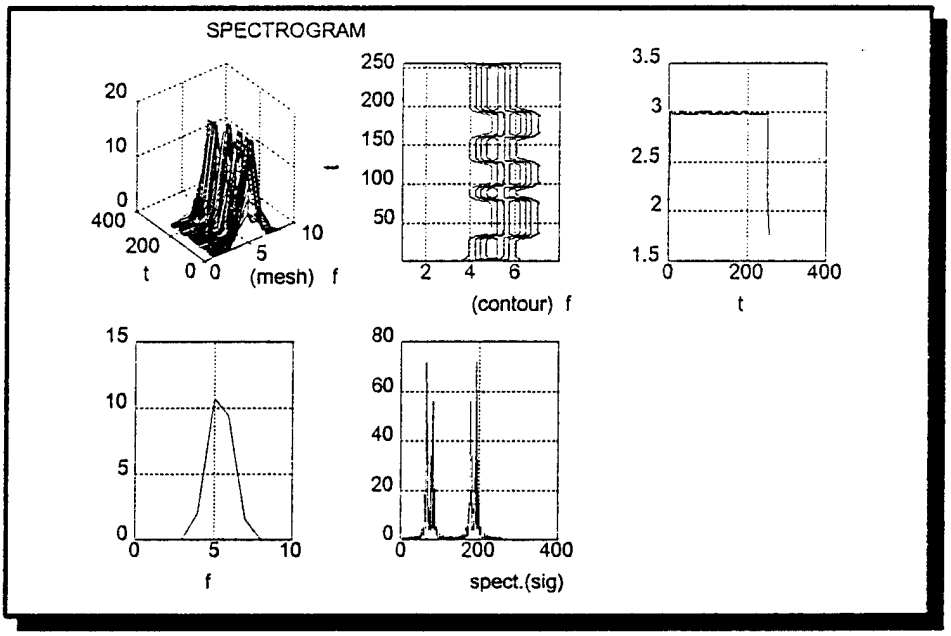

Figure 4.30: FSK Spectrogram (Window Length is 16)

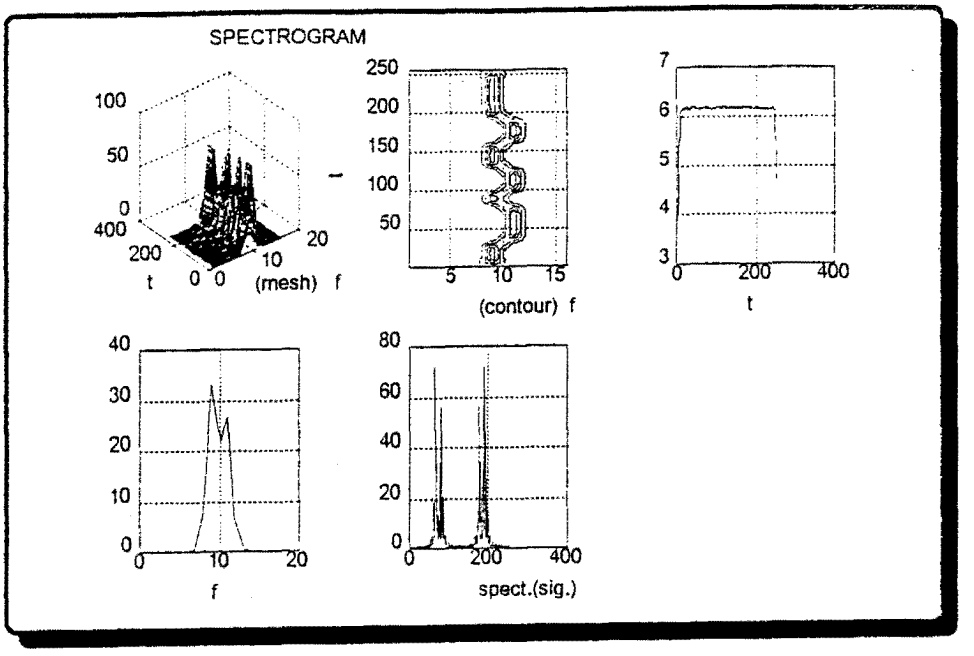

Figure 4.31: FSK Spectrogram (Window Length is 32)

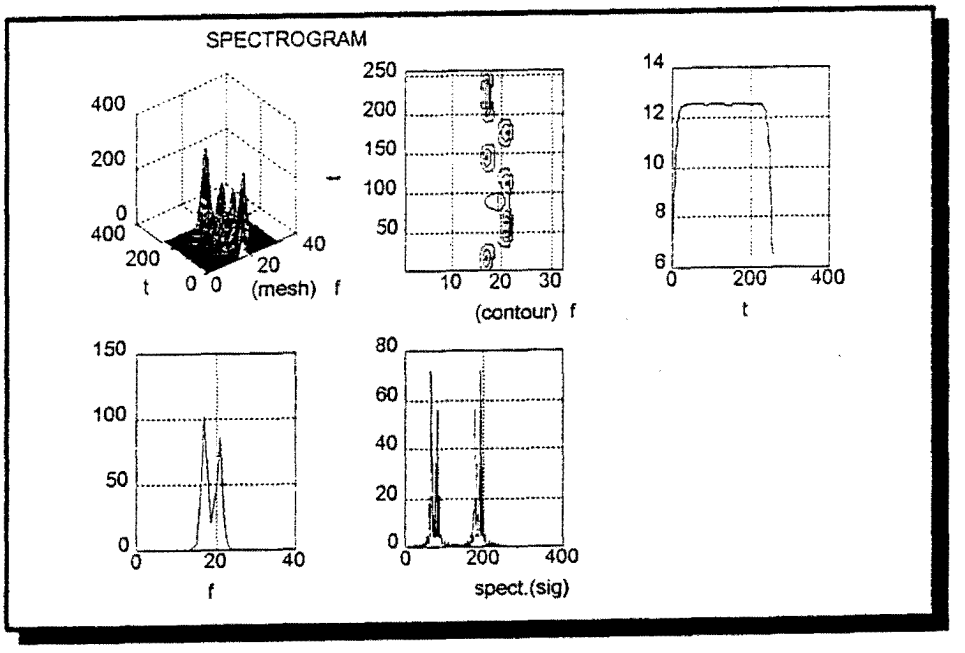

Figure 4.32: FSK Spectrogram (Window Length is 64)

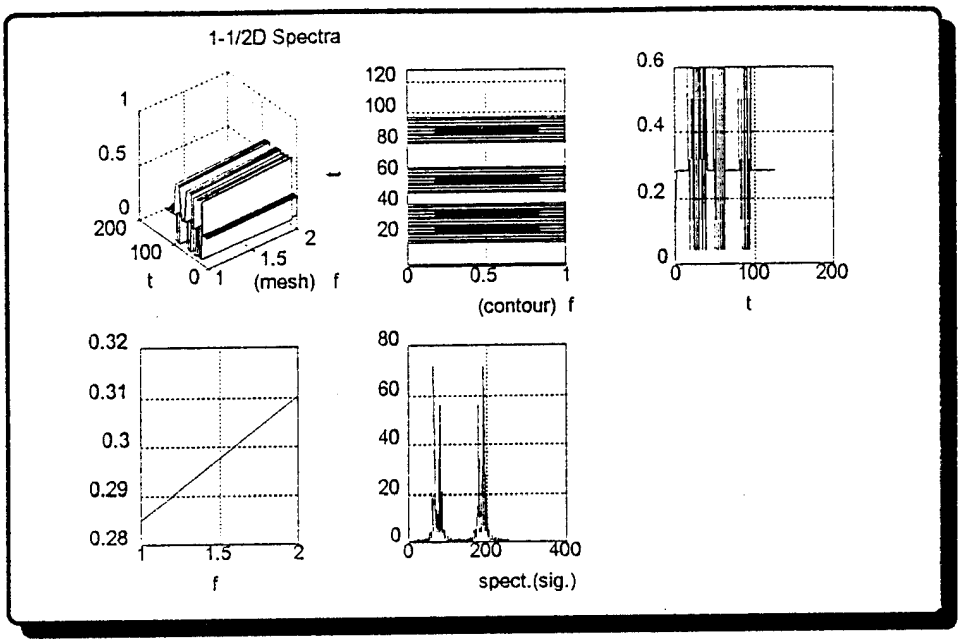

Figure 4.33: FSK 1-1/2D Spectra (Window Length is 4)

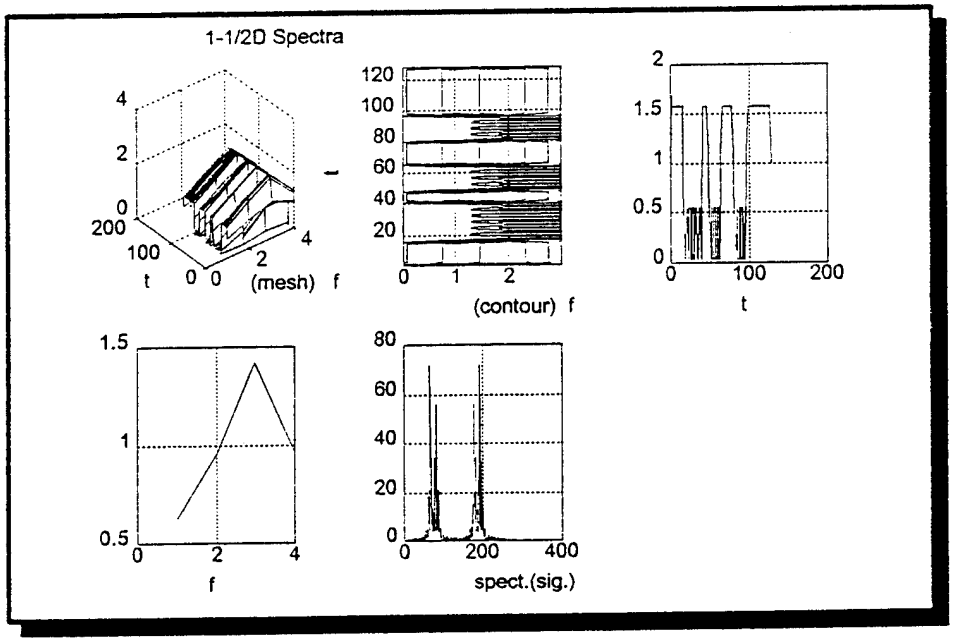

Figure 4.34: FSK 1-1/2D Spectra (Window Length is 8)

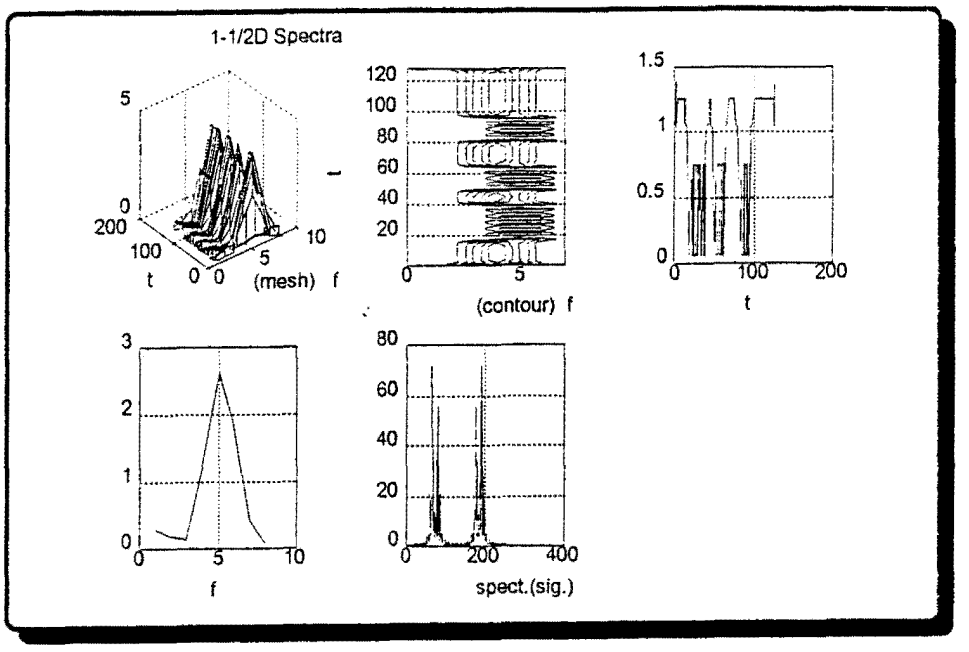

Figure 4.35: FSK 1-1/2D Spectra (Window Length is 16)

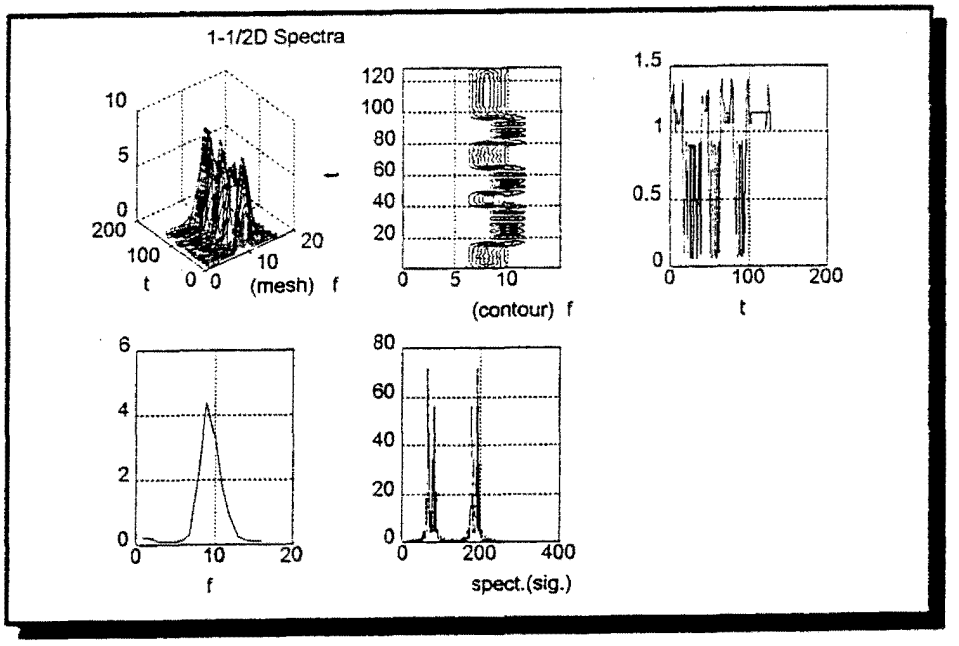

Figure 4.36: FSK 1-1/2D Spectra (Window Length is 32)

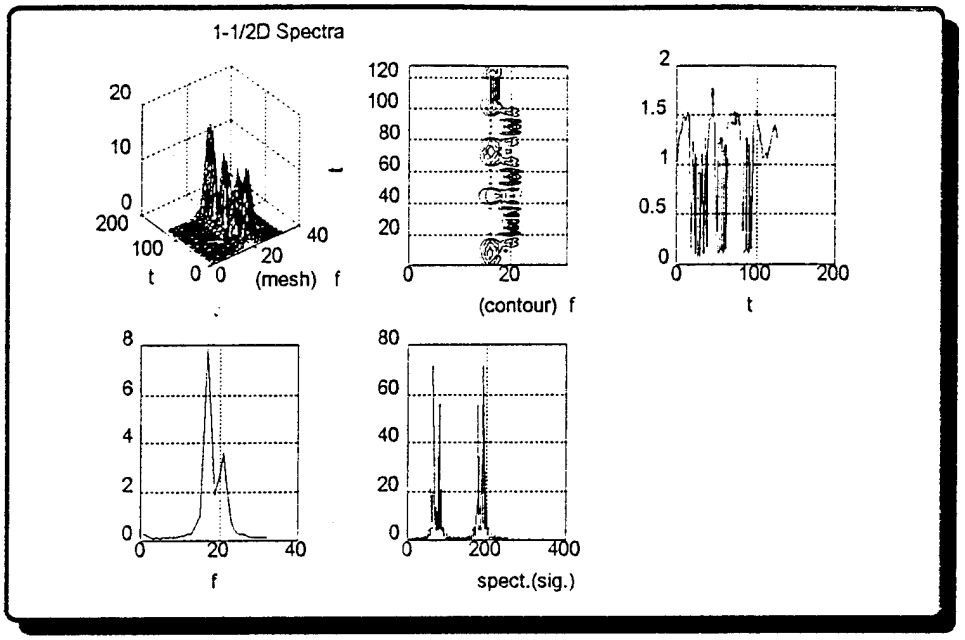

Figure 4.37: FSK 1-1/2D Spectra (Window Length is 64)

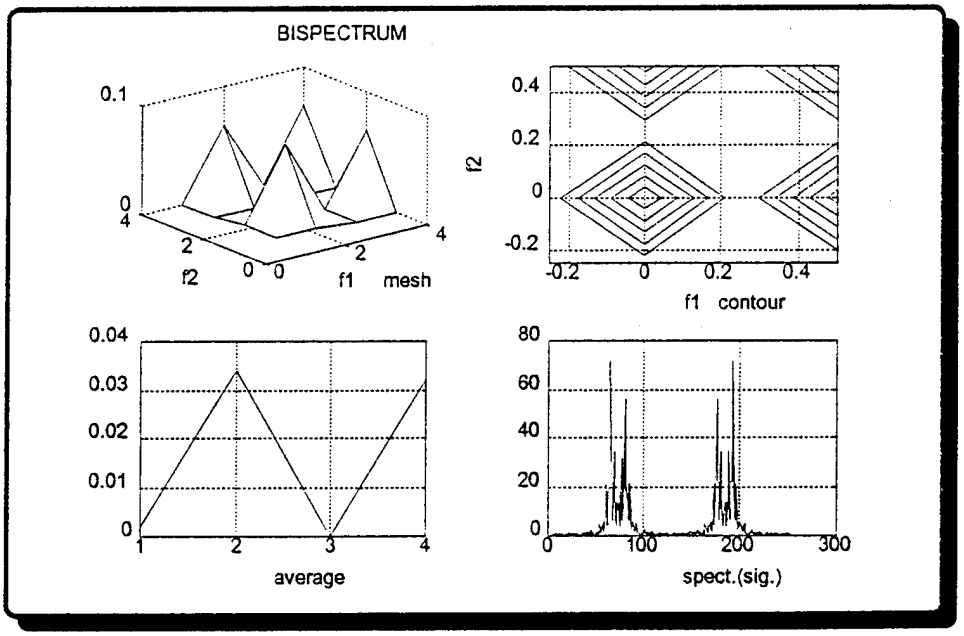

Figure 4.38: FSK Bispectrum (Fast Fourier Transform Length is 4)

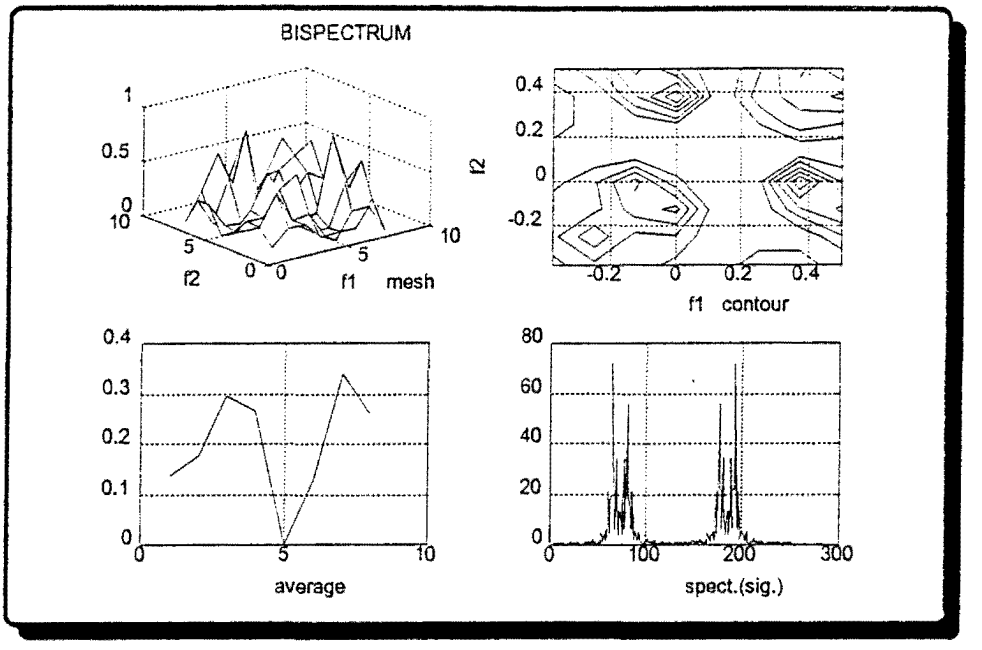

Figure 4.39: FSK Bispectrum (Fast Fourier Transform Length is 8)

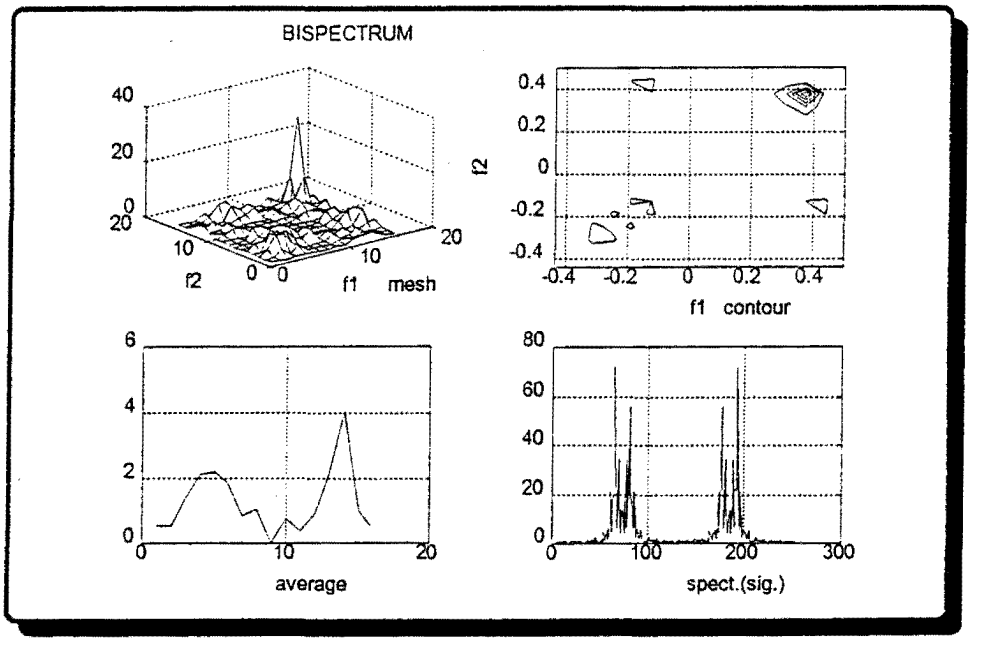

Figure 4.40: FSK Bispectrum (Fast Fourier Transform Length is 16)

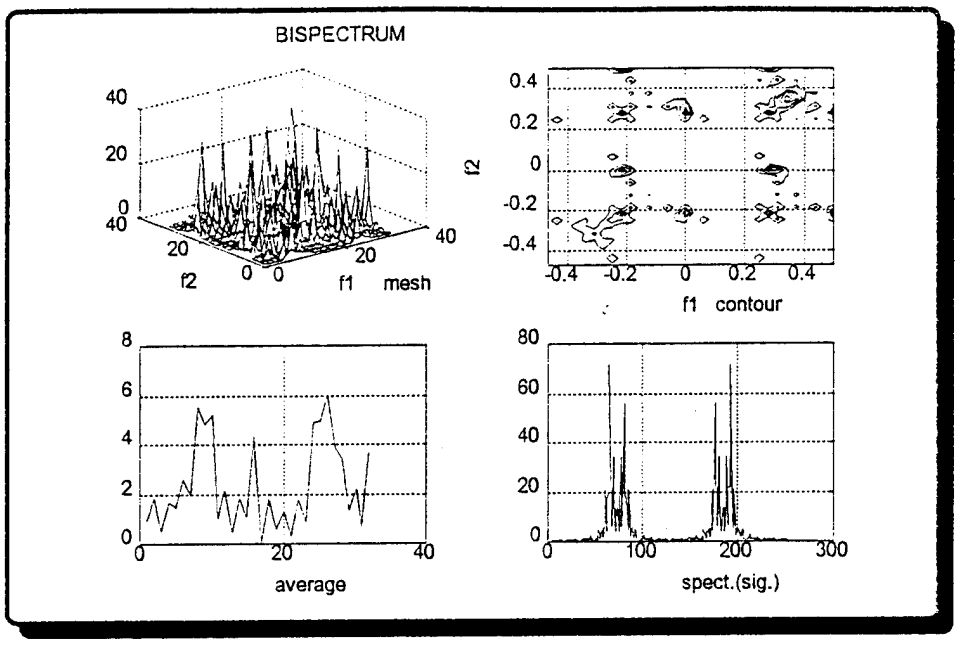

Figure 4.41: FSK Bispectrum (Fast Fourier Transform Length is 32)

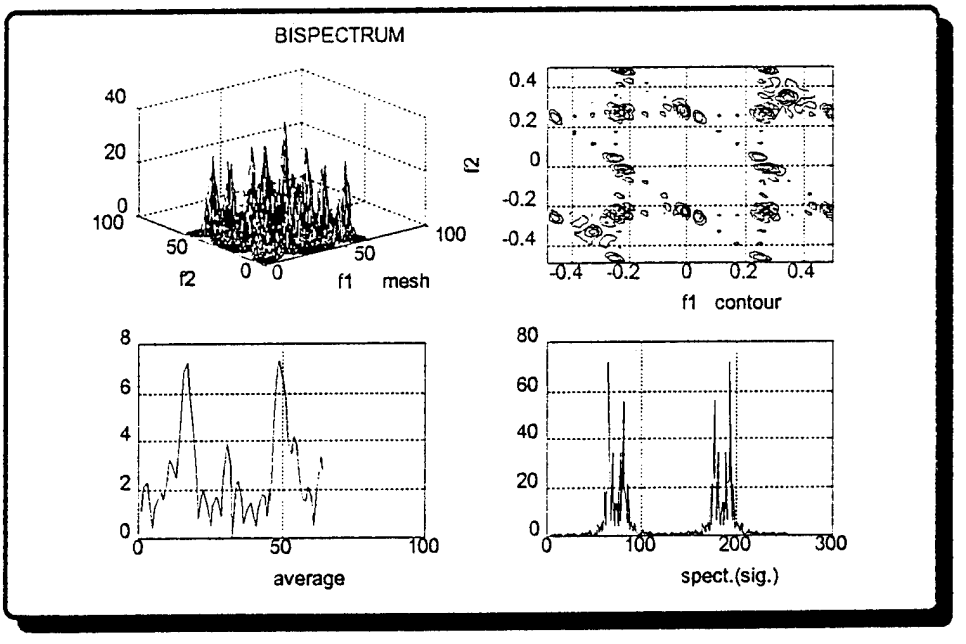

Figure 4.42: FSK Bispectrum (Fast Fourier Transform Length is 64)

Figure 4.43 through Figure 4.52 show the outer product representation of the FSK signal for FFT sizes of 4, 8, 16, 32, and 64. Figures for sizes of 4, 8, and 16 do not give clues about the modulation scheme nor present sufficiently different unique spectra for differentiating FSK from other modulation schemes. Figures 4.49 through 4.52 for sizes 32, and especially 64 give clues about the modulation scheme and present unique spectra for the FSK signal. In the contour plots and in the mesh plots of Figures 4.51 and 4.52 for FFT size of 64, the spectra showed the frequency shifts and the two different frequencies. Therefore, we choose the size of 64 for the outer product representation of the FSK signal (see Figures 4.51 and 4.52).

3. OOK

In the OOK scheme, there was no signal for the symbol 0 while there was a sinusoidal carrier for the symbol 1. In this study, OOK modulated signal was formulated as;

$$x(n) = \sin(2\pi(\frac{k}{N_1})n)$$

where k = 0 for symbol 0

k = 4 for symbol 1

$N_1 = 16$

n = 0,1,...,255.

We expected to see the sinusoidal carrier at the segments of the signal between location 33 and 81, 97 and 129, and 161 and 193. Conversely, at the other segments, we expected to see no carrier signal.

Figure 4.53 shows the plot of the sinusoidal carrier, message, and the OOK signal. Figure 4.54 through Figure 4.58 show spectrograms for FFT sizes 4, 8, 16, 32, and 64. A Hamming window was used. It can be seen that the changes

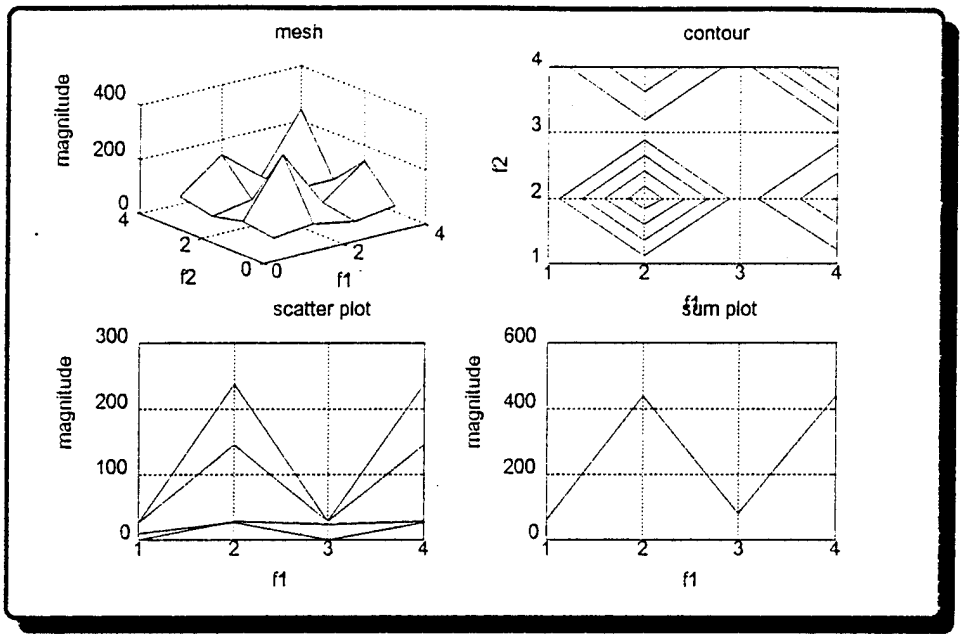

Figure 4.43: FSK Outer Product Representation (Transform Length is 4, Coherent)

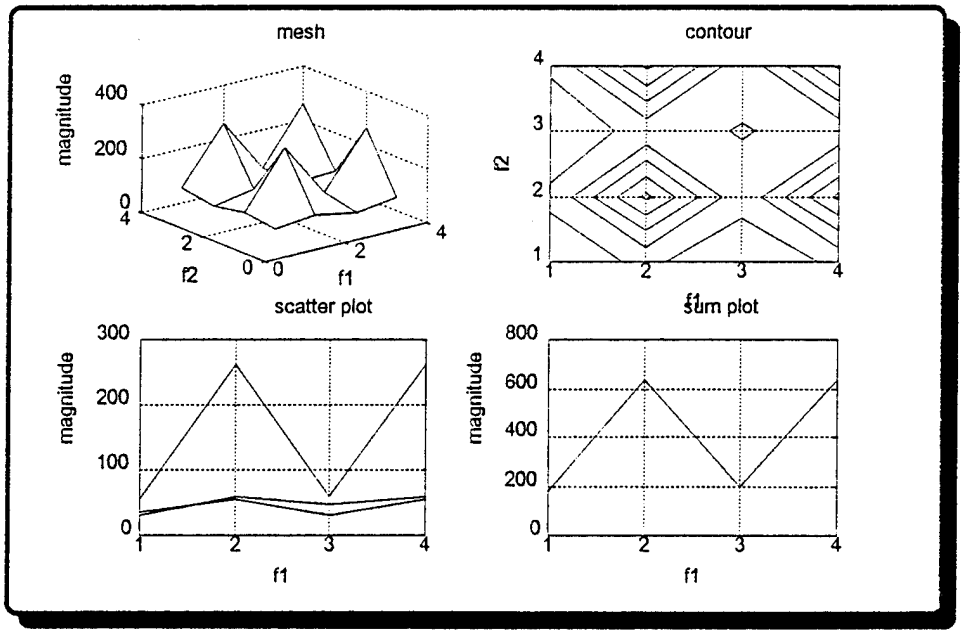

Figure 4.44: FSK Outer Product Representation (Transform Length is 4, Incoherent)

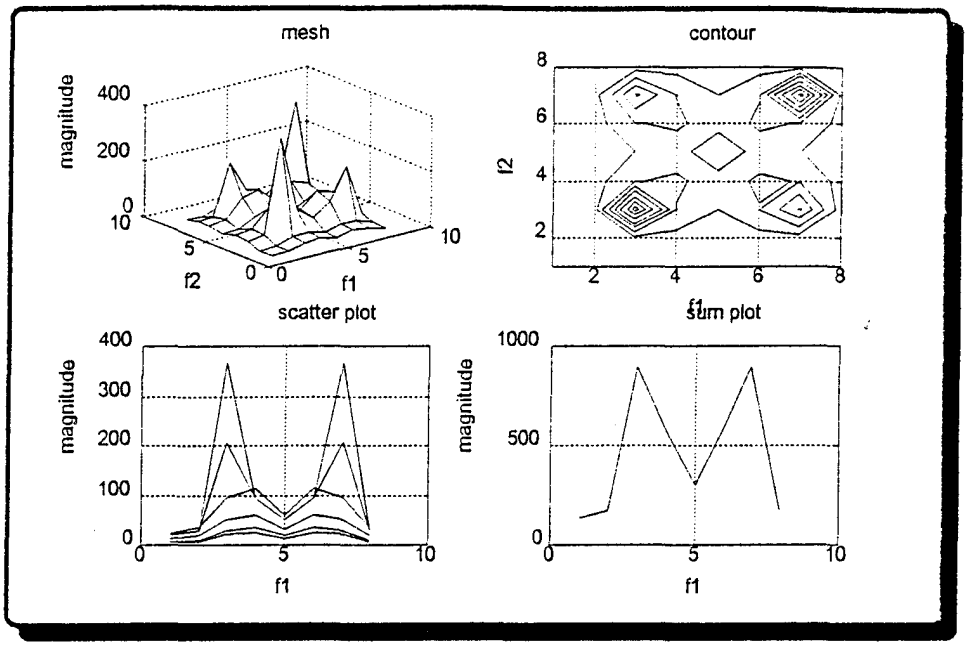

Figure 4.45: FSK Outer Product Representation (Transform Length is 8, Coherent)

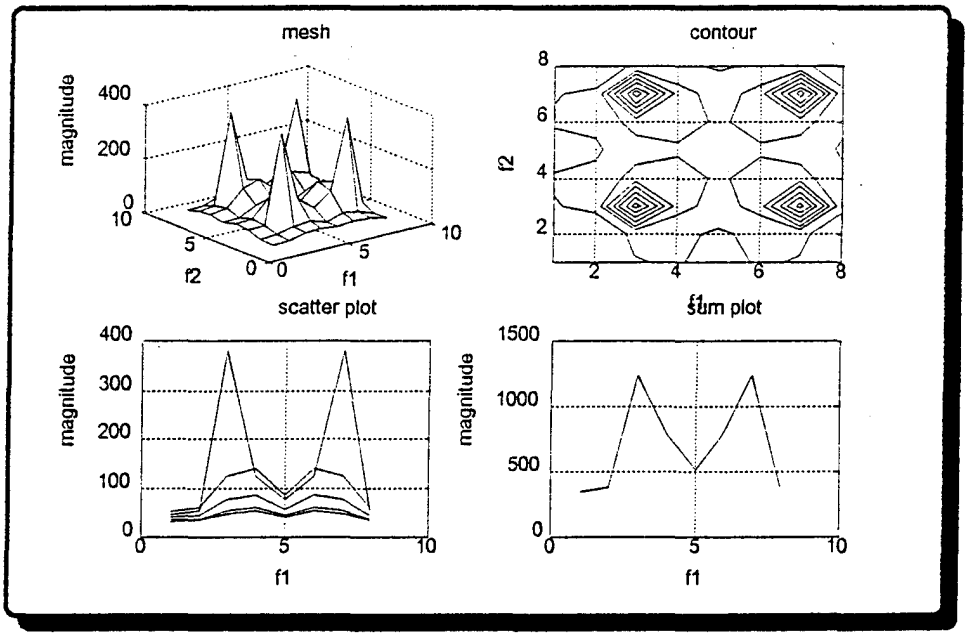

Figure 4.46: FSK Outer Product Representation (Transform Length is 8, Incoherent)

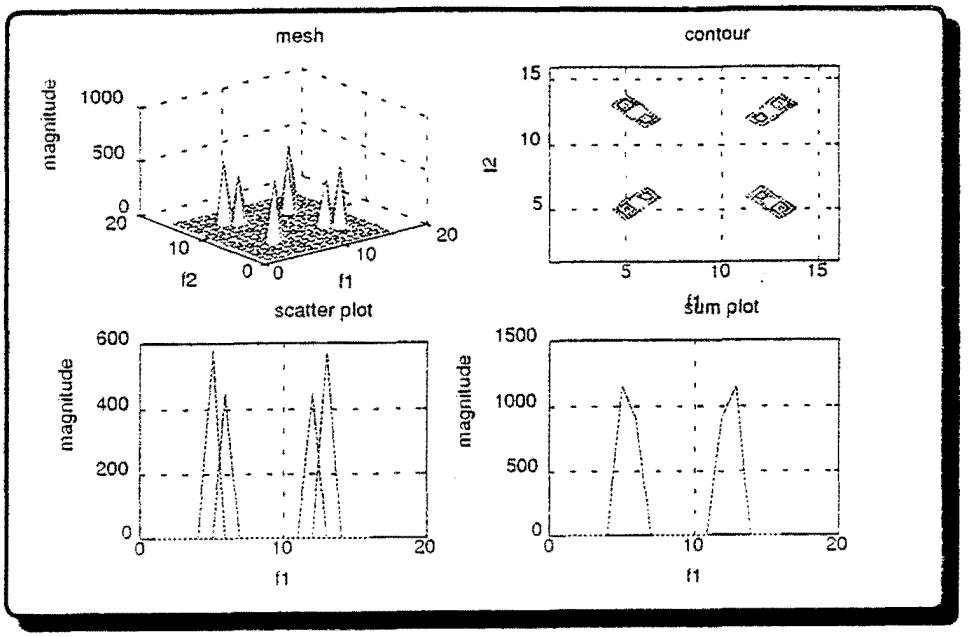

Figure 4.47: FSK Outer Product Representation
(Transform Length is 16, Coherent)

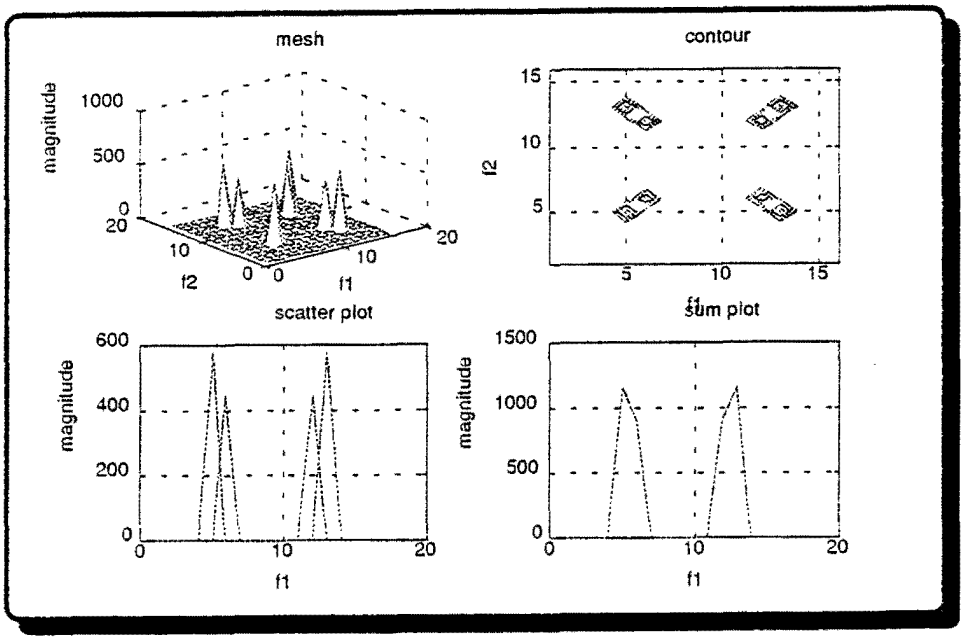

Figure 4.48: FSK Outer Product Representation
(Transform Length is 16, Incoherent)

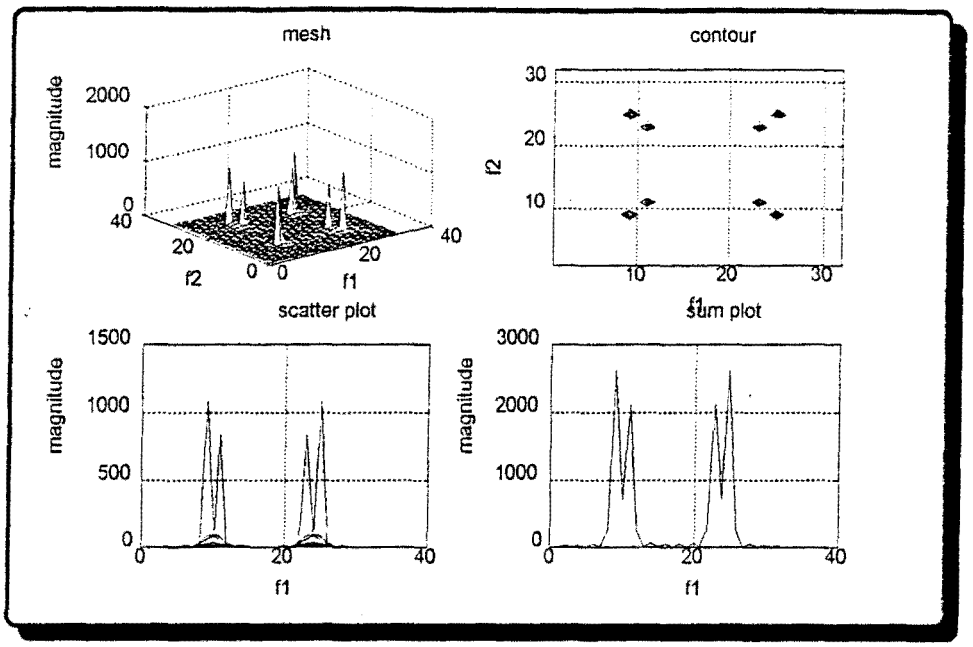

Figure 4.49: FSK Outer Product Representation (Transform Length is 32, Coherent)

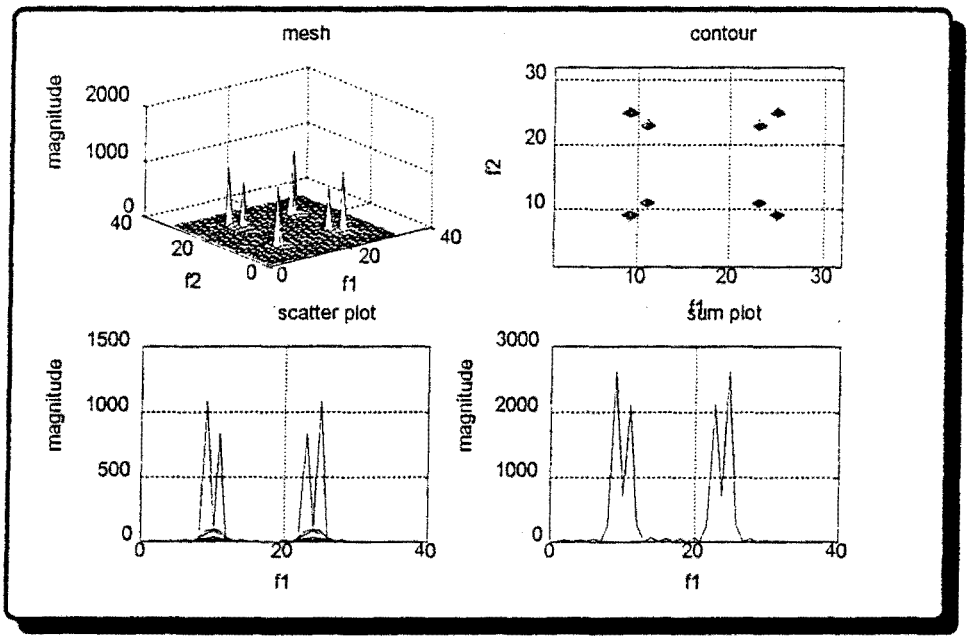

Figure 4.50: FSK Outer Product Representation (Transform Length is 32, Incoherent)

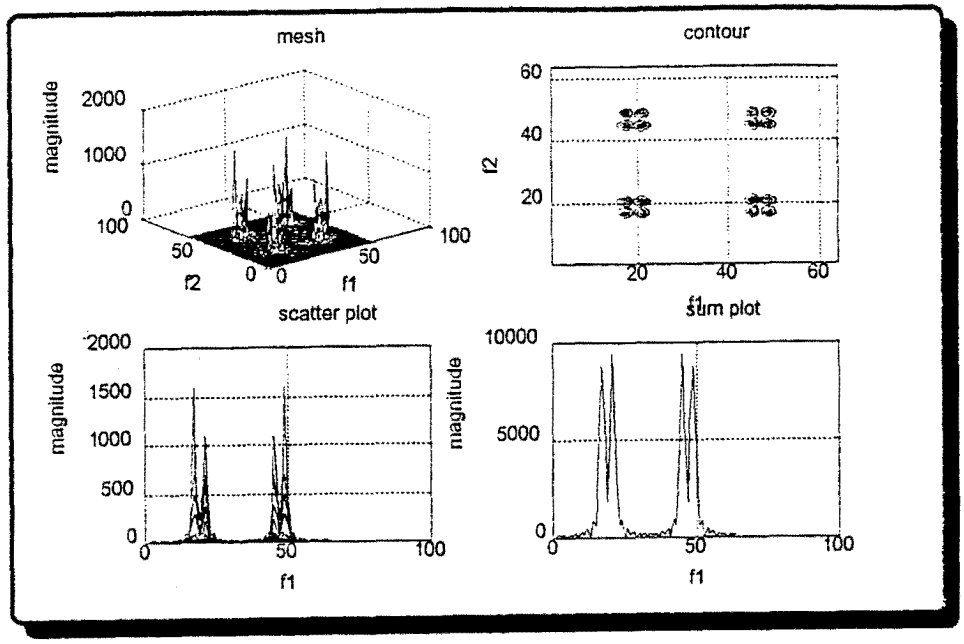

Figure 4.51: FSK Outer Product Representation (Transform Length is 64, Coherent)

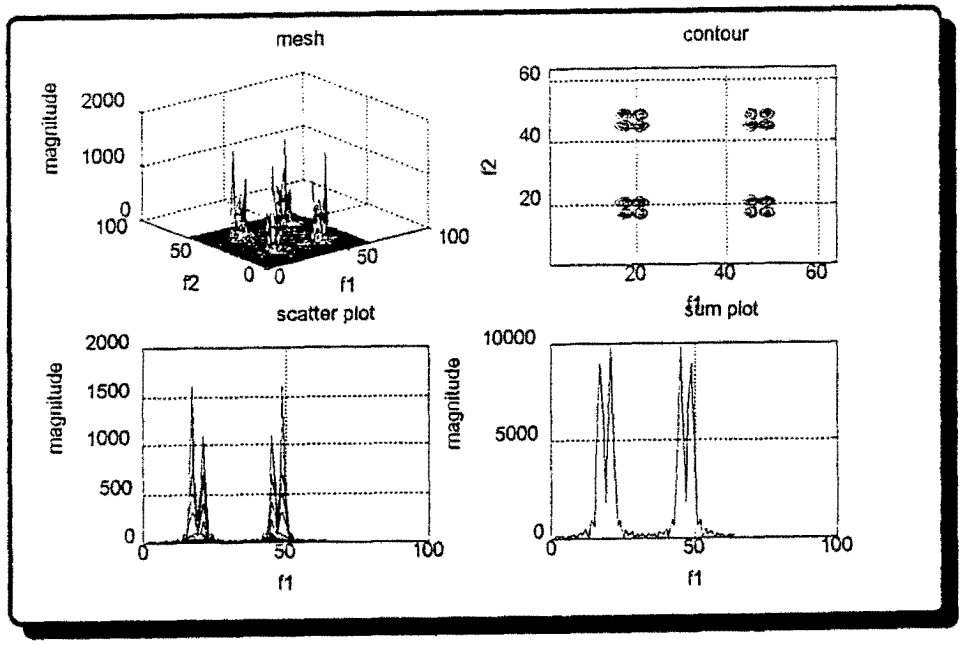

Figure 4.52: FSK Outer Product Representation (Transform Length is 64, Incoherent)

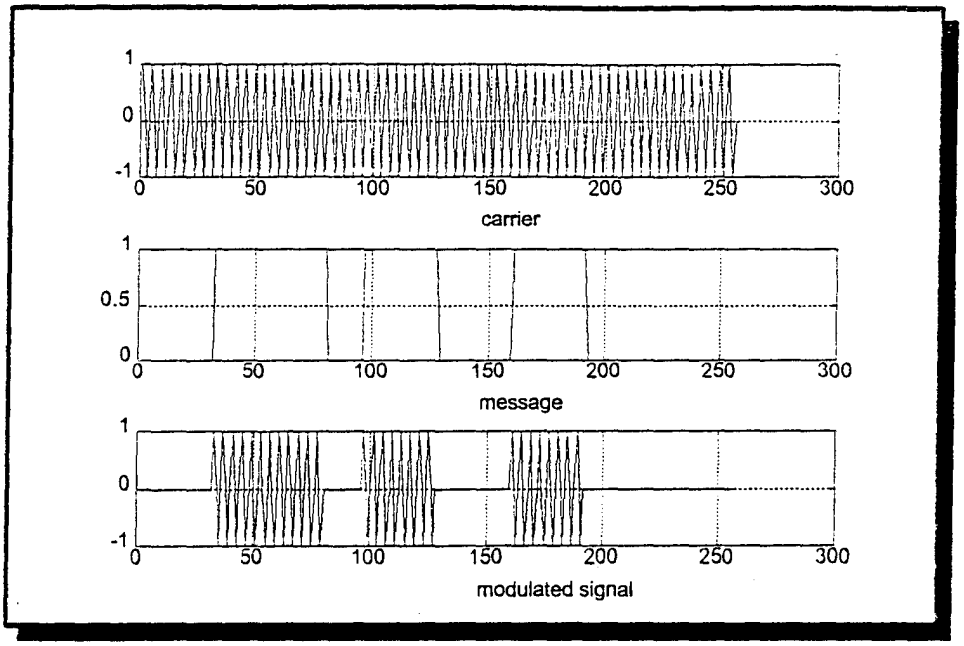

Figure 4.53: OOK Generation

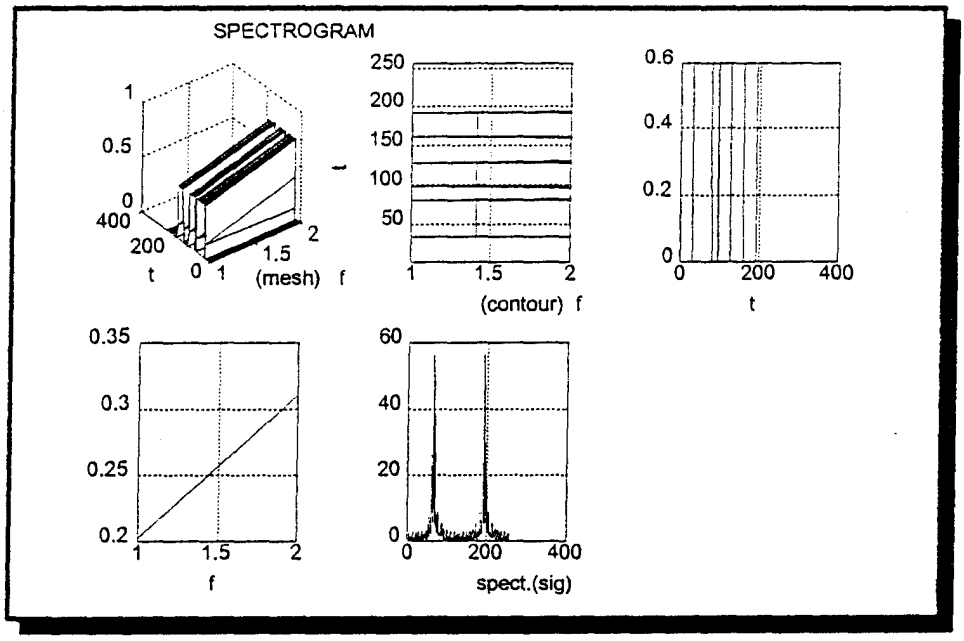

Figure 4.54: OOK Spectrogram (Window Length is 4)

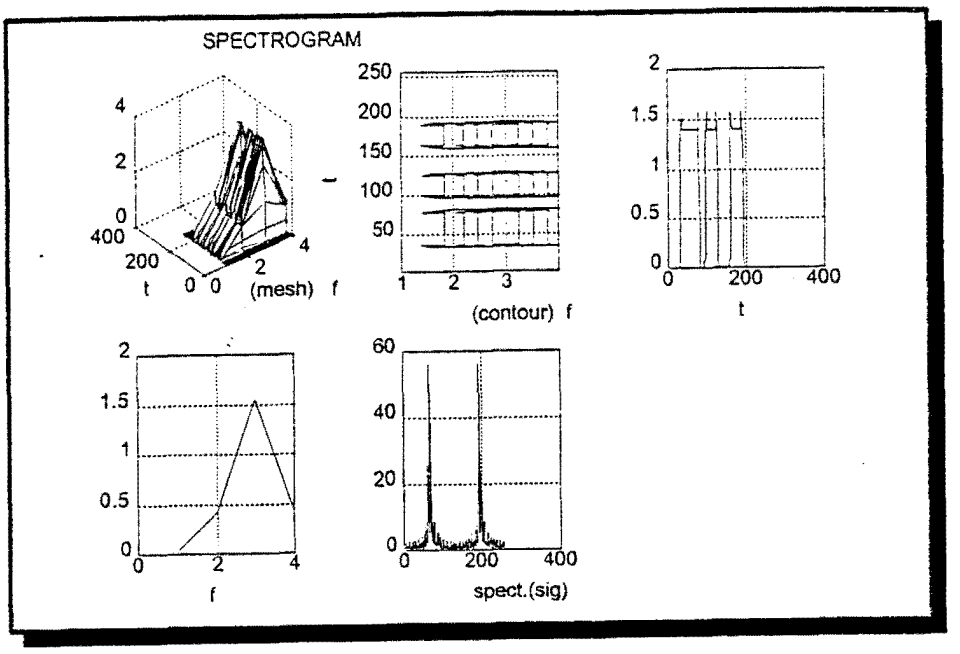

Figure 4.55: OOK Spectrogram (Window Length is 8)

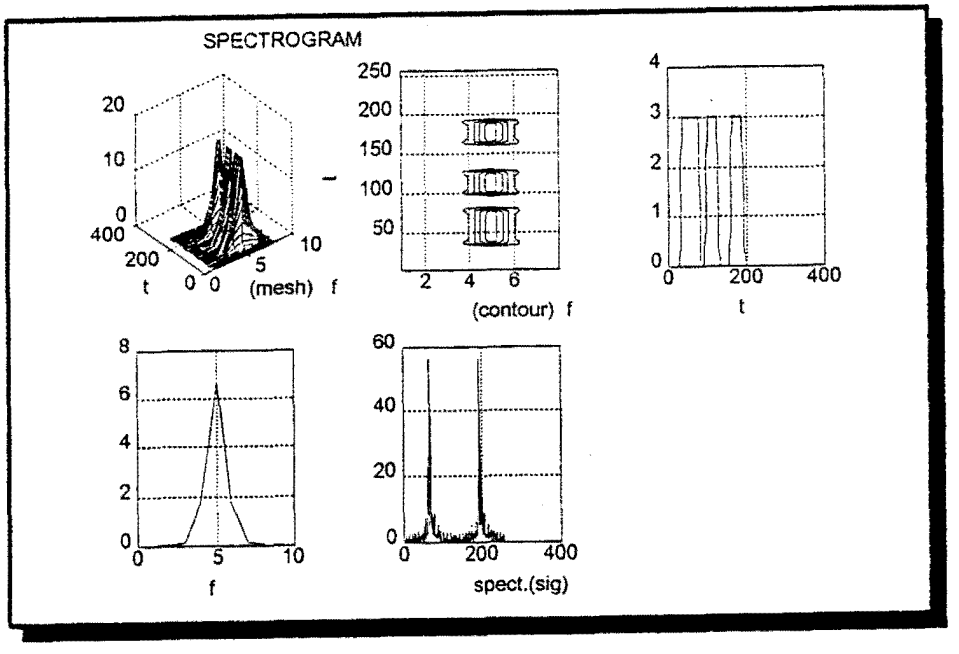

Figure 4.56: OOK Spectrogram (Window Length is 16)

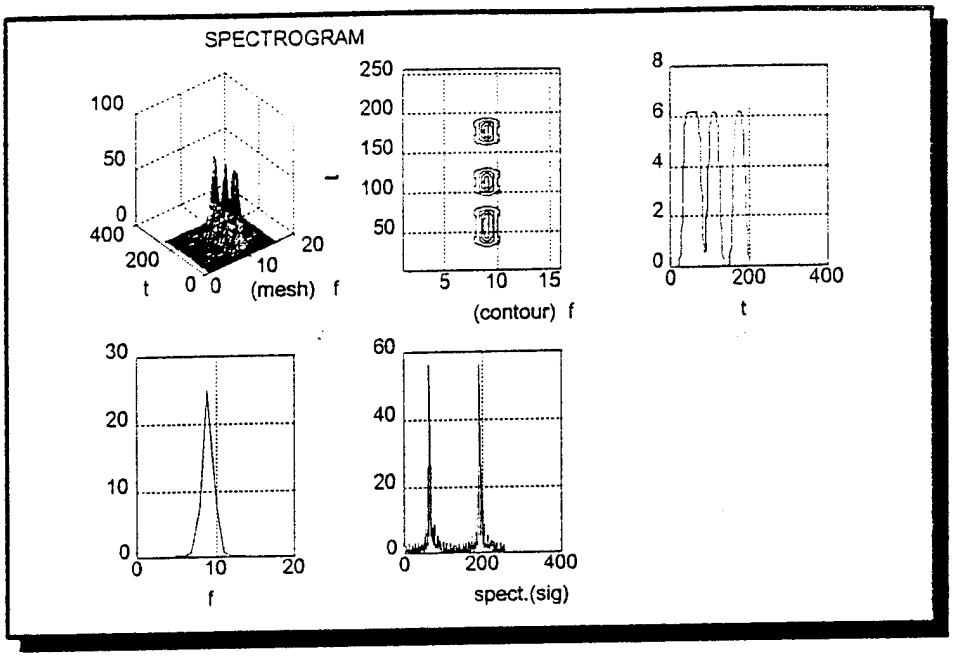

Figure 4.57: OOK Spectrogram (Window Length is 32)

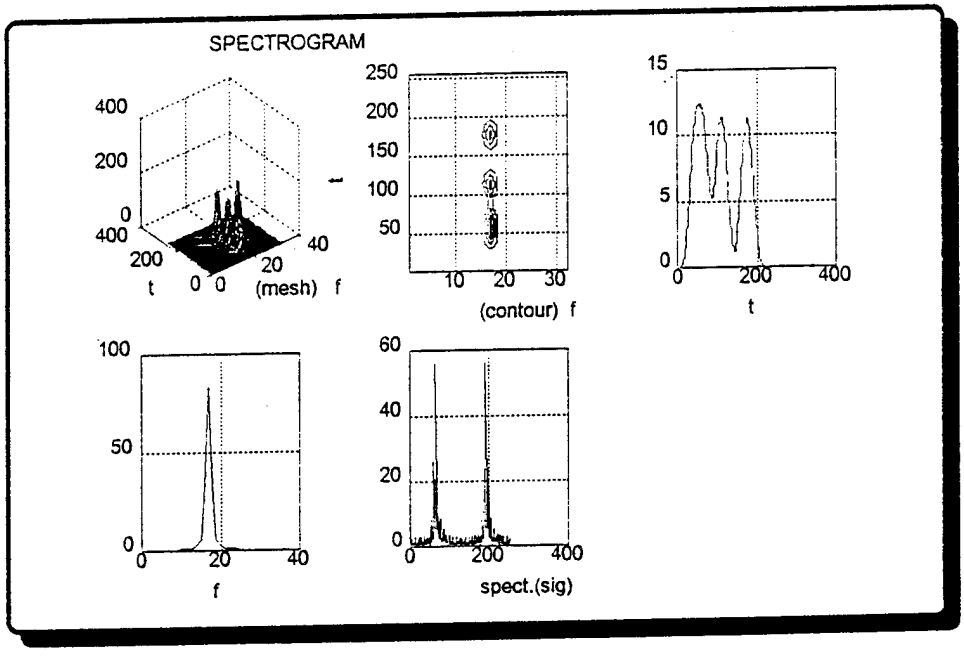

Figure 4.58: OOK Spectrogram (Window Length is 64)

at the relevant locations were apparent with the window lengths of N_1 /2 (which is 8), N_1 (which is 16) and 2 x N_1 (which is 32). For the other window lengths, it was difficult to determine the message by examining the mesh plot or contour plot. In Figure 4.55 (i.e., size 8), the time averaged plot does not present a complete picture since it was not centered and in the frequency averaged plot of Figure 4.57 (i.e., size 32) some distortions were observed which made it hard to see the amplitude shifts at the relevant locations. Figure 4.56 (i.e., size 16) was the best since the time averaged plot was centered and it showed the amplitude shifts at their relevant locations in the mesh, contour, and frequency averaged plots.

Figure 4.59 through Figure 4.63 show the 1-1/2 D instantaneous power spectrum for FFT sizes 4, 8, 16, 32, and 64. A Hamming window and a step size of 2 were used. Amplitude transition points at the right locations can be seen on the mesh, contour and frequency average plots when using FFT sizes of 8,16 and 32 (see Figures 4.60, 4.61, and 4.62). We choose 16 (i.e., matched signal bit length) as the transform length for 1-1/2 D spectral analysis of the OOK signal since the time averaged plot was centered and the frequency averaged plot showed the exact locations of the amplitude shifts (see Figure 4.61). In Figure 4.60 for a FFT size 8, the time averaged plot was not centered and in Figure 4.62 we observed some distortion in the mesh, contour and frequency averaged plot which made it hard to locate the exact points where the amplitude shifts occurred.

Figure 4.64 through Figure 4.68 show the bispectrum for FFT sizes 4, 8, 16, 32, and 64. The window type was '1' , the overlap was 50 percent, and the number of samples per segment (nsamp) was 16. For the bispectral analysis, we choose an FFT length of 16 for the remainder of this study, adhering to the symbol length and conforming with the transform length choice of the spectrogram and 1-1/2D_{IPS} methods for OOK.

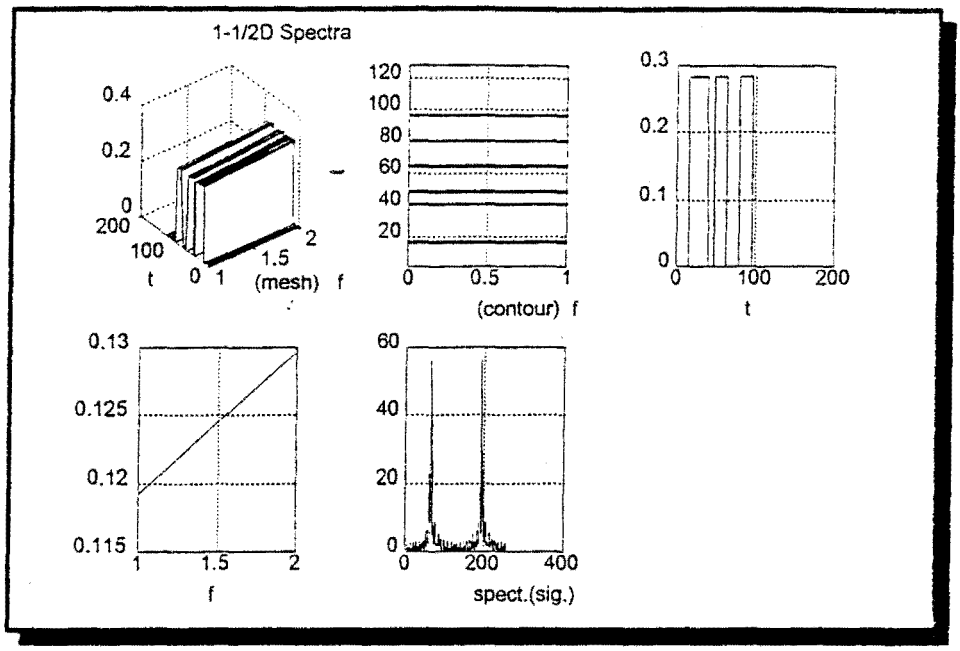

Figure 4.59: OOK 1-1/2D Spectra (Window Length is 4)

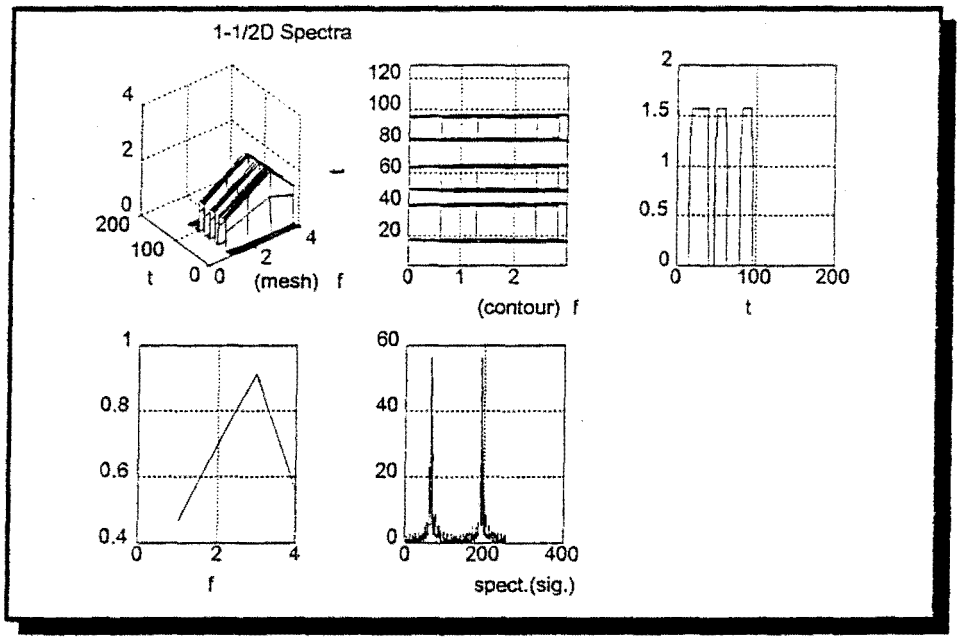

Figure 4.60: OOK 1-1/2D Spectra (Window Length is 8)

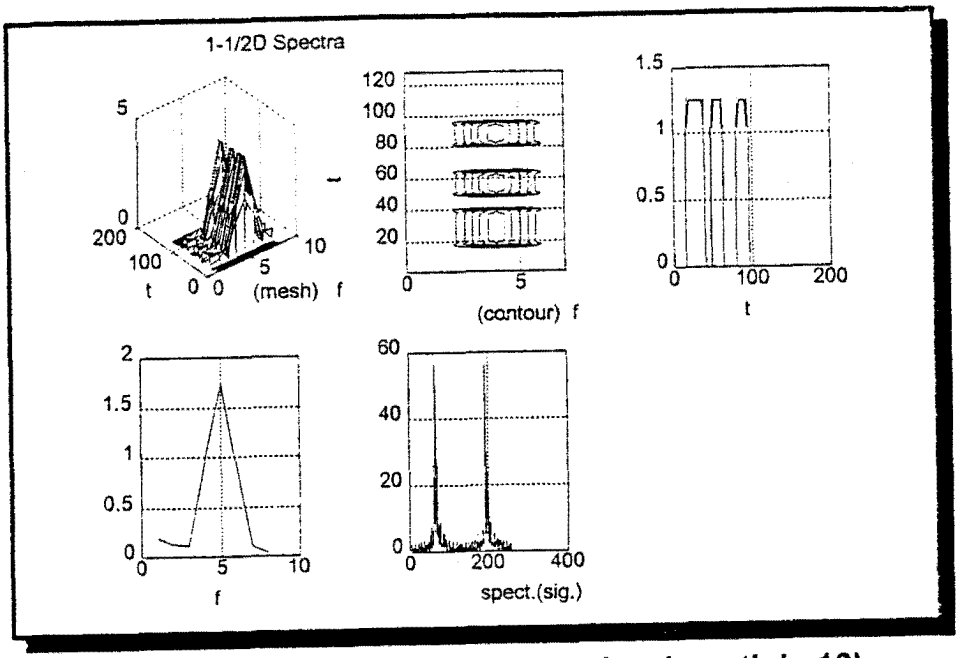

Figure 4.61: OOK 1-1/2D Spectra (Window Length is 16)

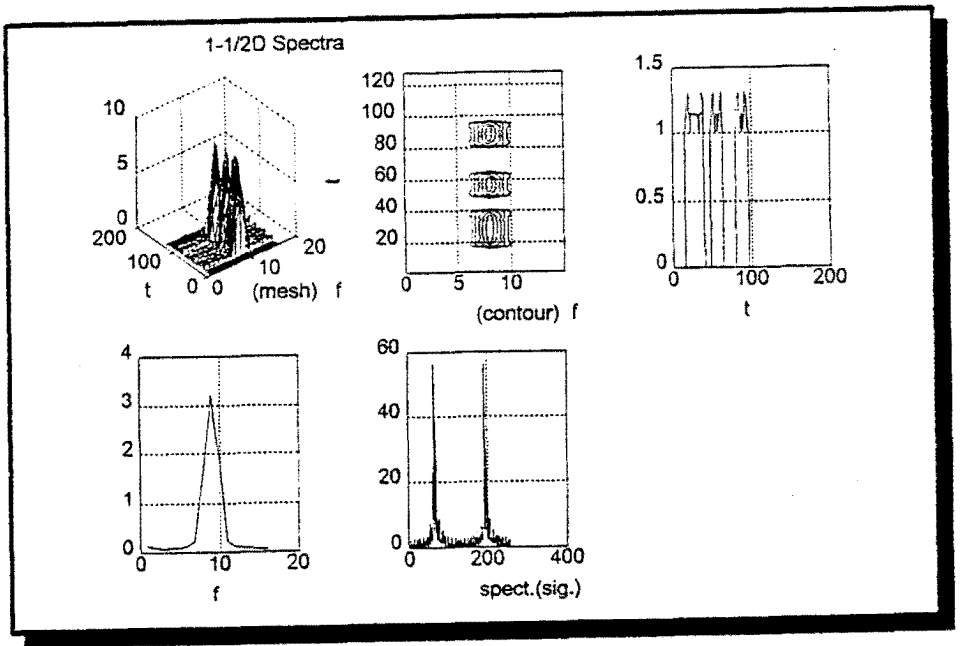

Figure 4.62: OOK 1-1/2D Spectra (Window Length is 32)

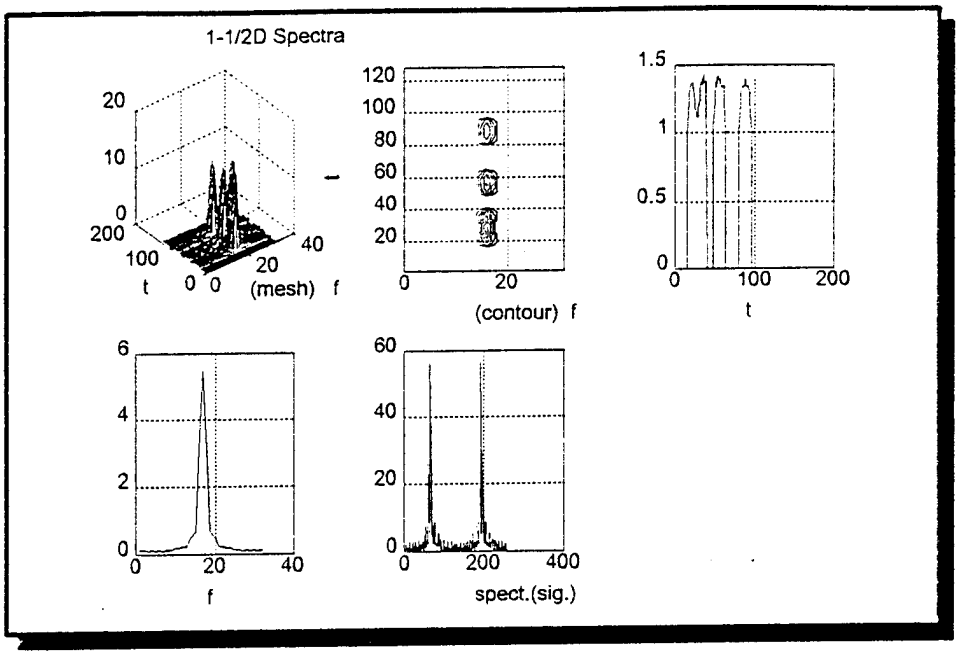

Figure 4.63: OOK 1-1/2D Spectra (Window Length is 64)

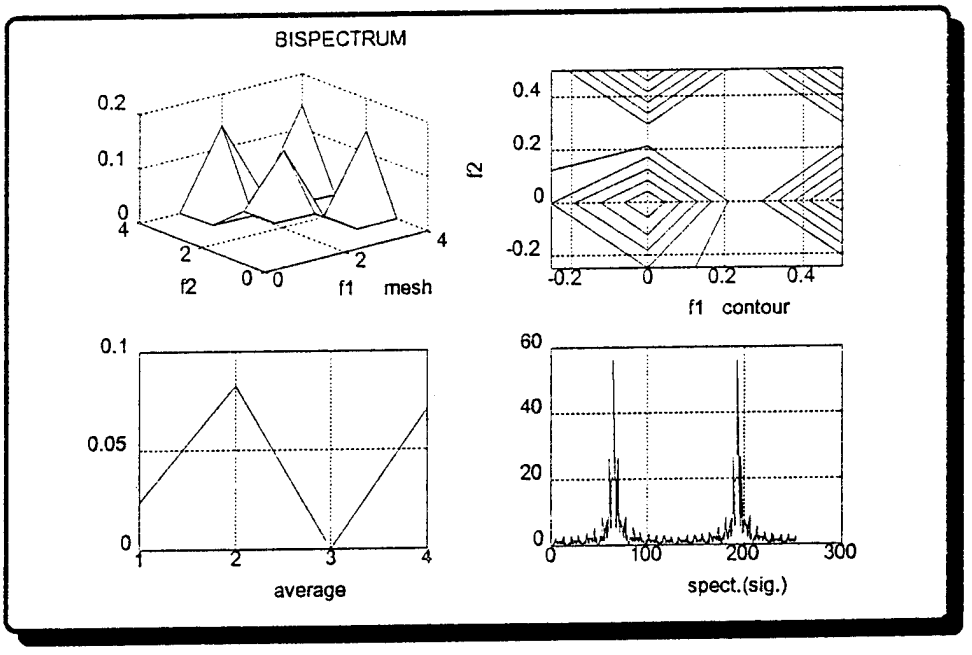

Figure 4.64: OOK Bispectrum (Fast Fourier Transform Length is 4)

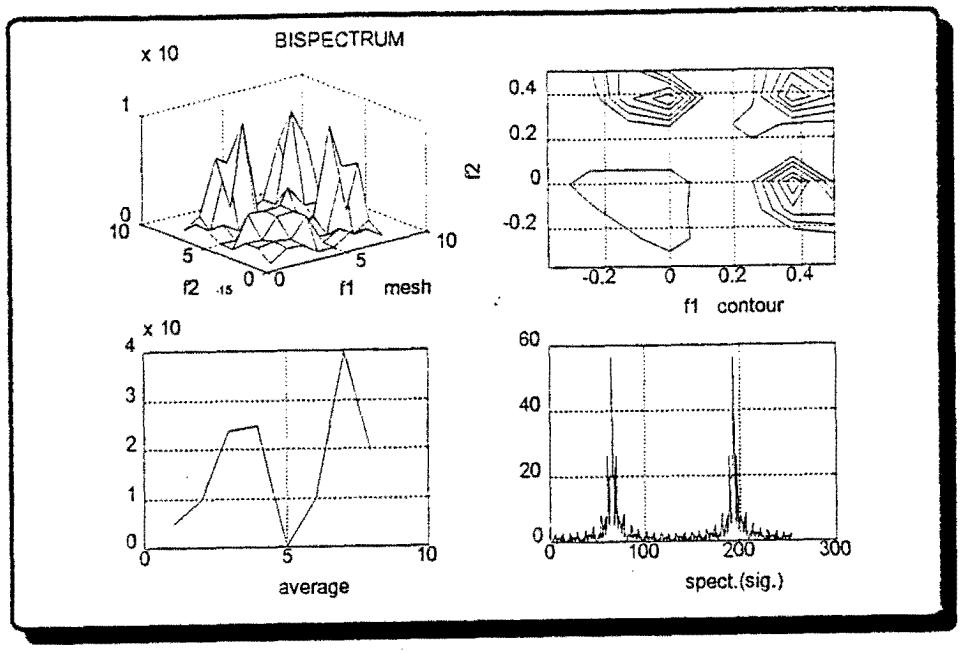

Figure 4.65: OOK Bispectrum (Fast Fourier Transform Length is 8)

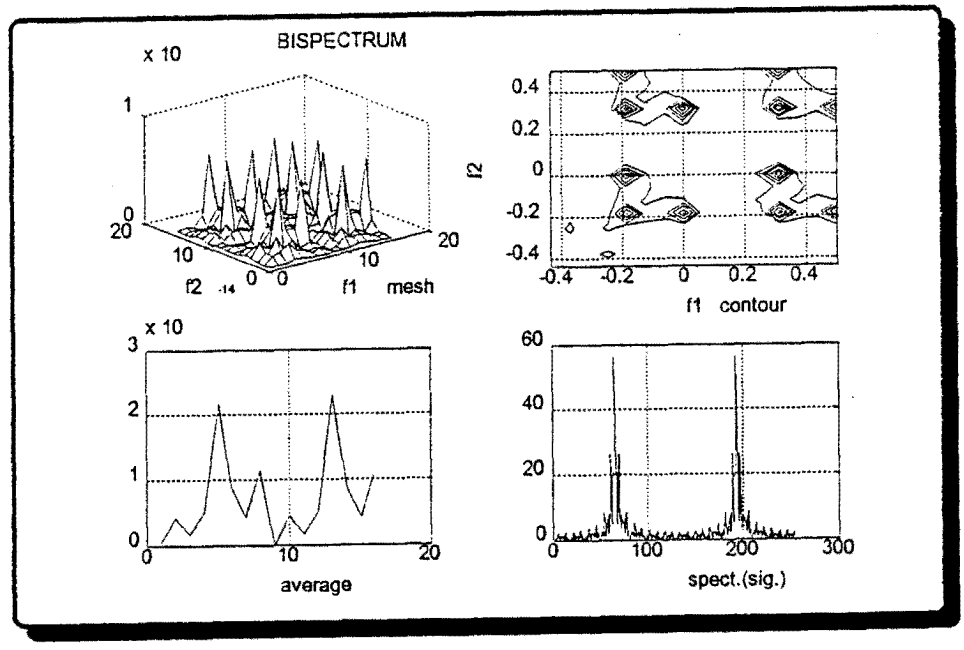

Figure 4.66: OOK Bispectrum (Fast Fourier Transform Length is 16)

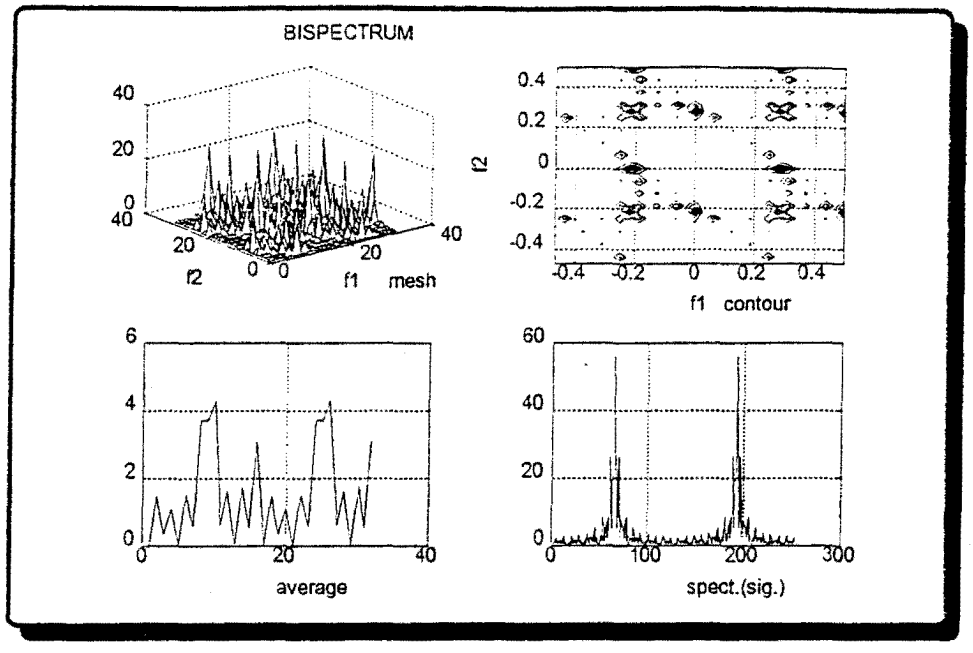

Figure 4.67: OOK Bispectrum (Fast Fourier Transform Length is 32)

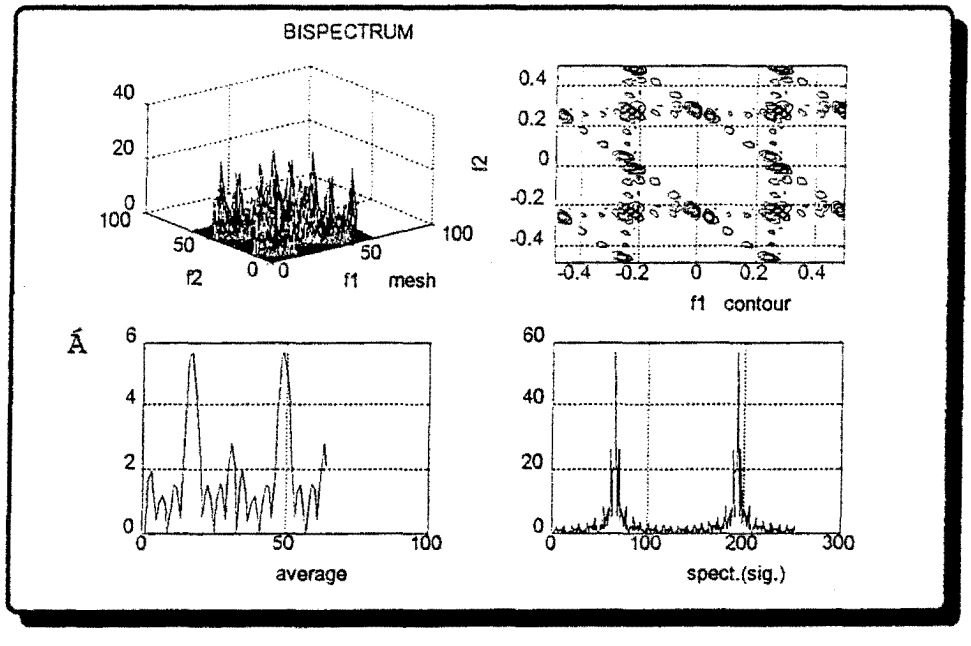

Figure 4.68: OOK Bispectrum (Fast Fourier Transform Length is 64)

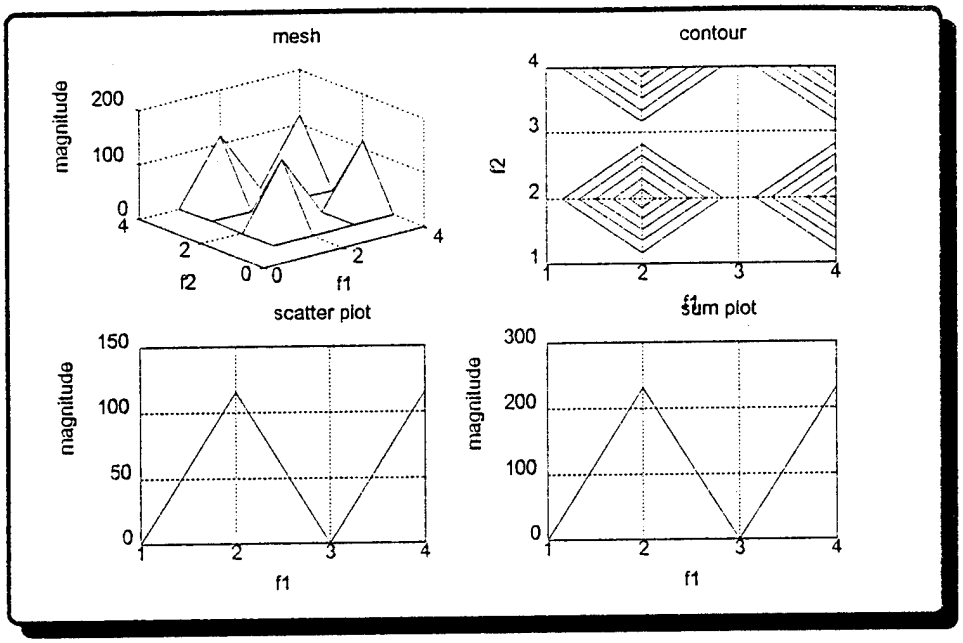

Figure 4.69: OOK Outer Product Representation (Transform Length is 4, Coherent)

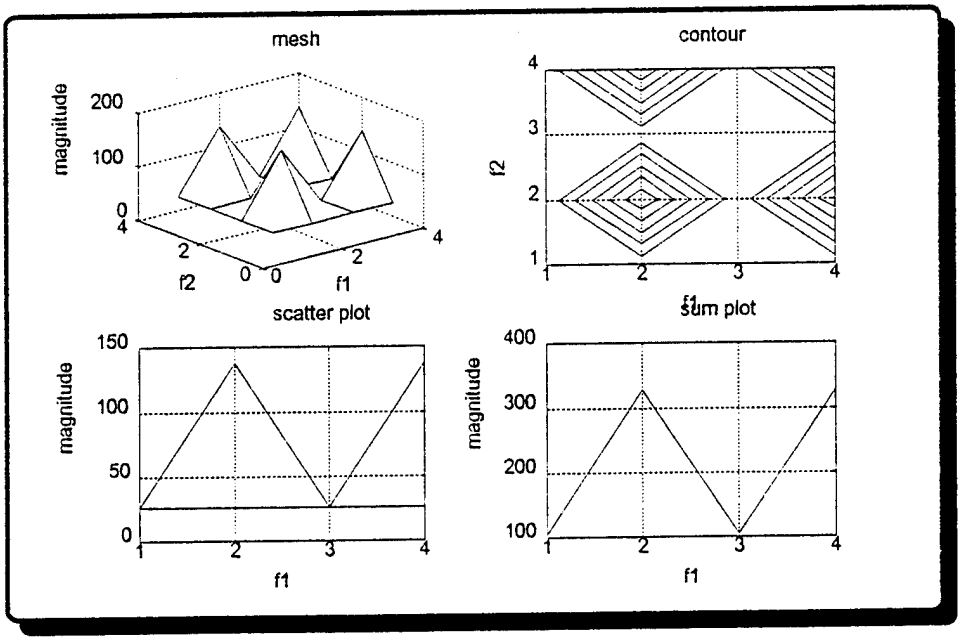

Figure 4.70: OOK Outer Product Representation (Transform Length is 4, Incoherent)

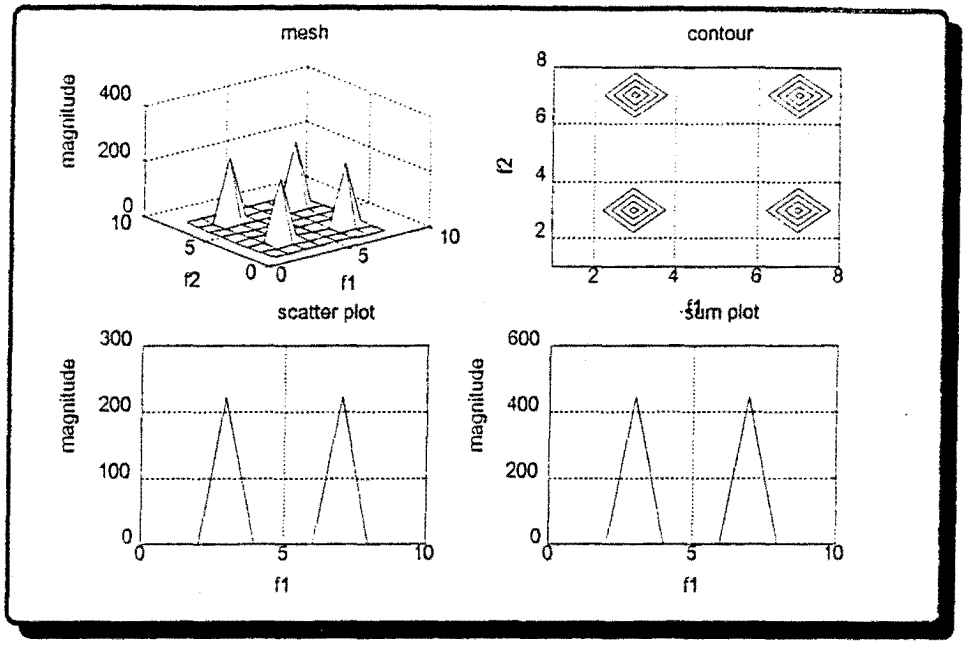

Figure 4.71: OOK Outer Product Representation (Transform Length is 8, Coherent)

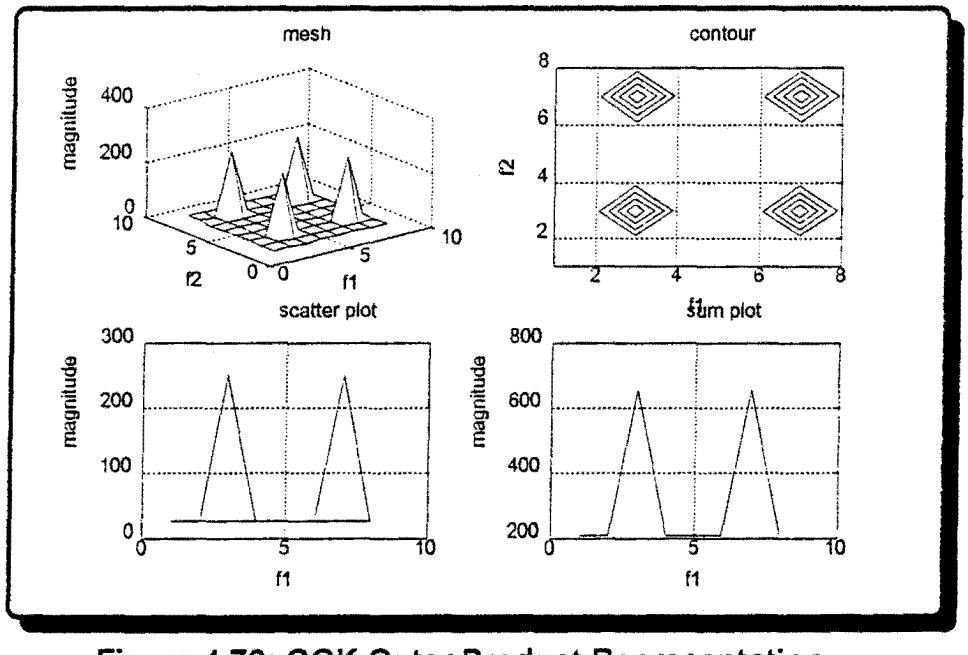

Figure 4.72: OOK Outer Product Representation (Transform Length is 8, Incoherent)

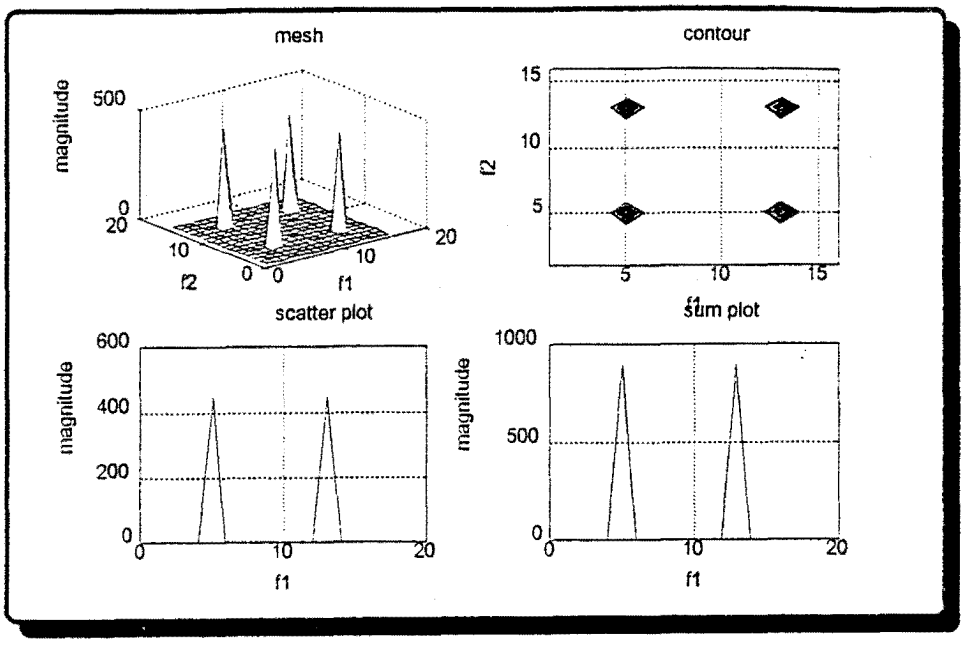

Figure 4.73: OOK Outer Product Representation (Transform Length is 16, Coherent)

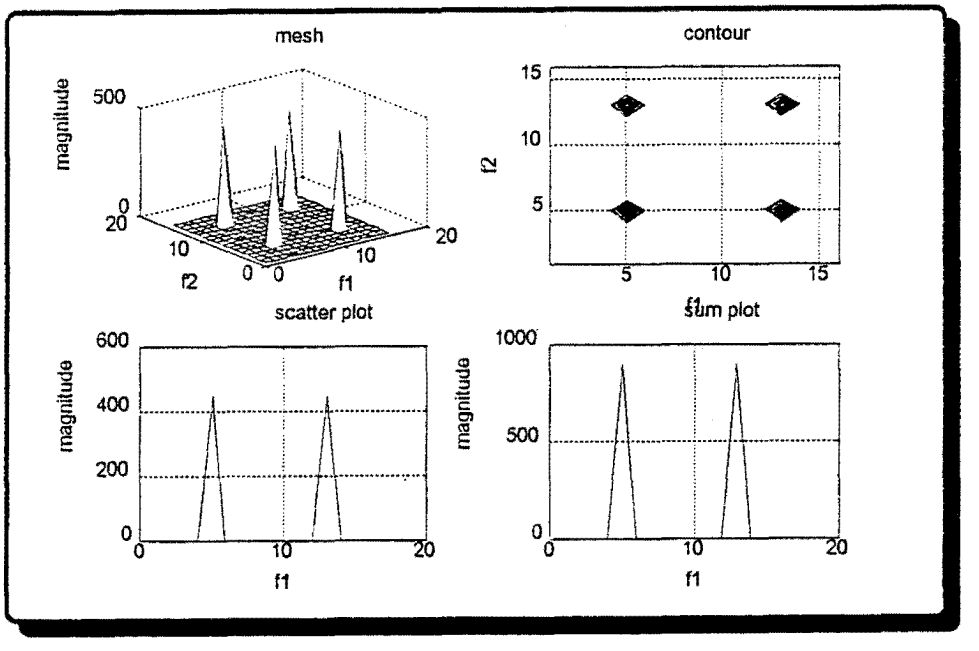

Figure 4.74: OOK Outer Product Representation (Transform Length is 16, Incoherent)

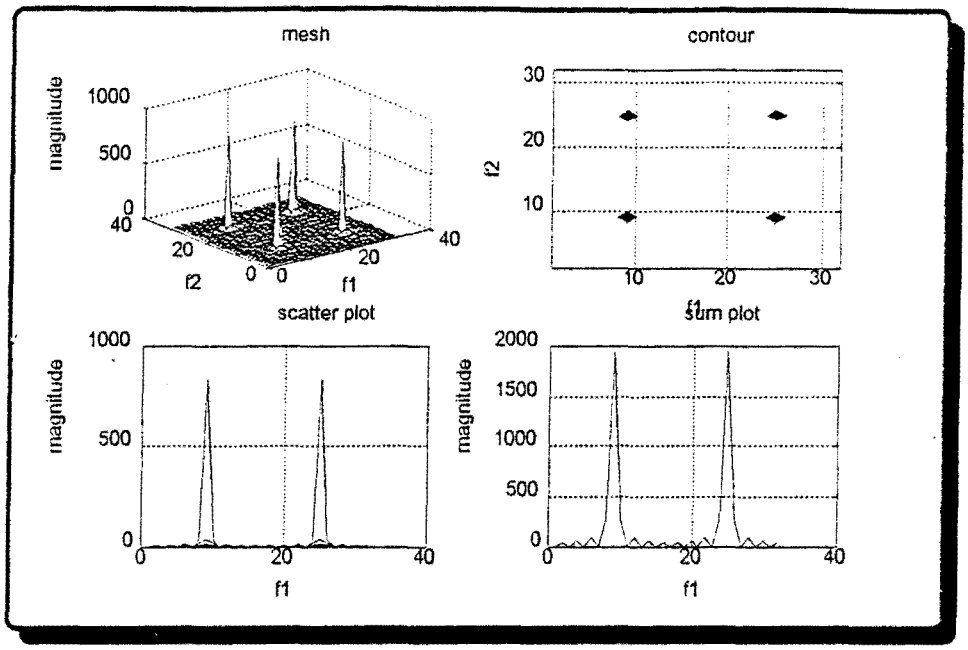

Figure 4.75: OOK Outer Product Representation (Transform Length is 32, Coherent)

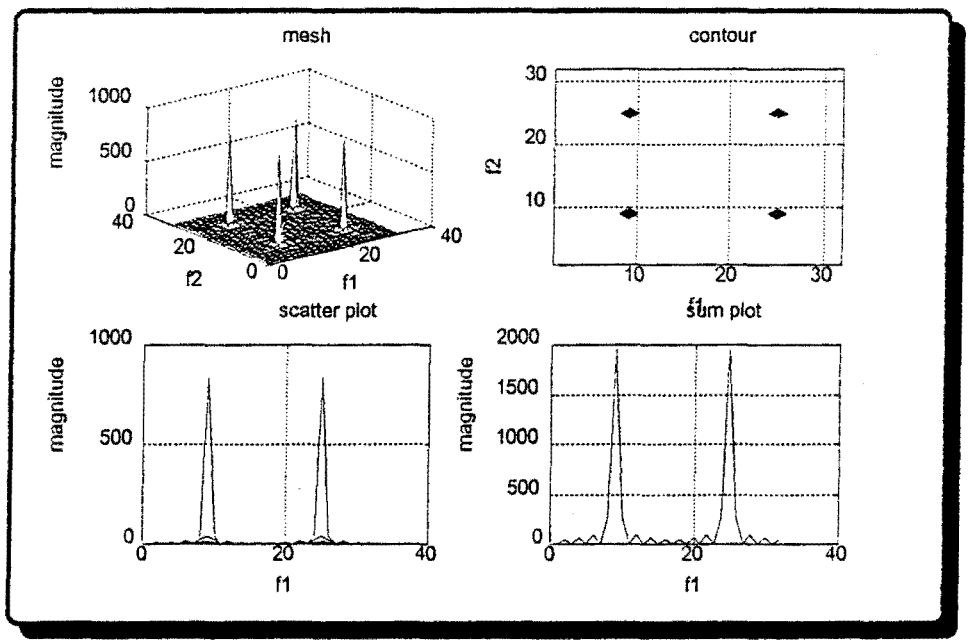

Figure 4.76: OOK Outer Product Representation (Transform Length is 32, Incoherent)

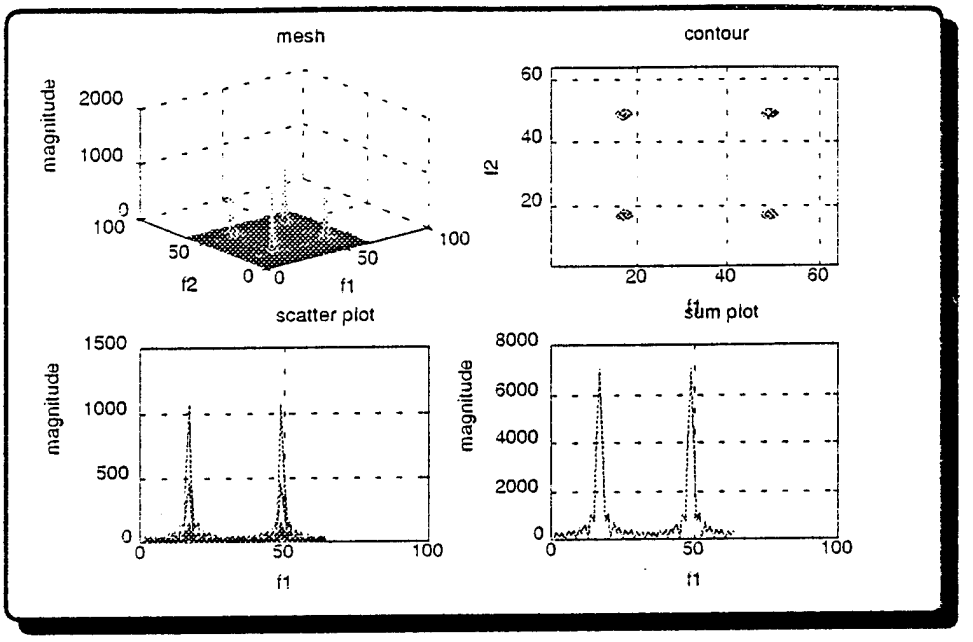

Figure 4.77: OOK Outer Product Representation
(Transform Length is 64, Coherent Case)

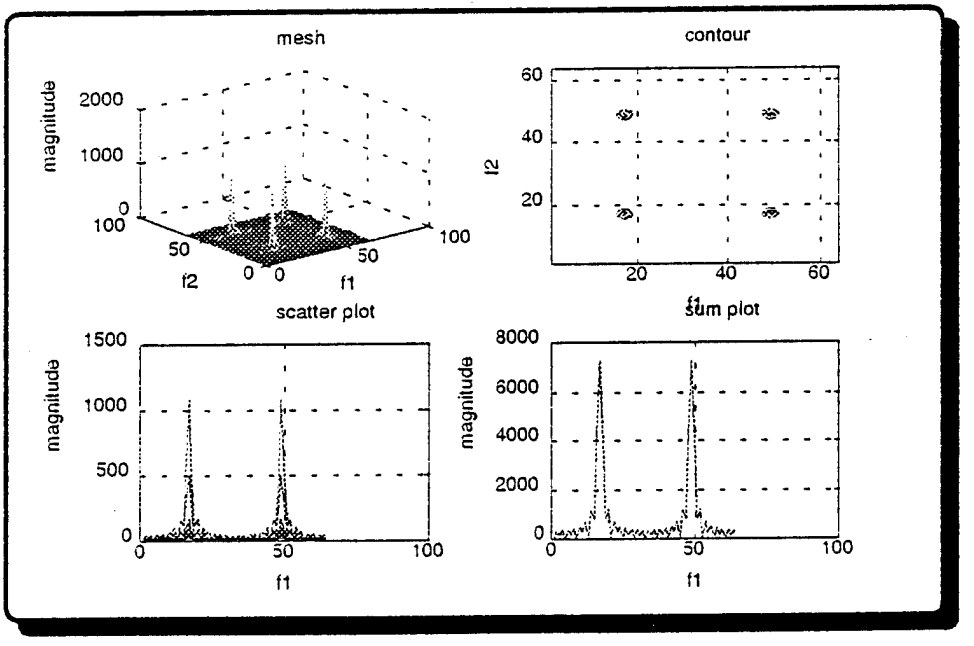

Figure 4.78: OOK Outer Product Representation
(Transform Length is 64, Incoherent Case)

Figure 4.69 through Figure 4.78 show the outer product representation for FFT sizes of 4, 8, 16, 32, and 64. The figures for sizes of 4, 8, and 16 do not provide clues about the modulation kind. Figures 4.75 through 4.78 for sizes 32, and especially 64 give some information about the modulation type. We choose a size of 64 for the outer product representation of the OOK signal since the sum plot presented the classical OOK spectrum and the contour plot showed an identical picture for the OOK signal (four solid points) which was useful for differentiating the OOK signal from other signals (see Figures 4.77 and 4.78).

4. QPSK

In the QPSK scheme, there are four phase changes for the four possible symbols. In this study, the QPSK modulated signal was formulated as

$$x(n) = \sin(2\pi(\frac{k}{N_1})n + \Phi)$$

where $\Phi = 0$ for symbol 3
$\Phi = \pi/2$ for symbol 2
$\Phi = \pi$ for symbol 1
$\Phi = 3\pi/2$ for symbol 0
k = 4
N_1 = 16
n = 0,1,....,255.

The 16 symbol message for QPSK was {3 3 1 1 0 2 1 0 3 3 1 1 3 2 3 2} where every symbol was 16 data points long. We expected a 90° phase shift at locations 65, 97, 113, 209, 225 and 241 , a 180° phase shift at locations 33, 81, 161, and 193 , a 270° phase shift at location 129, and no phase shifts at locations 17, 49, 145, and 177. The phase shifts were relative to the unmodulated carrier phase.

Figure 4.79 shows the plot of the sinusoidal carrier, message, and the QPSK modulated signal. Figure 4.80 through Figure 4.84 show spectrograms for FFT sizes of 4, 8, 16, 32, and 64. A Hamming window was used. It can be seen that changes at the relevant locations were revealed with window lengths of N_1 /2 (which is 8), N_1 (which is 16) and 2 x N_1 (which is 32). Figure (4.83), with transform length of 8, was the best since some phase transitions (at the right locations especially in the contour plot) were easier to see than in figures with other transform sizes.

Figure 4.85 through Figure 4.89 show the 1-1/2 D spectrum for FFT sizes of 4, 8, 16, 32, and 64. A Hamming window and the step size 2 were used. Some phase transition points appeared better on the mesh, contour and frequency averaged plots when using an FFT size of 4 and 8. We choose 8 (Figure 4.86) as the optimum transform length for 1-1/2 D spectra analysis of QPSK signal to conform with the choice made for the spectrogram.

Figure 4.90 through Figure 4.94 show the bispectrum for FFT sizes of 4, 8, 16, 32, and 64. The window type was '1' , overlap was 50, and number of samples per segment (nsamp) was 16. We choose an FFT length of 8 (Figure 4.91) for the bispectrum analysis of the QPSK signal to conform with the choice made for the spectrogram and 1-1/2D_{IPS} .

Figure 4.95 through Figure 4.104 show the outer product representation of the QPSK signal for FFT sizes of 4, 8, 16, 32, and 64. The figures for FFT sizes of 4, 8, and 16 did not provide information about the modulation scheme. But the figures for sizes 32, and especially 64 showed evidence of the modulation scheme and present unique spectra for QPSK signal. The contour plots of Figures 4.103 and 4.104 for FFT size of 64 show a spot consisting of many peaks which represent various phase transitions and the sum plot shows the spike with various peaks with various heights which also represent phase shifts.

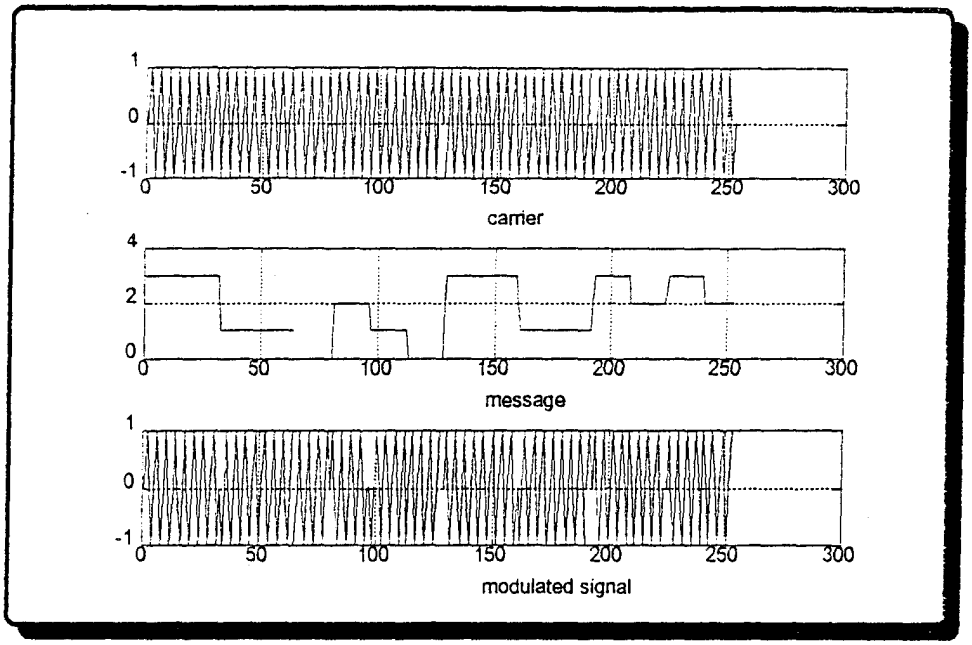

Figure 4.79: QPSK Generation

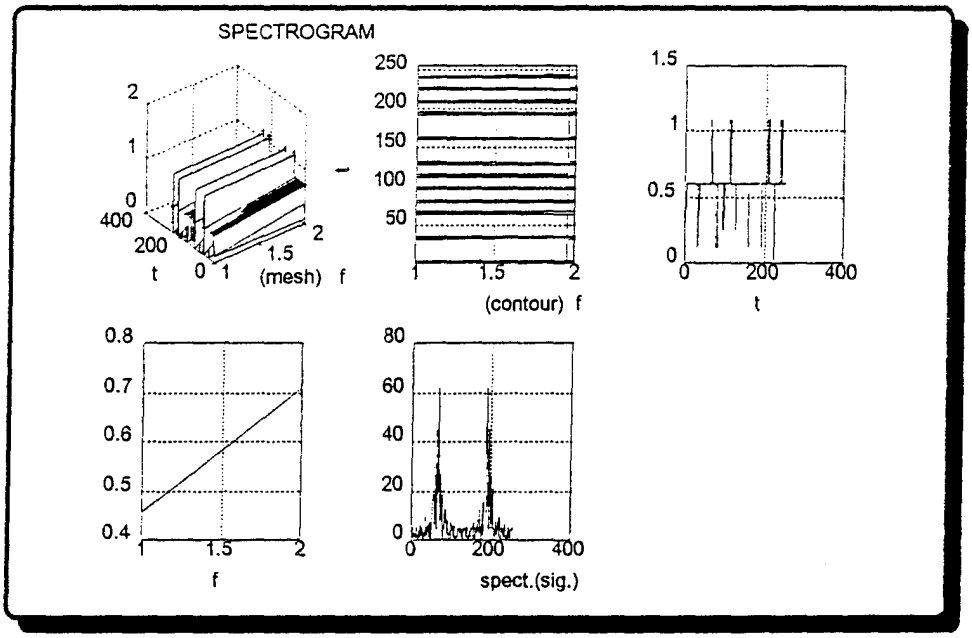

Figure 4.80: QPSK Spectrogram (Window Length is 4)

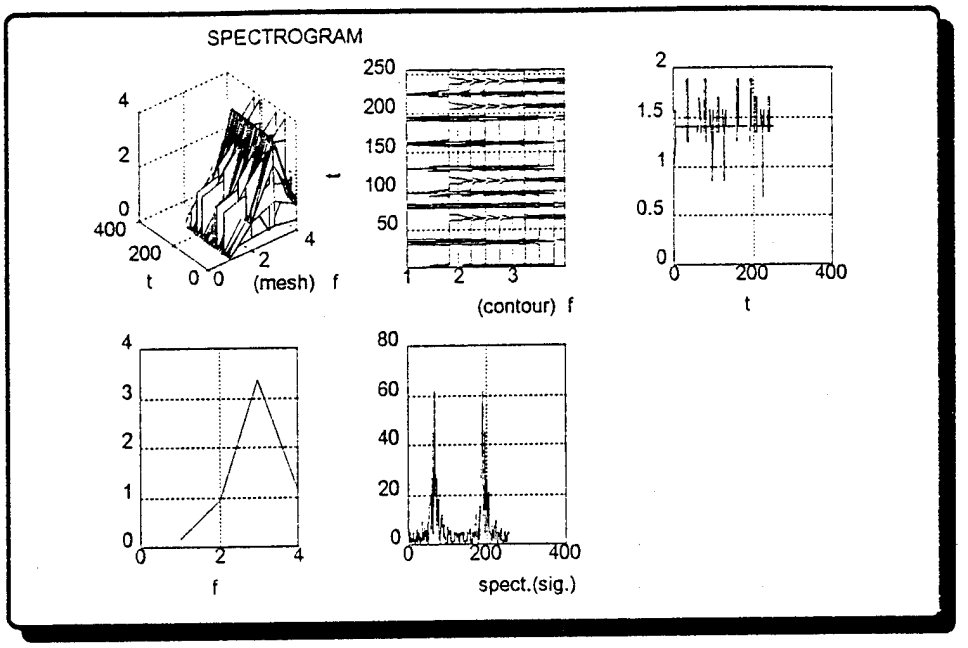

Figure 4.81: QPSK Spectrogram (Window Length is 8)

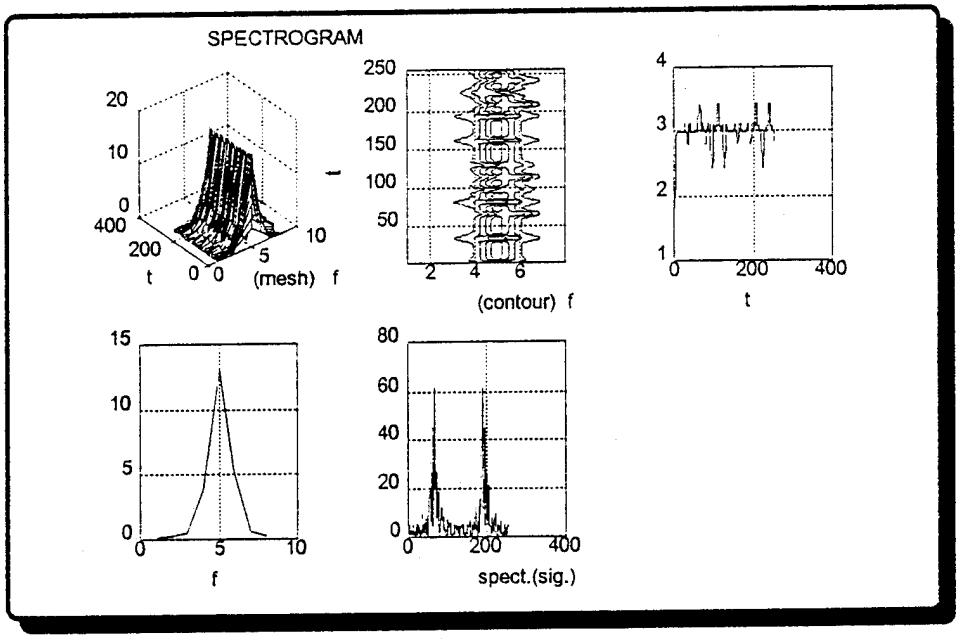

Figure 4.82: QPSK Spectrogram (Window Length is 16)

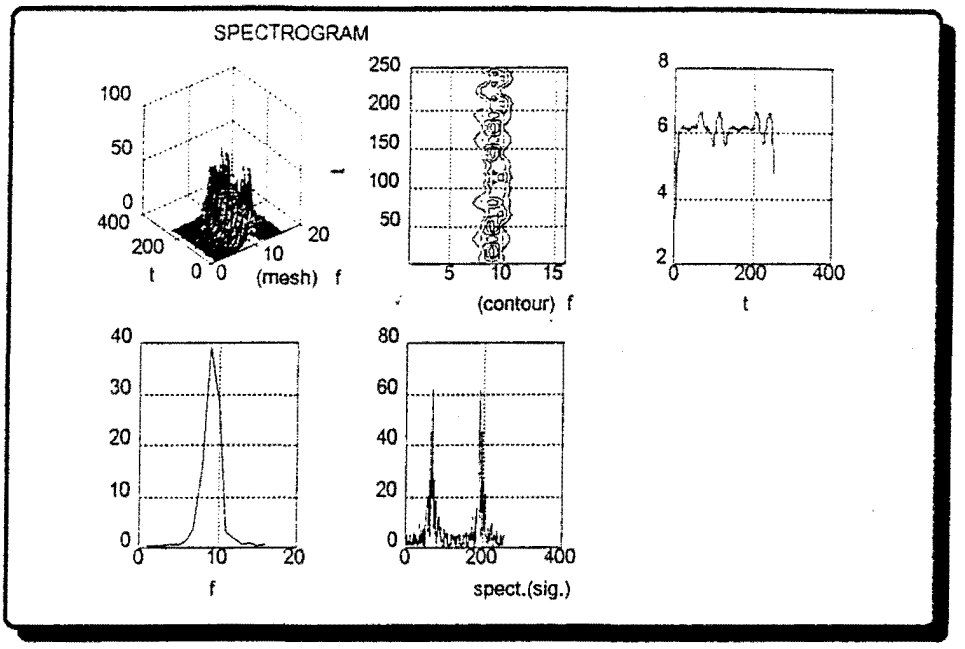

Figure 4.83: QPSK Spectrogram (Window Length is 32)

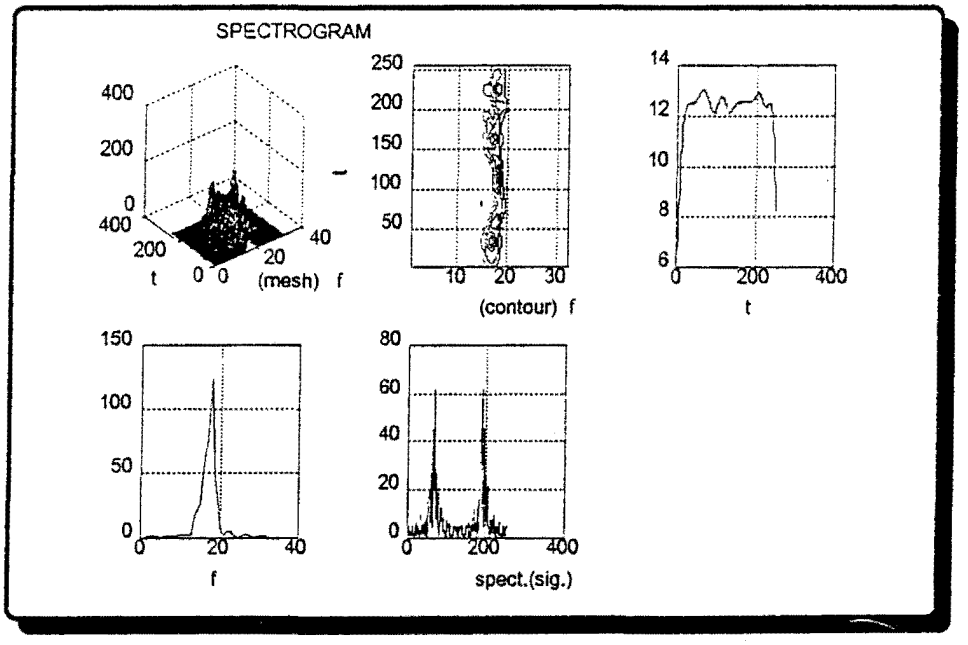

Figure 4.84: QPSK Spectrogram (Window Length is 64)

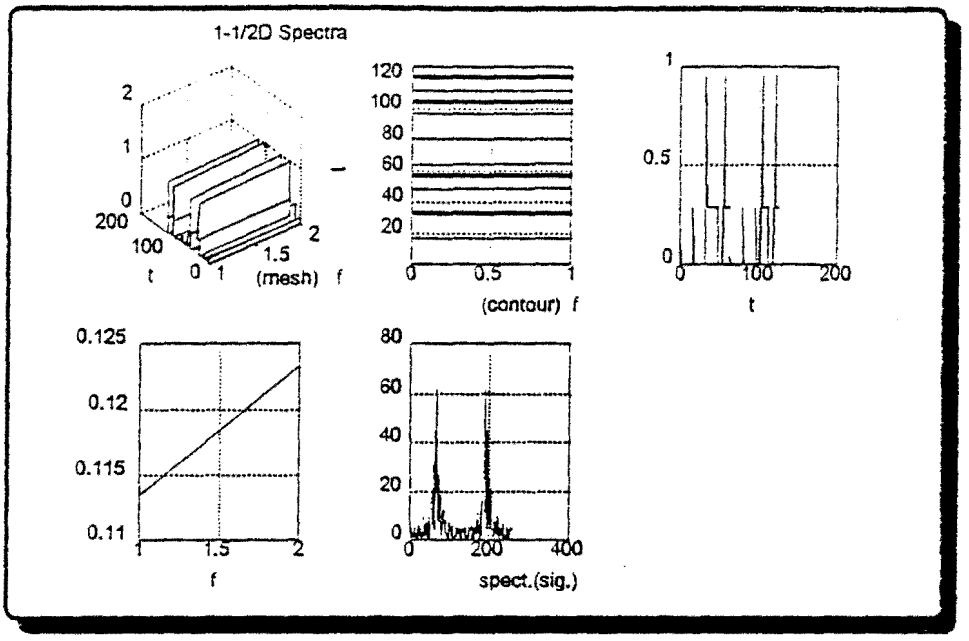

Figure 4.85: QPSK 1-1/2D Spectra (Window Length is 4)

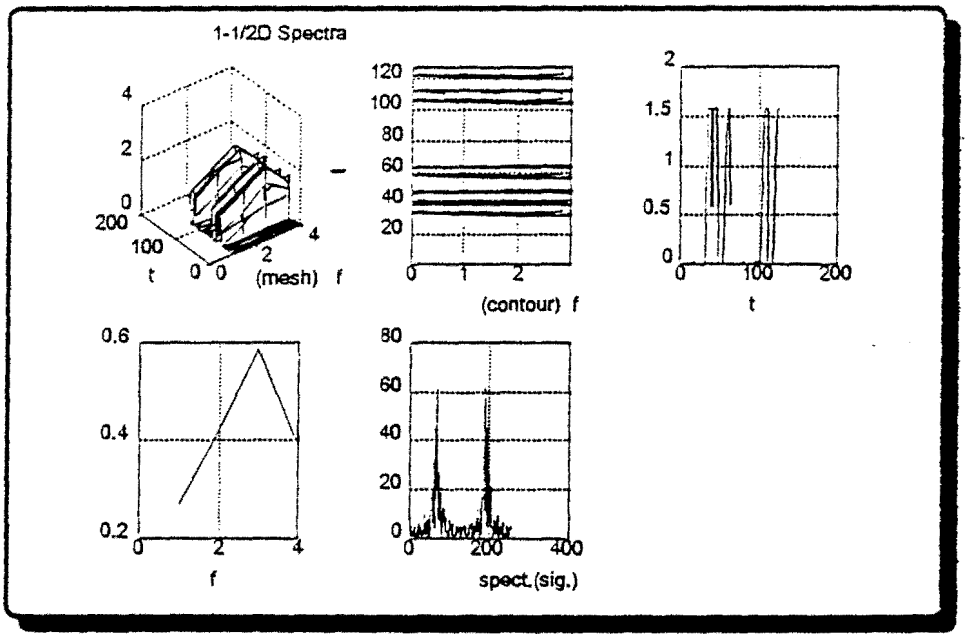

Figure 4.86: QPSK 1-1/2D Spectra (Window Length is 8)

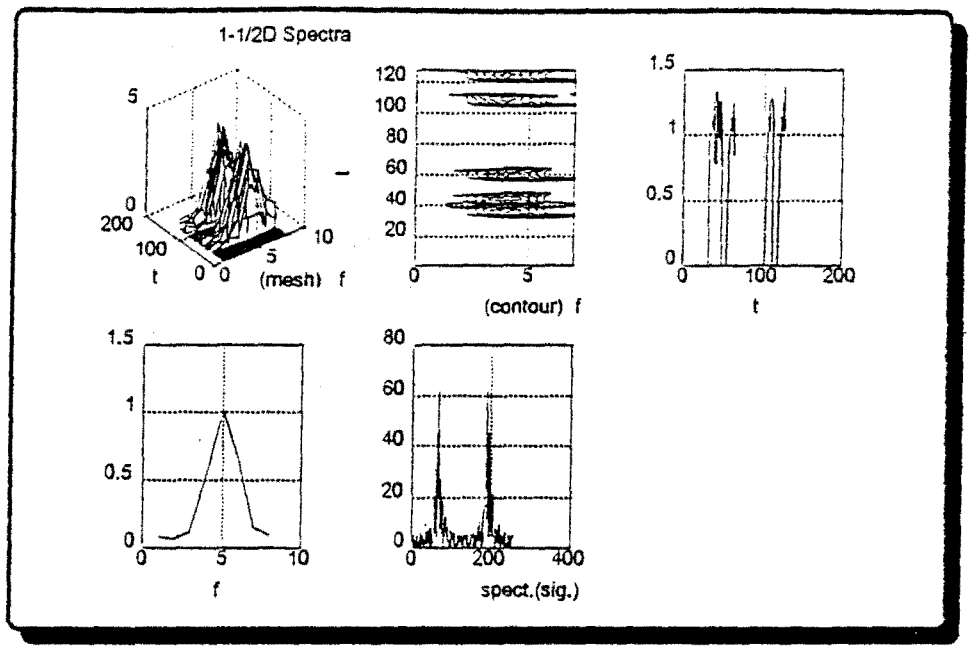

Figure 4.87: QPSK 1-1/2D Spectra (Window Length is 16)

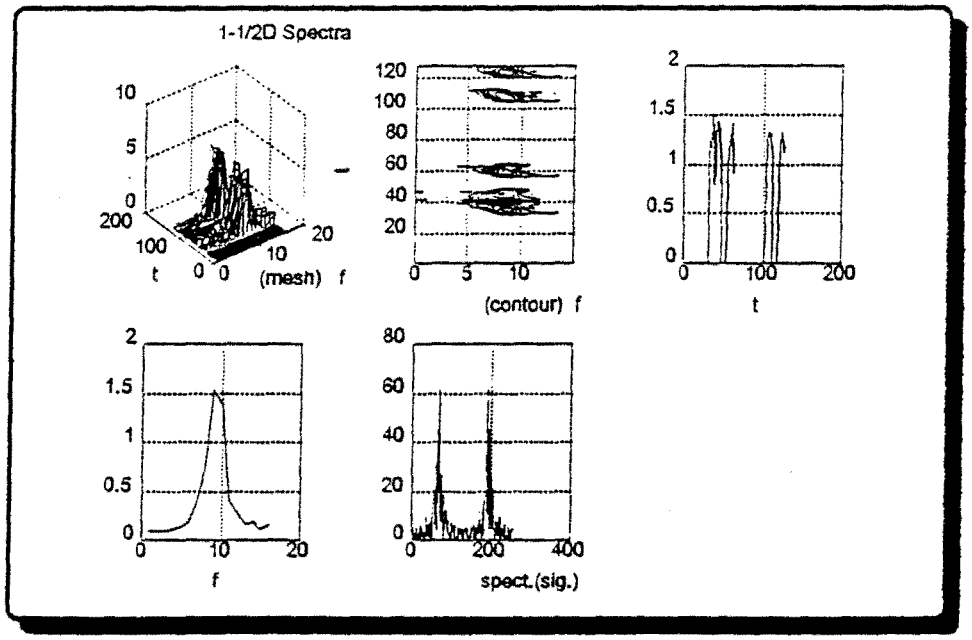

Figure 4.88: QPSK 1-1/2D Spectra (Window Length is 32)

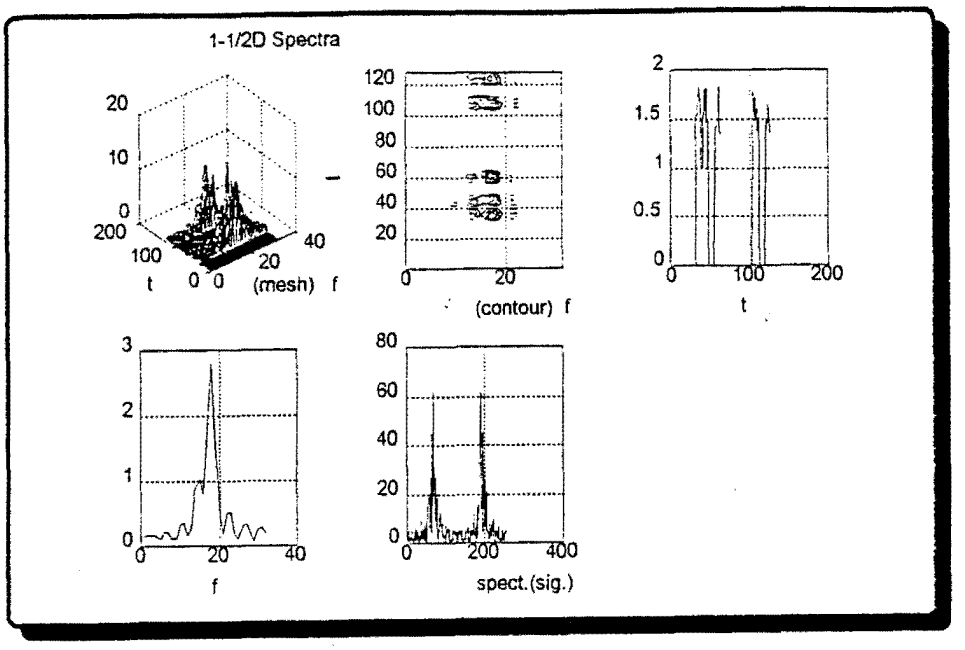

Figure 4.89: QPSK 1-1/2D Spectra (Window Length is 64)

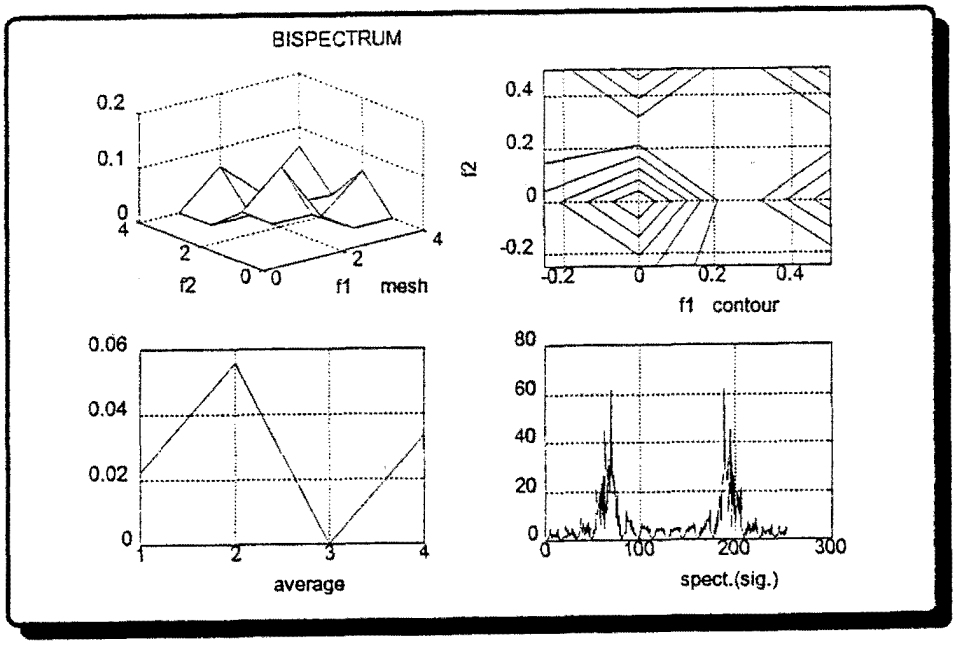

Figure 4.90: QPSK Bispectrum (Fast Fourier Transform Length is 4)

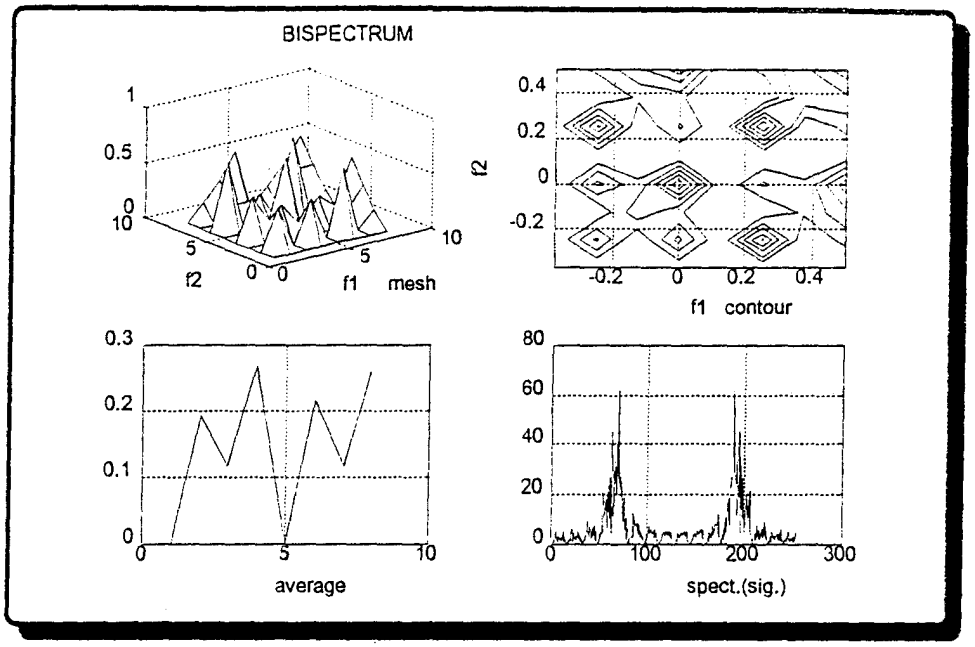

Figure 4.91: QPSK Bispectrum (Fast Fourier Transform Length is 8)

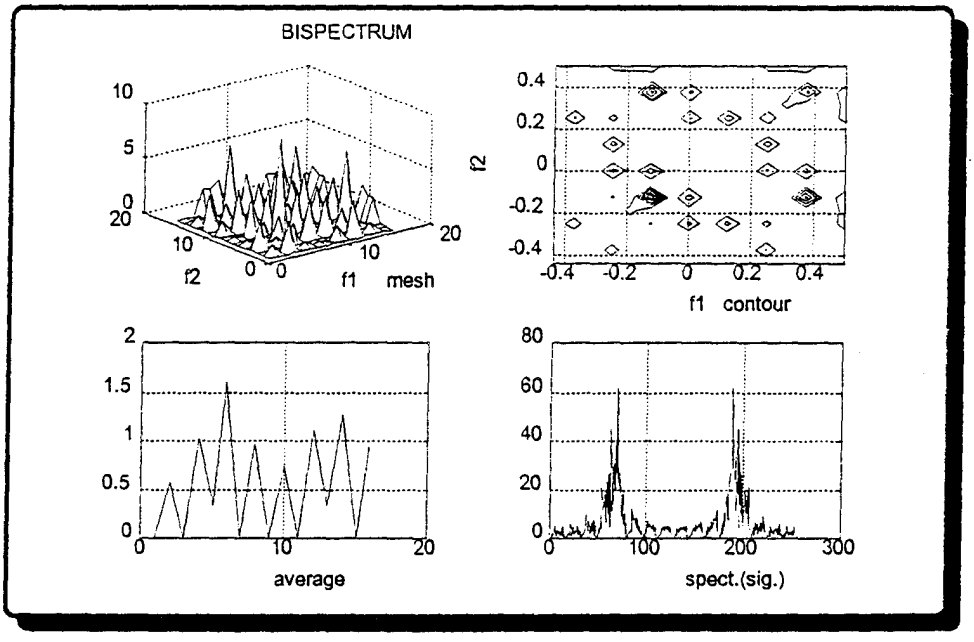

Figure 4.92: QPSK Bispectrum (Fast Fourier Transform Length is 16)

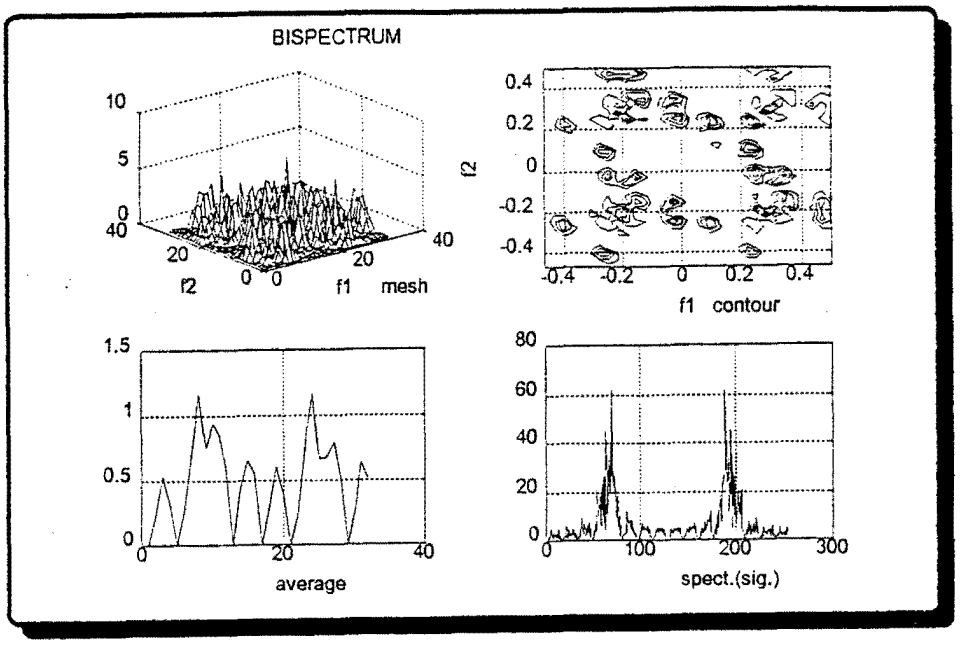

Figure 4.93: QPSK Bispectrum (Fast Fourier Transform Length is 32)

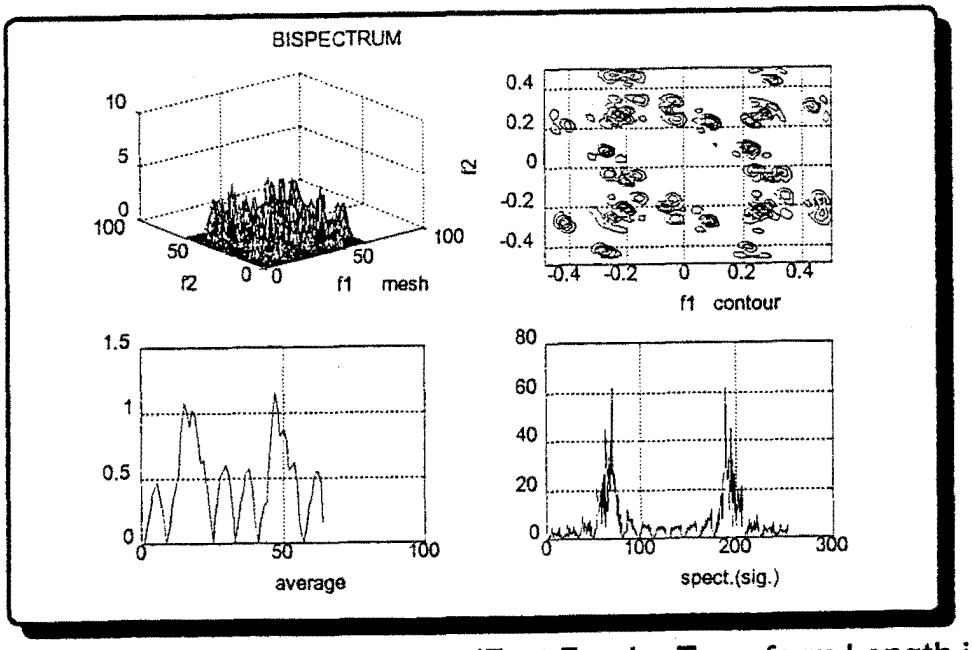

Figure 4.94: QPSK Bispectrum (Fast Fourier Transform Length is 64)

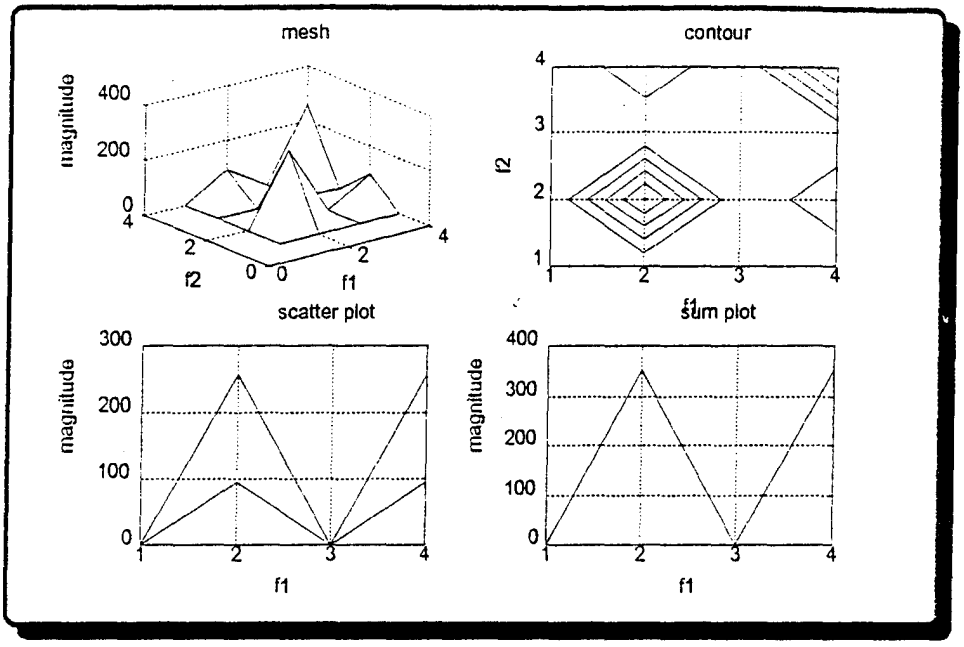

Figure 4.95: QPSK Outer Product Representation (Transform Length is 4, Coherent)

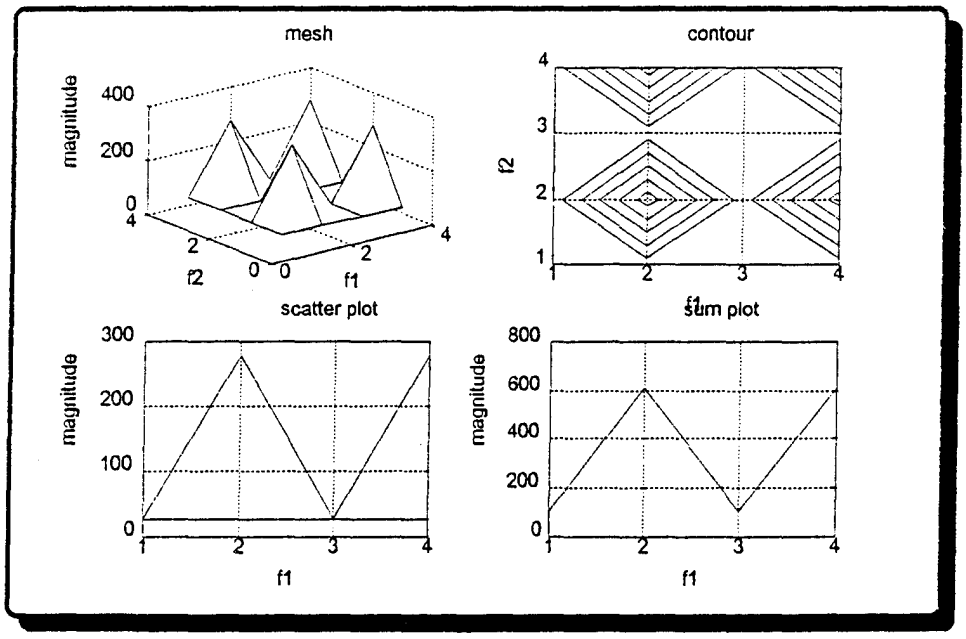

Figure 4.96: QPSK Outer Product Representation (Transform Length is 4, Incoherent)

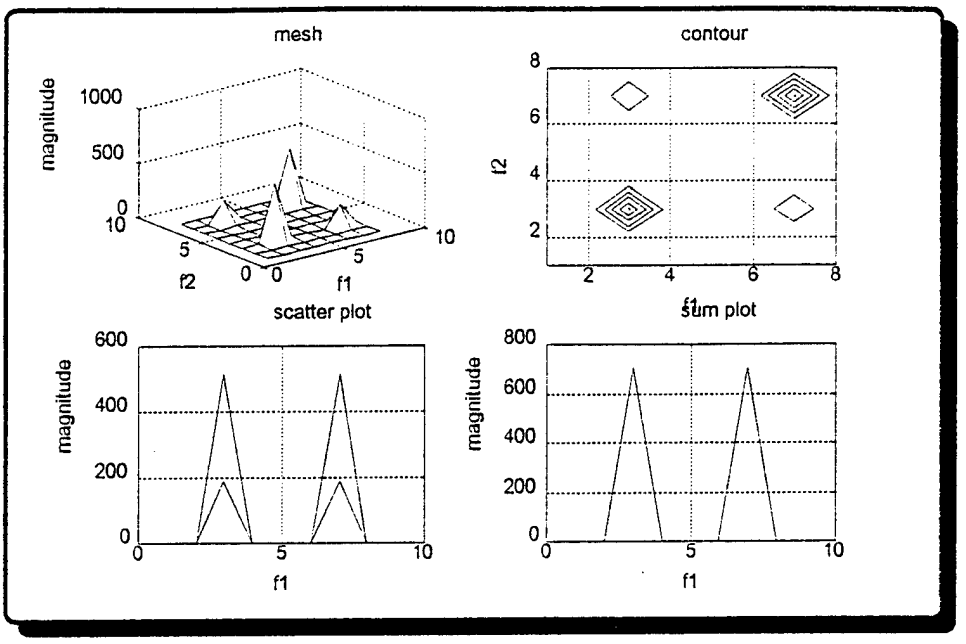

Figure 4.97: QPSK Outer Product Representation (Transform Length is 8, Coherent)

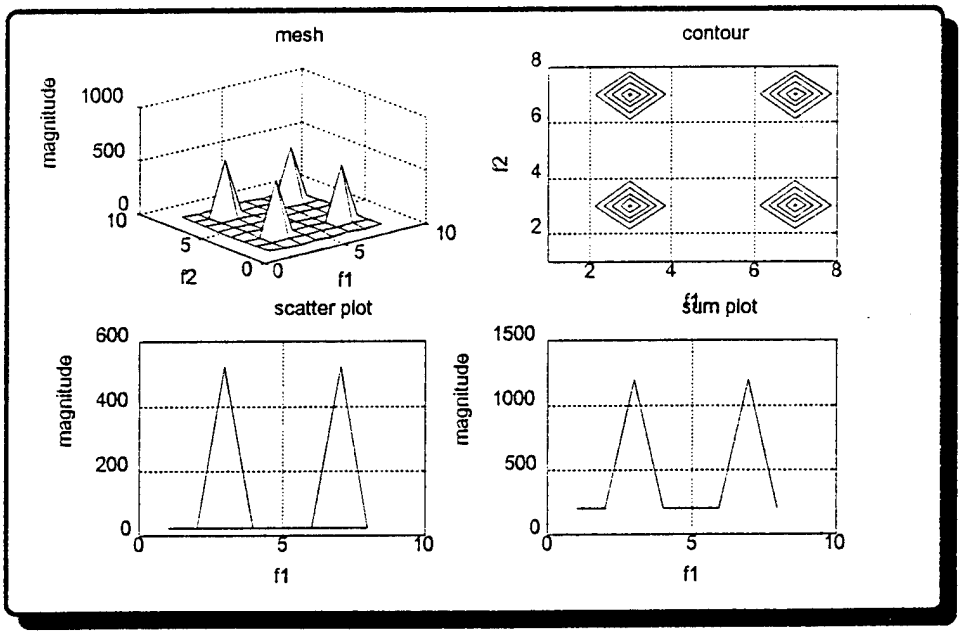

Figure 4.98: QPSK Outer Product Representation (Transform Length is 8, Incoherent)

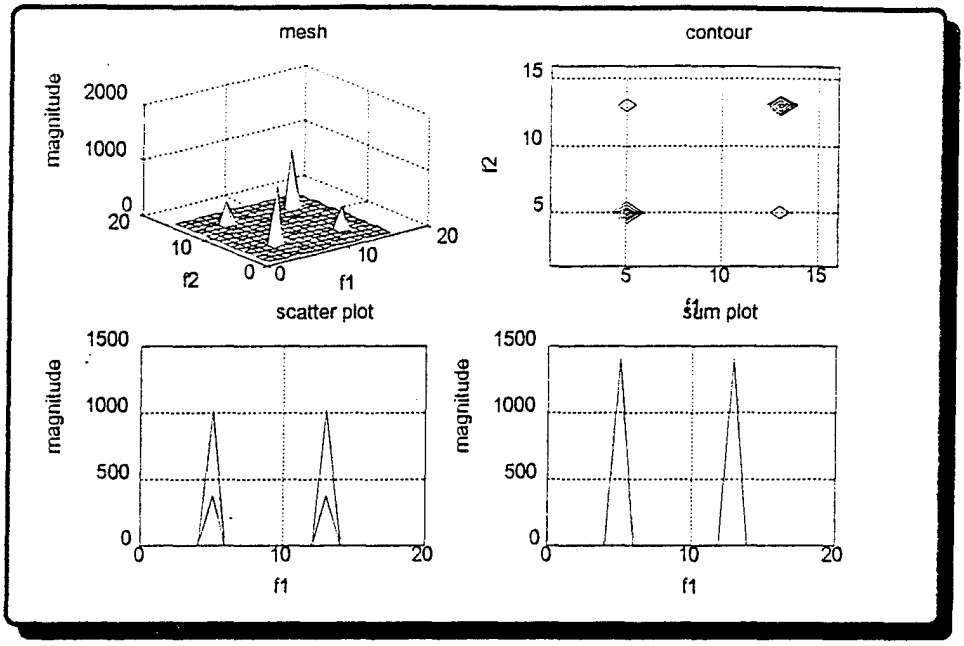

Figure 4.99: QPSK Outer Product Representation (Transform Length is 16, Coherent)

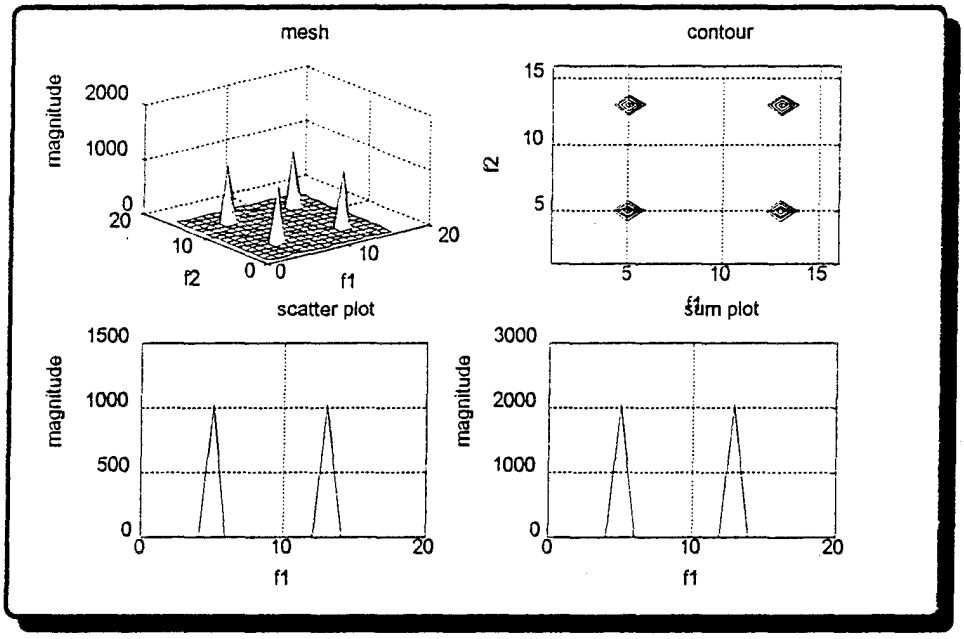

Figure 4.100: QPSK Outer Product Representation (Transform Length is 16, Incoherent)

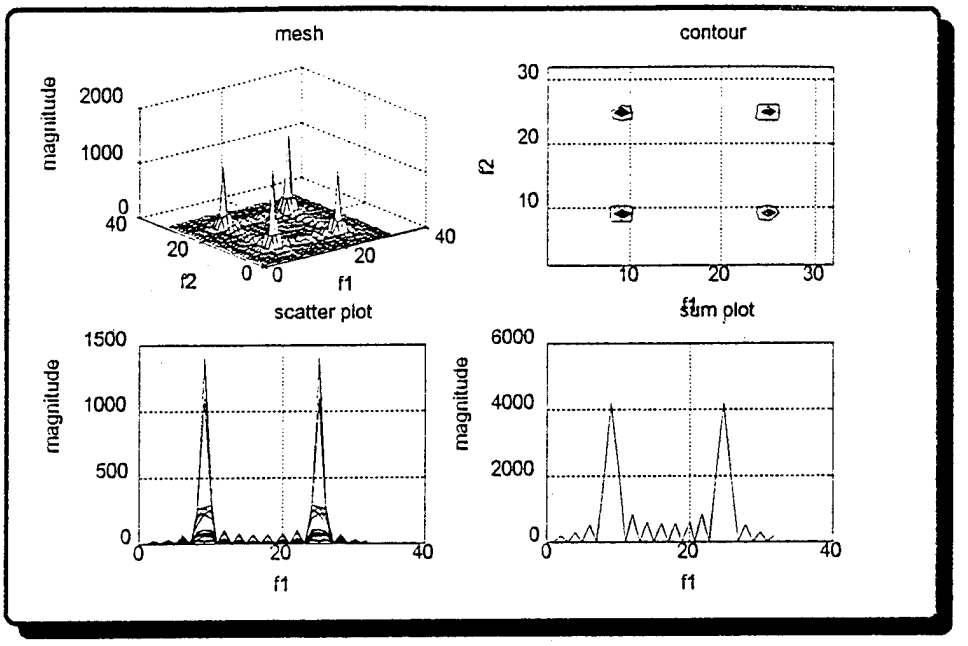

Figure 4.101: QPSK Outer Product Representation (Transform Length is 32, Coherent)

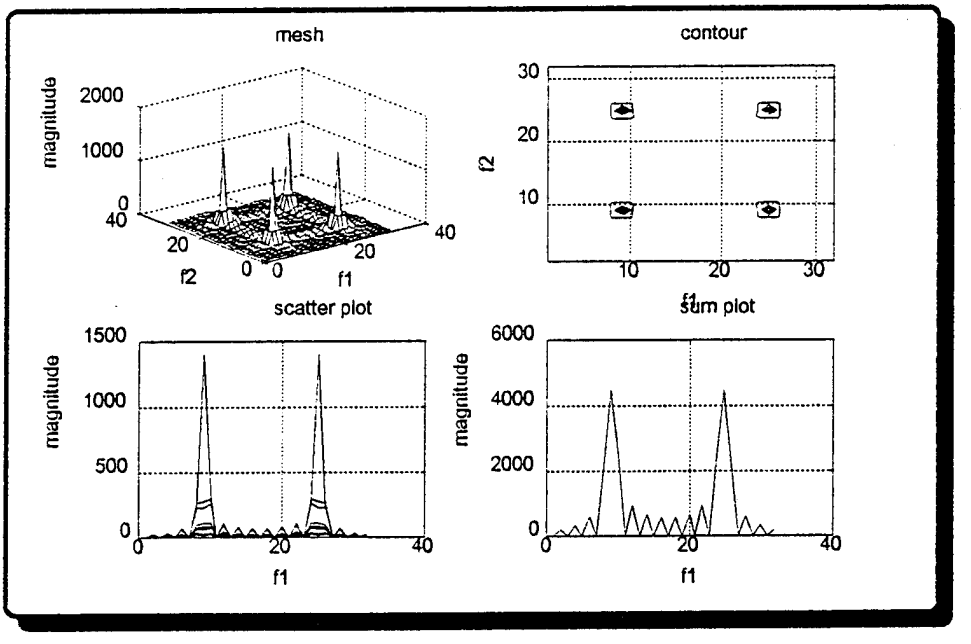

Figure 4.102: QPSK Outer Product Representation (Transform Length is 32, Incoherent)

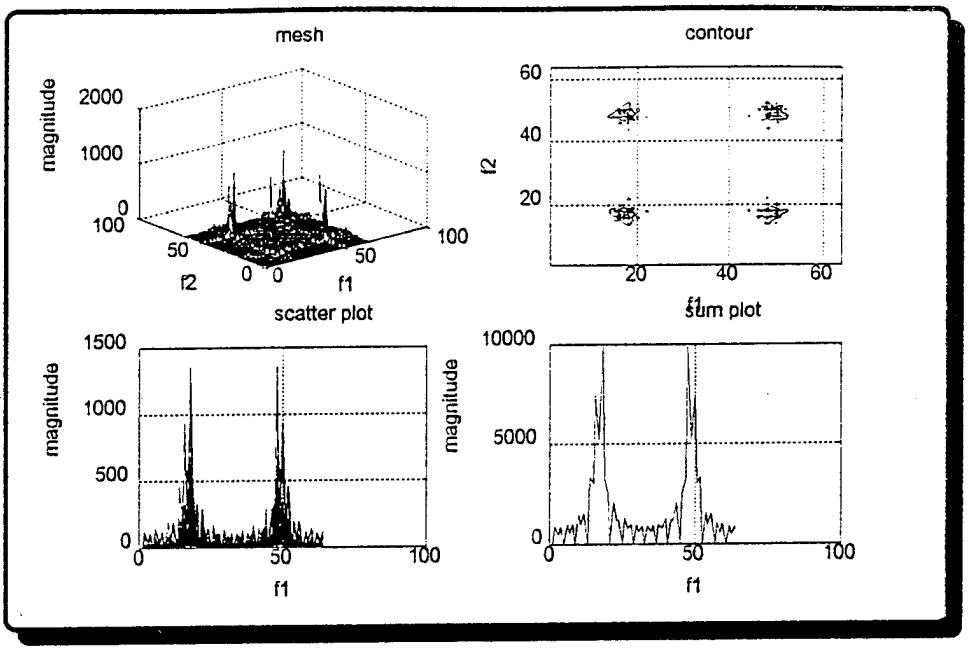

Figure 4.103: QPSK Outer Product Representation (Transform Length is 64, Coherent)

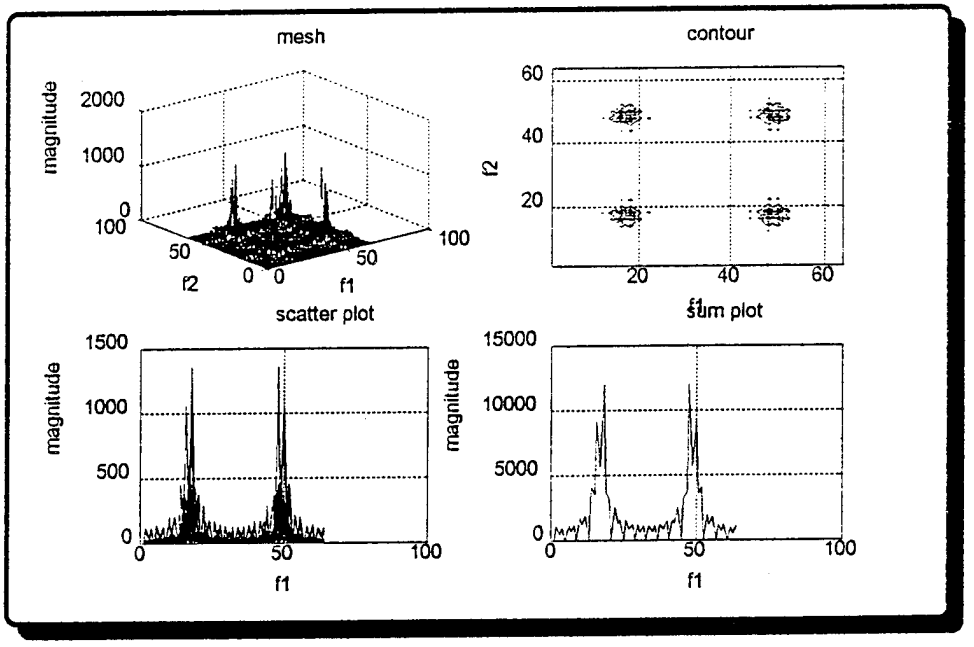

Figure 4.104: QPSK Outer Product Representation (Transform Length is 64, Incoherent)

Therefore, we choose a FFT size of 64 for the outer product representation of the QPSK signal.

For the remainder of this study, the following transform sizes were used: For BPSK, OOK, and FSK, in context of the spectrogram, the 1-1/2D_{IPS}, and the bispectrum analysis, a transform length equal to the symbol length (i.e., 16) was chosen. Half of the symbol length (i.e., 8) was chosen for QPSK. Four times the symbol length (i.e., 64) was chosen as the transform length for the outer product representation method.

V. SIGNAL PLUS NOISE ANALYSIS

In this chapter we compare the performance of the spectrogram, the 1-1/2D_{IPS}, the bispectrum, and the outer product representation methods. For the comparison, BPSK, QPSK, FSK, and OOK signals were used as input data. Gaussian noise was added to the original signals to create different SNR's. This allowed determination of the lowest SNR level at which the modulation type could be recognized.

Under some conditions, the two time-frequency methods (spectrogram and 1-1/2D_{IPS}) could recover the original signal (message) with a sign or phase uncertainty. The other two frequency-frequency methods (bispectrum and outer product representation) only revealed the modulation type. Unless otherwise specified, the transform lengths for the spectrograms, the 1-1/2D_{IPS} spectra and the bispectra were 16 and 64 for outer product representations.

A. BPSK

In this section, white Gaussian noise (AWGN) was added to the binary phase shift keyed (BPSK) signal. As stated, we expected 180° phase shifts at locations 33, 81, 97, 129, 161, and 193. For message recovery, these phase shifts at their appropriate locations must be detected.

Figure 5.1 shows the plot of the sinusoidal carrier, the message, the BPSK signal, and the BPSK signal with noise. Figure 5.2 through Figure 5.7 show the spectrograms for SNR levels of infinity, 20 dB, 15 dB, 10 dB, 5 dB, and 0 dB.

The phase shifts were apparent at the appropriate locations in the contour plots of all SNR levels of 15 dB or more. Transients in the contour plot represent phase shifts. But at the 15 dB SNR level (Figure 5.4), other transients due to noise appear. They corrupt the signal and confuse the observer. As a result we lost some ability to collect correct information about the message, modulation type, and bit rate for SNR levels below 20 dB.

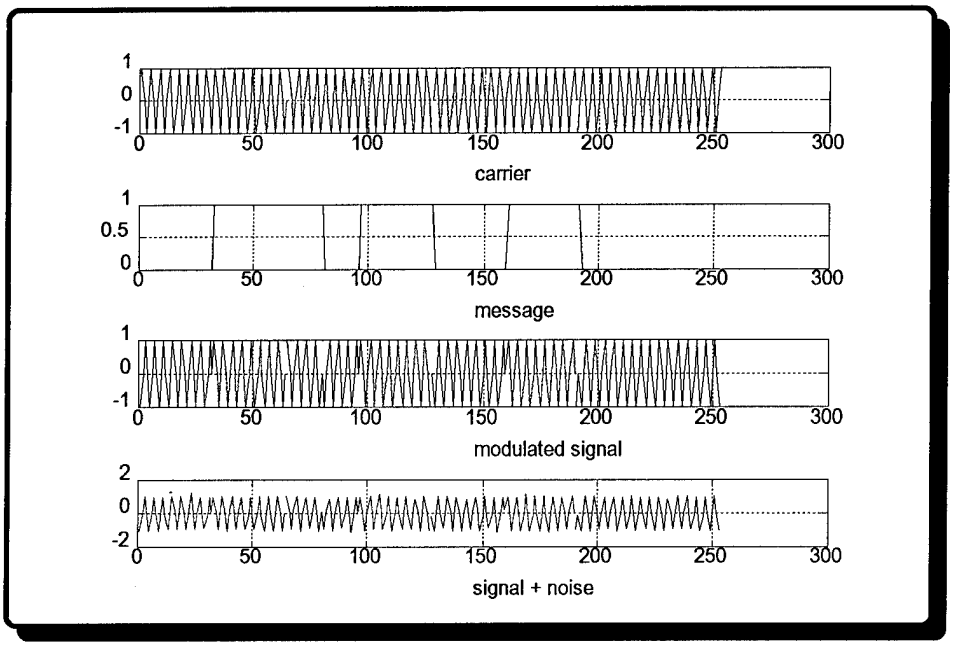

Figure 5.1: BPSK Generation with Noise

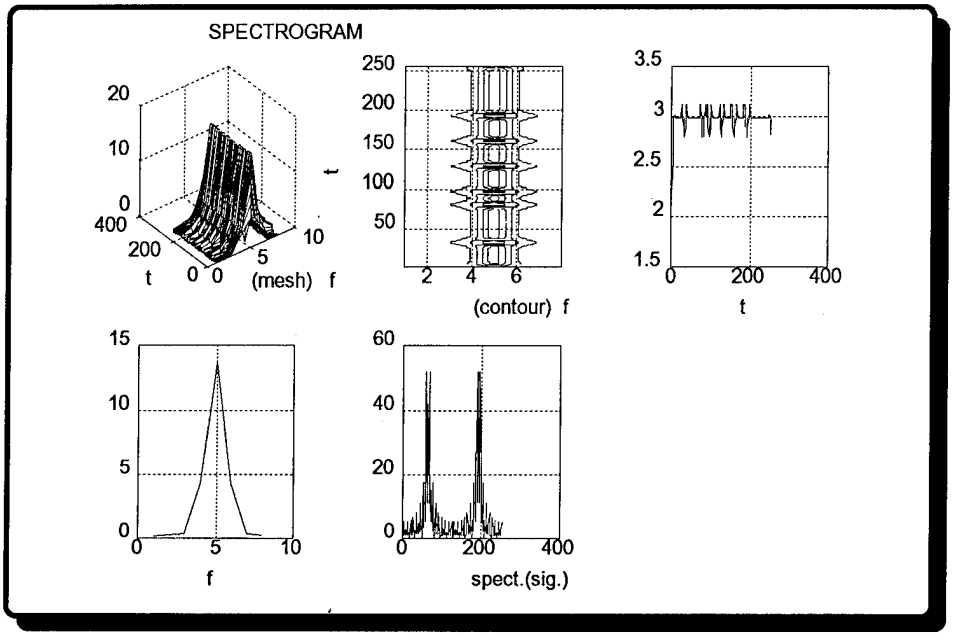

Figure 5.2: BPSK Spectrogram (Infinite SNR)

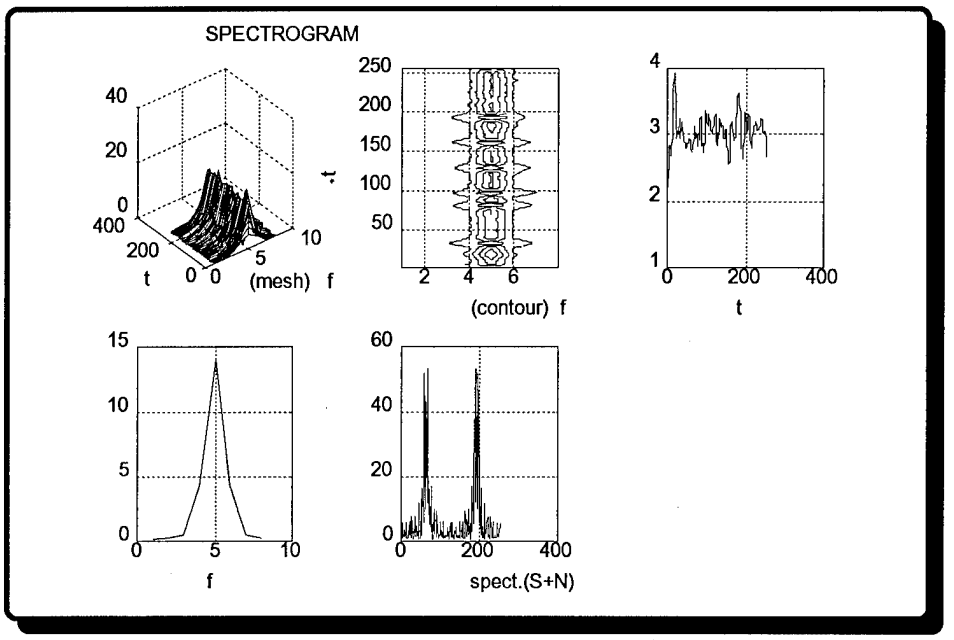

Figure 5.3: BPSK Spectrogram (SNR= +20 dB)

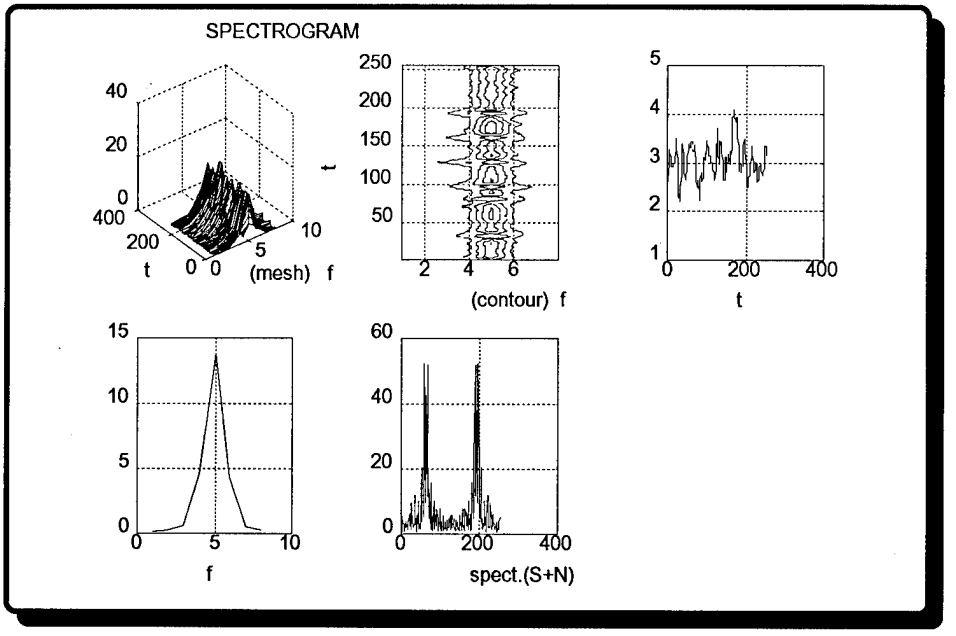

Figure 5.4: BPSK Spectrogram (SNR= +15 dB)

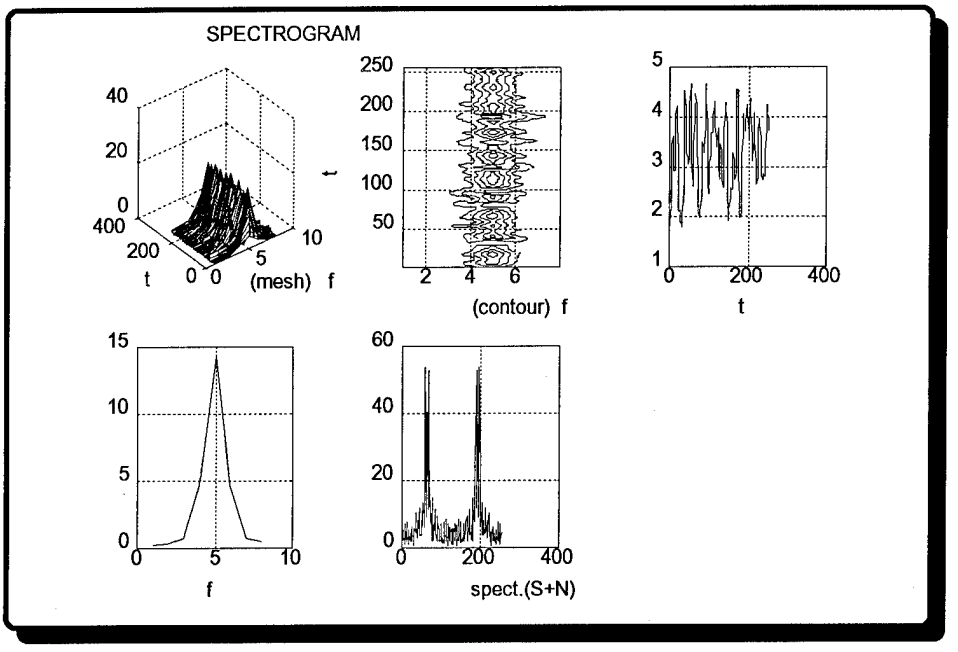

Figure 5.5: BPSK Spectrogram (SNR= +10 dB)

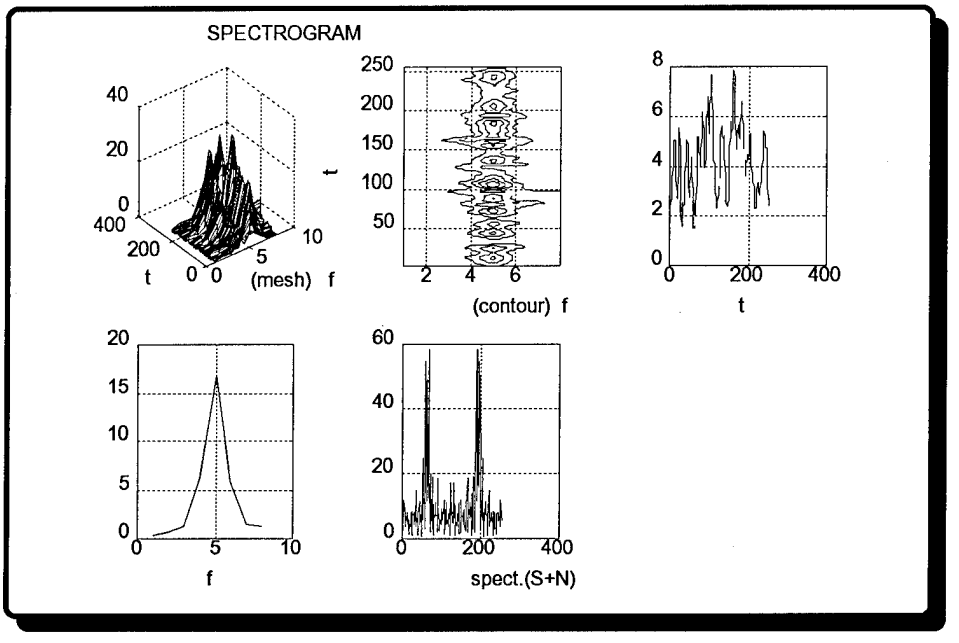

Figure 5.6: BPSK Spectrogram (SNR= +5 dB)

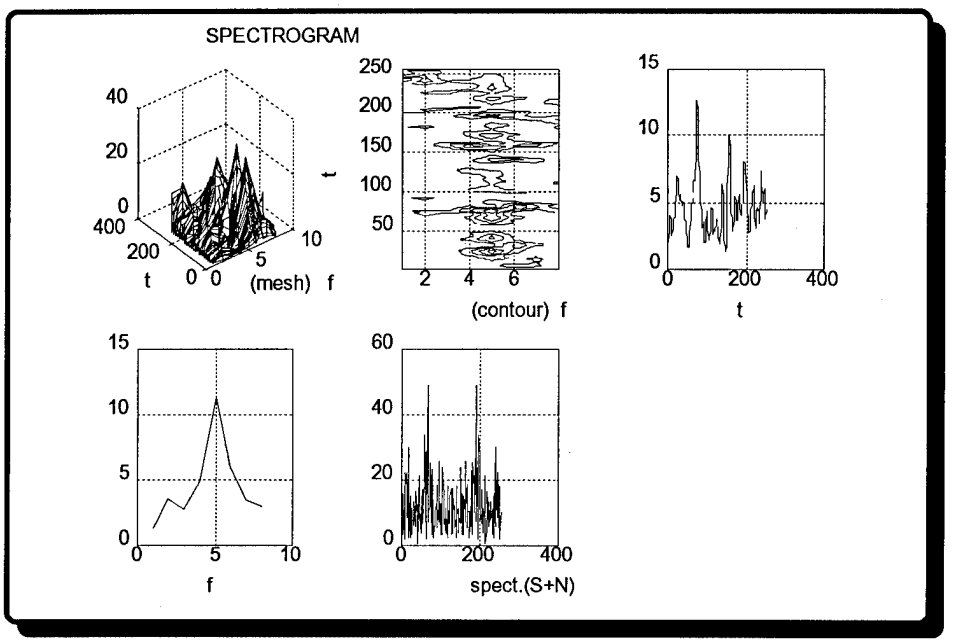

Figure 5.7: BPSK Spectrogram (SNR= +0 dB)

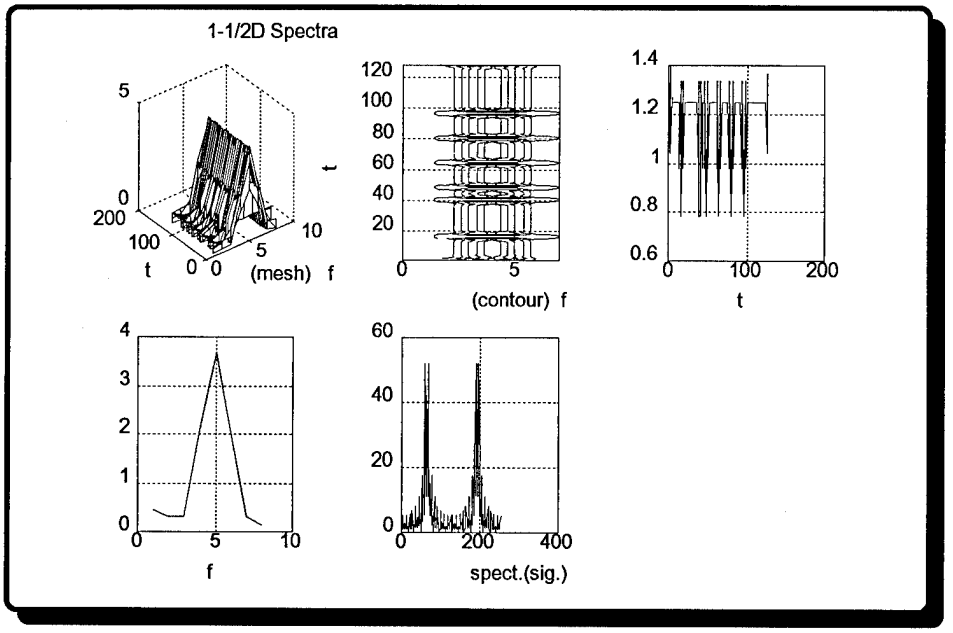

Figure 5.8: BPSK 1-1/2D Spectra (Infinite SNR)

Figure 5.8 through Figure 5.13 show the 1-1/2D_{IPS} spectra for SNR levels of infinity , 20 dB, 15 dB, 10 dB, 5 dB, and 0 dB. Phase shifts appear at the appropriate locations in the contour plots for 20 dB and above. Spreading (transients) in the contour plots represent these phase shifts. Below 20 dB, however, the noise makes the spectrum difficult to interpret.

Figure 5.14 through Figure 5.19 show the bispectrum for SNR levels of infinity, 20 dB, 15 dB, 10 dB, 5 dB, and 0 dB. From the bispectrum figures, we were not able to see any time-related information. They do, however, represent unique frequency-frequency spectra which were useful to differentiate between modulation schemes. At the infinite SNR level, there were many peaks in the mesh and corresponding contour plots. The heights of the peaks were very low. At 20 dB and 15 dB SNR levels, the magnitudes of the peaks became higher with a dominant peak approximately at location (0.36, 0.36) in the contour plots. This peak was most likely due to noise. As the SNR level decreased to 5 dB, this peak was still recognizable but it was no longer the dominant peak. Also, below the 15 dB SNR level, some other peaks emerged. Below the 5 dB SNR level, the original peak at (0.36, 0.36) was not recognizable.

Figure 5.20 through Figure 5.29 show the outer product representation (coherent and incoherent summation) for SNR levels of infinity, 20 dB, 10 dB, 0 dB, and -5 dB. These figures show that the outer product form was more noise tolerant than the other spectral methods. This may be a result of higher processing gain due to the larger transform length. We were able to get frequency related information but not time related information. The outer product representation was useful for differentiating BPSK modulation from the other modulations by interpreting the contour and frequency sum plots. BPSK has a spectral signature similar to pound sign (#) in the contour plot, and two spikes each with almost two equal peaks in the sum plot. This information was recognizable until the SNR fell below 10 dB.

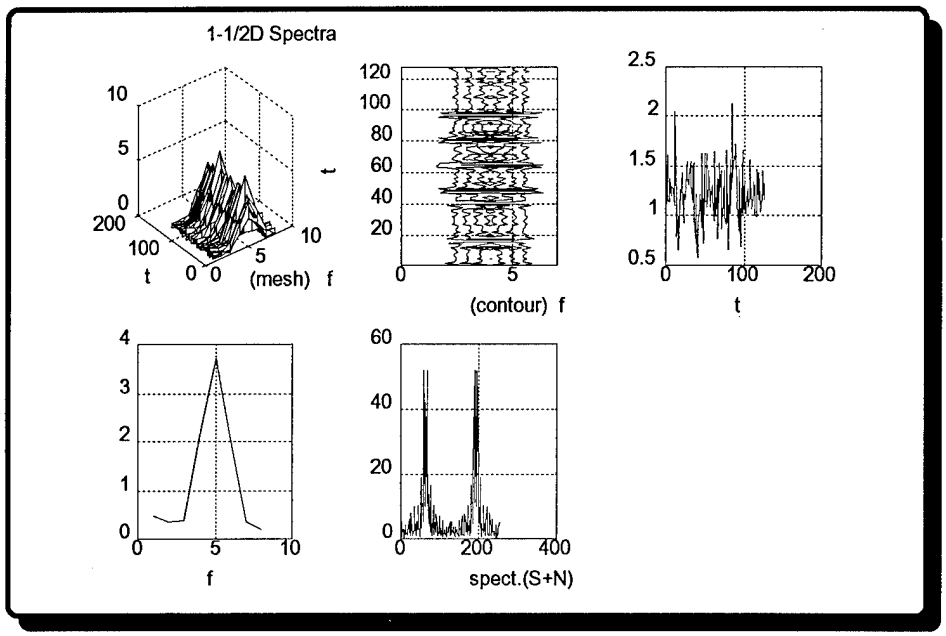

Figure 5.9: BPSK 1-1/2D Spectra (SNR= +20 dB)

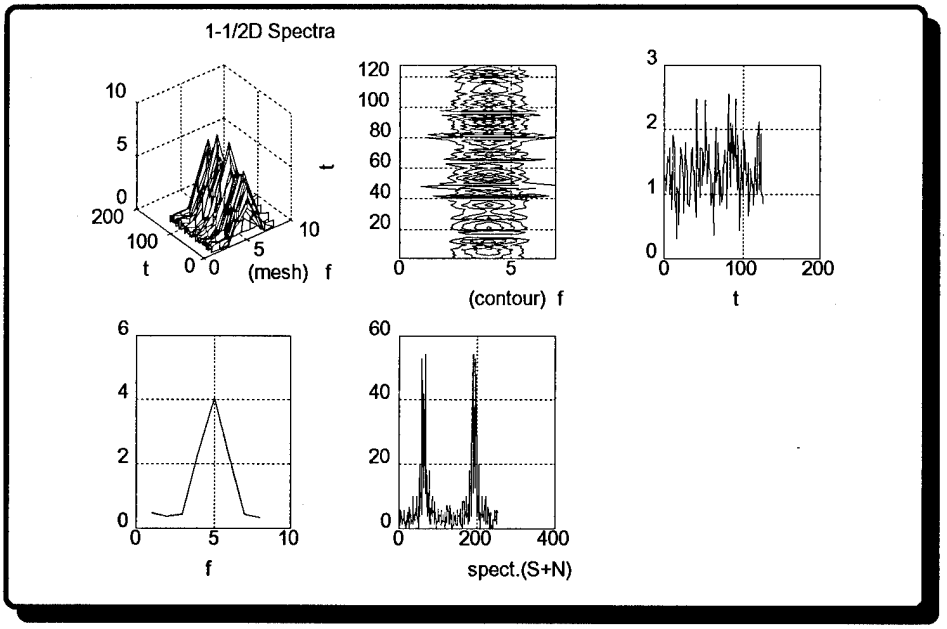

Figure 5.10: BPSK 1-1/2D Spectra (SNR= +15 dB)

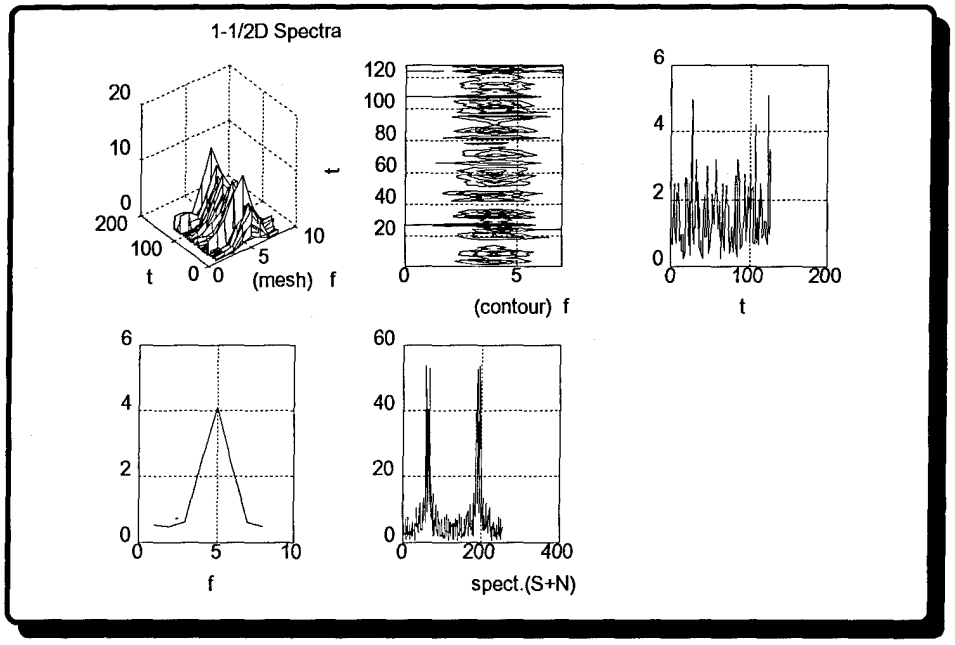

Figure 5.11: BPSK 1-1/2D Spectra (SNR= +10 dB)

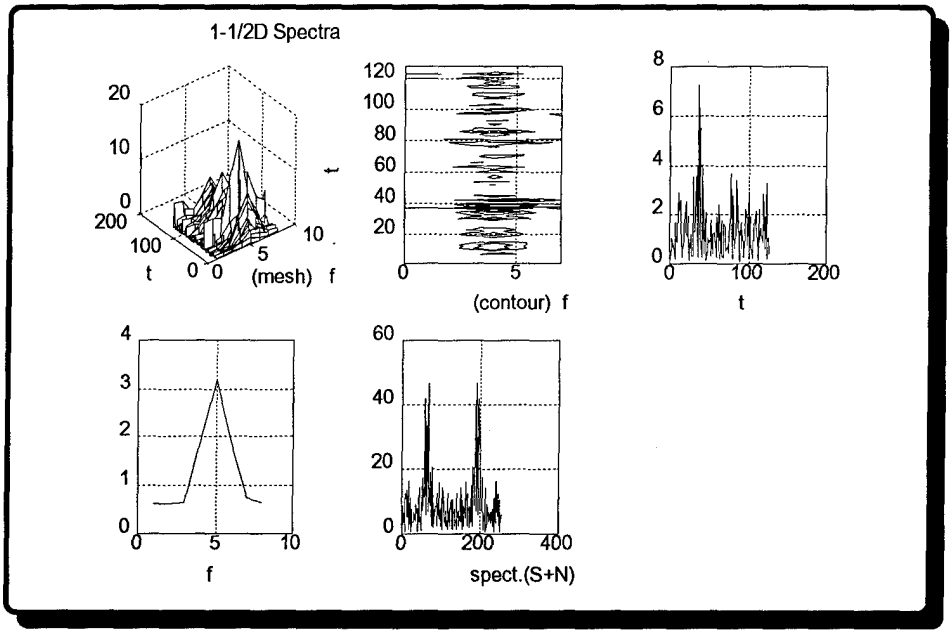

Figure 5.12: BPSK 1-1/2D Spectra (SNR= +5 dB)

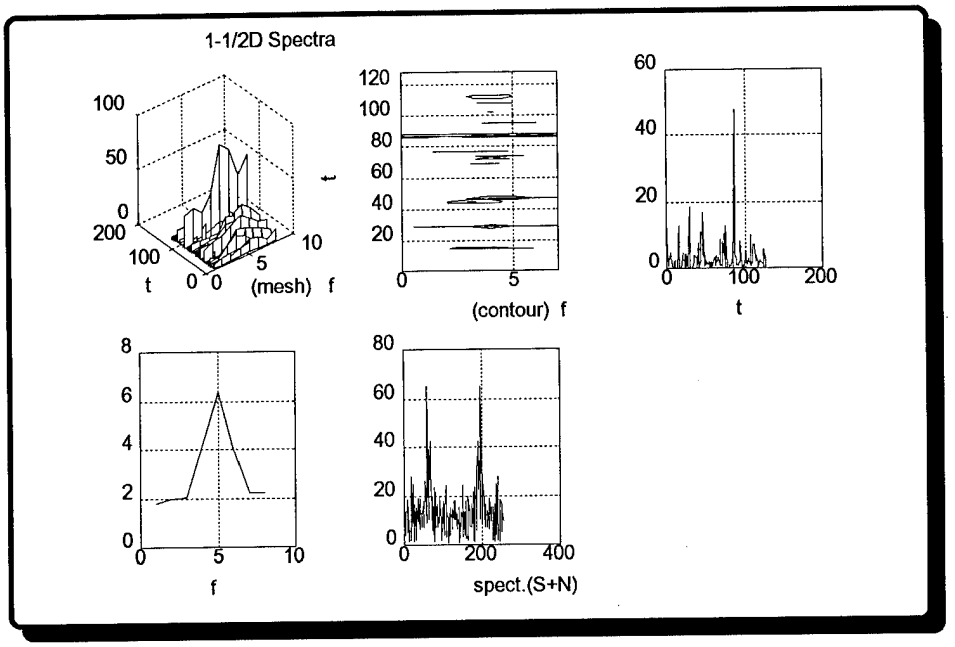

Figure 5.13: BPSK 1-1/2D Spectra (SNR= 0 dB)

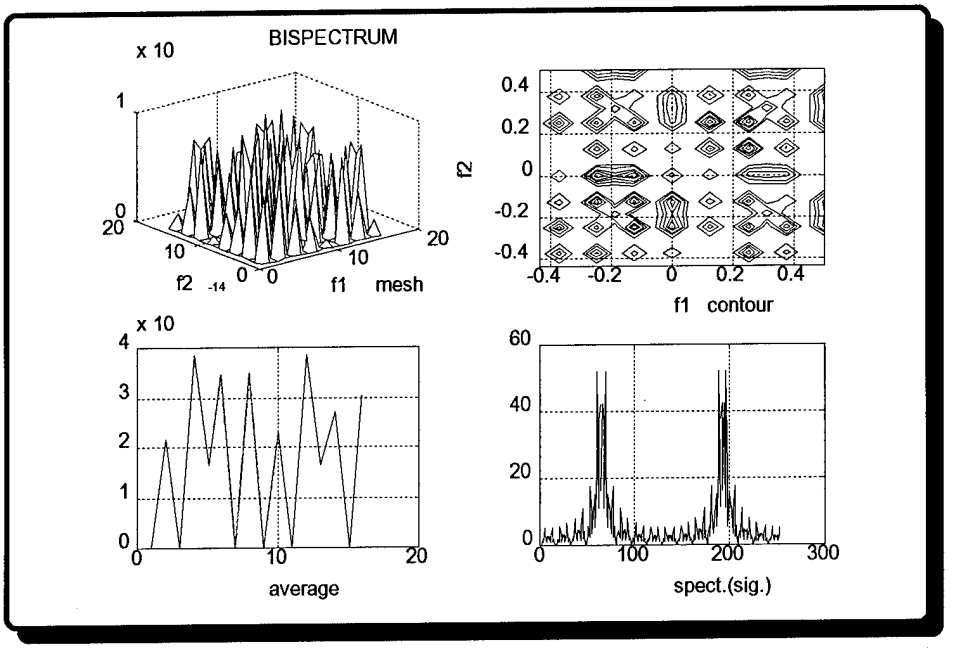

Figure 5.14: BPSK Bispectrum (Infinitive SNR)

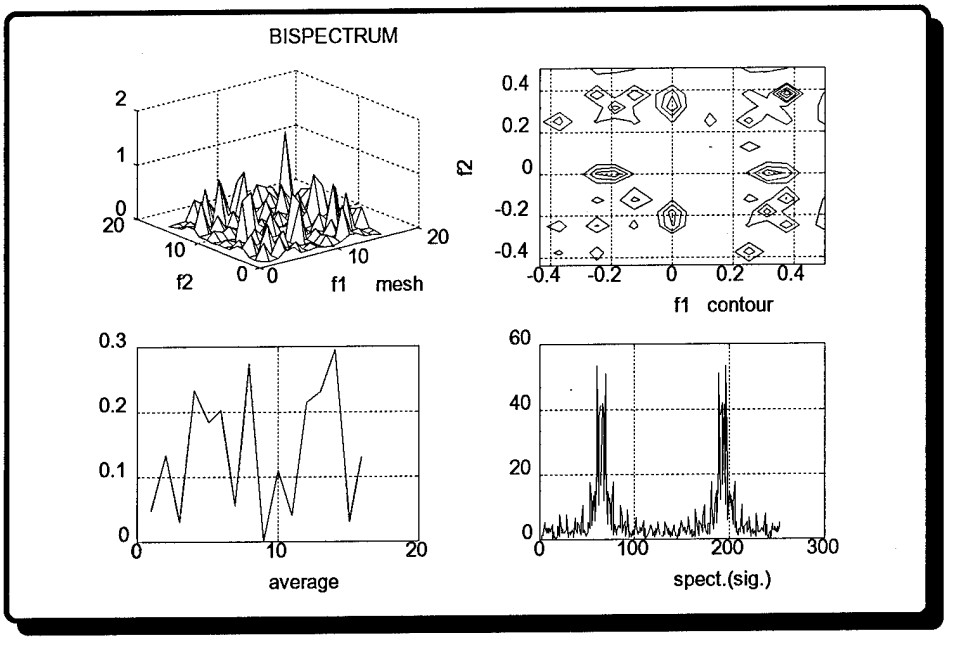

Figure 5.15: BPSK Bispectrum (SNR= +20 dB)

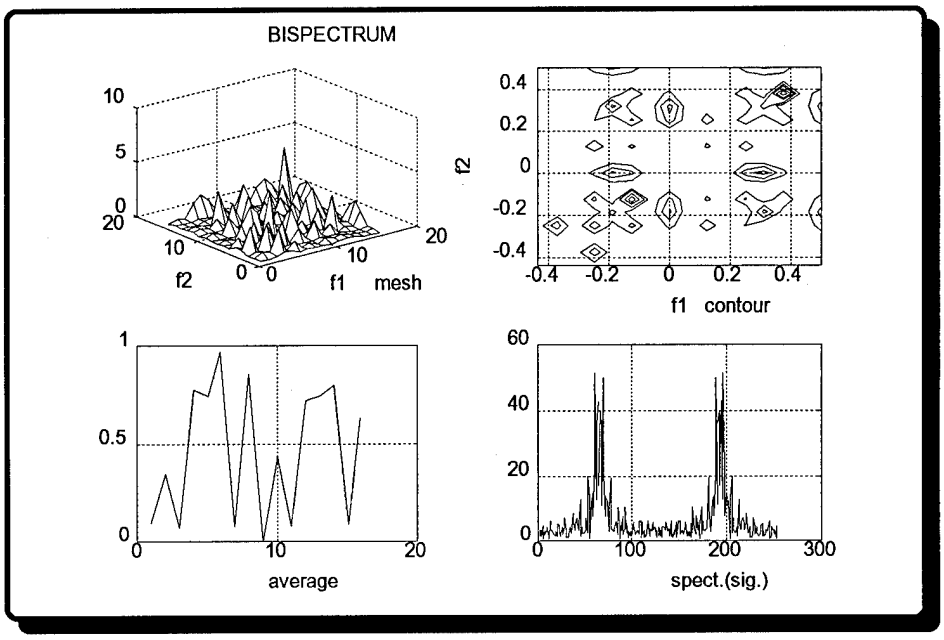

Figure 5.16: BPSK Bispectrum (SNR= +15 dB)

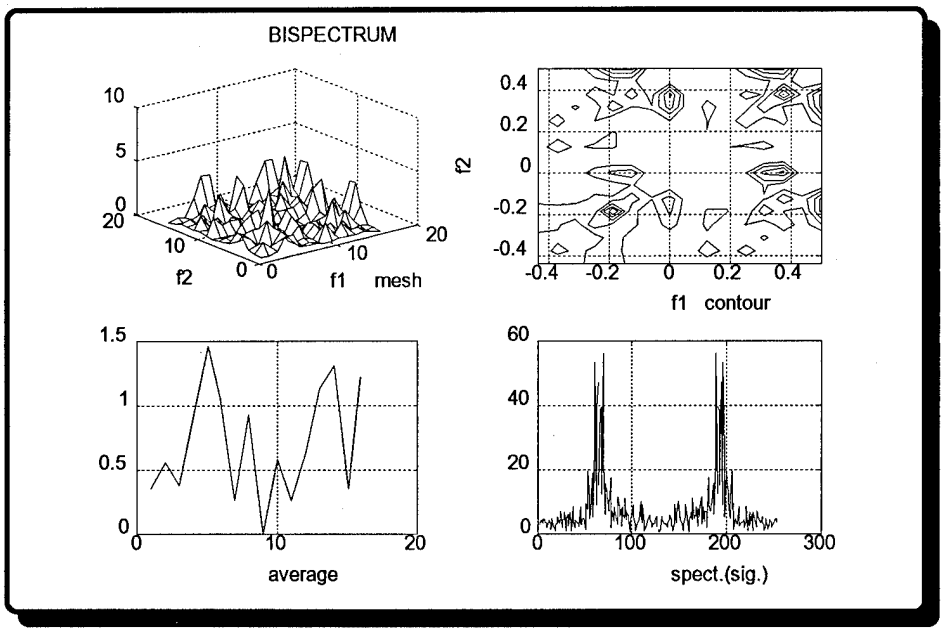

Figure 5.17: BPSK Bispectrum (SNR= +10 dB)

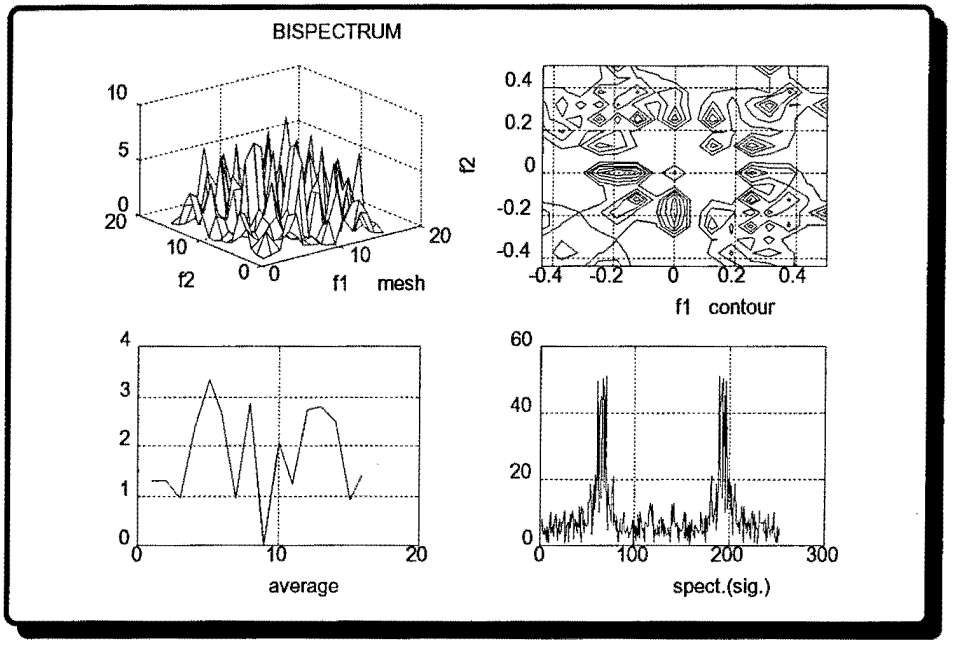

Figure 5.18: BPSK Bispectrum (SNR= +5 dB)

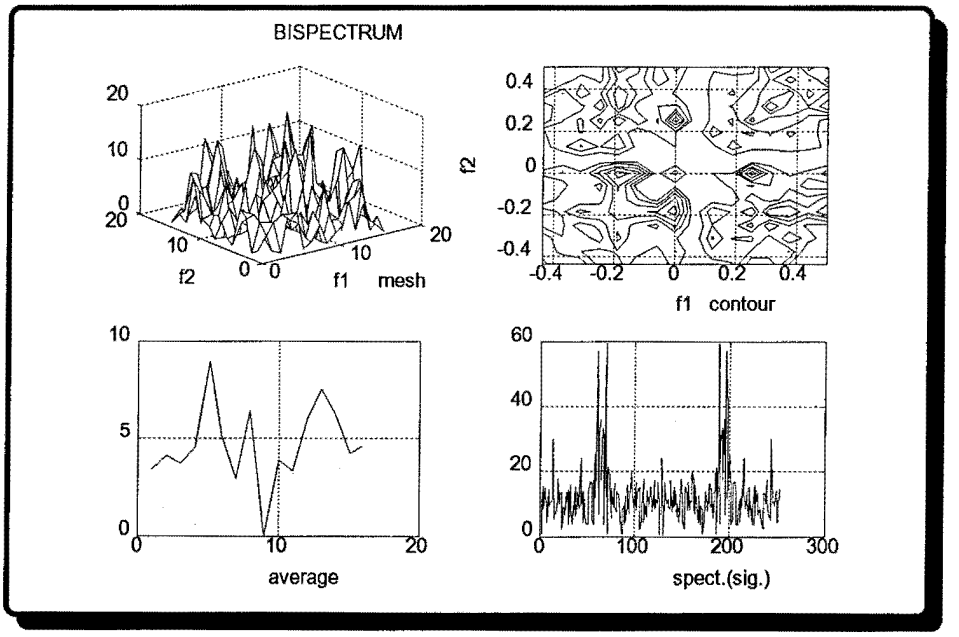

Figure 5.19: BPSK Bispectrum (SNR= +0 dB)

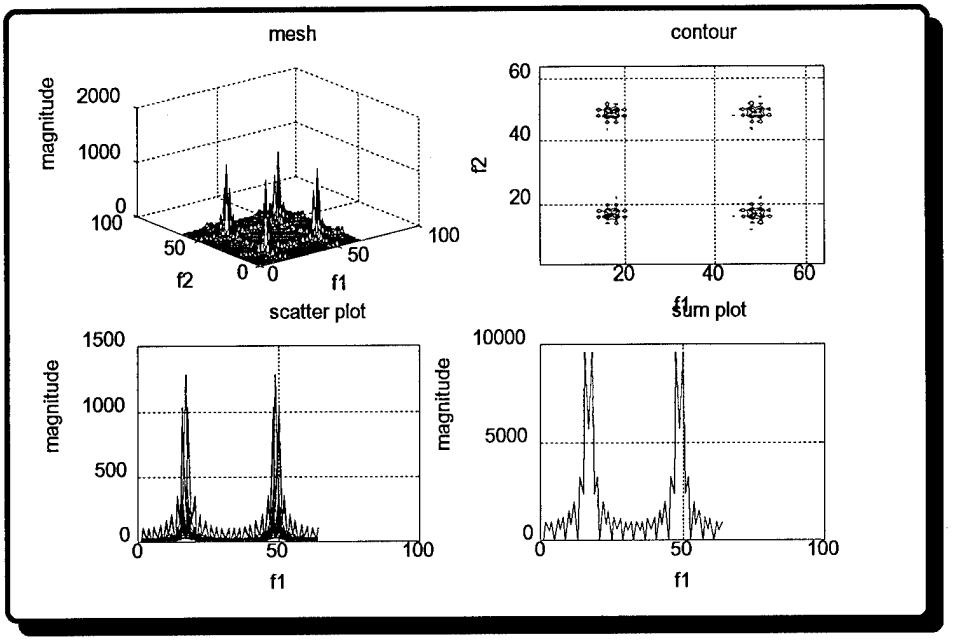

Figure 5.20: BPSK Outer Product Representation (Coherent, Infinite SNR)

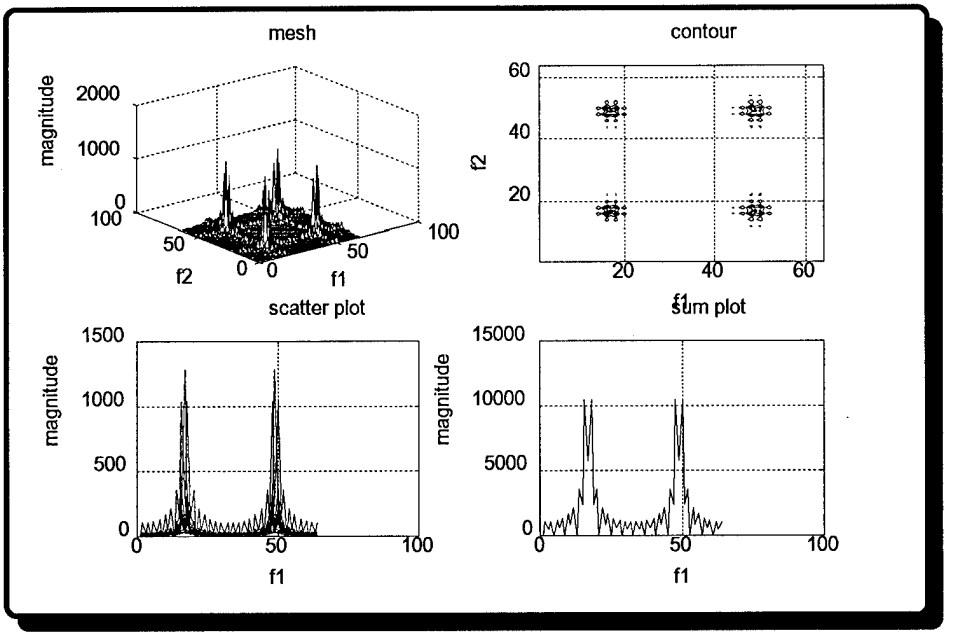

Figure 5.21: BPSK Outer Product Representation (Incoherent, Infinite SNR)

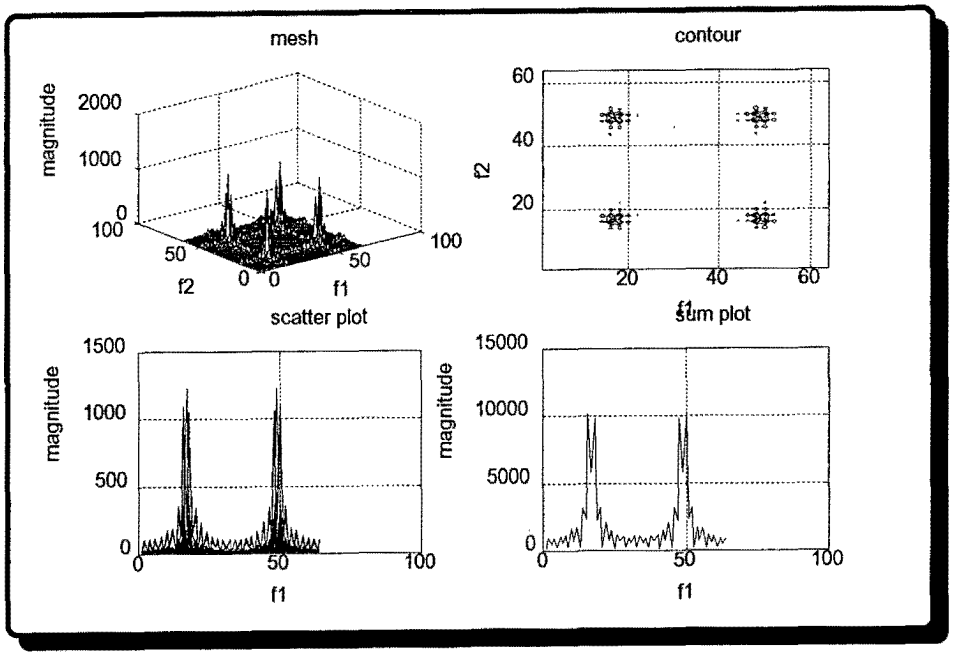

Figure 5.22: BPSK Outer Poduct Representation (Coherent, SNR= +20 dB)

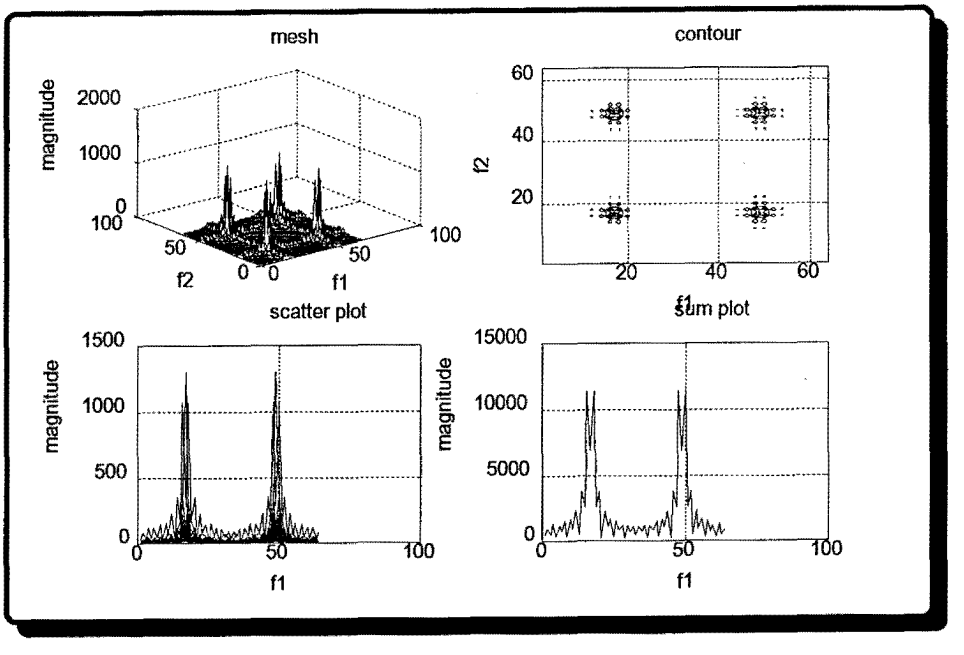

Figure 5.23: BPSK Outer Poduct Representation (Incoherent, SNR= +20 dB)

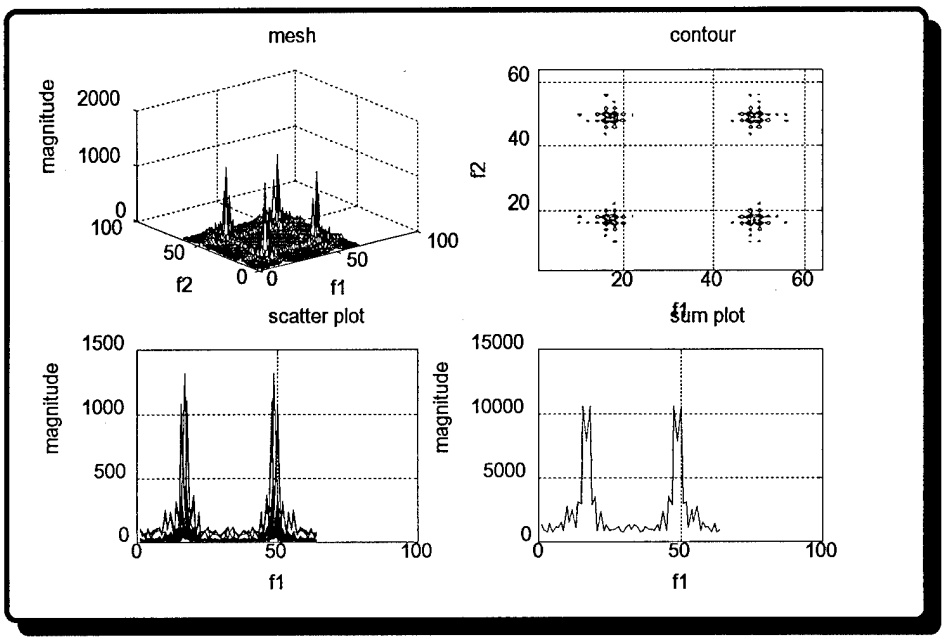

Figure 5.24: BPSK Outer Poduct Representation (Coherent, SNR= +10 dB)

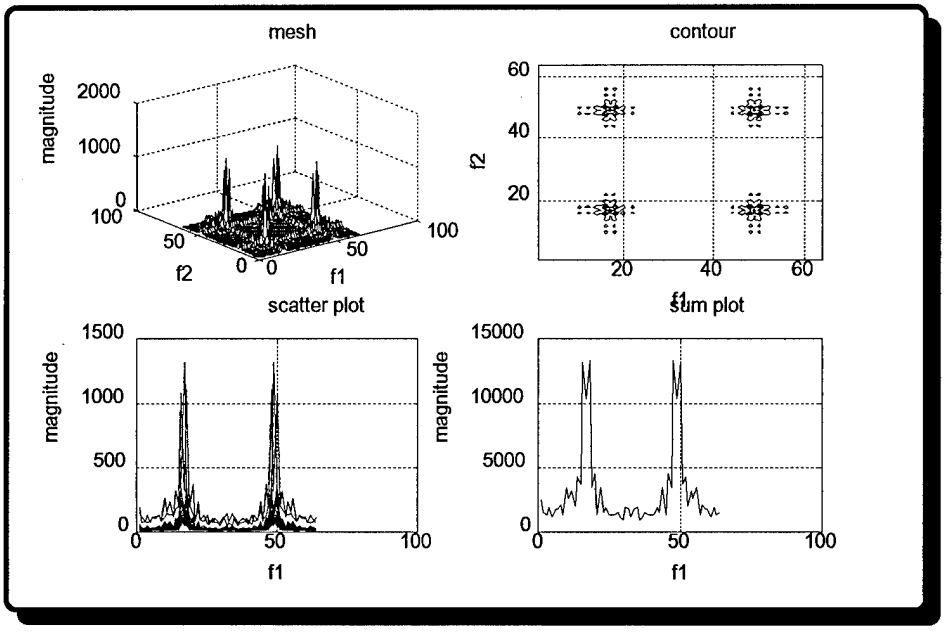

Figure 5.25: BPSK Outer Poduct Representation (Incoherent, SNR= +10 dB)

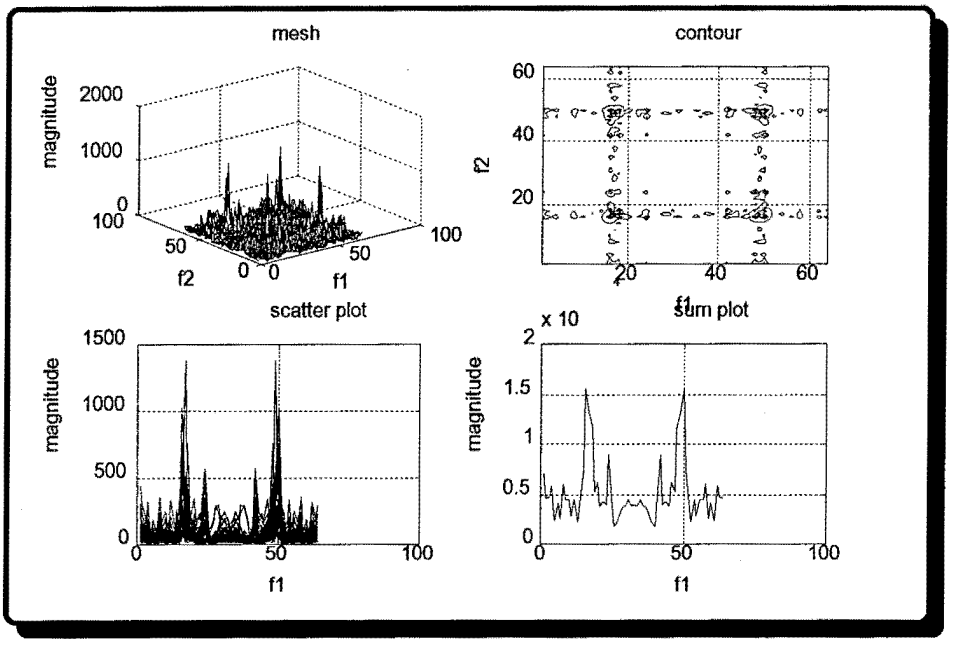

Figure 5.26: BPSK Outer Poduct Representation (Coherent, SNR= +0 dB)

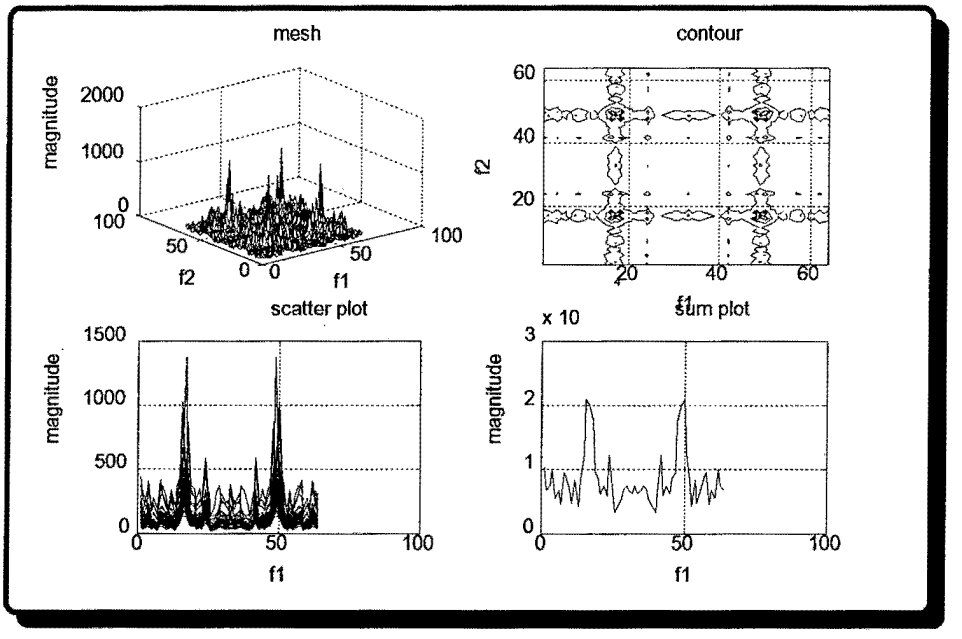

Figure 5.27: BPSK Outer Poduct Representation (Incoherent, SNR= +0 dB)

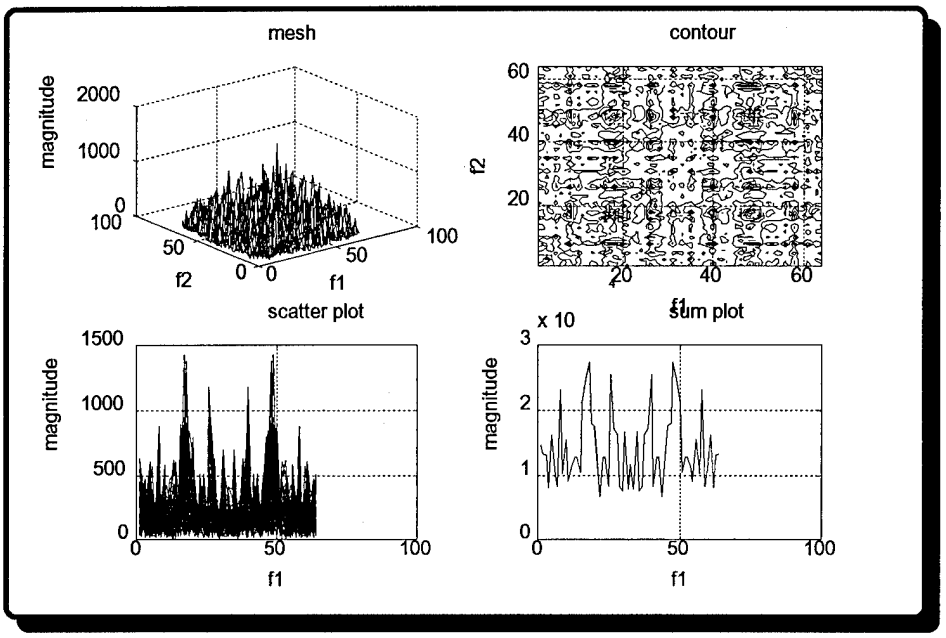

Figure 5.28: BPSK Outer Poduct Representation (Coherent, SNR= -5 dB)

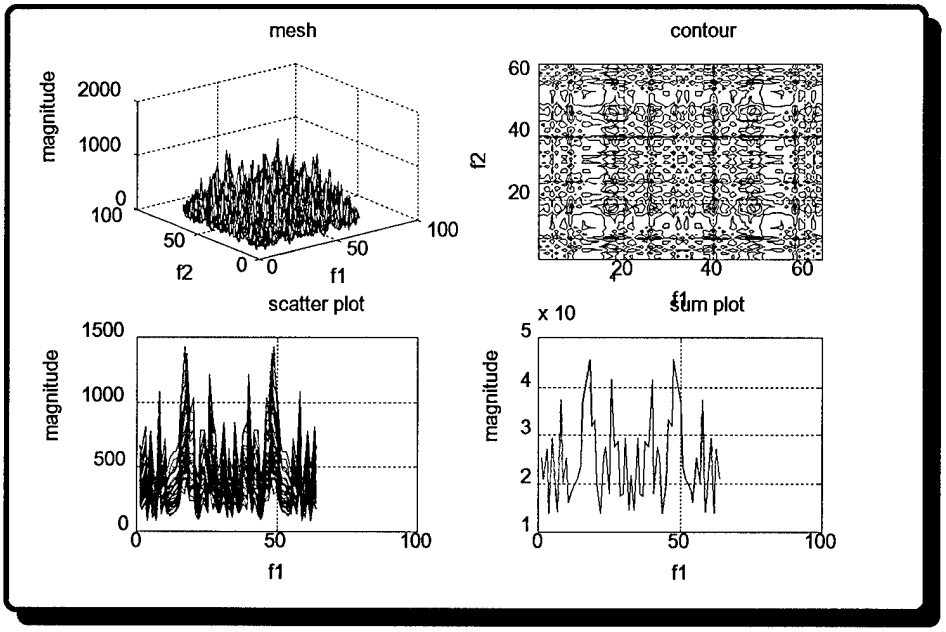

Figure 5.29: BPSK Outer Poduct Representation (Incoherent, SNR= -5 dB)

B. FSK

In this section, white Gaussian noise (WGN) was added to the binary frequency shift keyed (FSK) signal. Different SNR levels were used to examine the signal in the presence of noise. As stated previously, we expected frequency shifts at locations 33, 81, 97, 129, 161, and 193 when interpreting time-frequency plots.

Figure 5.30 shows the plot of the sinusoidal carrier, the message, the FSK modulated signal, and the FSK modulated signal with noise. Figure 5.31 through Figure 5.36 show the spectrograms for SNR levels of infinity, 20 dB, 15 dB, 10 dB, 5 dB, and 0 dB. The frequency shifts were apparent at the appropriate locations in the contour plots for SNR levels of 10 dB and above. Below 10 dB, we were unable to recognize frequency shifts at their appropriate locations, despite being able to estimate, to some extent, the modulation type. As a result, we were loosing the ability to obtain message information, modulation type, and bit rate for SNR levels below 10 dB.

Figure 5.37 through Figure 5.42 show the 1-1/2D_{IPS} spectral results. The frequency shifts appeared at their appropriate locations in the contour plots for SNR levels of 20 dB and above. Because of the noise components, the spectrum became hard to interpret below the 20 dB SNR level. As a result, we lost the ability to get the correct information about the message, modulation type, and bit rate at a SNR level below 20 dB.

Figure 5.43 through Figure 5.48 show the bispectral results. The bispectral figures have a unique frequency-frequency representation which was useful for differentiating FSK from the other modulation schemes. At an infinite SNR level, the FSK bispectrum pictures, especially the contour plot, were well defined (1 high peak, and 2 smaller peaks). This information was recognizable until the SNR fell below 15 dB. At the low SNR levels, we saw more noise peaks (see Fig. 5.46, 5.47 and 5.48).

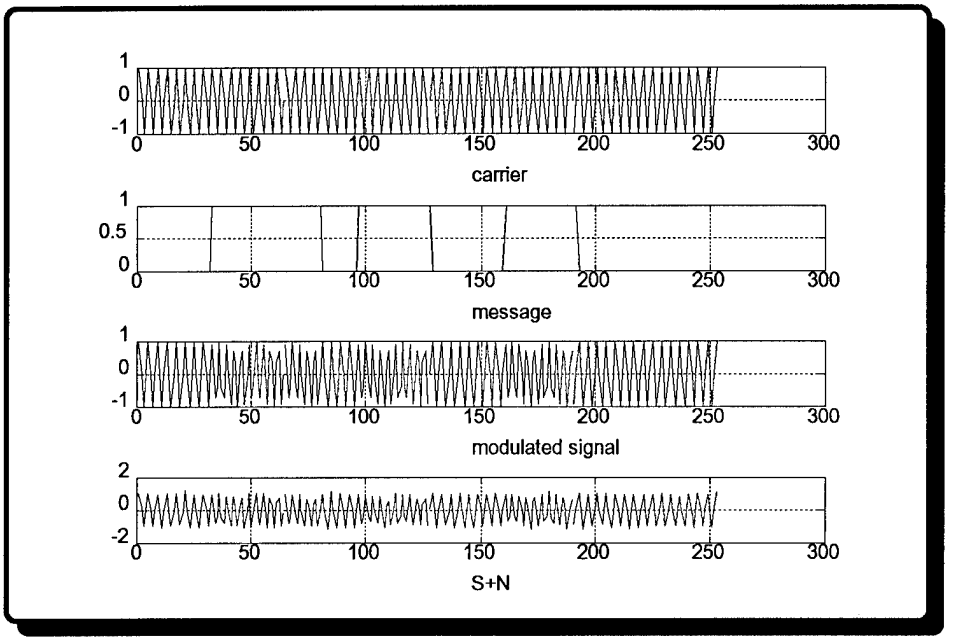

Figure 5.30: FSK Generation With Noise

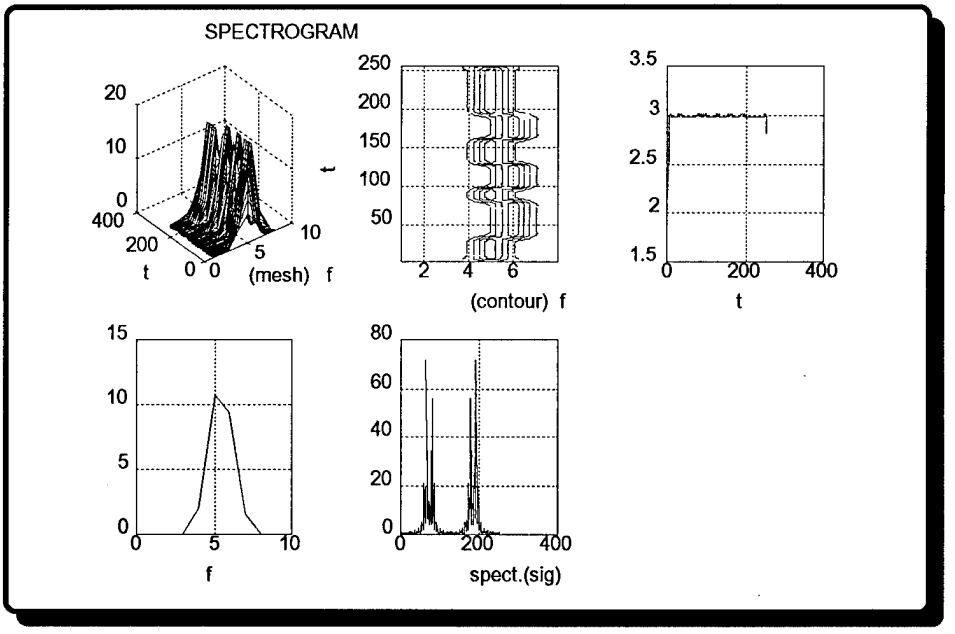

Figure 5.31: FSK Spectrogram (Infinite SNR)

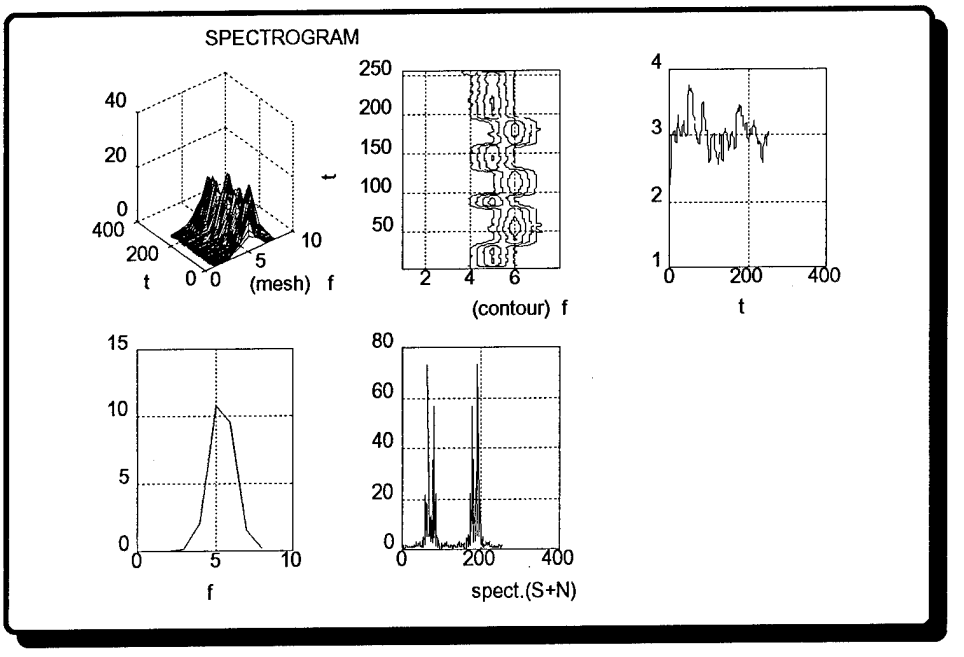

Figure 5.32: FSK Spectrogram (SNR= +20 dB)

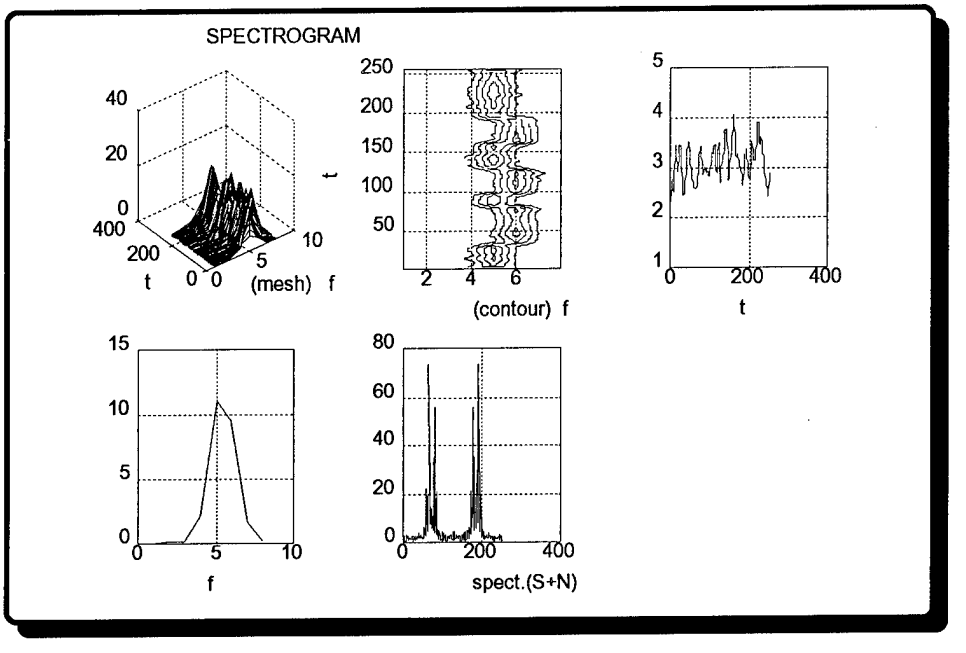

Figure 5.33: FSK Spectrogram (SNR= +15 dB)

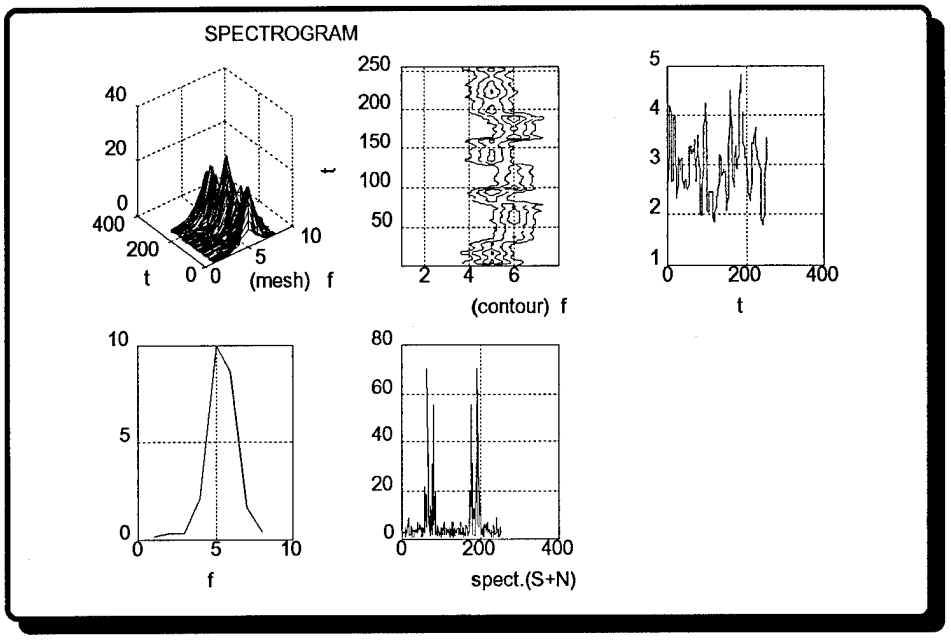

Figure 5.34: FSK Spectrogram (SNR= +10 dB)

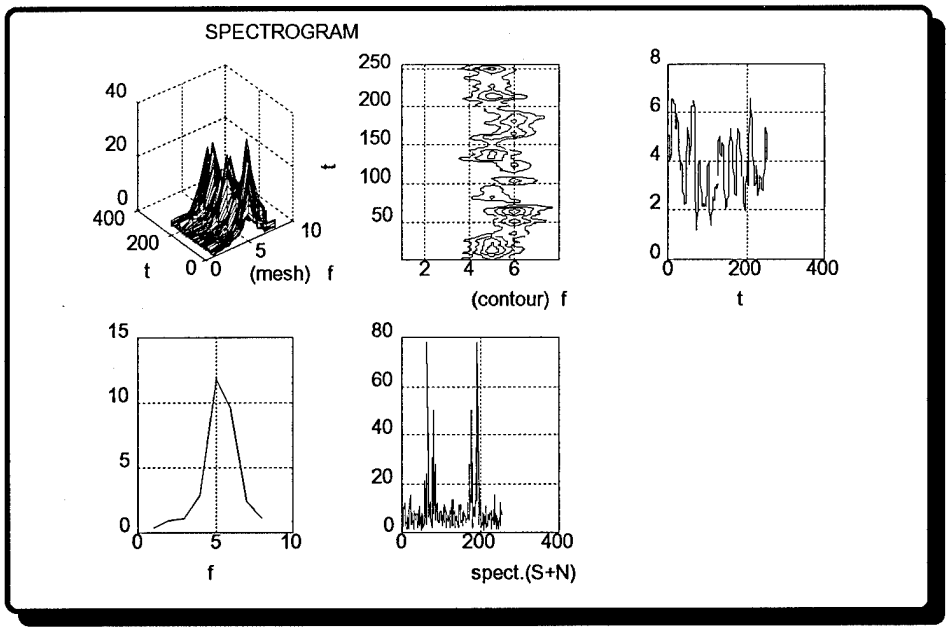

Figure 5.35: FSK Spectrogram (SNR= +5 dB)

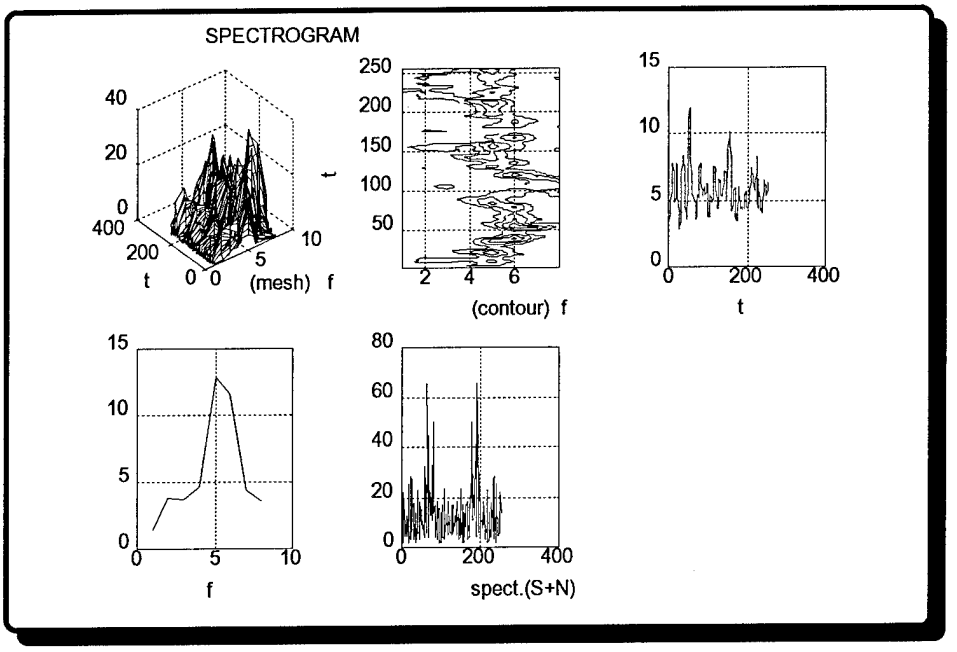

Figure 5.36: FSK Spectrogram (SNR= 0 dB)

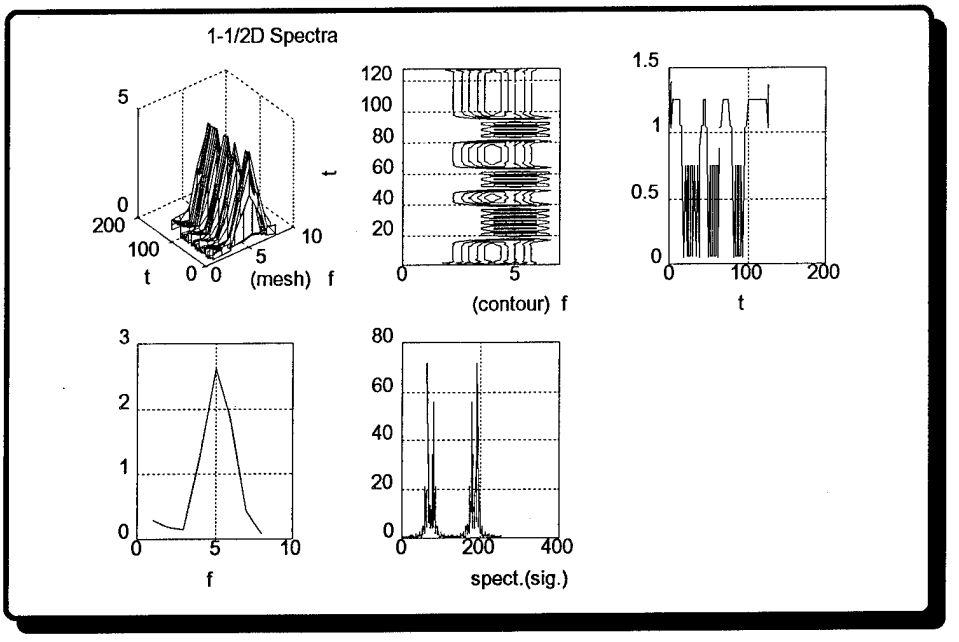

Figure 5.37: FSK 1-1/2D Spectra (Infinite SNR)

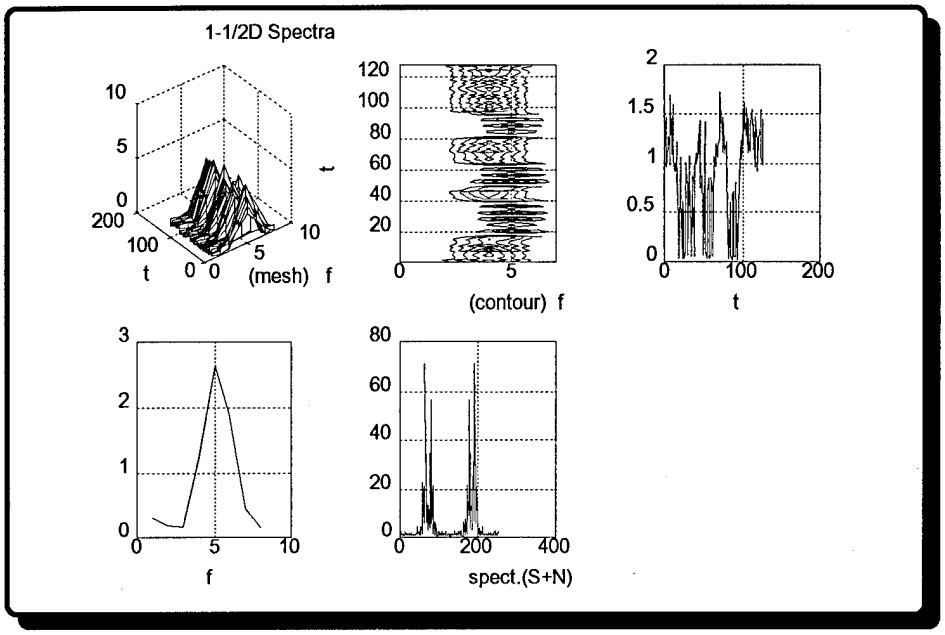

Figure 5.38: FSK 1-1/2D Spectra (SNR= +20 dB)

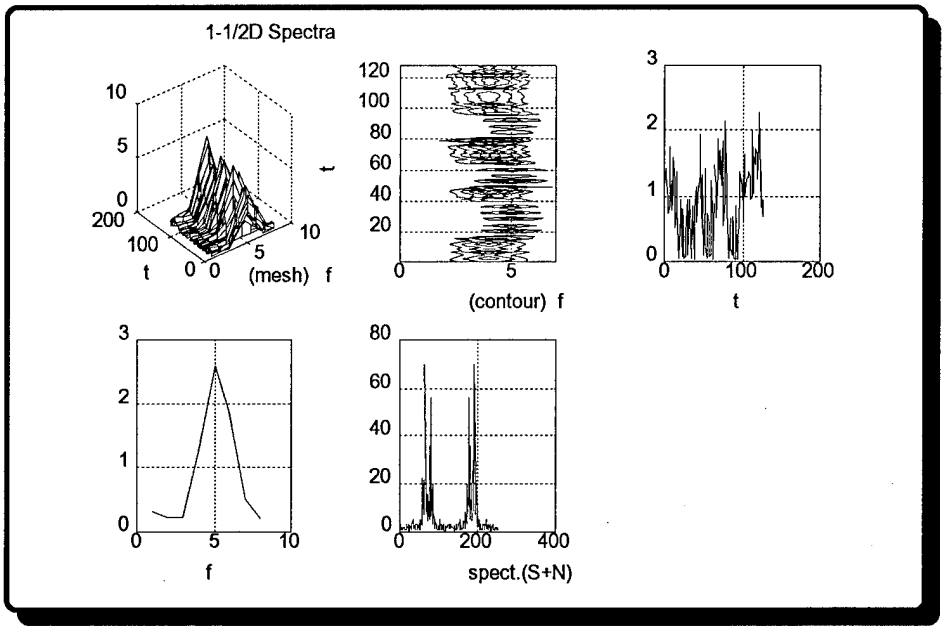

Figure 5.39: FSK 1-1/2D Spectra (SNR= +15 dB)

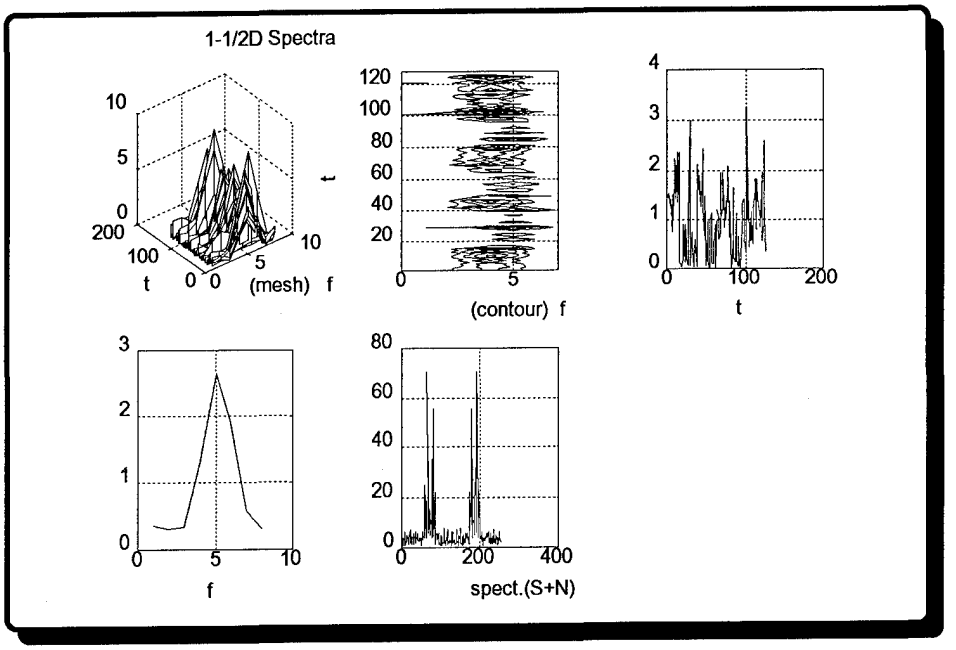

Figure 5.40: FSK 1-1/2D Spectra (SNR= +10 dB)

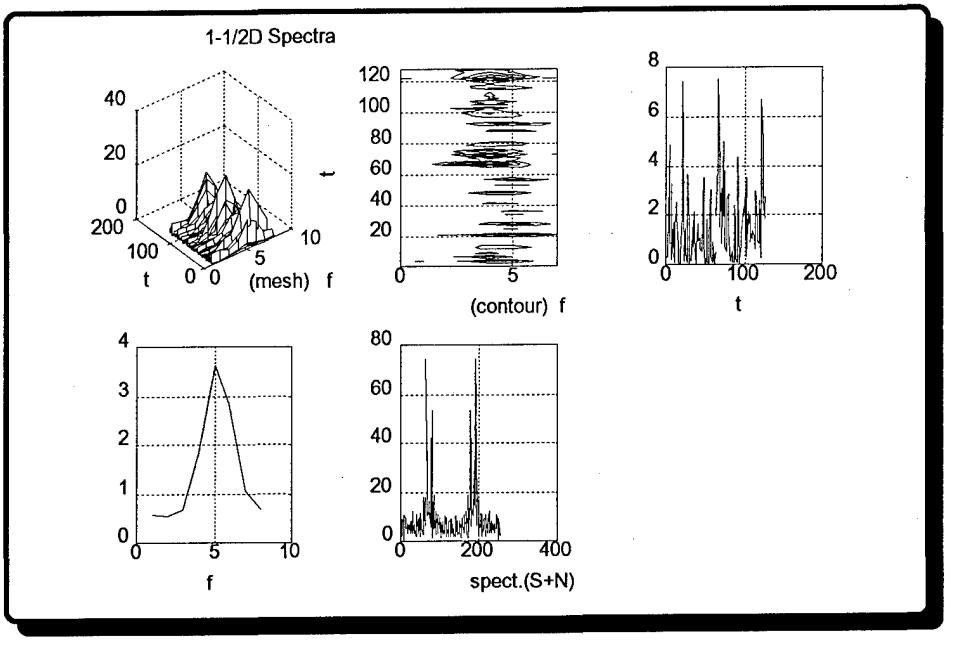

Figure 5.41: FSK 1-1/2D Spectra (SNR= +5 dB)

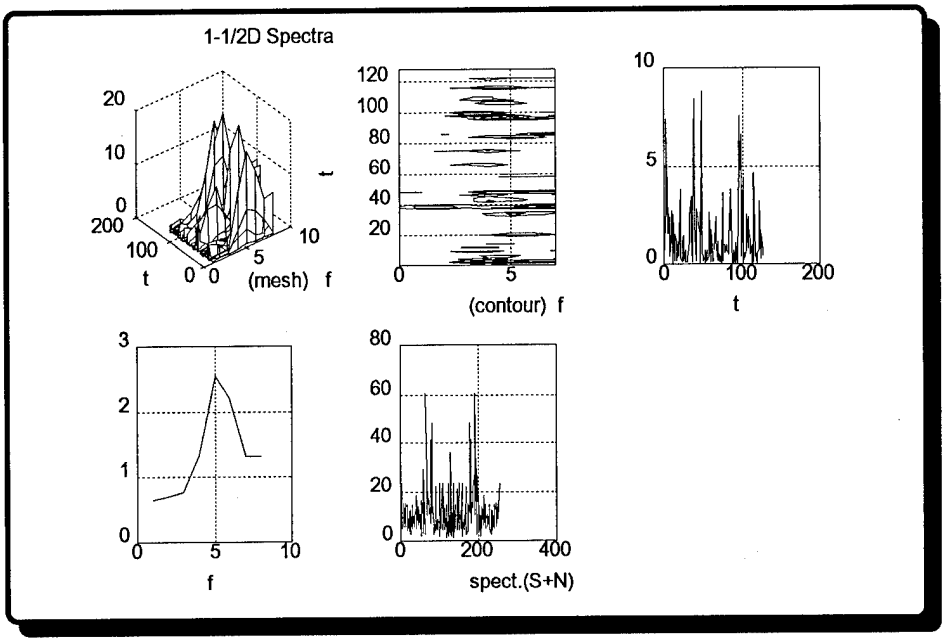

Figure 5.42: FSK 1-1/2D Spectra (SNR= +0 dB)

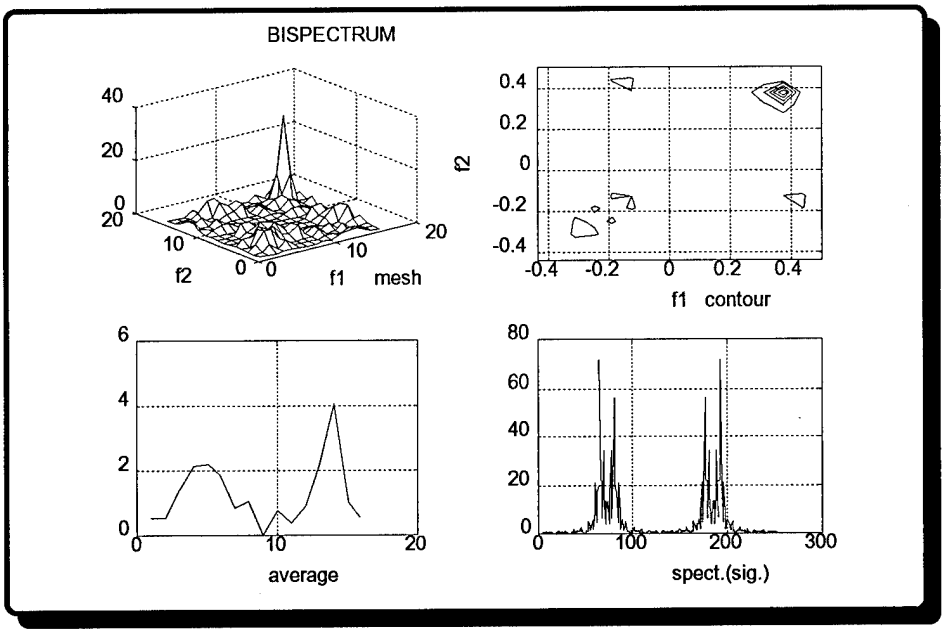

Figure 5.43: FSK Bispectrum (Infinite SNR)

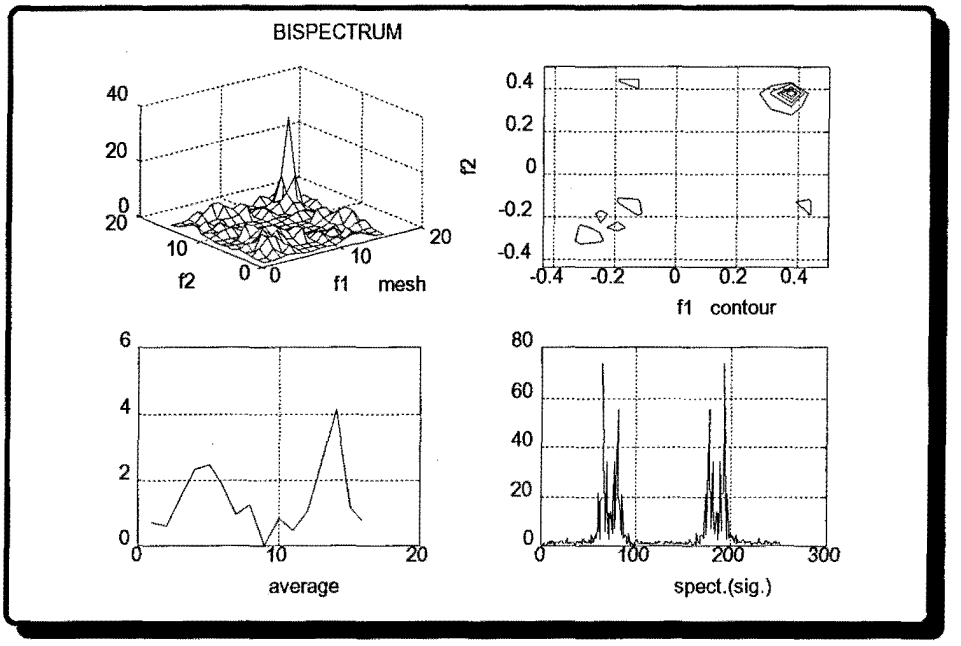

Figure 5.44: FSK Bispectrum (SNR= +20 dB)

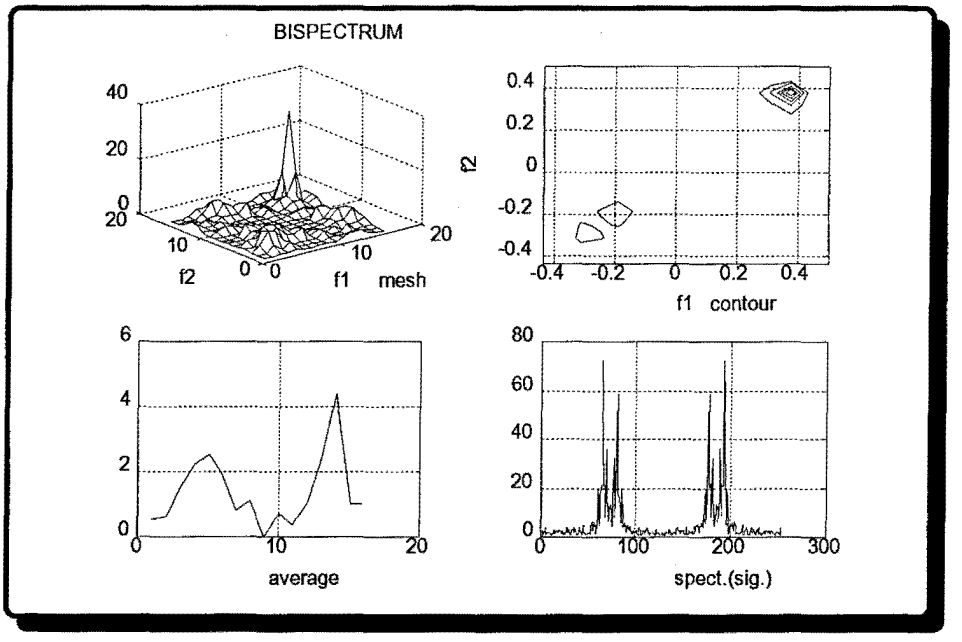

Figure 5.45: FSK Bispectrum (SNR= +15 dB)

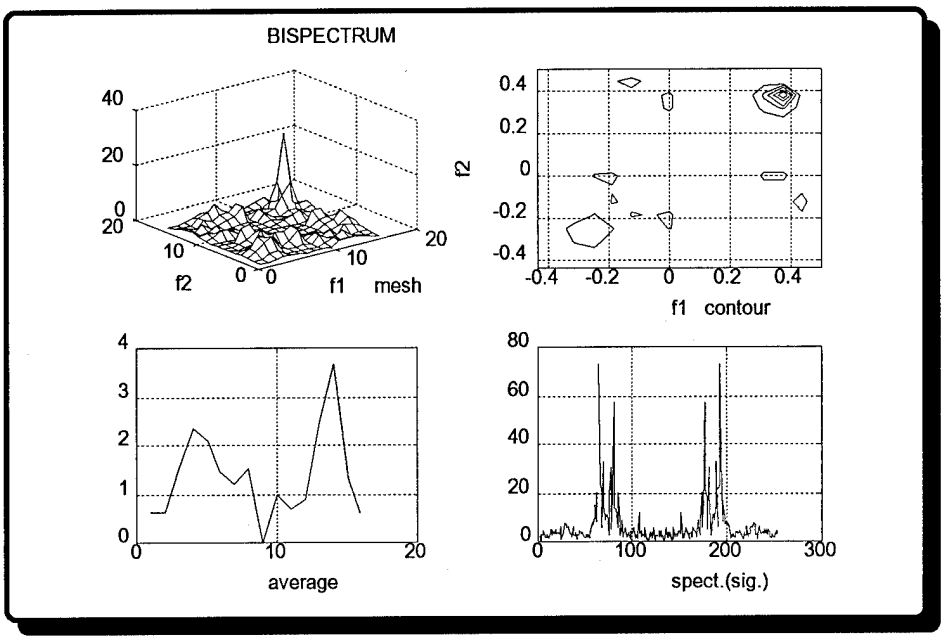

Figure 5.46: FSK Bispectrum (SNR= +10 dB)

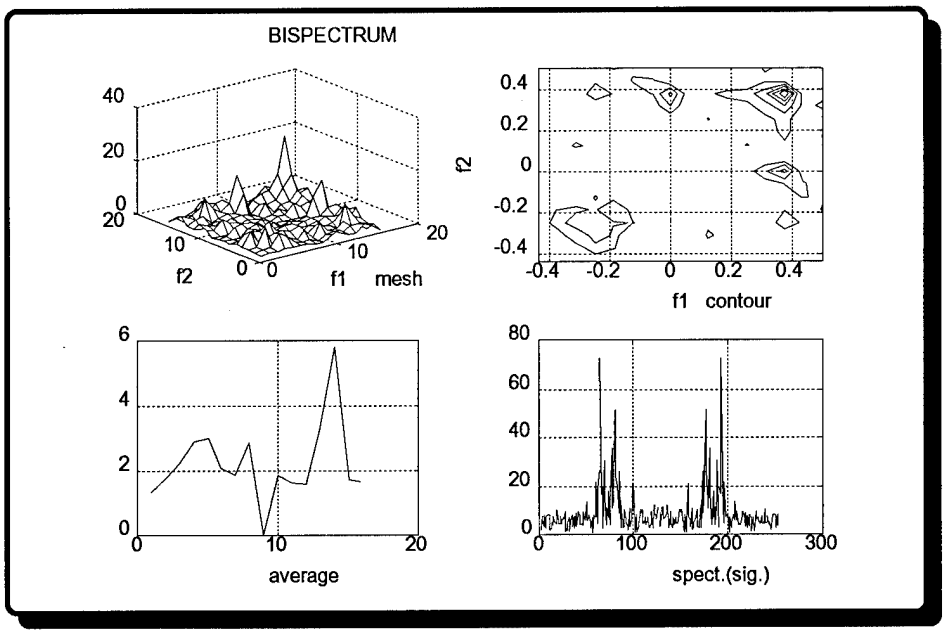

Figure 5.47: FSK Bispectrum (SNR= +5 dB)

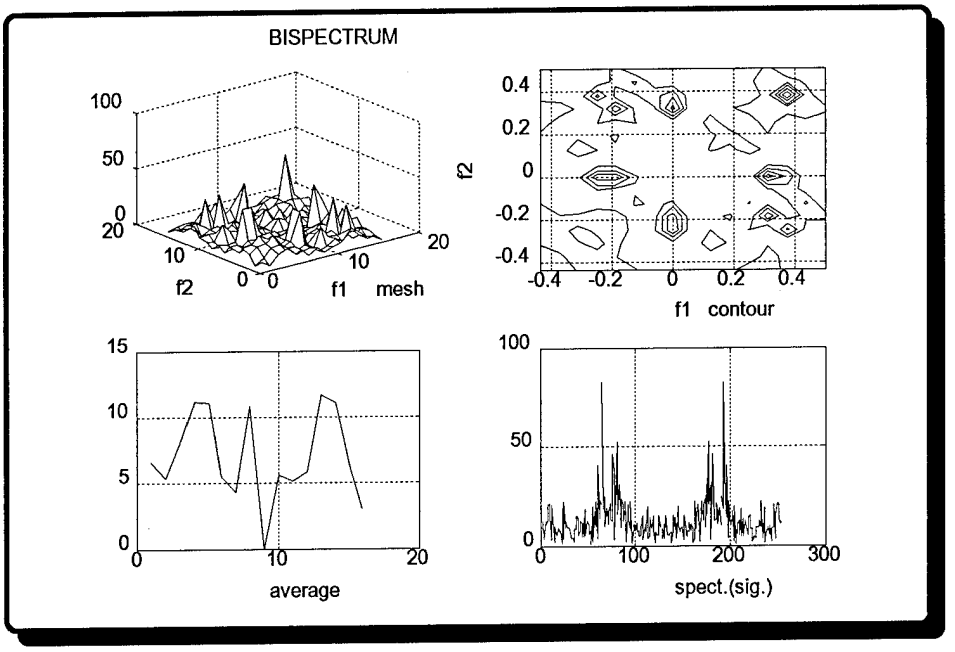

Figure 5.48: FSK Bispectrum (SNR= +0 dB)

Figure 5.49 through Figure 5.60 show the outer product representation (coherent and incoherent sum) for SNR levels of infinity, 20 dB, 10 dB, 0 dB, and -5 dB. These figures show that the outer product form was more tolerant of noise than the other spectrum methods. The outer product representation was useful for differentiating the FSK modulation scheme from other modulation schemes with the aid of the contour plots and frequency sum plots. FSK outer product spectra had four dominant peaks in which each peak had a different height in the mesh plots (one high peak and three relatively shorter peaks). In the contour plots, these transients were symmetric across the diagonal. The first part of the sum plots were useful since they had two symmetric regions. FSK spectra had two spectral spikes of unequal height until the SNR fell below 0 dB. These features were unique to FSK.

C. OOK

In this section, white Gaussian noise (WGN) was added to the OOK signal. Different SNR levels were used to examine the performance of the spectral representations in the presence of noise. As explained in chapter III, we expected to see the carrier at time locations 33 to 81, 97 to 129, and 161 to 193. At the other locations we expected to see no carrier. For message recovery the amplitude shifts at the appropriate locations must be detected.

Figure 5.61 shows the plot of the sinusoidal carrier, the message, the OOK modulated signal, and the OOK modulated signal with noise. Figure 5.62 through Figure 5.67 show the spectrograms for SNR levels of infinity, 20 dB, 15 dB, 10 dB, 5 dB, and 0 dB. Amplitude shifts were apparent at their appropriate locations in the contour plots for SNR levels of 10 dB and larger. Below the 10 dB SNR level, we were unable to recognize the amplitude shifts, but we were still able to identify the modulation type. As a result we had a degraded ability to collect

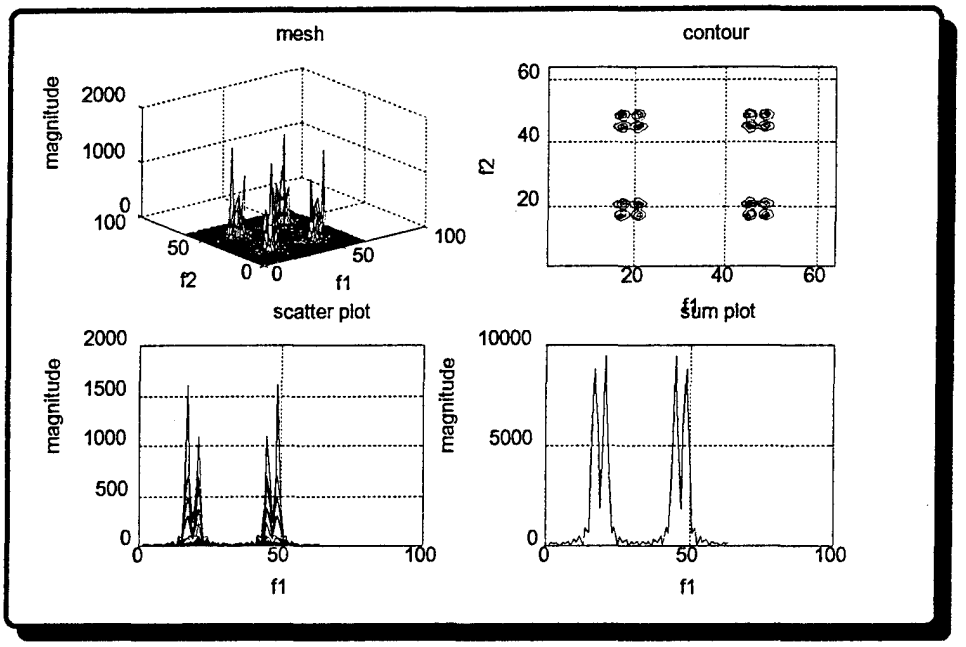

Figure 5.49: FSK Outer Product Representation (Coherent, Infinite SNR)

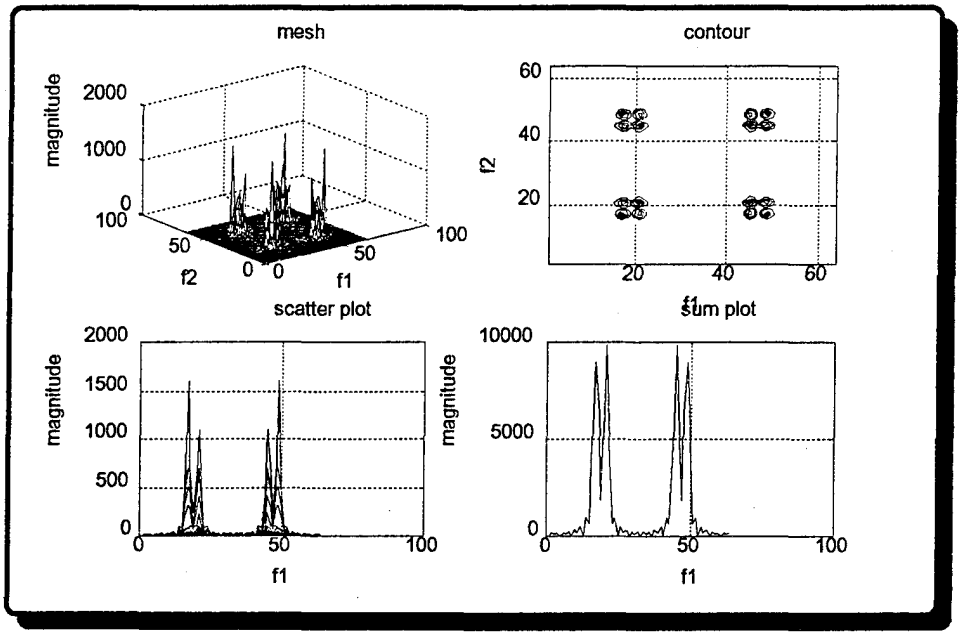

Figure 5.50: FSK Outer Product Representation (Incoherent, Infinite SNR)

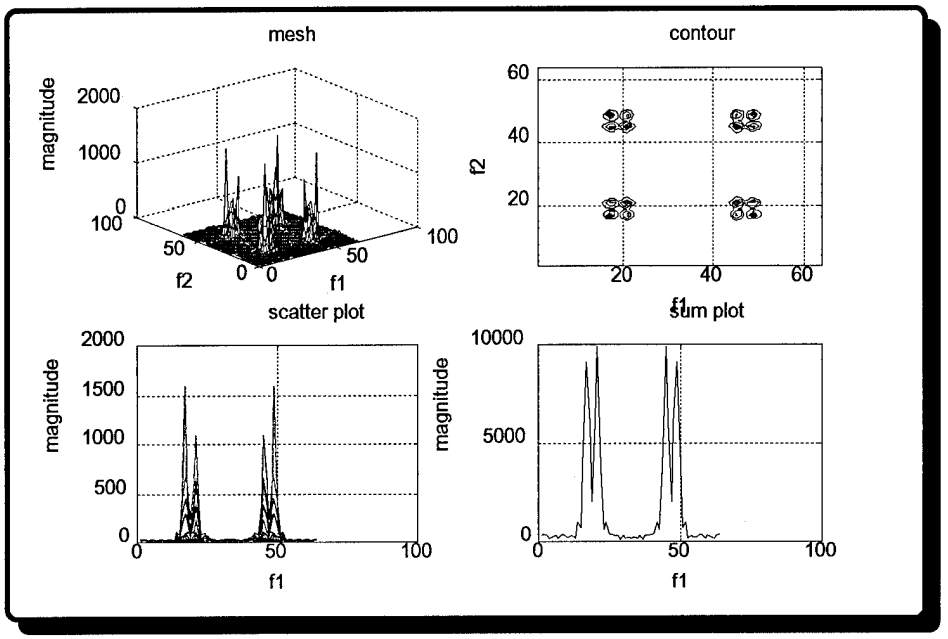

Figure 5.51: FSK Outer Poduct Representation (Coherent, SNR= +20 dB)

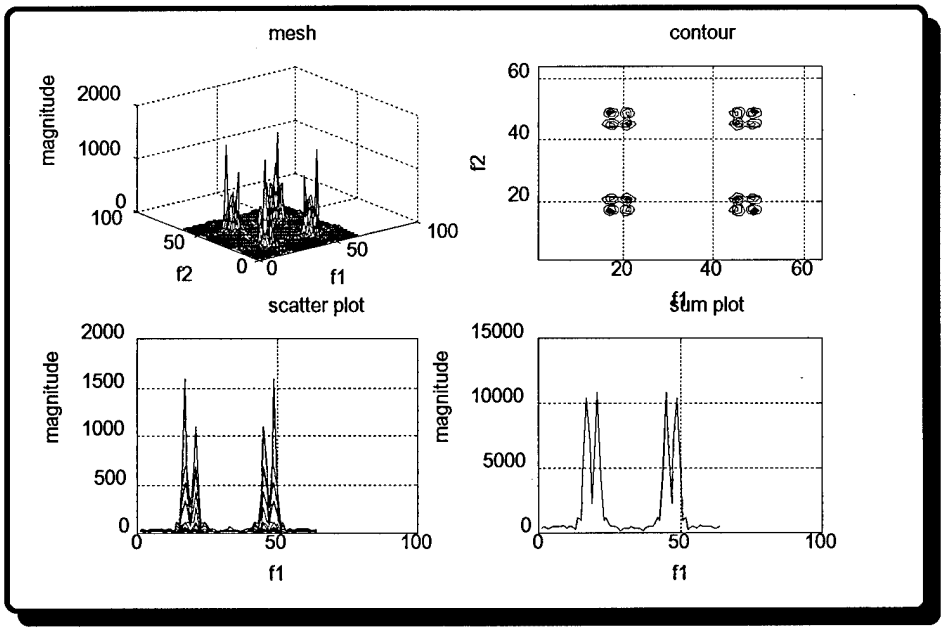

Figure 5.52: FSK Outer Poduct Representation (Incoherent, SNR= +20 dB)

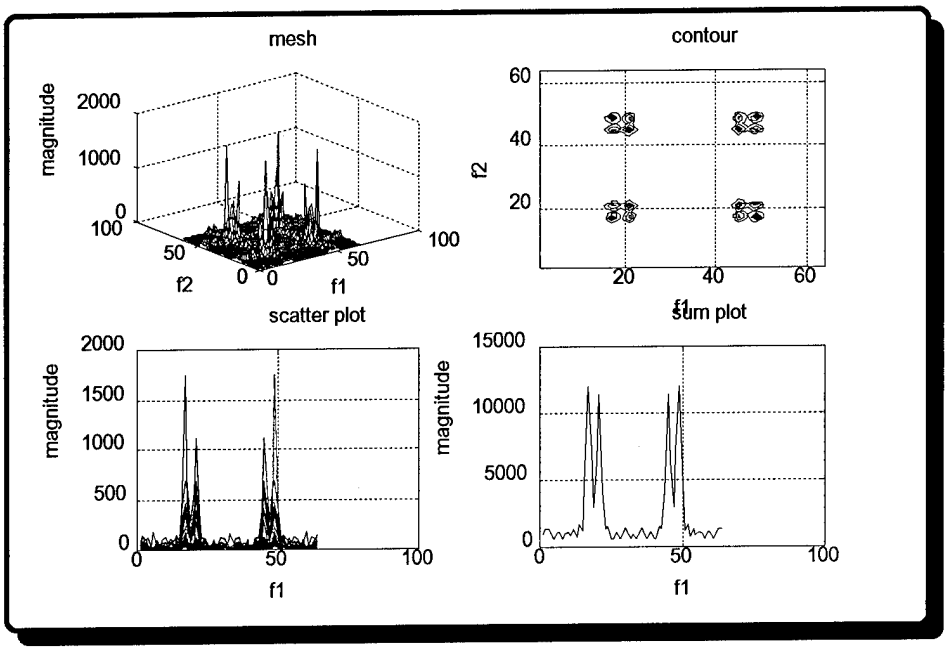

Figure 5.53: FSK Outer Poduct Representation (Coherent, SNR= +10 dB)

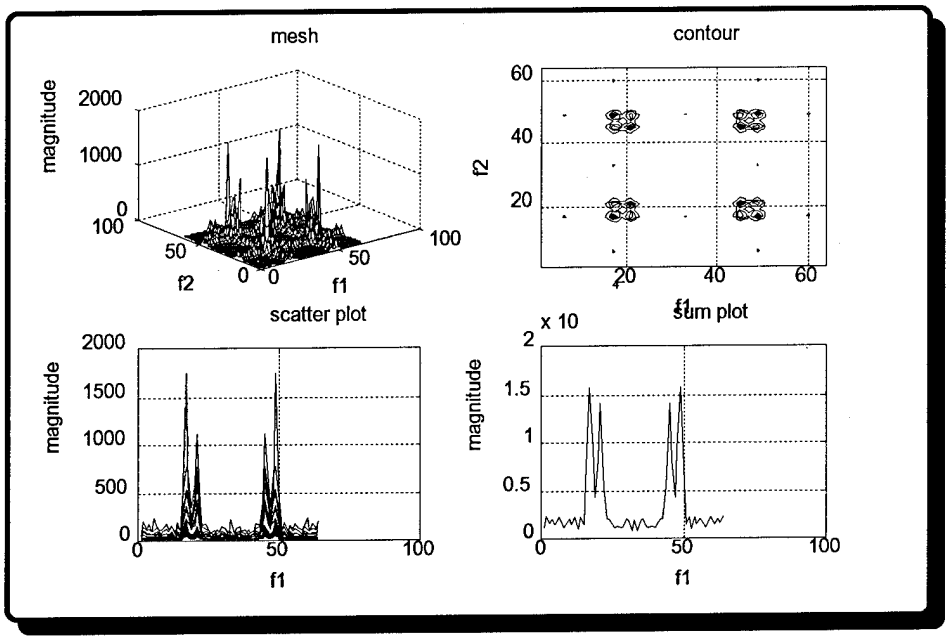

Figure 5.54: FSK Outer Poduct Representation (Incoherent, SNR= +10dB)

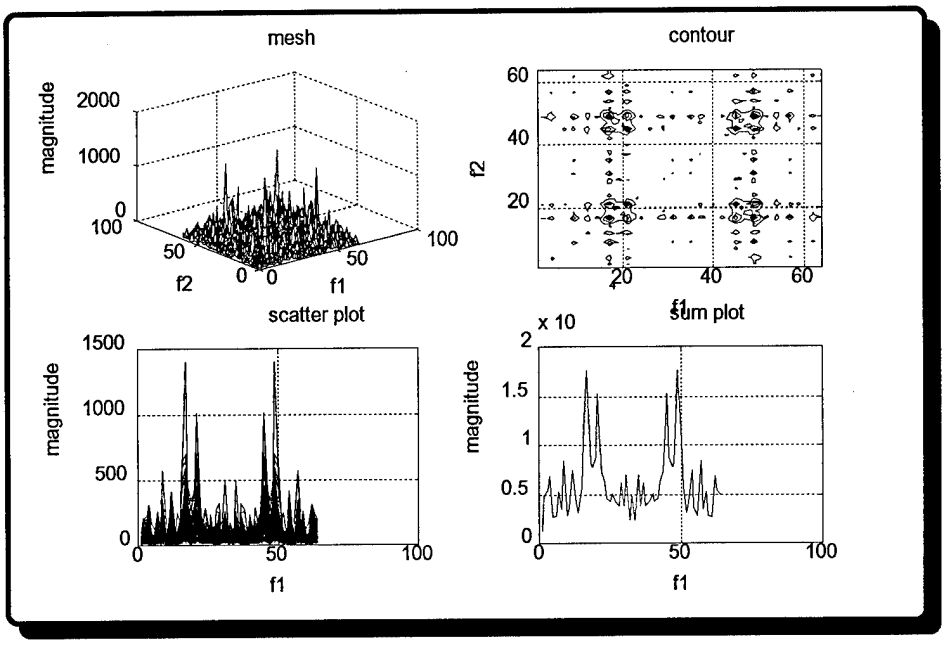

Figure 5.55: FSK Outer Poduct Representation (Coherent, SNR= +0 dB)

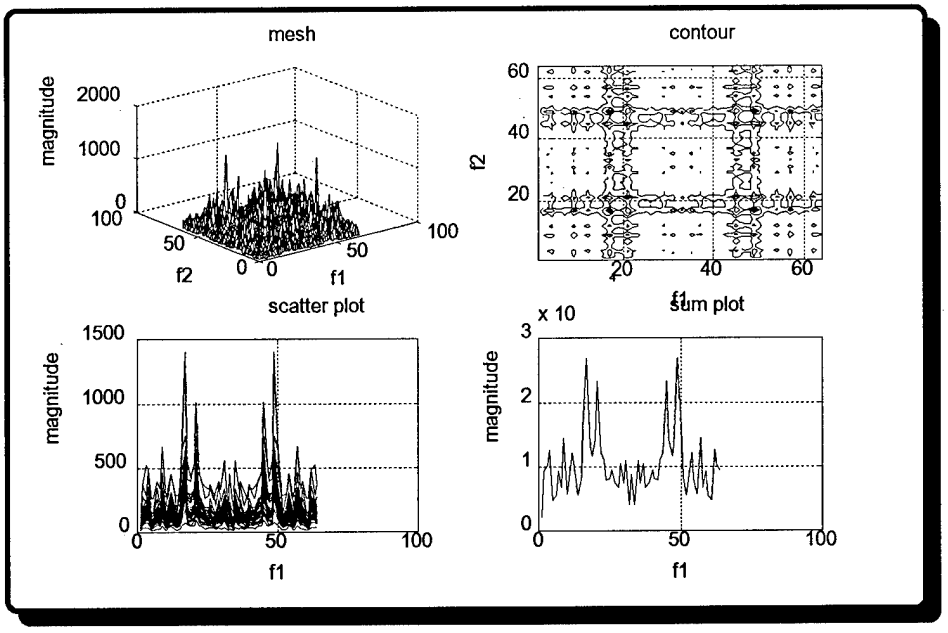

Figure 5.56: FSK Outer Poduct Representation (Incoherent, SNR= +0 dB)

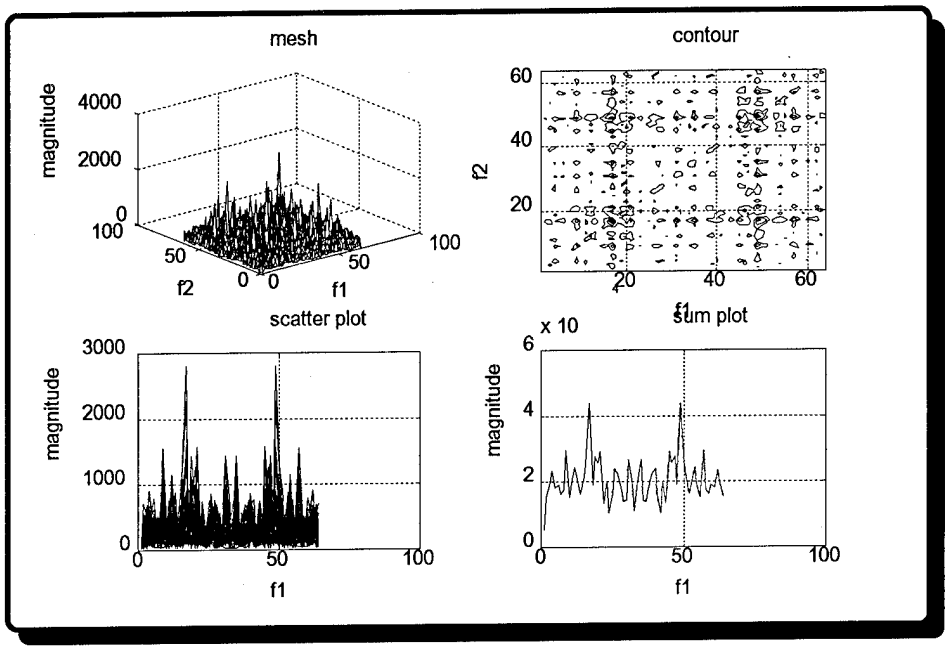

Figure 5.57: FSK Outer Poduct Representation (Coherent, SNR= -5 dB)

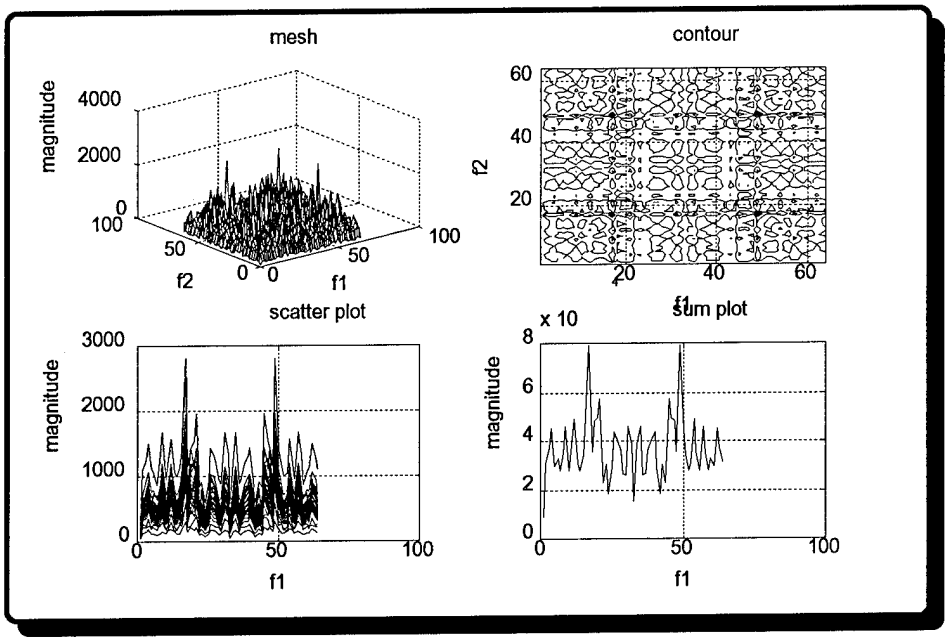

Figure 5.58: FSK Outer Poduct Representation (Incoherent, SNR= -5 dB)

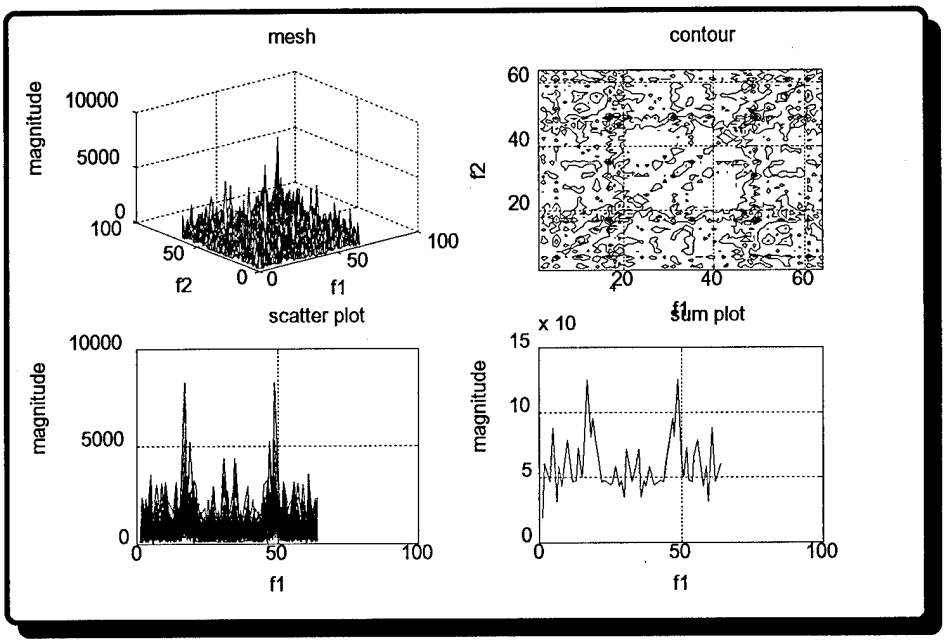

Figure 5.59: FSK Outer Poduct Representation (Coherent, SNR= -10 dB)

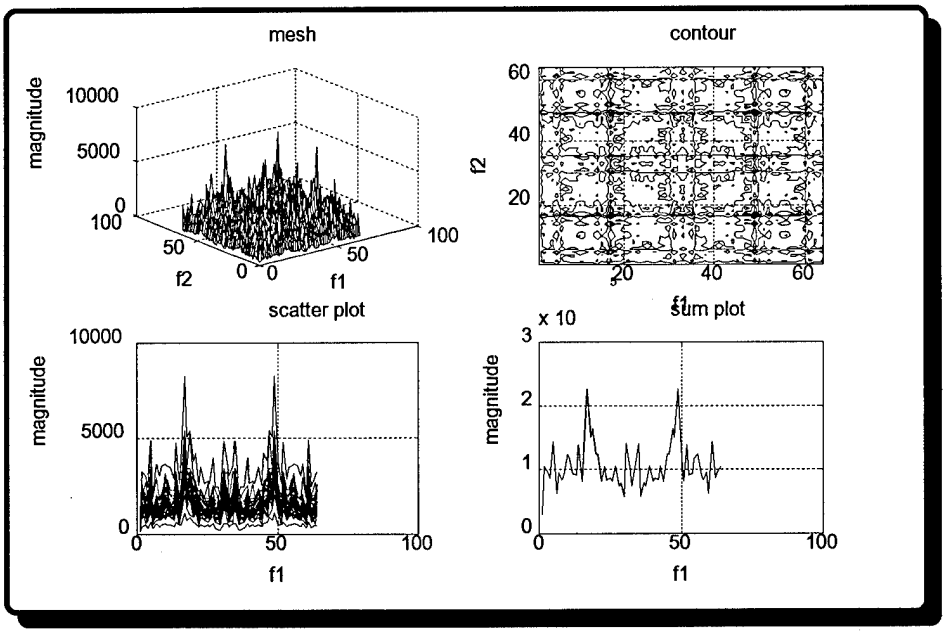

Figure 5.60: FSK Outer Poduct Representation (Incoherent, SNR= -10 dB)

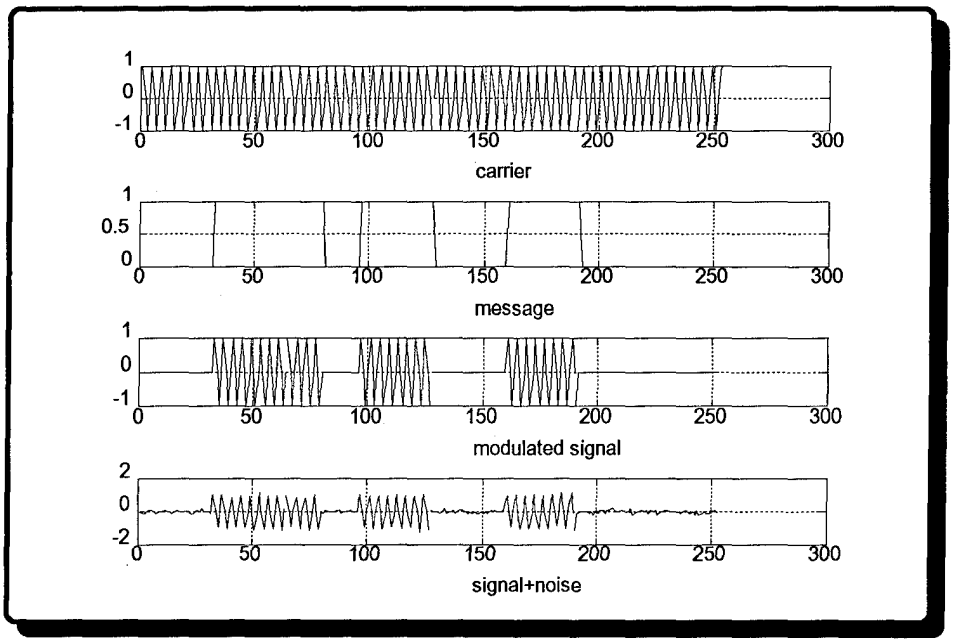

Figure 5.61: OOK Generation with Noise

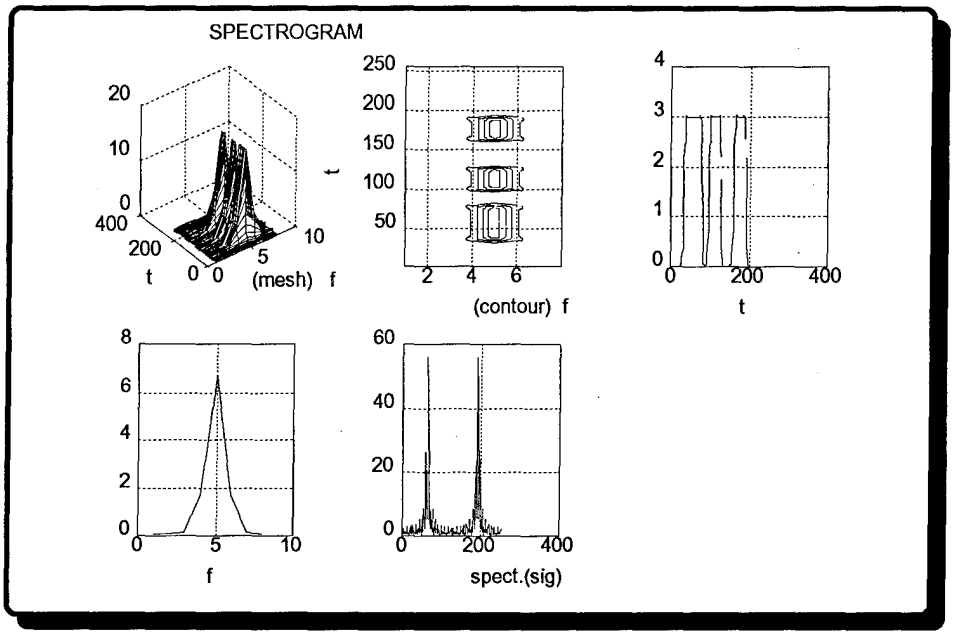

Figure 5.62: OOK Spectrogram (Infinite SNR)

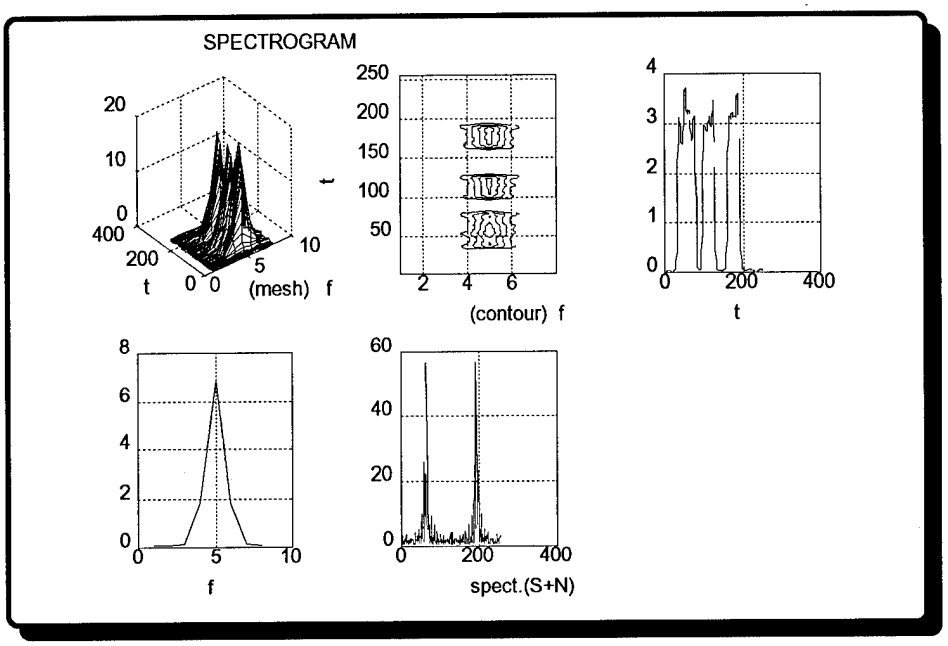

Figure 5.63: OOK Spectrogram (SNR= +20 dB)

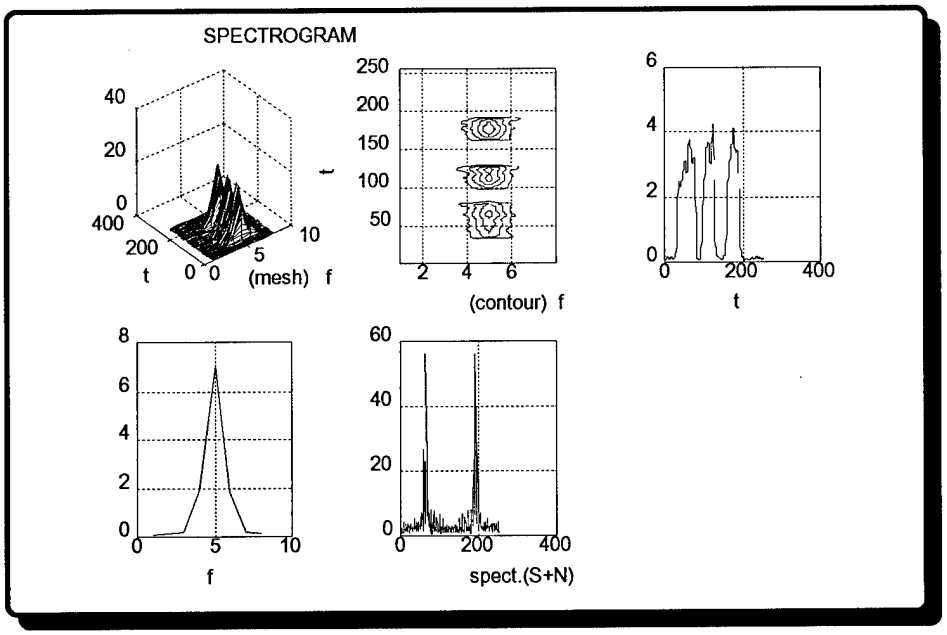

Figure 5.64: OOK Spectrogram (SNR= +15 dB)

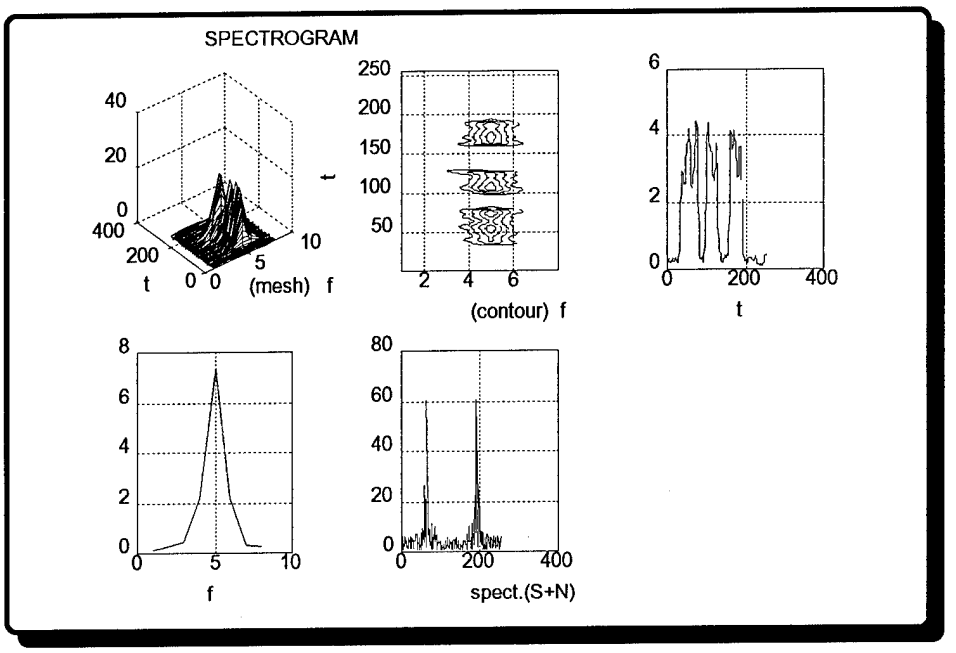

Figure 5.65: OOK Spectrogram (SNR= +10 dB)

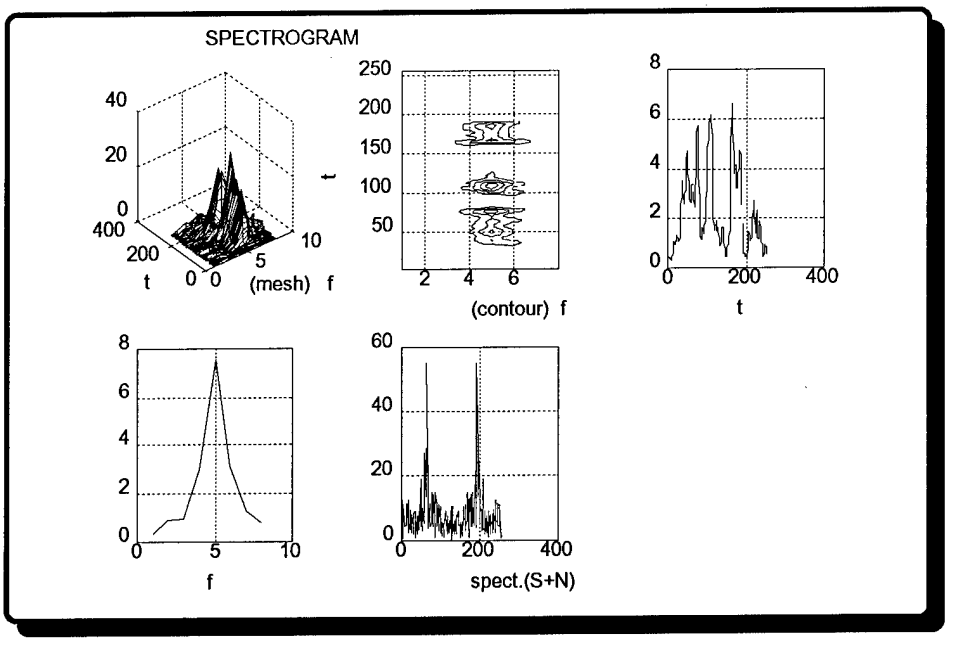

Figure 5.66: OOK Spectrogram (SNR= +5 dB)

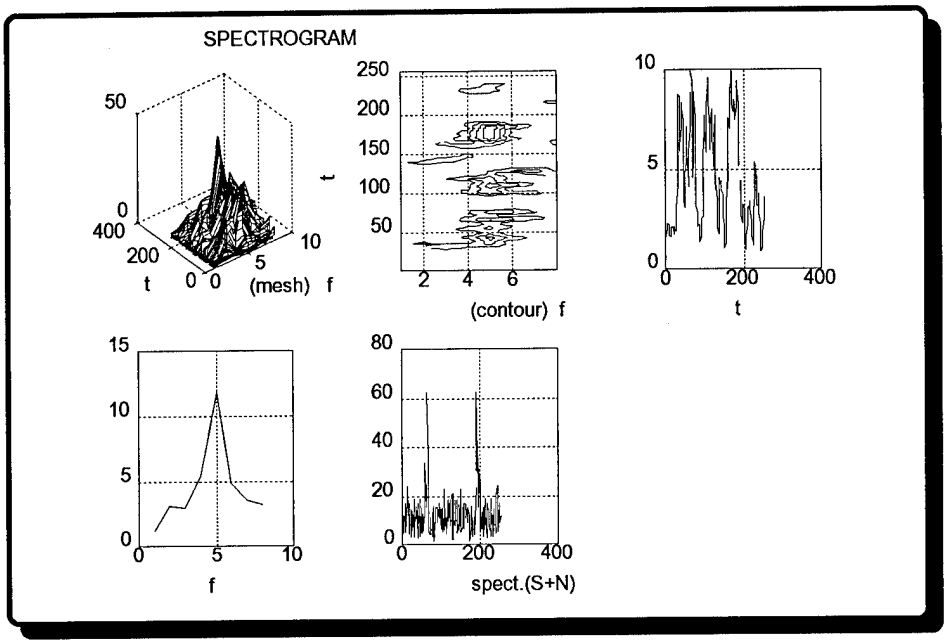

Figure 5.67: OOK Spectrogram (SNR= 0 dB)

correct information about the message, modulation type, and bit rate at and below 5 dB.

Figure 5.68 through Figure 5.73 shows the 1-1/2D_{IPS} spectra for SNR levels of infinity, 20 dB, 15 dB, 10 dB, 5 dB, 0 dB and -5 dB. The amplitude shifts were apparent at their appropriate locations for infinity, 20, 15 and 10 dB SNR levels. Below 10 dB, amplitude shifts did not occur at the correct locations. The spectrum became hard to interpret because of the noise component. As a result we lost the ability the message, modulation type, and bit rate for SNR levels below 10 dB.

Figure 5.74 through Figure 5.79 shows the bispectrum for SNR levels of infinity, 20 dB, 15 dB, 10 dB, 5 dB, and 0 dB. At an infinite SNR level, the OOK bispectral pictures, especially the contour plots were easy to interpret. The magnitudes of the peaks were very low and there were many similar peaks in the mesh plot. The dominant peaks were located, approximately, at location (-0.2,-0.2; -0.2,0; 0,-0.2) in the contour plot. As the SNR level decreased, we saw more peaks (except at 20 dB) with larger amplitudes than the peaks at higher SNR levels. However, at 20 dB SNR level, the peak at location (-0.2,-0.2) became unrecognizable while the other peaks were still apparent and their magnitudes become greater with respect to the infinite SNR level. Below 20 dB SNR level, (until the SNR level drops to under 10 dB) the peak at location (-0.2,-0.2) was still identifiable but below 10 dB SNR the other two peaks were lost.

Figure 5.80 through Figure 5.91 shows the outer product representation (coherent and incoherent sum) for SNR levels of infinity, 20 dB, 10 dB, 0 dB, and -5 dB. These figures show that the outer product form was more tolerant of noise than the other approaches. The outer product representation was useful for differentiating the OOK modulation scheme from other modulation schemes when using contour plots and frequency sum plots. OOK had one solid spike in

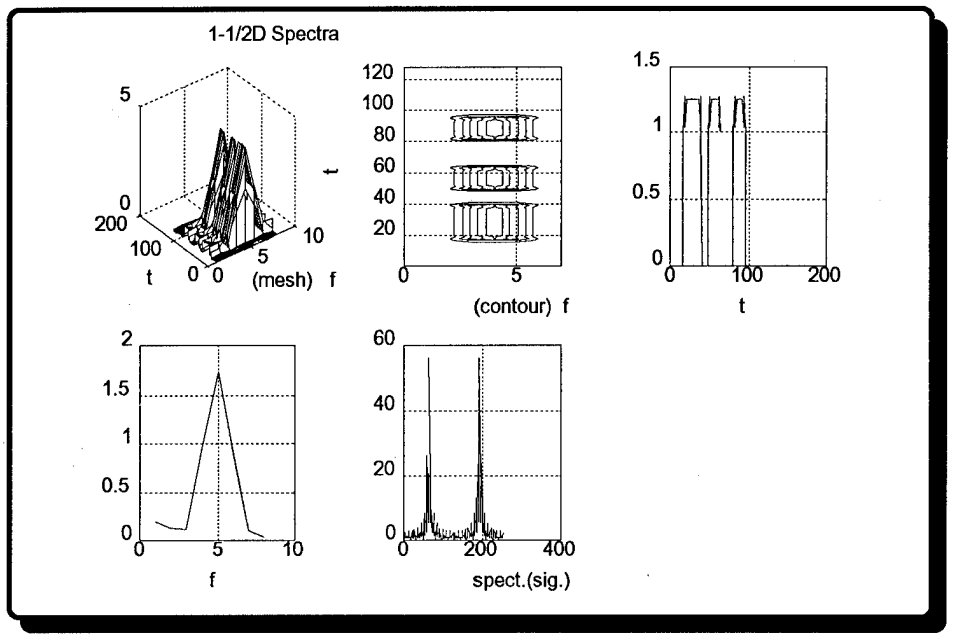

Figure 5.68: OOK 1-1/2D Spectra (Infinite SNR)

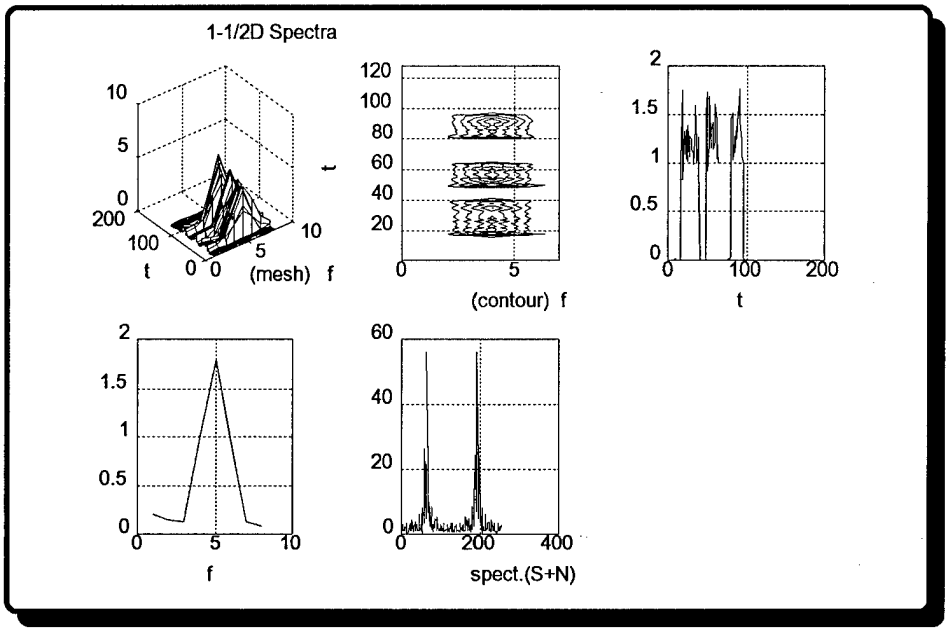

Figure 5.69: OOK 1-1/2D Spectra (SNR= +20dB)

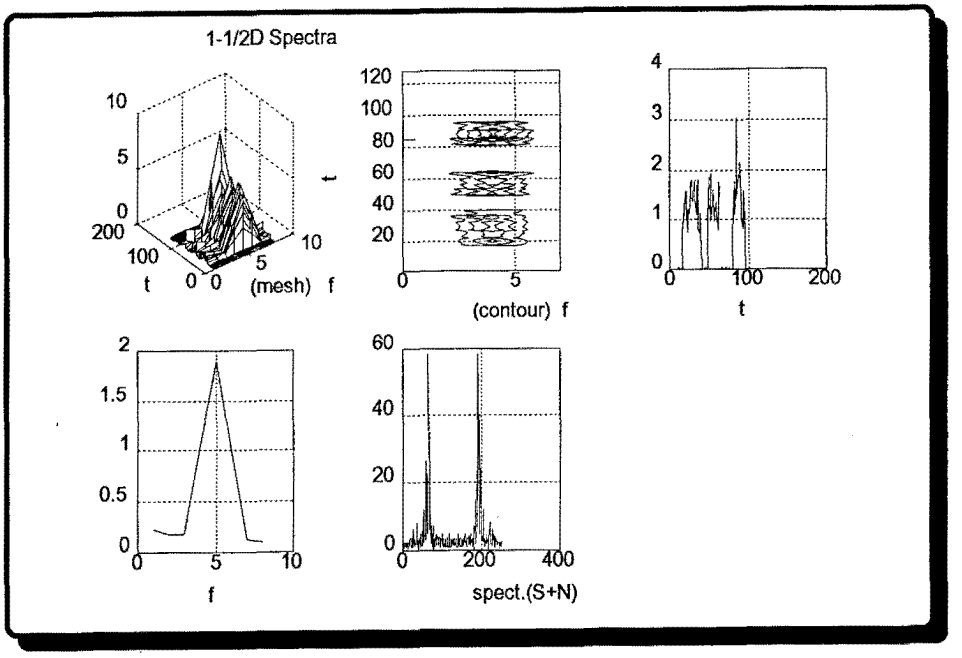

Figure 5.70: OOK 1-1/2D Spectra (SNR= +15dB)

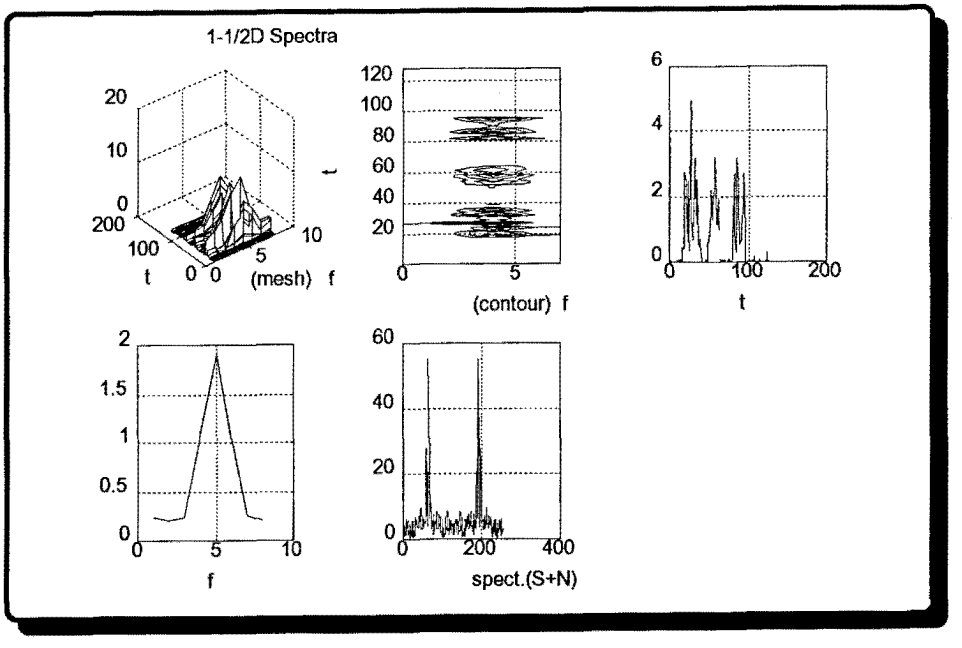

Figure 5.71: OOK 1-1/2D Spectra (SNR= +10dB)

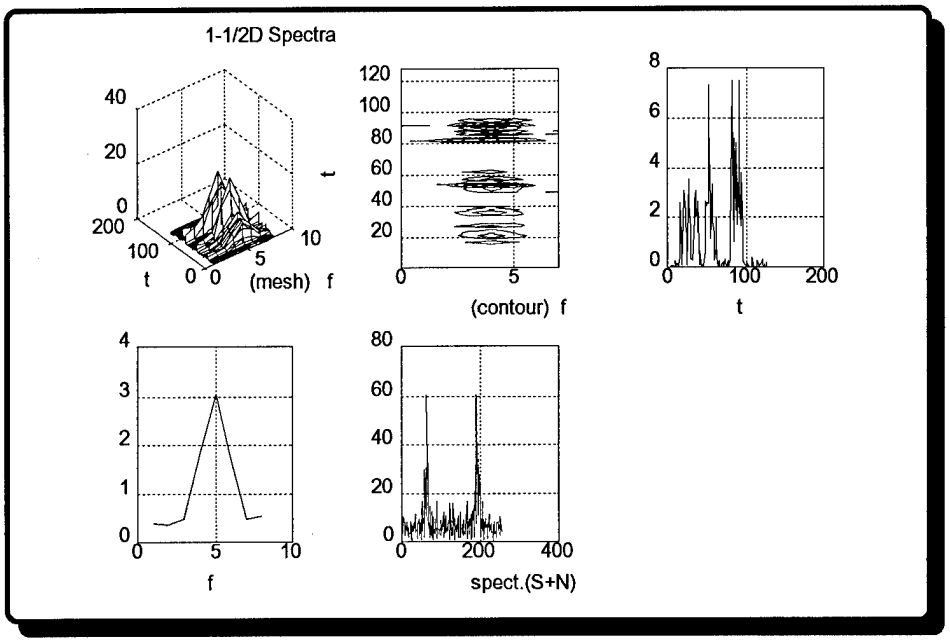

Figure 5.72: OOK 1-1/2D Spectra (SNR= +5dB)

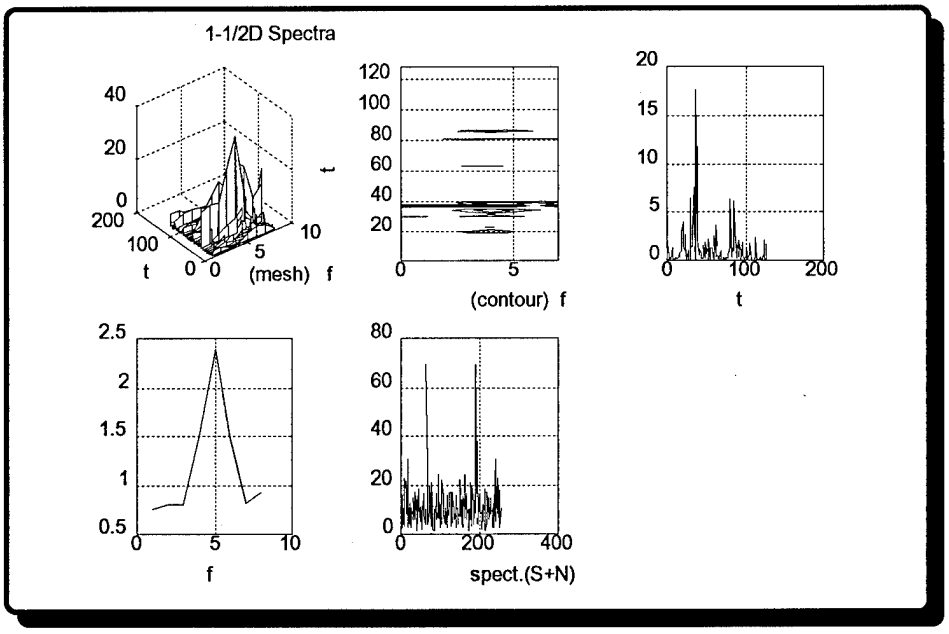

Figure 5.73: OOK 1-1/2D Spectra (SNR= 0 dB)

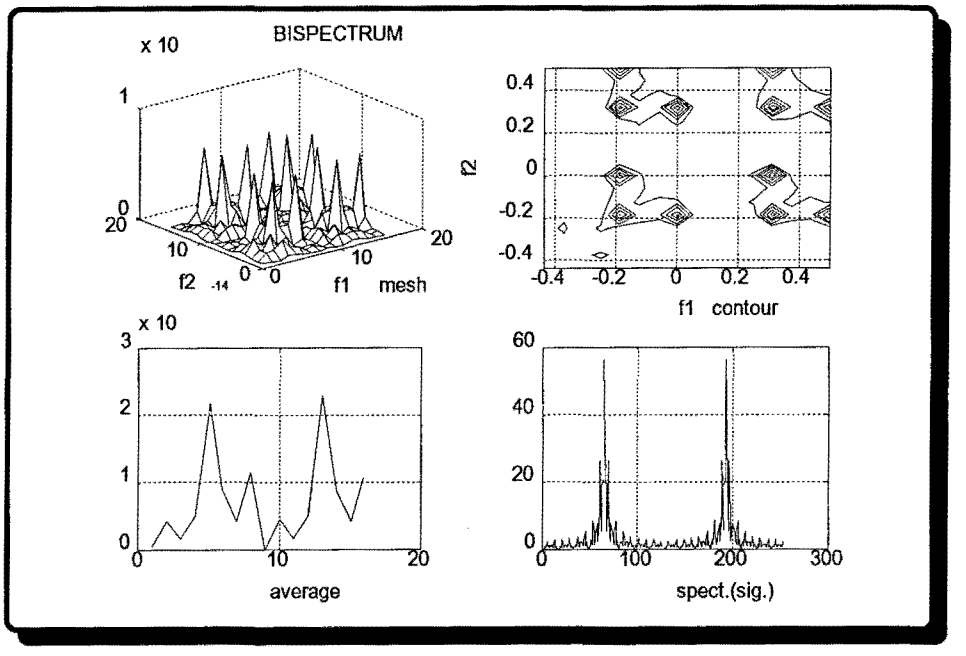

Figure 5.74: OOK Bispectrum (Infinite SNR)

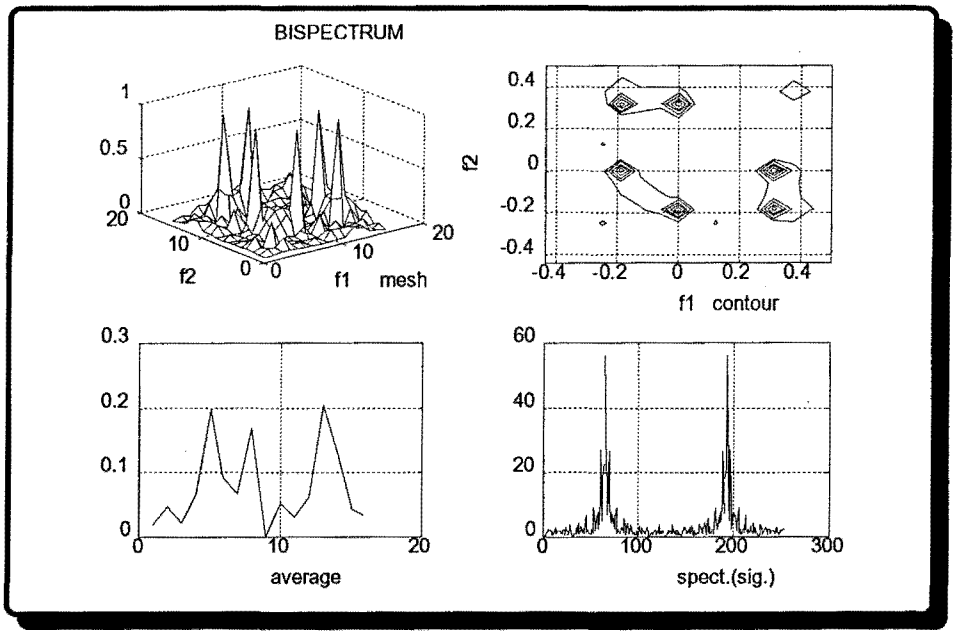

Figure 5.75: OOK Bispectrum (SNR= +20 dB)

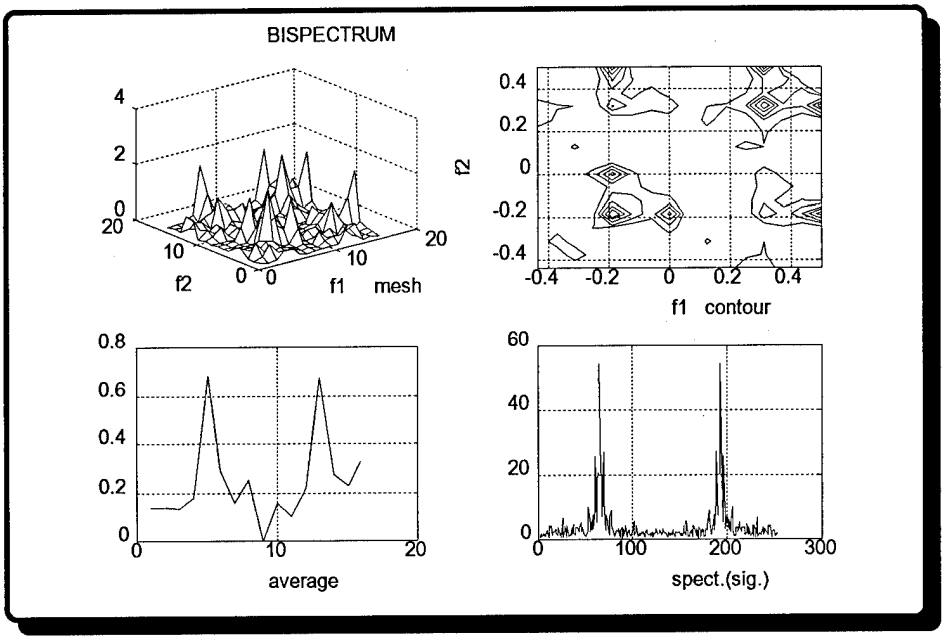

Figure 5.76: OOK Bispectrum (SNR= +15 dB)

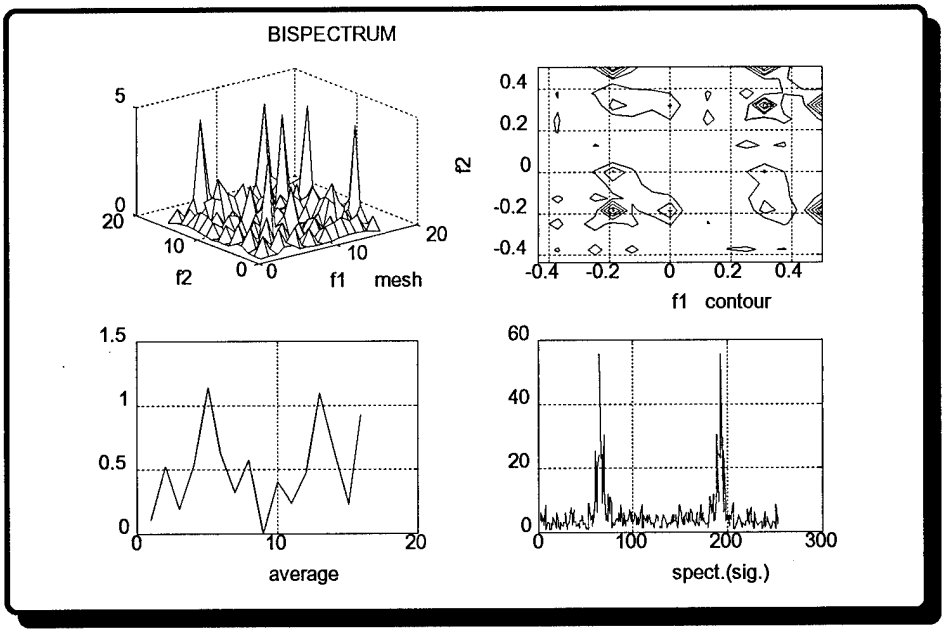

Figure 5.77: OOK Bispectrum (SNR= +10 dB)

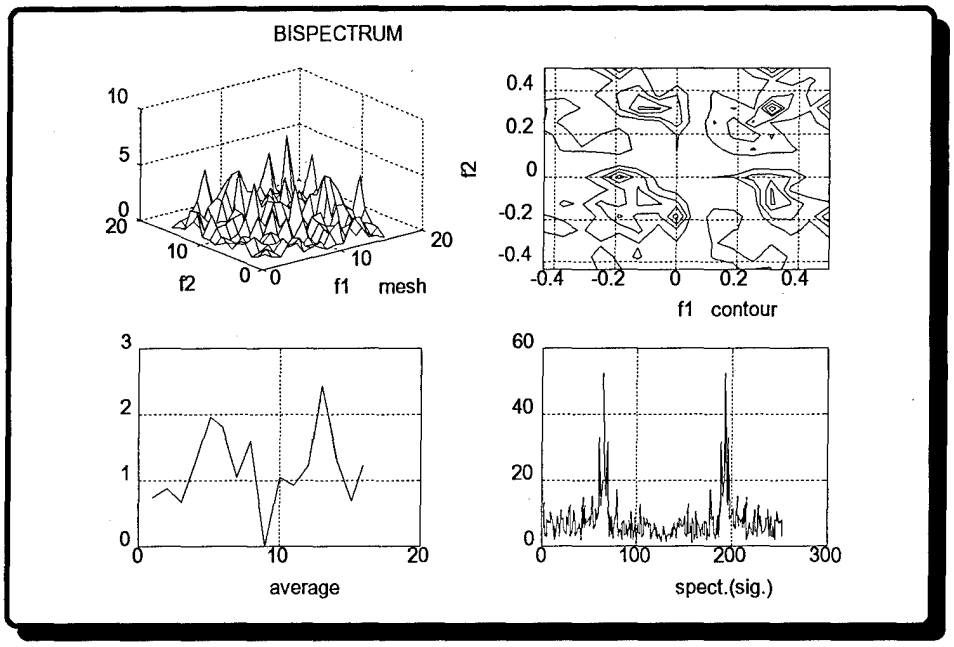

Figure 5.78: OOK Bispectrum (SNR= +5 dB)

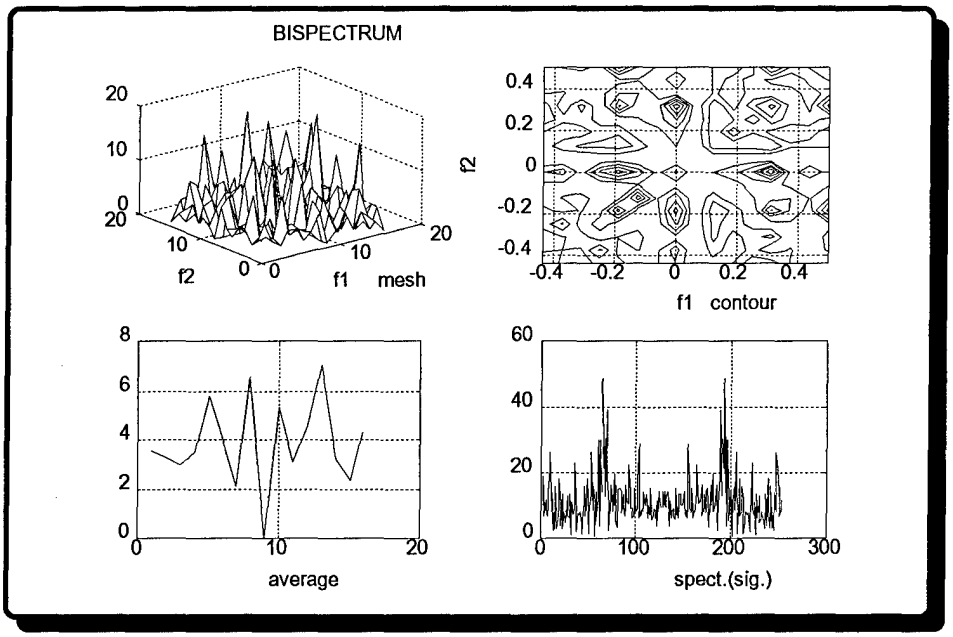

Figure 5.79: OOK Bispectrum (SNR= 0 dB)

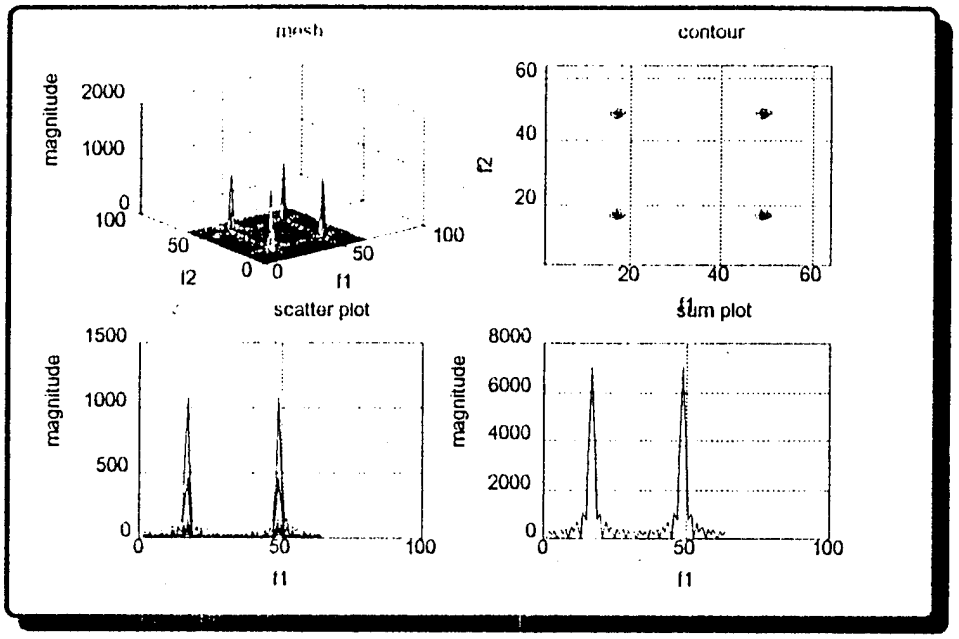

Figure 5.80: OOK Outer Product Representation (Coherent, Infinite SNR)

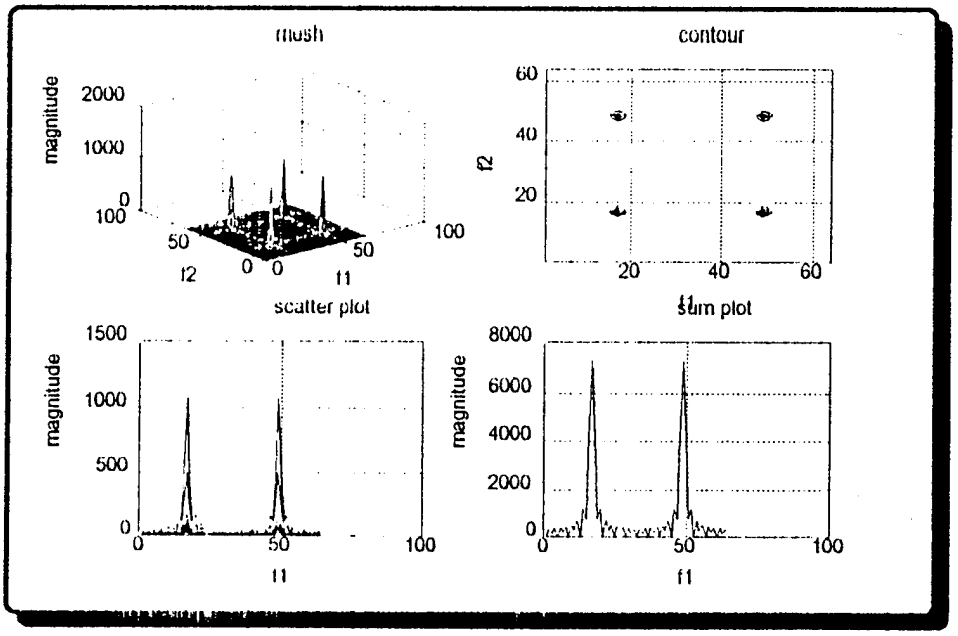

Figure 5.81: OOK Outer Product Representation (Incoherent, Infinite SNR)

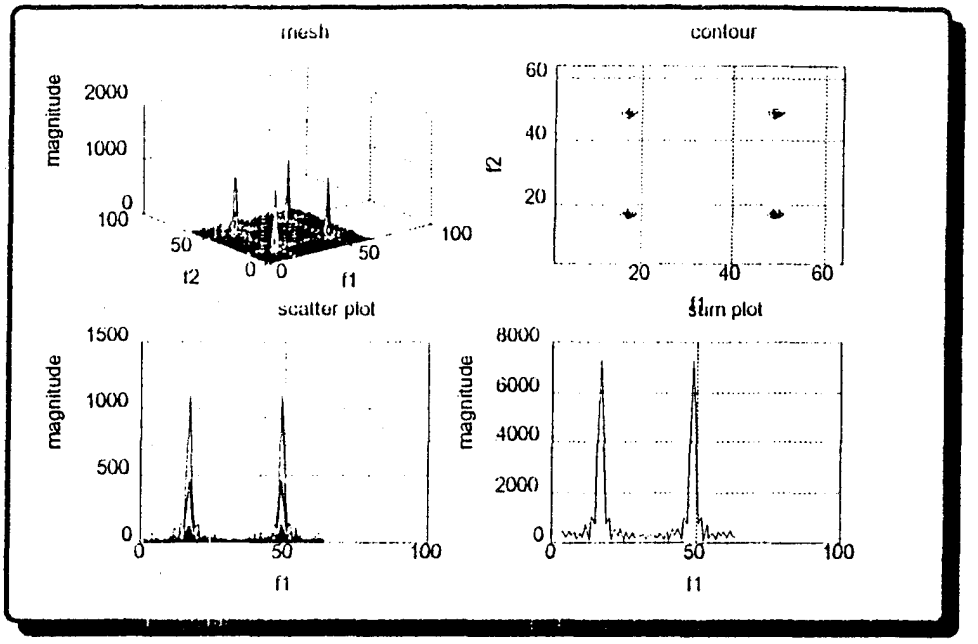

Figure 5.82: OOK Outer Poduct Representation (Coherent, SNR= +20 dB)

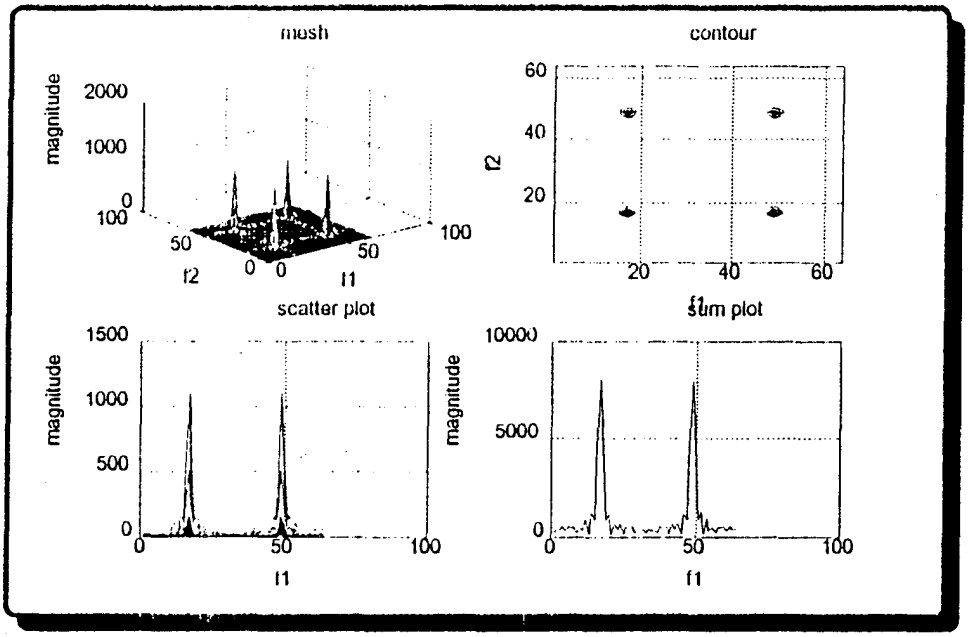

Figure 5.83: OOK Outer Poduct Representation (Incoherent, SNR= +20 dB)

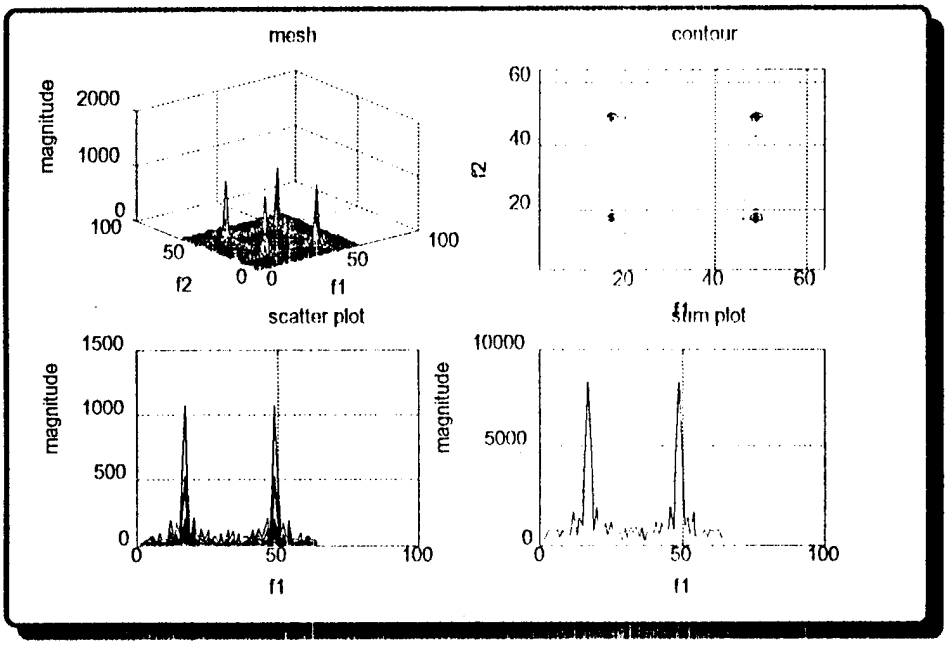

Figure 5.84: OOK Outer Poduct Representation (Coherent, SNR= +10 dB)

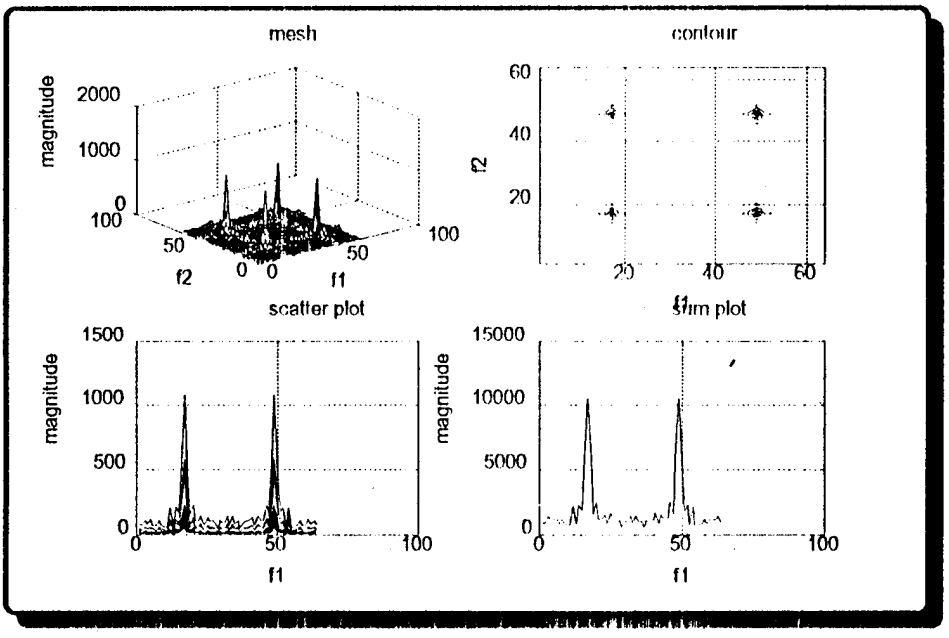

Figure 5.85: OOK Outer Poduct Representation (Incoherent, SNR= +10 dB)

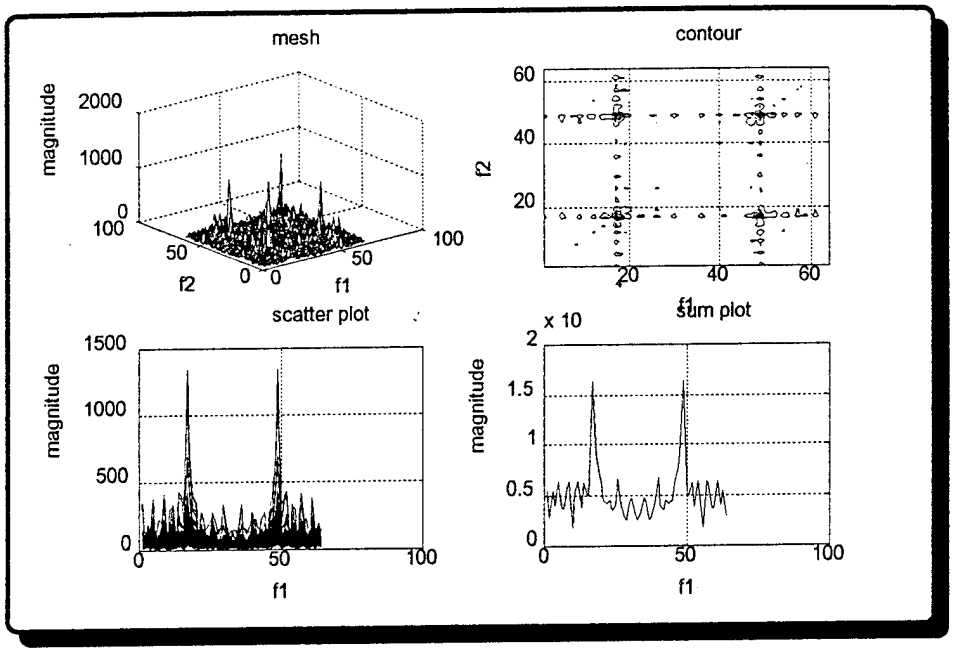

Figure 5.86: OOK Outer Poduct Representation (Coherent, SNR= +0dB)

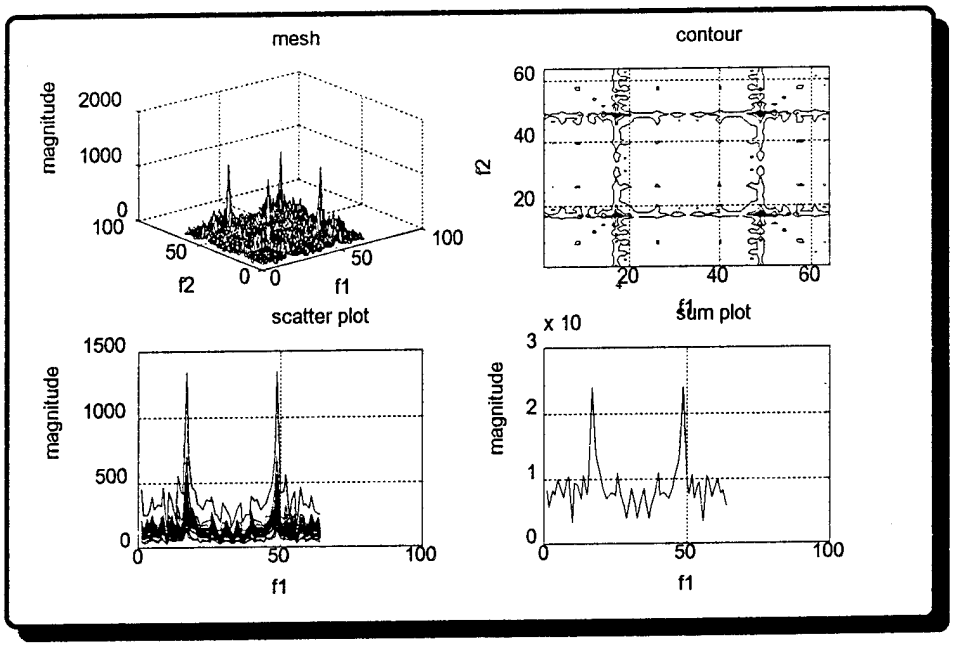

Figure 5.87: OOK Outer Poduct Representation (Incoherent, SNR= +0dB)

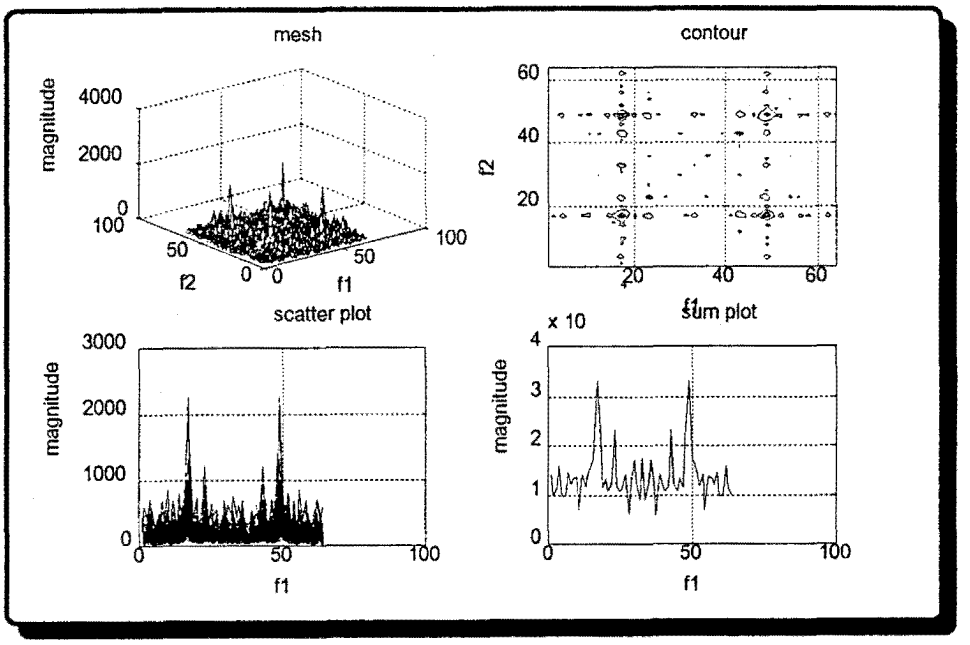

Figure 5.88: OOK Outer Poduct Representation (Coherent, SNR= -5dB)

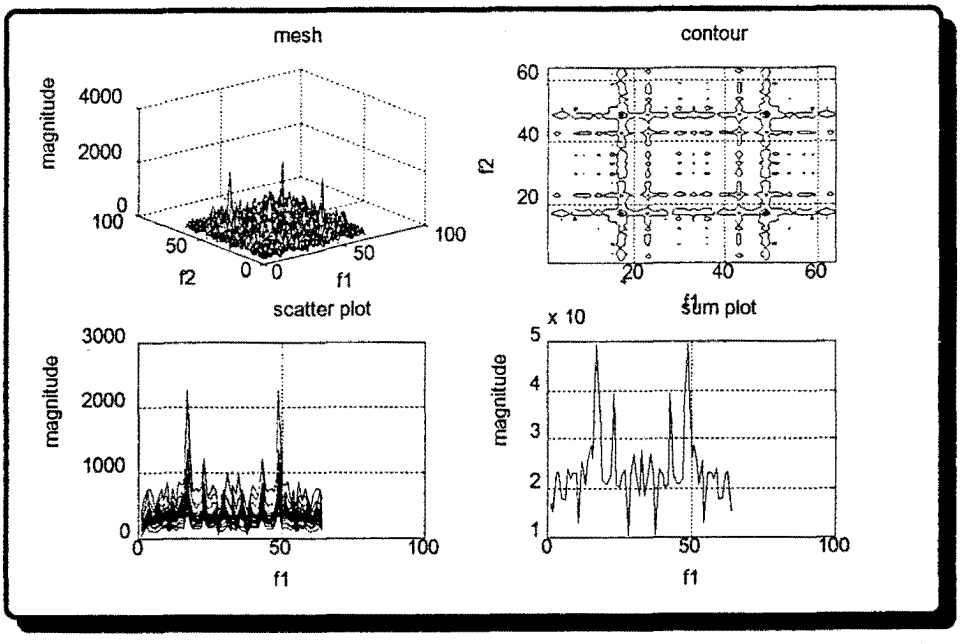

Figure 5.89: OOK Outer Poduct Representation (Incoherent, SNR= -5dB)

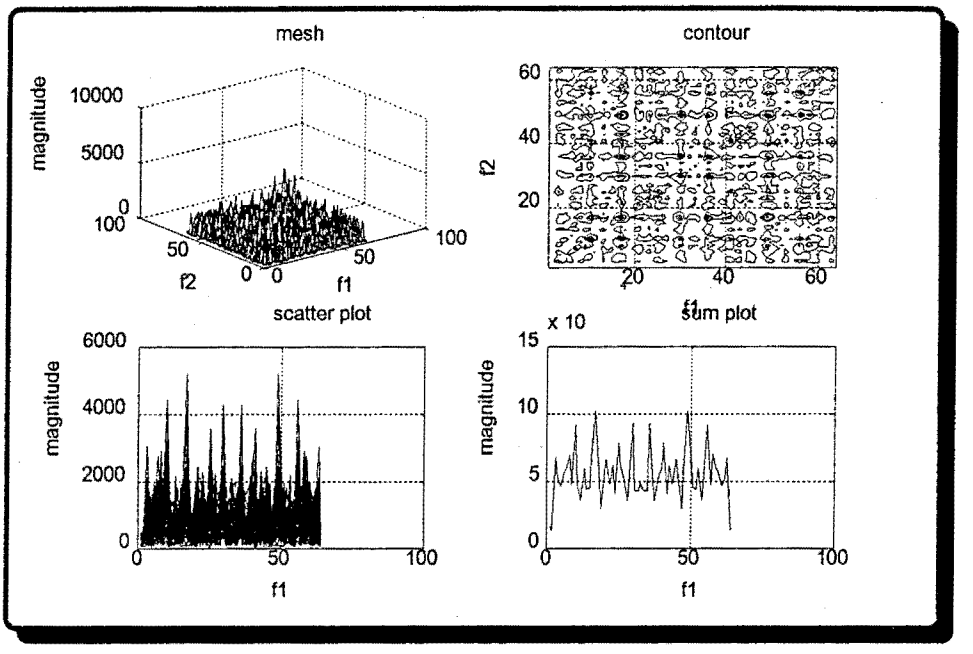

Figure 5.90: OOK Outer Poduct Representation (Coherent, SNR= -10 dB)

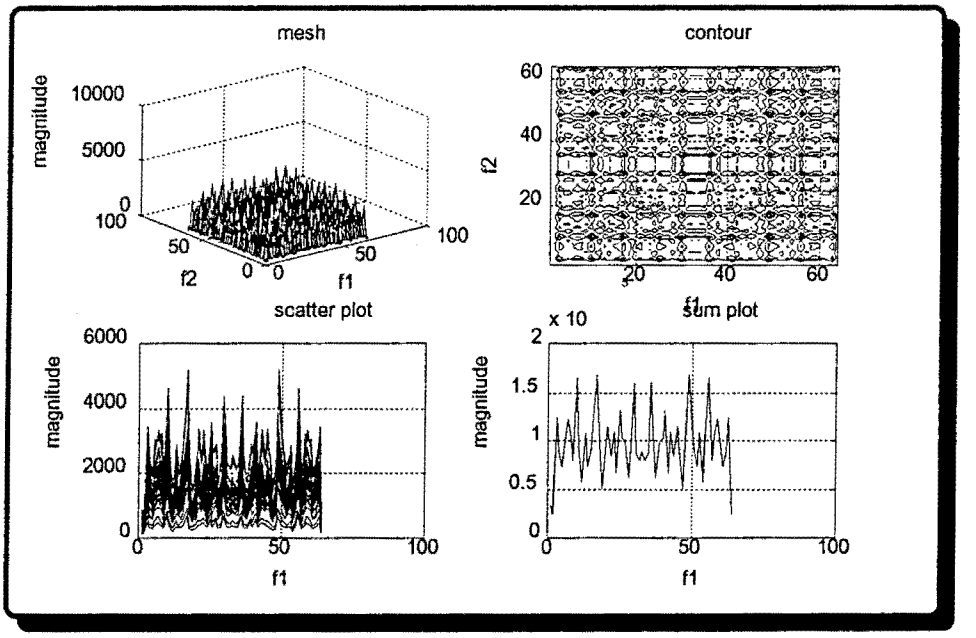

Figure 5.91: OOK Outer Poduct Representation (Incoherent, SNR= -10 dB)

the contour plots. In the mesh plots, there were four dominant transients that was connected to each other with lines produced by smaller transients. The whole shape was similar to a square (this is apparent when Fig. 5.84 and Fig. 5.86 were compared to each other). In the sum plots, OOK had one spectral spike. This information was distinguishable until the SNR fell below 10 dB. We were still able to identify the modulation type at 0 dB. These features were unique to OOK.

D. QPSK

In this section, white Gaussian noise (AWGN) was added to the quadrature phase shift keyed (QPSK) signal. As stated in earlier chapters, for the time-frequency representation we expected a 90° phase shift at locations 65, 97, 113, 209,225 and 241 , a 180° phase shift at locations 33, 81, 161, and 193 ,and a 270° phase shift at location 129. The phase shifts were relative to the unmodulated carrier phase. The transform length for the spectrogram, the 1-1/2D_{IPS} spectrum, and the bispectrum was 8 while it is 64 for the outer product representation.

Figure 5.92 shows a plot of the sinusoidal carrier, message, the QPSK modulated signal, and the QPSK modulated signal with noise. Figure 5.93 through Figure 5.98 show the spectrograms for SNR levels of infinity, 20 dB, 15 dB, 10 dB, 5 dB, and 0 dB. It can be seen that the phase shifts were apparent at their appropriate locations in contour plots for SNR levels of 20 dB and above. But below 20 dB, we were unable to recognize phase shift at their proper locations. As a result we lost the ability to identify information about the message, modulation type, and bit rate for SNR levels below 20 dB.

Figure 5.99 through Figure 5.105 show the 1-1/2D_{IPS} spectral results. Phase shifts were apparent at their appropriate locations in contour plots at 20 dB and above. Below 20 dB, these phase shifts did not occur at the correct locations.

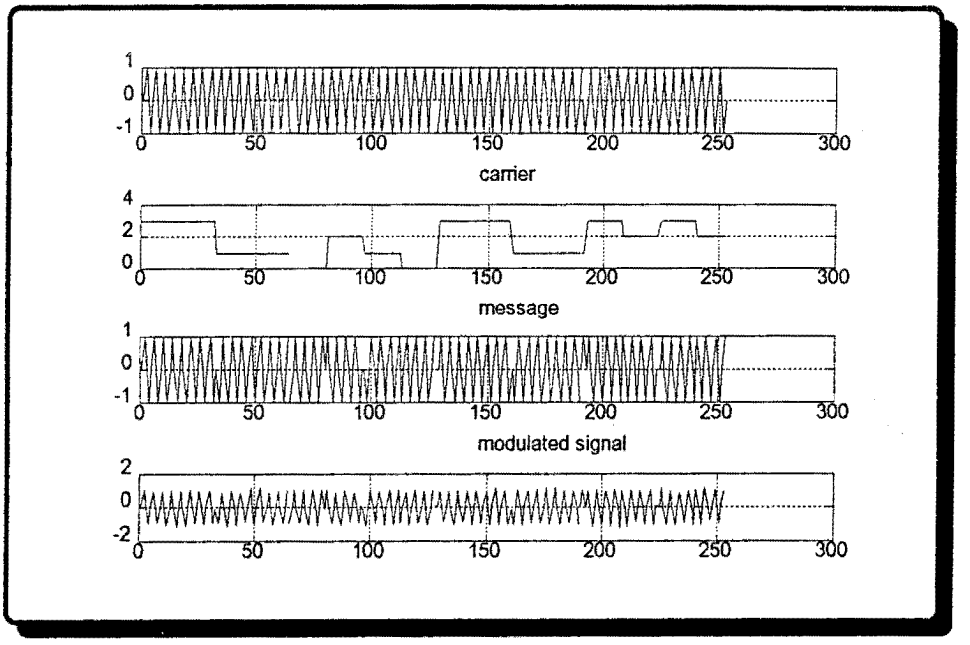

Figure 5.92: QPSK Generation with Noise

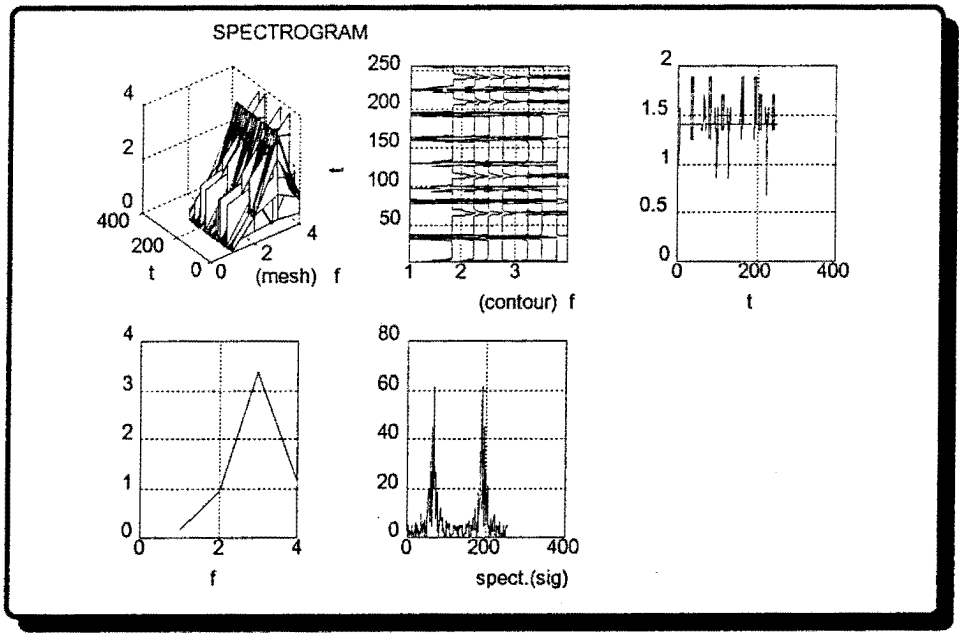

Figure 5.93: QPSK Spectrogram (Infinite SNR)

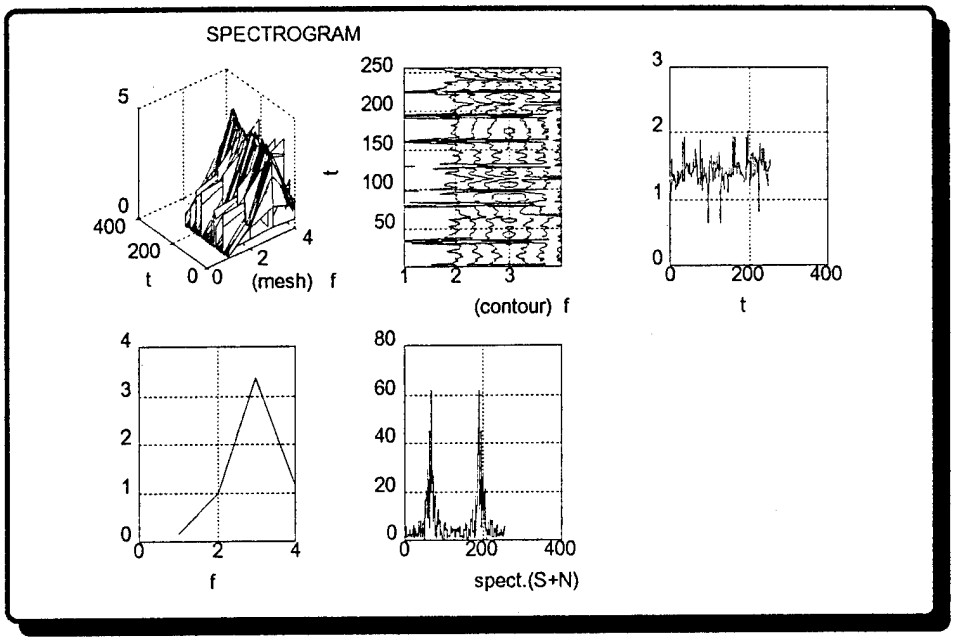

Figure 5.94: QPSK Spectrogram (SNR= +20 dB)

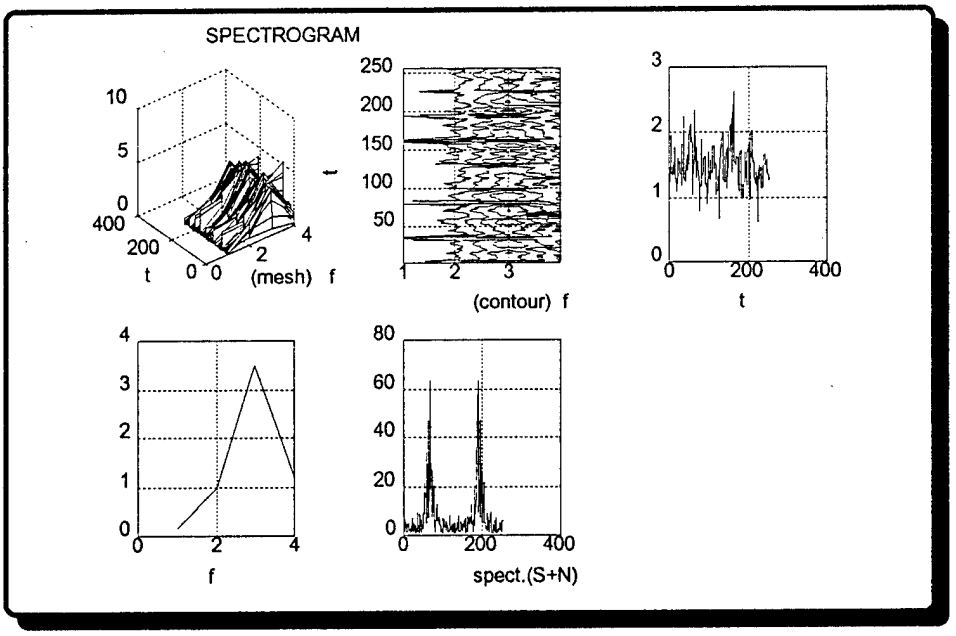

Figure 5.95: QPSK Spectrogram (SNR= +15 dB)

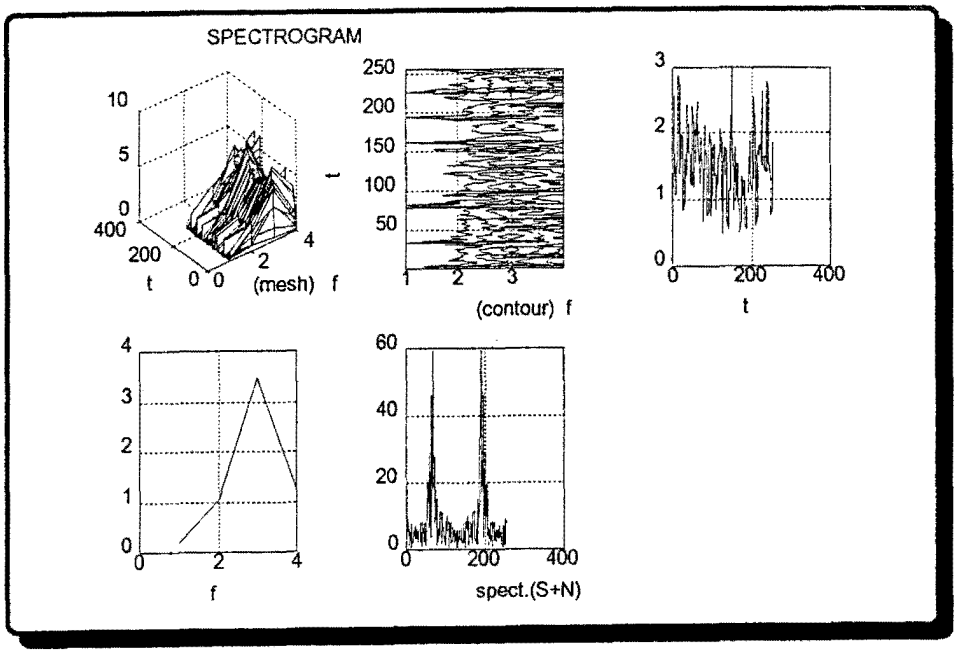

Figure 5.96: QPSK Spectrogram (SNR= +10 dB)

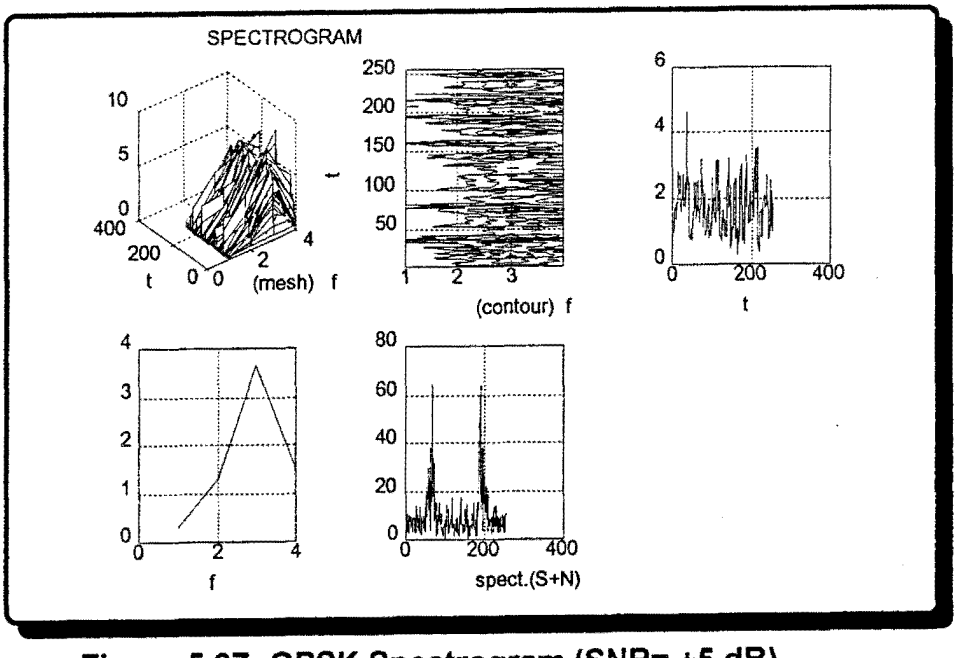

Figure 5.97: QPSK Spectrogram (SNR= +5 dB)

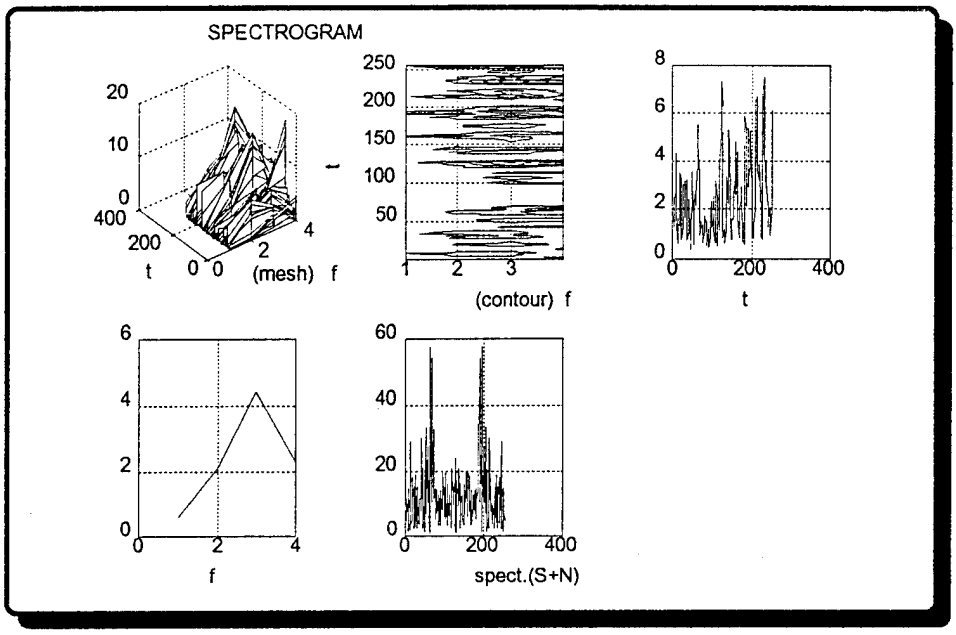

Figure 5.98: QPSK Spectrogram (SNR= 0 dB)

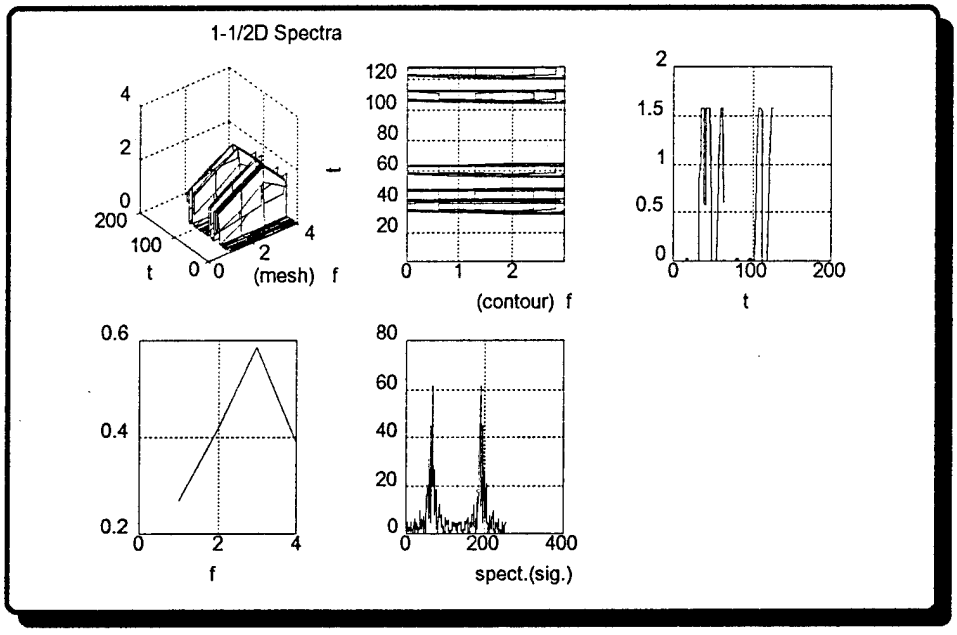

Figure 5.99: QPSK 1-1/2D Spectra (Infinite SNR)

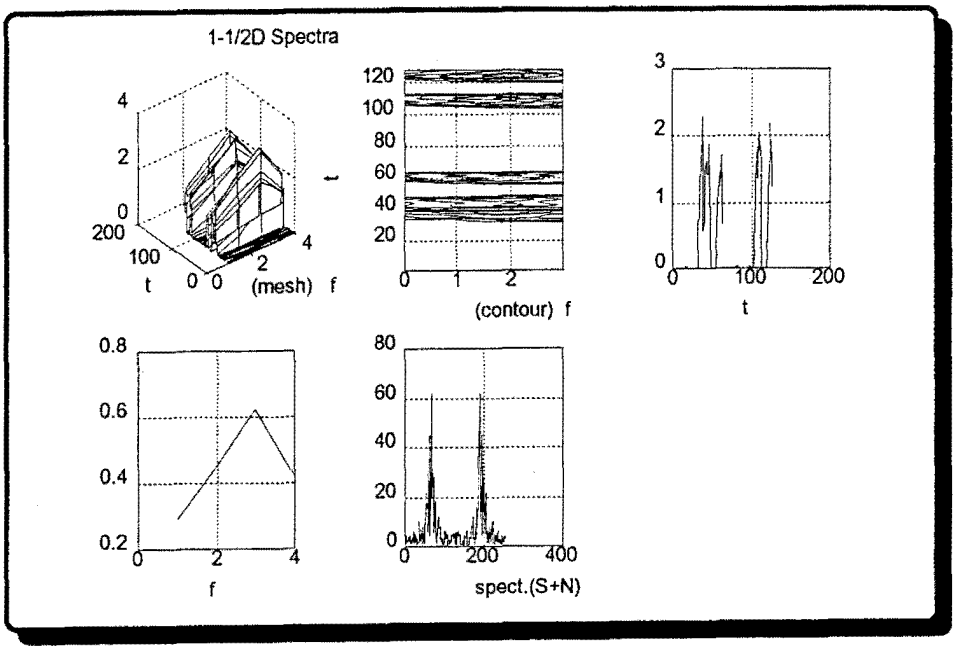

Figure 5.100: QPSK 1-1/2D Spectra (SNR= +20 dB)

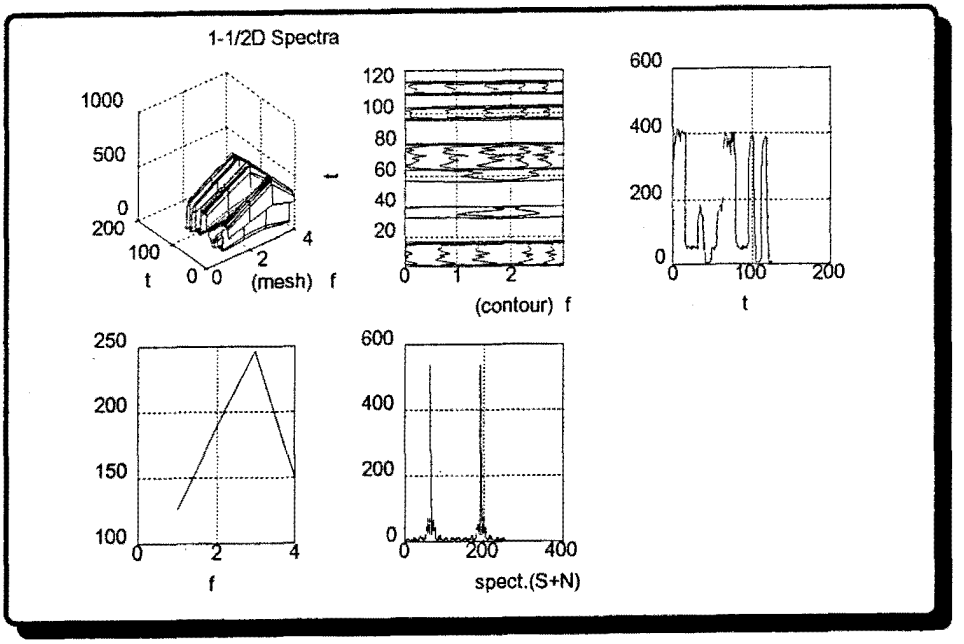

Figure 5.101: QPSK 1-1/2D Spectra (SNR= +15 dB)

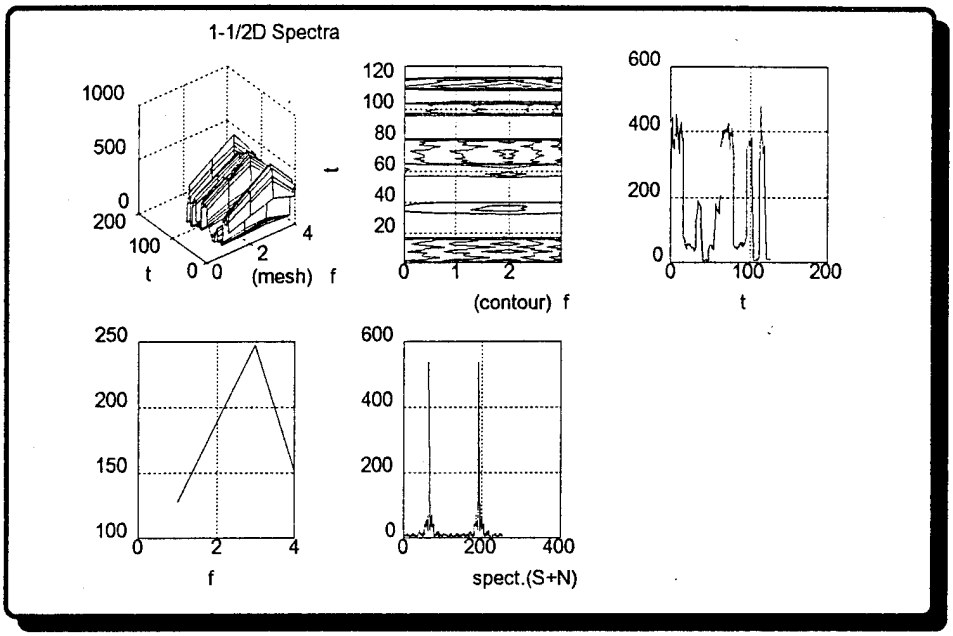

Figure 5.102: QPSK 1-1/2D Spectra (SNR= +10dB)

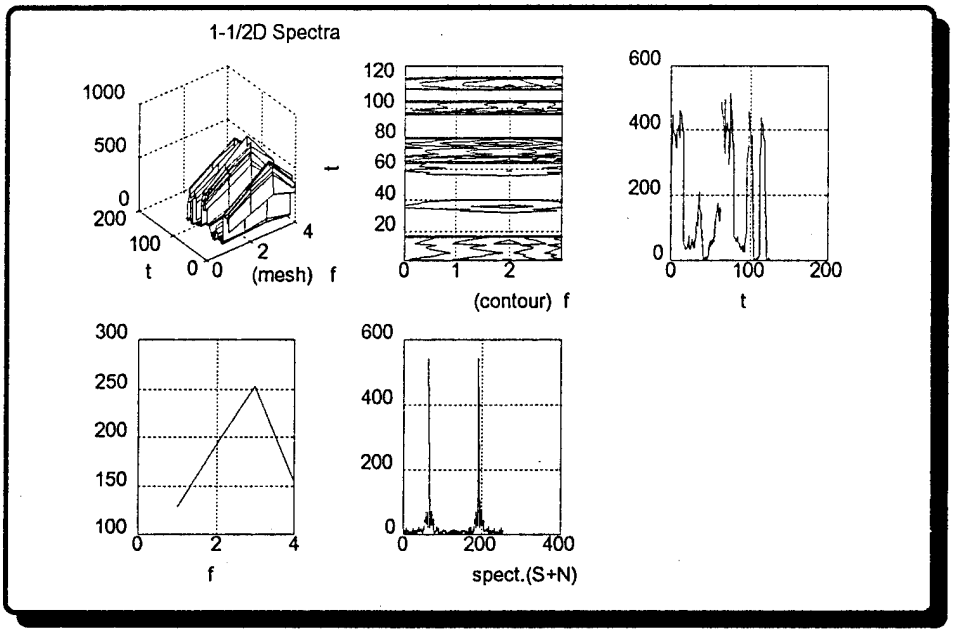

Figure 5.103: QPSK 1-1/2D Spectra (SNR= +5dB)

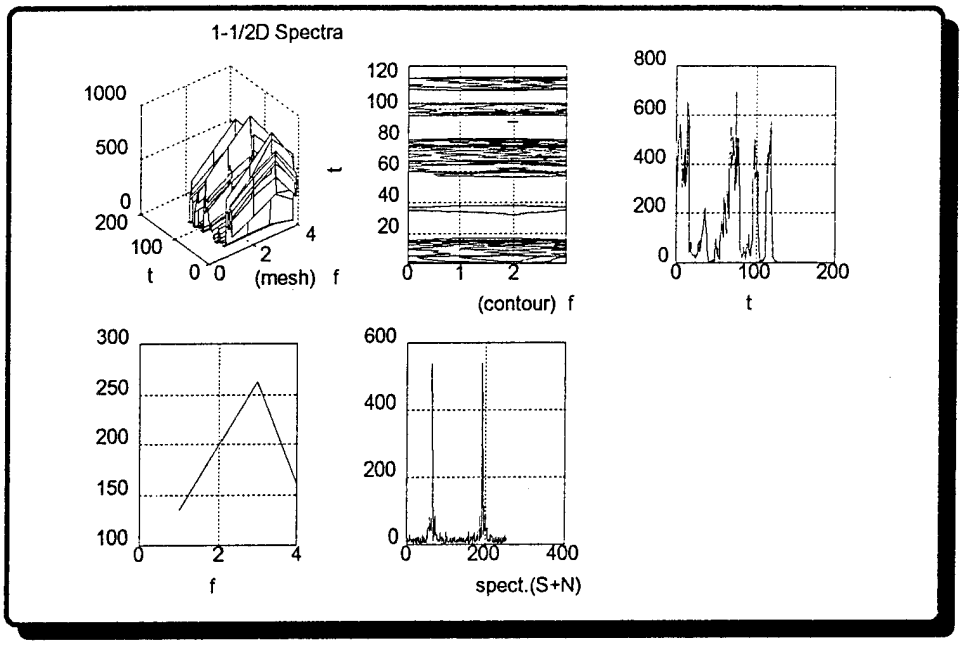

Figure 5.104: QPSK 1-1/2D Spectra (SNR= 0dB)

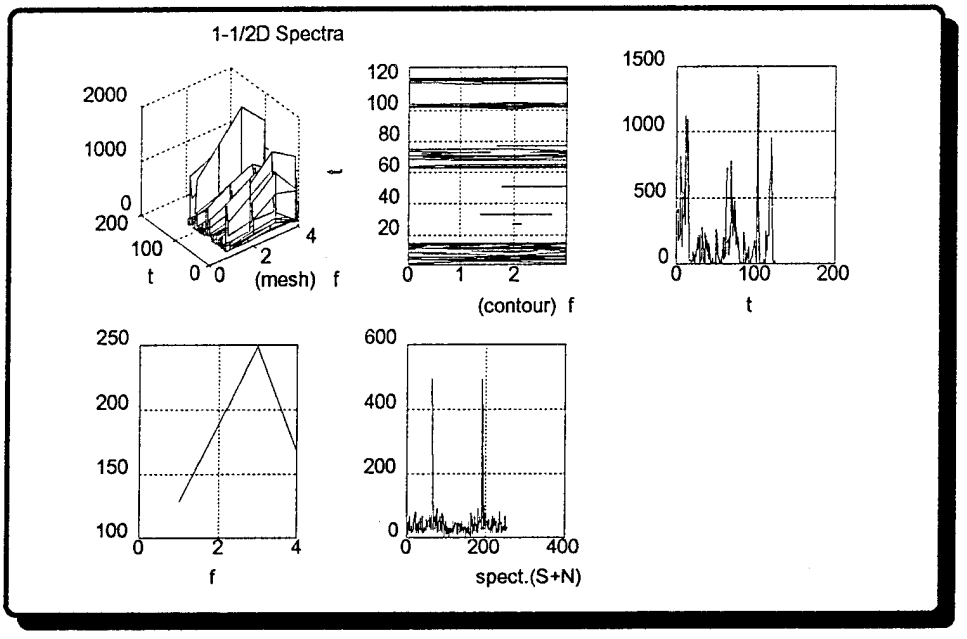

Figure 5.105: QPSK 1-1/2D Spectra (SNR= -10dB)

Because of noise components, the spectrum was difficult to interpret. Correct information about the message, modulation type, and bit rate for SNR levels below 20 dB were also difficult to determine.

Figure 5.106 through Figure 5.111 show the bispectral results. At an infinite SNR level, the QPSK bispectral pictures, especially the contour and mesh plots, showed a peak at location approximately (0.26,0.26). As the SNR level decreased, the magnitude of the peaks increased. A peak was recognizable at 20 dB and 15 dB. At SNR levels below 15 dB, this peak was not recognizable and any dominant peaks became harder to identify.

Figure 5.112 through Figure 5.121 show the outer product representation (coherent and incoherent sum) for SNR levels of infinity, 20 dB, 10 dB, 0 dB, and -5 dB. From these figures, it can be seen that the outer product form was more tolerant to noise than the other spectrum methods. The outer product representation was useful for differentiating the QPSK modulation scheme from other modulation schemes when using the contour and frequency sum plots. In the contour plots, QPSK had many peaks, all together these peaks may look like a point. This point does not look like a solid point as in the OOK's case. In the sum plots, QPSK had two spectral spikes of unequal height. The width of the QPSK's spectral spikes is narrower than the width of FSK's spectral spikes. This information was identifiable until the SNR fell below 10 dB. These features were unique to QPSK.

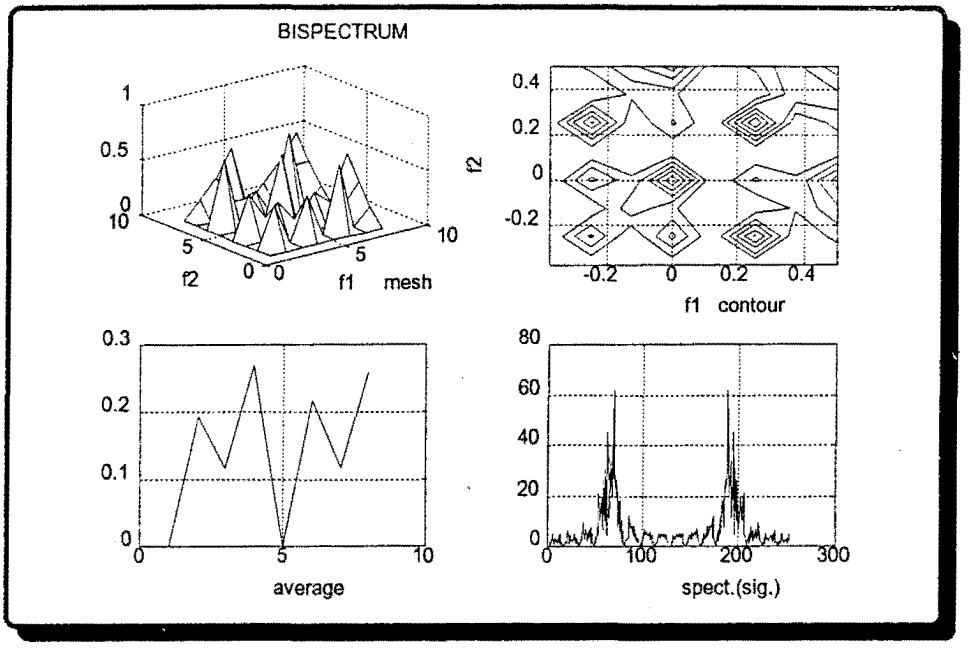

Figure 5.106: QPSK Bispectrum (Infinite SNR)

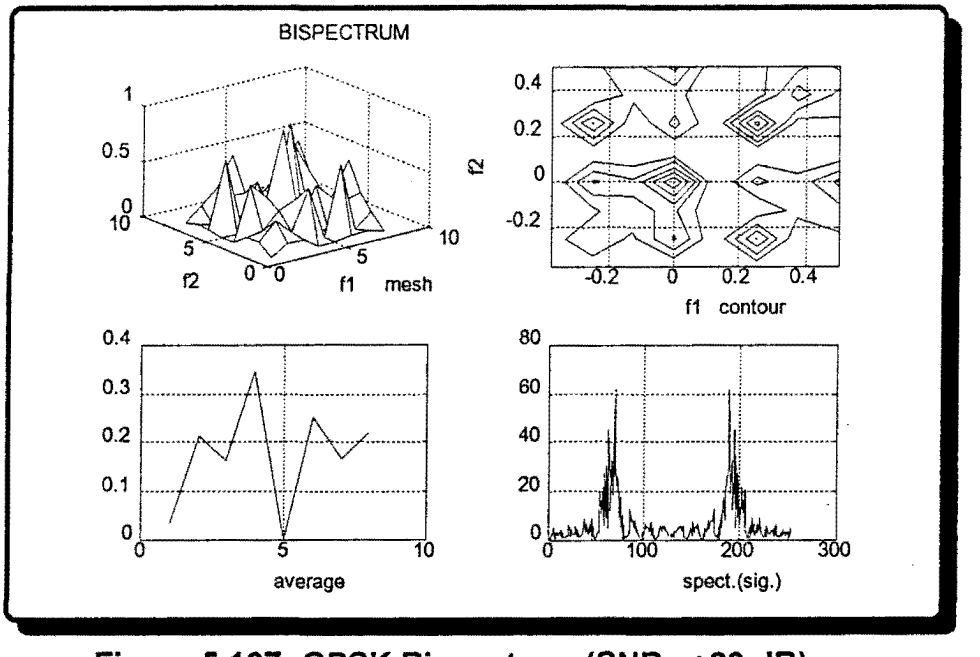

Figure 5.107: QPSK Bispectrum (SNR= +20 dB)

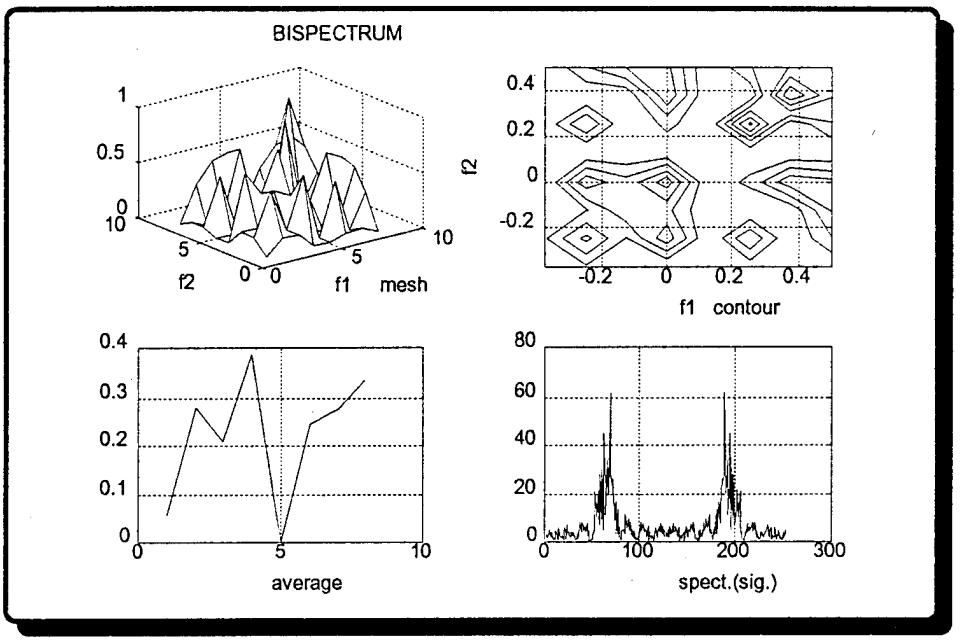

Figure 5.108: QPSK Bispectrum (SNR= +15 dB)

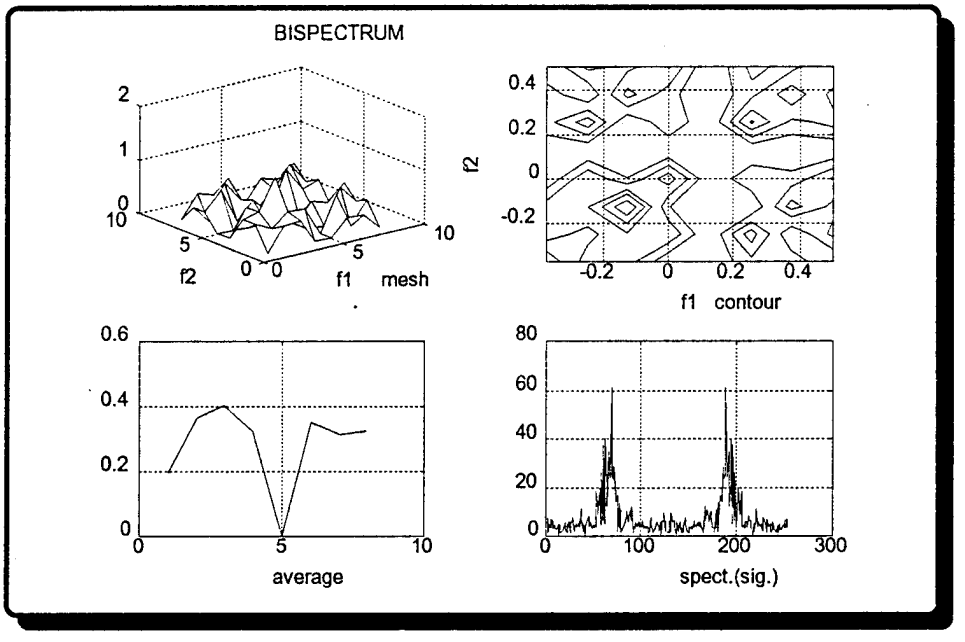

Figure 5.109: QPSK Bispectrum (SNR= +10 dB)

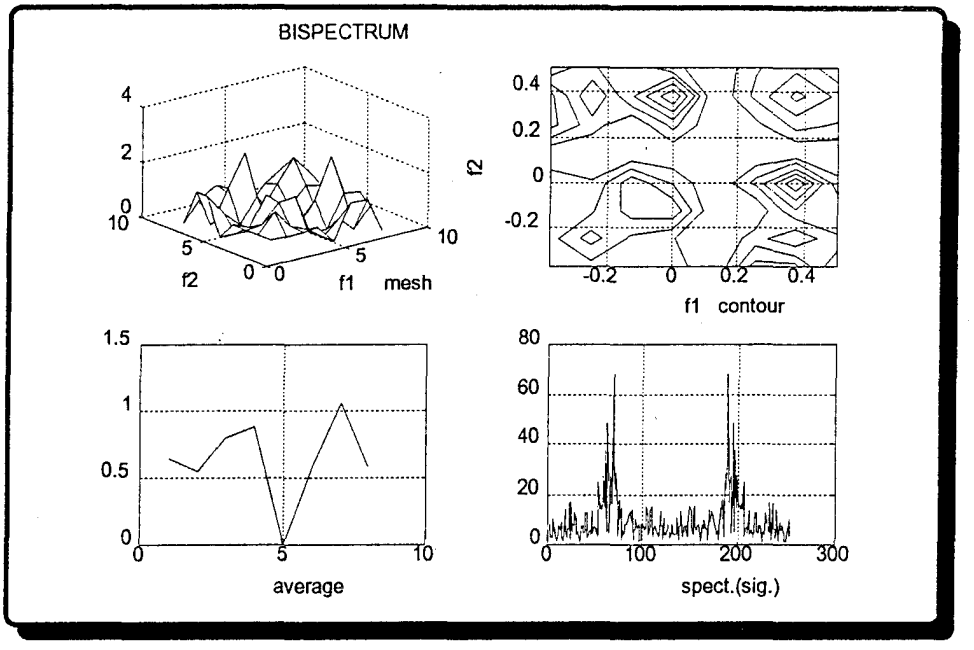

Figure 5.110: QPSK Bispectrum (SNR= +5 dB)

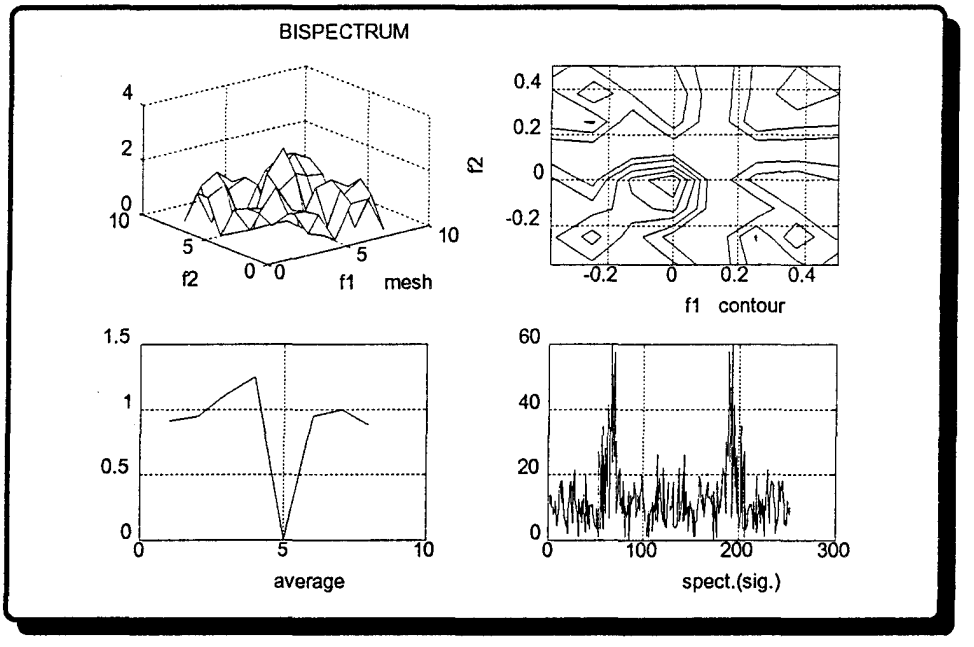

Figure 5.111: QPSK Bispectrum (SNR= +0 dB)

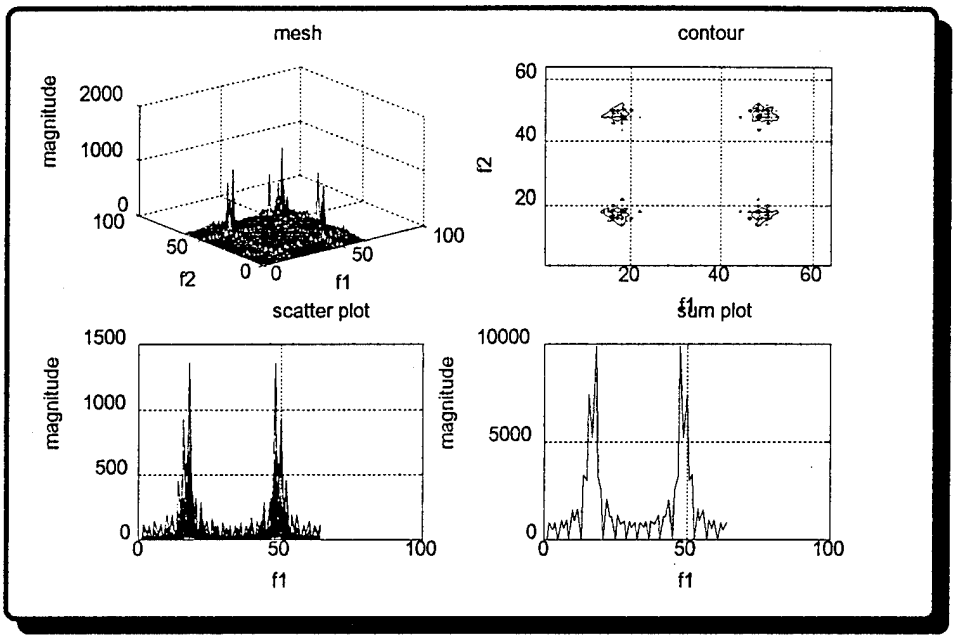

Figure 5.112: QPSK Outer Product Representation (Coherent, Infinite SNR)

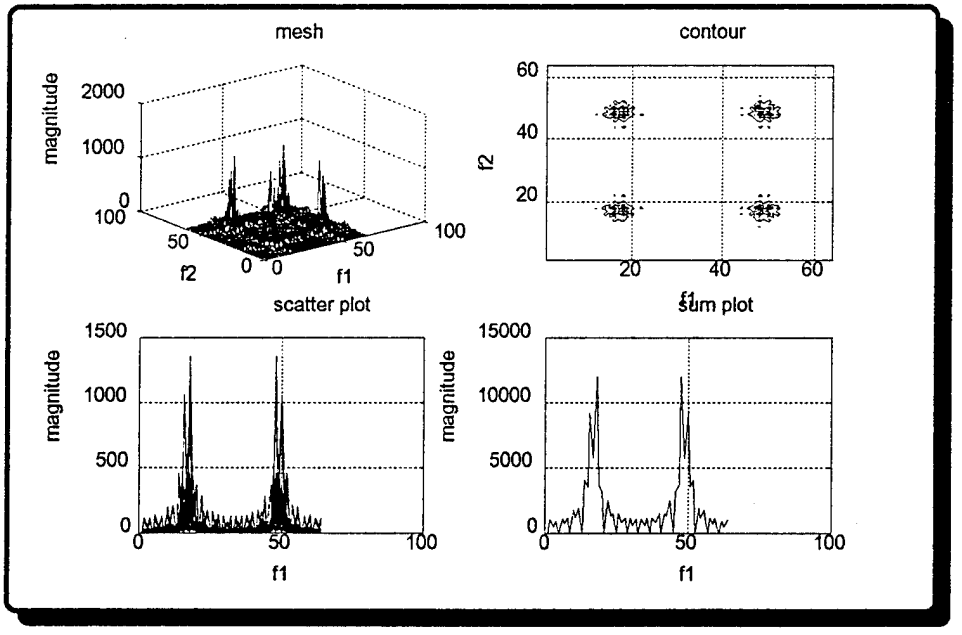

Figure 5.113: QPSK Outer Product Representation (Incoherent, Infinite SNR)

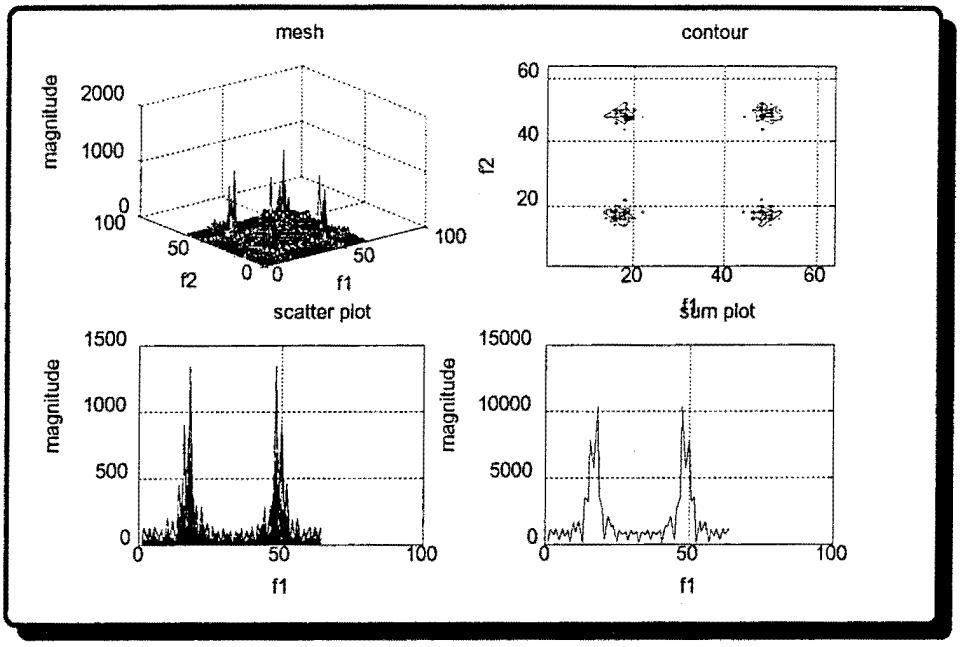

Figure 5.114: QPSK Outer Product Representation (Coherent, SNR= +20 dB)

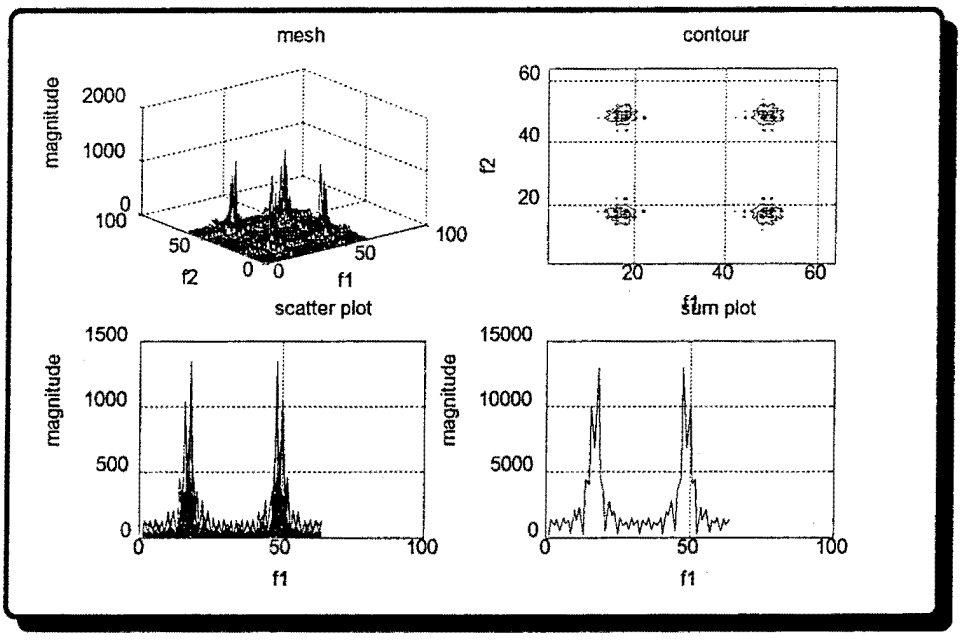

Figure 5.115: QPSK Outer Product Representation (Incoherent, SNR= +20 dB)

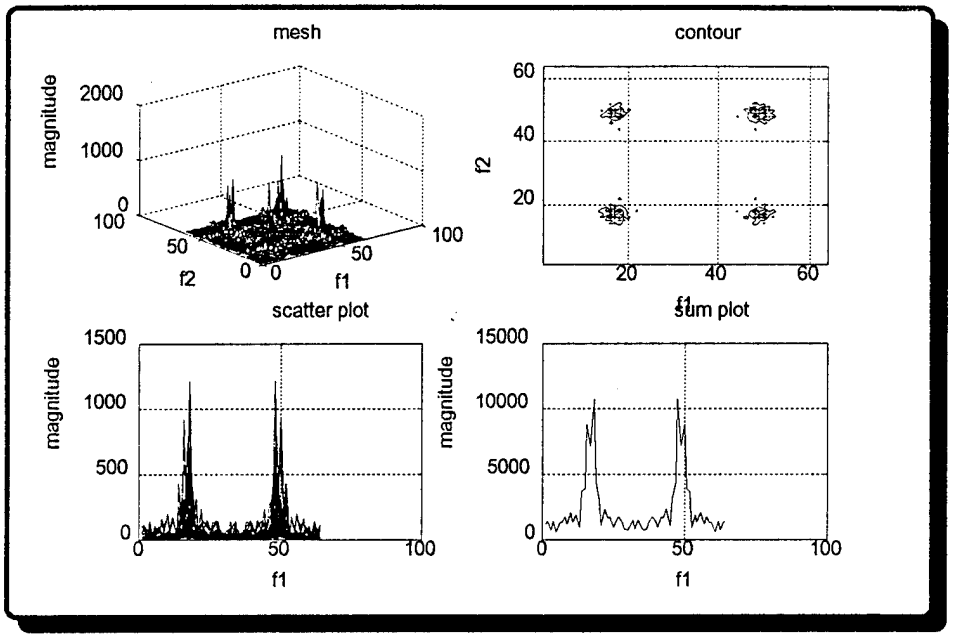

Figure 5.116: QPSK Outer Product Representation (Coherent, SNR= +10 dB)

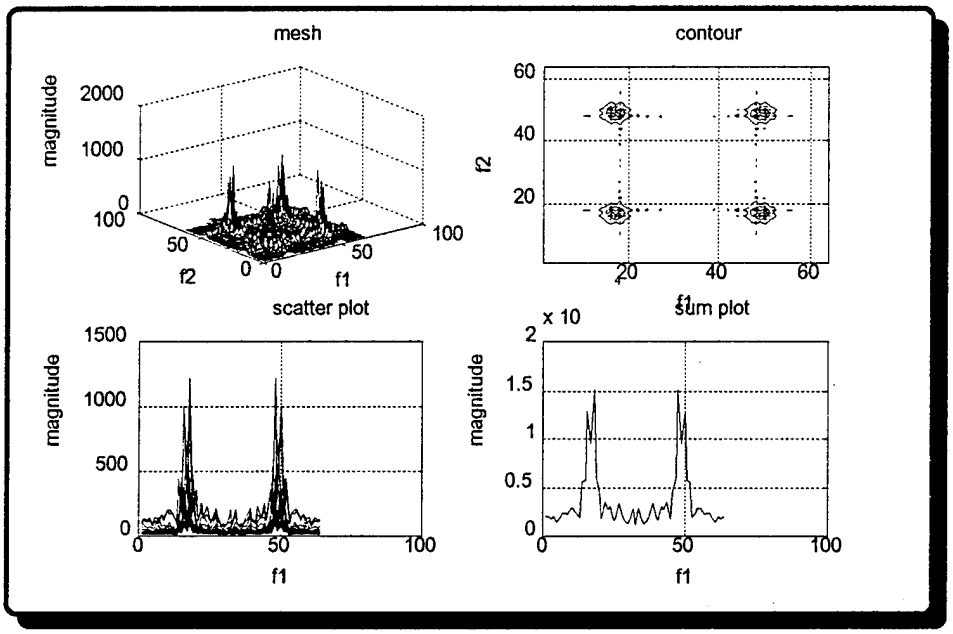

Figure 5.117: QPSK Outer Product Representation (Incoherent, SNR= +10 dB)

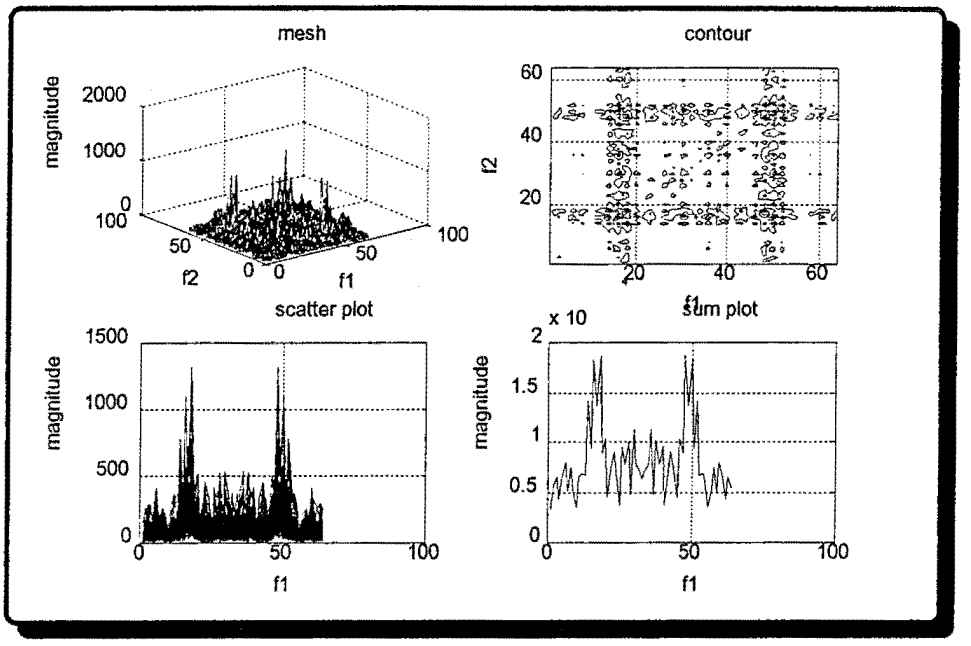

Figure 5.118: QPSK Outer Product Representation (Coherent, SNR= 0 dB)

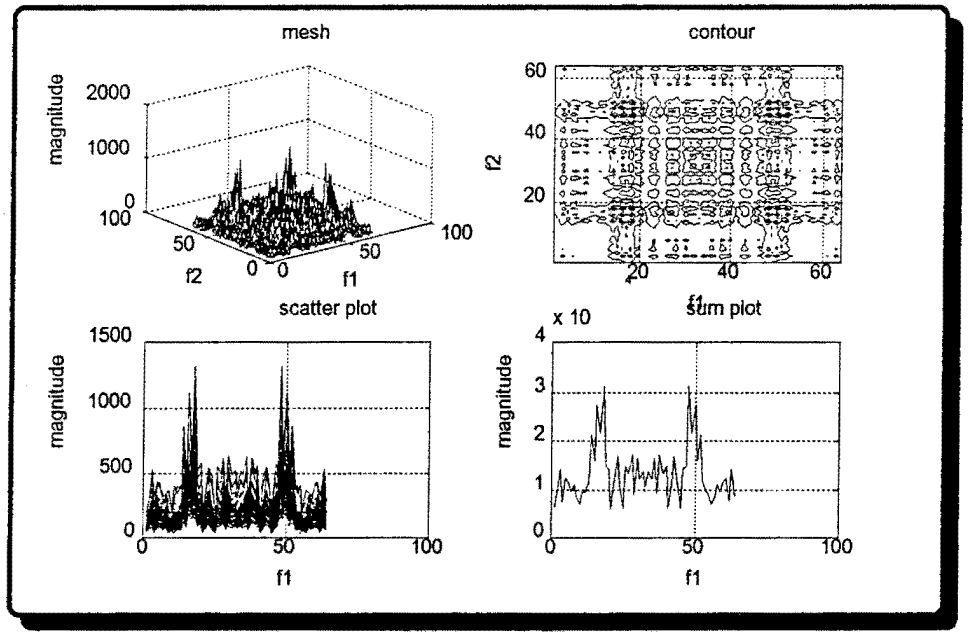

Figure 5.119: QPSK Outer Product Representation (Incoherent, SNR= 0 dB)

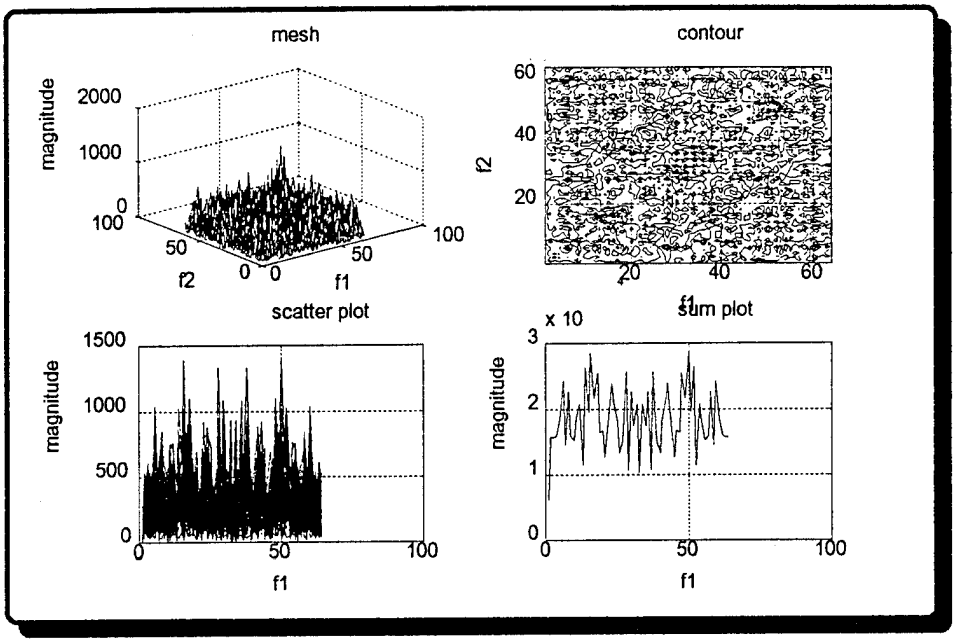

Figure 5.120: QPSK Outer Product Representation (Coherent, SNR= -5 dB)

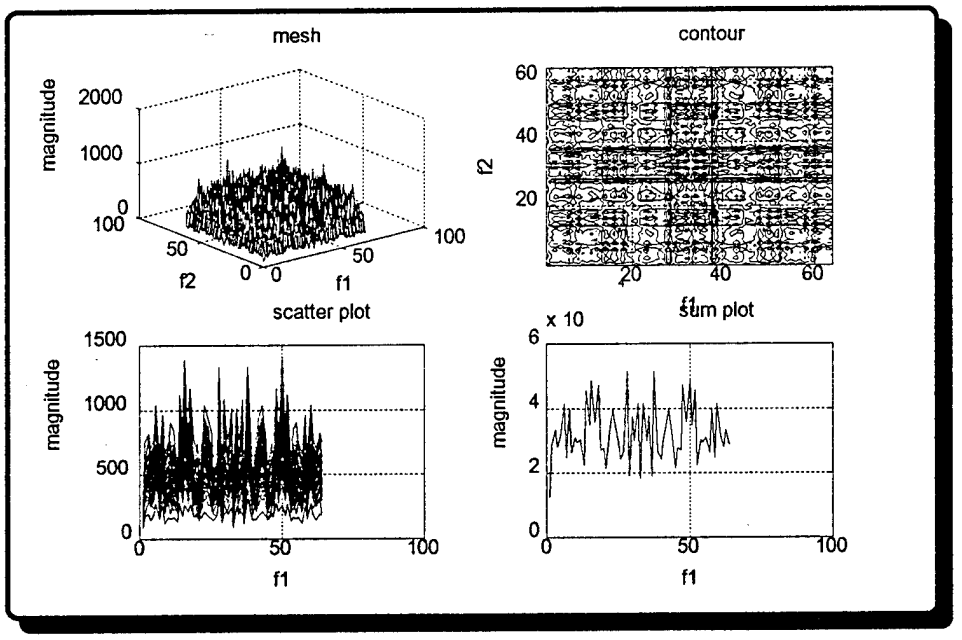

Figure 5.121: QPSK Outer Product Representation (Incoherent, SNR= -5 dB)

VI. CONCLUSIONS

A. RESULTS

This thesis investigated four spectral analysis techniques on four signal modulation forms (binary phase shift keying (BPSK), frequency shift keying (FSK), on-off keying (OOK), and quadrature phase shift keying (QPSK)). The first part of the thesis determined the optimum number of points needed for each spectral analysis and modulation choice. The second part provided the minimum SNR level able to extract information about the message, modulation type, and bit rate for each spectral estimation method.

1. Transform Length

The following table summarizes the number of signal samples needed for all modulation types and spectral estimation methods.

	spectrogram	1-1/2D_{IPS}	bispectrum	outer product form
BPSK	N_1	N_1	N_1	$4N_1$
QPSK	$N_1/2$	$N_1/2$	$N_1/2$	$4N_1$
OOK	N_1	N_1	N_1	$4N_1$
FSK	N_1	N_1	N_1	$4N_1$

Table 6.1: Transform Length versus Modulation and Detection Type

In this table, N_1 is the number of samples per symbol (or symbol length) which was 16 for all test cases. The transform length as indicated in Table 6.1 was determined from the ability to see time and spectral features in the spectral plots. In all simulations, carrier synchronization and bit synchronization were assumed.

2. Minimum SNR Level

The minimum SNR levels for detecting the modulation type versus spectral estimation method are shown in the Table 6.2.

	spectrogram	1-1/2D_{IPS}	bispectrum	outer product represent.
BPSK	20 dB	20 dB	10 dB	10 dB
QPSK	20 dB	20 dB	15 dB	10 dB
OOK	5 dB	10 dB	10 dB	0 dB
FSK	10 dB	20 dB	15 dB	0 dB

Table 6.2: The Minimum SNR Level For Identifying The Modulation Type

Under some conditions, two methods (spectrogram and 1-1/2D_{IPS}) could be used to recover the original signal (message) with some sign or phase ambiguity. The other two methods (bispectrum and outer product representation) could only determine the modulation type.

From Table 6.2, the signal modulation techniques ranked in terms of the detectability, ease of classification and recognizability and arranged in decreasing order are:

1. OOK
2. FSK
3. BPSK
4. QPSK

The bispectrum and outer product representations were the most noise tolerant methods for all modulation types investigated. Both of these techniques preserved the phase and frequency information of the signal. In addition the outer product representation had a longer transform length which improved the SNR level. The spectrogram was more noise tolerant than 1-1/2D_{IPS}. The bispectrum was useful in identifying the modulation type.

B. SUGGESTIONS FOR FUTURE STUDY

In the future, the effects of different symbol lengths, modulation types, window functions, and carrier and/or synchronization mismatch should be studied in the context of optimal processing parameters.

Information from the bispectral plane should be examined. In particular, transforms along lines of constant frequency or along linear frequency indices should be examined for use in signal classification.

Other cumulant spectral methods which are higher than third order could also be used for analyzing signals.

Implementing an alternate bispectral calculation method relying on polar rasters looks like a promising starting point. Evaluation of parametric methods and comparison to the non-parametric methods of computing the bispectrum might prove worthwhile.

For the outer product representation, coherent and incoherent sums should be studied in conjugation with different transform lengths. The phase information which can be obtained from the coherent sum should be analyzed.

APPENDIX A: BPSK CODE

```
%created by Cihat YAYCI,Turkish Navy ,July 1994
%This code generates BPSK signal.
%N is the number of information symbols (for example 16,32,64,..)
%fs is equal to k in the formulation of sinusoidal signal cos(2*pi*k/(N*c))
%c is the number of bits which are used for representing each symbol .
 %d is the desired Fourier transform length.
clear
N=input('ENTER THE NUMBER OF INFORMATION SYMBOLS...=');
fs =input('ENTER THE SAMPLING FREQUENCY..=');
c=input('ENTER THE BIT LENGTH OF EACH INFORMATION SYMBOL..=');
d=input('ENTER THE FFT LENGTH..=');
a=ones(1:N);
if N==16
x16
end
if N==32
x32
end
if N==64
x64
end
if N==128
x128
end
for i=1:N;
if x(i)<.5
x(i)=-1;
else
x(i)=1;
end
end
y=boxcar(c);
data1=y*x;
z=N*c;
data1=reshape(data1,1,z)
s=sin(2*pi*(fs/length(a)).*(1:z));
data=data1.*s;
ff=fft(data);
fff=abs(ff);
```

figure,subplot(221),plot(s) subplot(222),plot(data1) subplot(223),plot(data)
subplot(224),plot(fff)

APPENDIX B: FSK CODE

```
%created by Cihat YAYCI,Turkish Navy ,July 1994
%This code generates FSK signal.
%N is the number of information symbols (for example 16,32,64,..)
%fs is equal to k in the formulation of sinusoidal signal cos(2*pi*k/(N*c))
%f is the frequency(i.e. cos(2*pi*(k+f)/(N*c))  )
%c is the number of bits which are used for representing each symbol
%d is the desired Fourier transform length.
clear N=input('ENTER THE NUMBER OF SAMPLES...=');
fs = input('ENTER THE SAMPLING FREQUENCY..=');
f=input('ENTER THE FREQUENCY SHIFT...=')
c=input('ENTER THE DATA POINT LENGTH..=');
d=input('ENTER THE FFT LENGTH..=');
a=ones(1:N);
if N==16
x16
end
if N==32
x32
end
 if N==64
x64
end
if N==128
x128
end
for i=1:N;
if x(i)<.5
x(i)=0; else
x(i)=f;
end
end
y=boxcar(c);
 z=N*c;
data1=y*x;
data1=reshape(data1,1,z)
s=sin(2*pi*((fs+data1)/length(a)).*(1:z));
ss=fft(s); sss=abs(ss);
figure,subplot(311),plot(data1) subplot(312),plot(s) subplot(313),plot(sss)
```

APPENDIX C: OOK CODE

```
%created by Cihat YAYCI,Turkish Navy ,July 1994
%This code generates OOK signal.
%N is the number of information symbols (for example 16,32,64,..)
%fs is equal to k in the formulation of sinusoidal signal cos(2*pi*k/(N*c)).
%c is the number of bits which are used for representing each symbol
%d is the desired Fourier transform length.
clear
N=input('ENTER THE NUMBER OF SAMPLES...=');
fs = input('ENTER THE SAMPLING FREQUENCY..=');
c=input('ENTER THE DATA POINT LENGTH..=')
d=input('ENTER THE FFT LENGTH..=');
a=ones(1:N);
if N==16
x16
end
if N==32
x32
end
if N==64
x64
end
if N==128
x128
end
for i=1:N;
if x(i)<.5
x(i)=0;
else
x(i)=1;
end
end
y=boxcar(c);
data1=y*x;
z=N*c;
data1=reshape(data1,1,z)
s=sin(2*pi*(fs/length(a)).*(1:z));
data=data1.*s;
ff=fft(data);
fff=abs(ff);
```

figure,subplot(221),plot(s) subplot(222),plot(data1) subplot(223),plot(data)
subplot(224),plot(fff)

APPENDIX D: QPSK CODE

```
%created by Cihat YAYCI,Turkish Navy ,July 1994
%This code generates QPSK signal.
%N is the number of information symbols (for example 16,32,64,..)
%fs is equal to k in the formulation of sinusoidal signal cos(2*pi*k/(N*c))
%c is the number of bits which are used for representing each symbol
%of information symbols.
%d is the desired Fourier transform length.
clear
N=input('ENTER THE NUMBER OF SAMPLES...=');
fs = input('ENTER THE SAMPLING FREQUENCY..=');
c=input('ENTER THE DATA POINT LENGTH..=')
d=input('ENTER THE FFT LENGTH..=');
a=ones(1:N);
if N==16
x16
end
if N==32
x32
end
if N==64
x64
end
if N==128
x128
end
for i=1:N;
 if x(i)<.25
x(i)=2*pi;
end
end
for i=1:N;
if x(i)<.5
x(i)=pi/2;
end
end
for i=1:N;
if x(i)<.75
x(i)=pi;
end
end
```

```
for i=1:N;
if x(i)<=1.0
x(i)=3*pi/2;
end
end
y=boxcar(c);
data2=y*x;
z=N*c;
data1=reshape(data2,1,z)
s1=sin((2*pi*fs/N).*(0:z-1));
s=sin(((2*pi*fs/N).*(0:z-1))+data1);
ss=fft(s);
sss=abs(ss);
figure,subplot(311),plot(data1) subplot(312),plot(s) subplot(313),plot(sss)
```

APPENDIX E: SPECTROGRAM CODE

```
% function [P,freqaxis,timeaxis]=spectro(data,wintype,winlen);
% This function calculates spectrogram of the the supplied sequence,
% "data". The user must specify:
% "wintype" - "0" for a rectangular window.
% "1" for a Hamming window.
% "winlen" - The desired length of the data window.
% The time step is fixed at one and the spectrogram is calculated with
 % non-normalized periodograms. The time-frequency surface is returned
% in the "P" matrix. The columns of "P" are the frequency bins while the
% rows are the time steps. Time-frequency axis labeling vectors,
% "freqindex" and"imeindex" are also returned to aid in the plotting of results.
% prepared by Jeff McAloon, 01 June 1993.
% modified by Cihat Yayci, 26 July 1994.
 function [pow,freqaxis,timeaxis] = spectro(data,wintype,winlen)
x=data; xlen=length(x);
N=winlen; [row, col]=size(x);
 if row > 1
x=x.';
end
x=[zeros(1,N/2) x zeros(1,N/2)];
if wintype == 1
win=hamming(N)';
elseif wintype == 0
win=ones(1,N);
end
for ind=1:xlen
xseg=x(ind:(N-1+ind));
xseg=xseg-mean(xseg);
SP=((abs(fft(xseg.*win,N))).^2)/1;
POW(ind,:)=fftshift(SP);
end
pow=POW(:,N/2+1:N);
[prow,pcol]=size(pow);
%pow=POW;
% for noise.m timeaxis=0:xlen-1;
freqaxis=0:N/2-1;
figure,subplot(231),mesh(pow) subplot(232),contour(pow)
subplot(233),plot(mean(pow')) subplot(234),plot(mean(pow))
```

APPENDIX F: ONE_HALF D_{IPS} CODE

```
%function [P,freqindex,timeindex]=one_half(data,wintype,winlen,step);
%This function will calculate the 1 1/2 D Spectral surface.
% The 1 1/2  D surface characteristics are determined by the selection of window
%type (wintype), window length (winlen) and the distance that the window
%is moved through the data sequence (step).  The magnitude of the positive
%half of the 1 1/2 D  spectral plane is returned in the "P" matrix.
%Outputs "timeindex" and "freqindex" aid in axis labeling.
%The inputs are:
%data -The input observations vector. The length should be a power  of 2, e.g.
%64,128,512
%wintype:  '0' Rectangular Window
%  '1' Hamming Window
%winlen   - The desired width of the window, normally half of the input
% length %step     - Time step desired, can be '1' or a multiple of '2'
%prepared by Karen A. Hagerman, 06 May 1992.
%modified by Jeff McAloon,  01 June 1993.
%modified by Cihat Yayci, 24 July 1994.

function [P,freqindex,timeindex]=one_half(data,wintype,winlen,step)
[datarows,datacolumns]=size(data);
if datarows~=1 data=data.';
end
siglen=length(data);
 if wintype==0
win=ones(winlen-1,1);
elseif
wintype==1
win=hamming(winlen-1);
end
W=[win(winlen/2:-1:1)];
x=[zeros(1,winlen) data zeros(1,winlen)].';
 p=zeros(siglen/step,winlen);
index=1;
for n=winlen+1:step:
siglen+winlen-step+1
 xt=x;
ll=max((winlen+1),
(n-(winlen/2-1)));
ul=min((n+(winlen/2-1)),
(siglen+winlen));
```

```
 ctp=xt(ll:ul);
 mtp=mean(ctp);
xt(ll:ul)=ctp-mtp;
xdt=xt((n-(winlen/2-1)):
(n+(winlen/2-1)));
Xn=[abs(xt(n))^2;abs(xt(n))^2];
Xm=[conj(xt(n:-1:n-(winlen/2-1))) xt(n:n+(winlen/2-1))];
product=((Xm*Xn).*W).';
product=[product 0 conj(product(winlen/2:-1:2))];
pt=0.5*fftshift(fft(product));  p(index,:)=pt;
 index=index+1;
end
P=abs(p(:,winlen/2+1:winlen));
[Prow,Pcol]=size(P);
%P=abs(p);
 % for noise.m
 [prow,pcolumn]=size(P);
freqindex=[0:pcolumn-1]; timeindex=[1:prow];
%subplot(221),plot(freqindex,timeindex,P)
figure,subplot(231),
mesh(P)
title('1-1/2D Spectral Surface')
xlabel('f1'), ylabel('f2')
subplot(232),
contour(P,5,freqindex,timeindex)
title('1-1/2D Spectral Surface')
xlabel('f1'), ylabel('f2')
subplot(233),
plot(mean(P'))
subplot(234),
plot(mean(P))
```

APPENDIX G: OUTER PRODUCT FORM CODE

(for BPSK of FFT size 64)

```
%created by Cihat YAYCI,Turkish Navy ,July 1994
%This code creates the outer product representation of the BPSK signal for a FFT
%length of 64.  For the other modulated signals and different transform
%lengths the same logic can be used.
%N is the number of information symbols (for example 16,32,64,..)
%fs is equal to k in the formulation of sinusoidal signal cos(2*pi*k/(N*c))
%f is the frequency(i.e. cos(2*pi*(k+f)/(N*c))  )
%c is the number of bits which are used for representing each symbol
%d is the desired Fourier transform length.

clear
N=input('ENTER THE NUMBER OF SAMPLES...=');
fs =input('ENTER THE SAMPLING FREQUENCY..=');
c=input('ENTER THE DATA POINT LENGTH..=');
d=input('ENTER THE FFT LENGTH..=');
a=ones(1:N);
if N==16
x16
end
if N==32
x32
end
if N==64
x64
end
if N==128
x128
end
for i=1:N;
if x(i)<.5
x(i)=-1;
else
x(i)=1;
end
end
y=boxcar(c);
data1=y*x;
z=N*c;
data1=reshape(data1,1,z)
```

```
s=sin(2*pi*(fs/length(a)).*(1:z));
data=data1.*s;
 ffx1=fft(data(1:64));
ffx2=fft(data(65:128));
ffx3=fft(data(129:192));
ffx4=fft(data(193:256));
Z1=ffx1'*ffx1;
Z2=ffx2'*ffx2;
Z3=ffx3'*ffx3;
Z4=ffx4'*ffx4;
ZC=zeros(N,N);
coherent case Z=Z1+Z2+Z3+Z4;
cc=atan2(imag(Z),real(Z));
figure,subplot(223),plot(abs(Z)),grid
title('scatter plot') ylabel('magnitude') xlabel('f1')
subplot(224),plot(sum(abs(Z))),grid
title('sum plot') xlabel('f1') ylabel('magnitude')
subplot(221),mesh(abs(Z)),grid
xlabel('f1') zlabel('magnitude') ylabel('f2') title('mesh')
subplot(222),contour(abs(Z)),grid
xlabel('f1') ylabel('f2') title('contour')
%figure,subplot(311),plot(abs(cc)),grid
%title('BPSK (coherent case)')
%subplot(312),contour(cc),grid
%ylabel('phase')
%subplot(313),mesh(cc),grid
%ylabel('phase')
%xlabel('Z')
%Incoherent Case
ZP=abs(Z1)+abs(Z2)+abs(Z3)+abs(Z4);
figure,subplot(411),plot(ZP),grid
title('BPSK Incoherent (Power) Case')
subplot(412),plot(sum(ZP)),grid
subplot(413),plot(sum(ZP')),grid
ylabel('magnitude')
subplot(414),contour(ZP),grid
```

REFERENCES

1. Nikias, C. L., *Higher Order Spectral Analysis*, Prentice-Hall, Englewood Cliffs, New Jersey, 1993.

2. Mendel, J. M., "Tutorial on Higher Order Statistics (Spectra) in Signal Processing and System Theory: Theoretical Results and Some Applications," *Proceedings of IEEE*, Vol. 79, pp. 278-305, 1991.

3. Nikias, C. L., and Fonollosa, J. R., "Analysis of QAM Signals Using Higher-Order Spectra-Based Time-Frequency Distributions," *Proceedings of IEEE*, Vol 78, pp. 255-259, 1993.

4. Zhou, G., and Giannakis, B. G., "Comparison of Higher-Order and Cyclic Approaches For Estimating Random Amplitude Modulated Harmonics," *Proceedings of IEEE*, vol 78, pp. 225-229, 1993.

5. Giannakis, B. G., and Shamsunder, S., "Ambiguity Function, Polynomial Phase Signals and Higher-Order Cyclostationarity," *Proceedings of IEEE*, vol 78, pp. 173-177, 1993.

6. Hippenstiel, R., *Analysis Using Bi-Spectral Related Technique, Technical Report No. NPSEC-93-020*, U.S. Naval Postgraduate School, Monterey, California, November 17,1993.

7. Whalen, A. D., Detection of Signals in Noise, Academic Press, San Diego, California, 1971.

8. Kay, S. M., *Modern Spectral Estimation*, Prentice-Hall, Englewood Cliffs, New Jersey, 1988.

9. McAloon, F. J., *Comparison of Higher Order Moment Spectrum Estimation Techniques*, Master's Thesis, U.S. Naval Postgraduate School, Monterey, California, September, 1993.

10. Haykin, S., *An Introduction to Analog and Digital Communications*, John Wiley & Sons Inc., New York, New York, 1989.

11. Proakis, J. G., *Digital Communications*, McGraw Hill Inc., San Francisco, California, 1989.

12. Couch II, L. W., *Digital and Analog Communication Systems*, Macmillan Publishing Co., New York, New York, 1993.

13. Hi-Spec Software Reference Manual for Signal Processing with Higher-Order Spectra, United Signals and Systems, Inc., 1990.

14. Papoulis, A., *Probability, Random Variables, and Stochastic Processes*, McGraw Hill Inc., New York, New York, 1991.

15. Leon-Garcia, A., *Probability of Random Processes for Electrical Engineering*, Addison-Wesley Publishing Co., Menio Park, California, 1989.

16. Hagerman, K. A., *Instanteneous Power Spectrum and 1-1/2D Instantaneous Power Spectrum Techniques*, Master's Thesis, U.S. Naval Postgraduate School. Monterey, California, June 1992.

17. Nikias, C. L., and Raghuveer, M.R., "Bispectrum Estimation: A Digital Signal Processing Framework," *Proceedings of the IEEE*, Vol. 75, pp. 869-891, 1987.

18. Haykin, S., editor. *Advances in Spectrum Analysis and Array Processing,* Vol 1, Prentice-Hall, Englewood Cliffs, New Jersey, 1991.

19. Therrien, C. W., *Discrete Random Signals and Statistical Signal Processing*, Prentice-Hall, Englewood Cliffs, New Jersey, 1992.

20. Torrieri, D.J., *Principles of Secure Communication Systems*, Artech House, Norwood, MA, 1992.

21. Hippenstiel, R.D., and De Oliveira, P.M., "Time-Varying Spectral Estimation Using the Instantaneous Power Spectrum (IPS)," *IEEE Transactions on Acoustics, Speech, and Signal Processing*, Vol. 38, No. 10, pp. 1752-1759, October 1990.

22. Ross, S., *A First Course in Probability*, MacMillian Publishing Co., New York, New York, 1988.

23. Hurd H.L., "Spectral Coherence of Nonstationary and Transient Stochastic Processes," *Proceedings of the IEEE*, Vol. 88, pp. 387-390, 1988.

24. Hinich. M.J., "Detecting a Transient Signal by Bispectral Analysis," *IEEE Transactions on Acoustics, Speech, and Signal Processing*, Vol. 38, No. 7, pp. 1277-1283, July 1990.

25. Wolinsky, M.A., *Invitation to the Bispectrum*, Tech. Report No. ARL-TR-88-7, Applied Research Laboratories, The University of Texas at Austin, August 1988.

26. Nikias C.L., and Mendel J.M., "Signal Processing with Higher-Order Spectra," *IEEE Signal Processing Magazine*, pp. 10-37, July 1993.

27. Fontanella J.C., and Seve A., "Reconstruction of Turbulence-Degraded Images Using the Knox-Thompson Algorithm," *Optical Society of America,* Volume 4, No. 3, pp 438-448, March 1987.

28. Nakajima T., "Signal-to-Noise Ratio of the Bispectral Analysis of Speckle Interferometry," *Optical Society of America,* Volume 5, No. 9, pp 1477-1491, September 1988.

INITIAL DISTRIBUTION LIST

		No. Copies
1.	Defense Information Center Cameron Station Alexandria, VA 22304-6145	2
2.	Library Code 52 Naval Postgraduate School Monterey, CA 93943-5101	2
3.	Chairman, Code EC Department of Electrical and Computer Engineering Naval Postgraduate School Monterey, CA 93943-5121	1
4.	Chairman, Code Ph Department of Physics Naval Postgraduate School Monterey, CA 93943-5117	1
5.	Professor Ralph Hippenstiel, Code EC/Hi Department of Electrical and Computer Engineering Naval Postgraduate School Monterey, CA 93943-5121	2
6.	Professor Donald Walters, Code Ph/We Department of Physics Naval Postgraduate School Monterey, CA 93943-5117	2
7.	CDL Program Manager Defense Support Project Office Washington DC 20330-1000	1
8.	Deniz Kuvvetleri Komutanligi Personel Daire Baskanligi Bakanliklar, Ankara, Turkey	2

		No. Copies
9.	Golcuk Tersanesi Komutanligi Golcuk, Kocaeli, Turkey	1
10.	Deniz Harp Okulu Komutanligi 81704 Tuzla, Istanbul, Turkey	1
11.	Taskizak Tersanesi Komutanligi Kasimpasa, Istanbul, Turkey	1
12.	Cihat Yayci Kaymakam Evi Yalova, Istanbul, Turkey	1
13.	Bogaziçi Üniversitesi Kütüphanesi Istanbul, Turkey	1
14.	Istanbul Teknik Üniversitesi Kütüphanesi Istanbul, Turkey	1
15.	Ortadoğu Teknik Üniversitesi Kütüphanesi Ankara, Turkey	1